



National Aeronautics and
Space Administration

ENERGY EFFICIENT ENGINE

FLIGHT PROPULSION SYSTEM PRELIMINARY ANALYSIS AND DESIGN

By

GENERAL ELECTRIC COMPANY

June 1980

Prepared For

National Aeronautics and Space Administration

LEWIS RESEARCH CENTER
21000 BROOKPARK ROAD
CLEVELAND, OHIO 44135

Contract NAS3-20643

(NASA-CR-159583) ENERGY EFFICIENT ENGINE:
FLIGHT PROPULSION SYSTEM PRELIMINARY
ANALYSIS AND DESIGN Topical Report, Jan. -
Nov. 1978 (General Electric Co.) 276 p
HC A12/MF A01

N81-18056

Unclas
41518



1. Report No. NASA CR-159583		2. Government Accession No.		3. Recipient's Catalog No.	
4. Title and Subtitle Energy Efficient Engine - Flight Propulsion System Preliminary Analysis and Design				5. Report Date November 1979	
				6. Performing Organization Code	
7. Author(s) R.P. Johnston, R.S. Beitler, R.O. Bobinger, C.L. Broman R.D. Gravitt, H. Heineke, P.R. Holloway, J.S. Klem, D.O. Nash, P. Ortiz, G.T. Sandusky, A.P. Sterman				8. Performing Organization Report No. R79AEG623	
				10. Work Unit No.	
9. Performing Organization Name and Address General Electric - Aircraft Engine Group Evendale, Ohio				11. Contract or Grant No. NAS3-20643	
				13. Type of Report and Period Covered Topical Report January 1978 - November 1978	
12. Sponsoring Agency Name and Address National Aeronautics and Space Administration Lewis Research Center 21000 Brookpark Road Cleveland, Ohio 44135				14. Sponsoring Agency Code	
15. Supplementary Notes Project Manager: Mr. N.T. Saunders, NASA-Lewis Research Center, Cleveland, Ohio					
16. Abstract The characteristics of an advanced Flight Propulsion System (FPS), suitable for introduction in the late 1980's to early 1990's, has been more fully defined. It has been determined that all NASA goals for efficiency, environmental considerations, and economics could be met or exceeded with the possible exception of NO _x emission. In evaluating the FPS, all aspects were considered including component design, performance, weight, initial cost, maintenance cost, engine-system integration (including nacelle), and aircraft integration considerations. In terms of the NASA goals, the current FPS installed specific fuel consumption has been reduced 14.2% from that of the CF6-50C reference engine. When integrated into an advanced, subsonic, study transport, the FPS produced a fuel-burn savings of 15 to 23% and a direct operating cost reduction of 5 to 12% depending on the mission and study-aircraft characteristics relative to the reference engine.					
17. Key Words (Suggested by Author(s)) Energy Conservation Subsonic Transport Turbine Engine Aircraft Turbine Engine Energy Efficient Engine			18. Distribution Statement Unclassified - Unlimited		
19. Security Classif. (of this report) Unclassified		20. Security Classif. (of this page) Unclassified		21. No. of Pages	22. Price*

* For sale by the National Technical Information Service, Springfield, Virginia 22151

FOREWORD

This report presents the results of preliminary analysis and design of an advanced Flight Propulsion System (FPS) conducted by the General Electric Company. This work was performed for the National Aeronautics and Space Administration (NASA), Lewis Research Center, under contract NAS3-20643 as part of the Aircraft Energy Efficiency (ACEE) Program, Energy Efficient Engine (E³) Project. Mr. Neal T. Saunders is the NASA E³ Project Manager; Mr. Lawrence E. Macioce is serving as NASA Assistant Project Manager. Mr. John Schaefer was the NASA Project Engineer responsible for the effort associated with the Flight Propulsion System - Preliminary Analysis and Design reported here. Mr. Martin C. Hemsworth served as manager of the E³ Project for the General Electric Company. This report was prepared by Mr. Richard P. Johnston with the assistance of the responsible engine component design managers.

PRECEDING PAGE BLANK PAGE

TABLE OF CONTENTS

<u>Section</u>		<u>Page</u>
1.0	SUMMARY	1
2.0	INTRODUCTION	5
3.0	FLIGHT PROPULSION SYSTEM PRELIMINARY DESIGN AND PERFORMANCE	7
3.1	Flight Propulsion System (FPS) Design	7
3.1.1	FPS Features	7
3.1.2	Design Requirements	12
3.1.3	Design Studies and Results	15
3.1.4	Active Clearance Control	18
3.1.5	System Compatibility	25
3.1.6	Maintainability	25
3.1.7	Weight, Cost, Maintenance Cost, Engine Performance, and Economic Benefits	27
3.1.8	Engine System Vibration	33
3.2	Cycle and Performance	42
3.2.1	Cycle History and Selection Criteria	42
3.2.2	Cycle Selection Process	48
3.2.3	Cycle Definition	48
3.2.4	Reference Engine Comparison	50
3.2.5	Growth Capability	52
3.3	Performance Retention	52
3.4	Materials and Processes	56
3.5	Acoustics	69
3.5.1	Acoustic Considerations	69
3.5.2	Component Design Features	70
3.6	Propulsion-System/Aircraft Integration	79
3.6.1	Aircraft Company Subcontracts	82
3.6.2	Economic Studies	93
4.0	COMPONENT PRELIMINARY ANALYSIS AND DESIGN	99
4.1	Fan	99
4.1.1	FPS Configuration	99
4.1.2	Alternate Fan Study	101
4.2	Compressor	112
4.2.1	Configuration and Design	112
4.2.2	Active Clearance Control	127

TABLE OF CONTENTS (Continued)

<u>Section</u>	<u>Page</u>
4.3 Combustor	131
4.3.1 Component Description	131
4.3.2 Aerodynamic Design	134
4.3.3 Impact of Broad-Specification Fuels	142
4.3.4 Mechanical Design	144
4.3.5 Alternate Combustor Design	150
4.3.6 Weight Estimate	154
4.4 High Pressure Turbine	157
4.4.1 General Description	157
4.4.2 Cooling	161
4.4.3 Stage 1 Design Features	165
4.4.4 Stage 2 Design Features	165
4.4.5 Materials	170
4.4.6 Active Clearance Control	175
4.4.7 Disk Life	175
4.5 Low Pressure Turbine	175
4.5.1 Component Description	175
4.5.2 Design Objectives	180
4.5.3 Cooling System	180
4.5.4 Active Clearance Control	183
4.5.5 Aerodynamic Design	183
4.5.6 Mechanical Design	187
4.6 Turbine Frame and Mixer	191
4.6.1 Turbine Frame	191
4.6.2 Mixer	195
4.7 Bearings Systems, Drives, and Configuration	201
4.8 Control System	219
4.8.1 Design Requirements	219
4.8.2 Control System Design	220
4.8.3 Digital Control Design	222
4.8.4 Fuel Control System	225
4.8.5 Stator Control System	229
4.8.6 Active Clearance Control	231
4.8.7 Starting Bleed	234
4.8.8 Fuel-Heating System	234
4.8.9 Aircraft Generator Cooling	235
4.8.10 Control System Configuration	236

TABLE OF CONTENTS (Concluded)

<u>Section</u>		<u>Page</u>
4.9	Nacelle Design	236
4.9.1	Fan Reverser	237
4.9.2	Engine Mount System	241
4.9.3	Accessory Package	243
4.9.4	Aircraft Company Subcontracts	247
5.0	CONCLUSIONS	251
6.0	REFERENCES	253

LIST OF ILLUSTRATIONS

<u>Figure</u>		<u>Page</u>
1.	E ³ FPS Features.	2
2.	Uninstalled FPS Features.	8
3.	Installed FPS Features.	11
4.	Engine Cycle Comparison.	13
5.	Installed Engine Piping and Mount Details.	14
6.	FPS Comparison.	16
7.	High Pressure Compressor ACC System.	19
8.	High/Low Pressure Turbine ACC System.	19
9.	Typical Tip-Clearance Behavior.	20
10.	Typical Mission Profile.	21
11.	HPT Stage 1 Rotor/Stator Transient Clearances.	23
12.	Average Stage Clearance Behavior.	24
13.	Sample Stability Stack Crosswind - Fan at T/O Thrust.	26
14.	Sample Stability Stack Crosswind - HPC at T/O Thrust.	26
15.	FPS On-Wing Access Provisions.	28
16.	Energy Efficient Engine Modules.	29
17.	FPS Maintainability Features.	30
18.	FPS Reliability Features.	31
19.	Combined Tuned Bearing Support and Damper Arrangement for the E ³ FPS Core Rotor.	37
20.	FPS Engine Dynamics Model with Component Descriptions.	38
21.	Maximum Value of No. 3 Bearing Force Versus Number of Shims for 0.0381 kg-m (1500 g-in) HPT Unbalance.	40

LIST OF ILLUSTRATIONS (Continued)

<u>Figure</u>		<u>Page</u>
22.	Maximum Value of No. 4 Bearing Force Versus Number of Shims for 0.0381 kg-m (1500 g-in) HPT Unbalance.	41
23.	E ³ FPS No. 3 Bearing Load Versus Core Speed for Combined Mode Response with 0.0381 kg-m (1500 g-in) HPT Unbalance.	43
24.	E ³ FPS No. 4 Bearing Load Versus Core Speed for Combined Mode Response with 0.0381 kg-m (1500 g-in) HPT Unbalance.	44
25.	E ³ FPS No. 3 Bearing Load Versus Core Speed for Combined Mode Response with 0.00762 kg-m (300 g-in) HPC Unbalance.	46
26.	E ³ FPS No. 4 Bearing Load Versus Core Speed for Combined Mode Response with 0.00762 kg-m (300 g-in) HPC Unbalance.	47
27.	E ³ Cycle Selection.	47
28.	E ³ Long-Term Performance Retention.	55
29.	Fan Frame and Nacelle.	59
30.	Fan Rotor and Stator.	60
31.	HP Compressor Rotor and Stator.	61
32.	FPS Combustor.	62
33.	Turbine Shroud Concepts.	63
34.	HPT Materials, Rotating Components.	64
35.	HPT Materials, Static Components.	65
36.	Low Pressure Turbine.	66
37.	Mixer and Turbine Frame.	67
38.	Bearings, Seals, Drives, and Shafting.	68
39.	Energy Efficient Engine - Low Noise Design Features.	71
40.	Fan Frame Acoustic Evaluation.	74
41.	Turbulence-Control Structure and Test Setup.	74

LIST OF ILLUSTRATIONS (Continued)

<u>Figure</u>		<u>Page</u>
42.	Effect of Cut-On Vane-Frame at Wide Spacing.	75
43.	E ³ Component Noise Levels.	76
44.	E ³ System Noise-Reduction Studies - Approach.	80
45.	Energy Efficient Engine, Model 768-868 Domestic Airplane (Boeing).	83
46.	General Arrangement, Domestic Transcontinental Range Version (McDonnell-Douglas).	84
47.	General Arrangement, Domestic Aircraft (Lockheed).	85
48.	General Arrangement, Intercontinental Aircraft (Lockheed).	86
49.	Block Fuel Savings (E ³ Engine Versus CF6-50C).	87
50.	Direct Operating Cost (DOC) Improvement (E ³ Versus CF6-50C).	98
51.	Fan Module Cross Section and Preliminary Operating Map.	100
52.	Particle Trajectories.	102
53.	Typical Tests and Particle Size Distribution.	103
54.	E ³ Initial-Study Fan - Baseline.	105
55.	Thirty-Eight-Blade Design - No Booster.	106
56.	Twenty-Eight-Blade Design - Pin Root.	107
57.	Thirty-Two-Blade Design - No Booster.	108
58.	Twenty-Blade Design - No Shroud or Booster.	109
59.	Thirty-Two-Blade Design - with Booster.	110
60.	E ³ 32-Blade Fan, Preliminary Coupled-Blade-Disk Campbell Diagram.	113
61.	E ³ Quarter-Stage Preliminary Blade Campbell Diagram.	114
62.	E ³ High Pressure Compressor.	116

LIST OF ILLUSTRATIONS (Continued)

<u>Figure</u>		<u>Page</u>
63.	Core Compressor Performance Map Estimated from Stage Characteristics, Without Starting Bleed.	118
64.	Configuration Changes from the Initial to the Current FPS Compressor.	121
65.	Compressor-Case Cooling Flow.	123
66.	Compressor Rotor Cooling.	125
67.	HP Compressor Aft Rotor Spool Stresses.	126
68.	Compressor Rotor Blade; Typical Campbell Diagram.	128
69.	Compressor Clearance Study.	129
70.	E ³ Combustor - Selected Design.	132
71.	Split Duct Diffuser Design.	132
72.	Dome/Swirl-Cup Design.	133
73.	Fuel Nozzle Design.	133
74.	Shingle Liner Design.	135
75.	E ³ Combustor Materials Selection.	136
76.	E ³ Combustor Design Technology.	136
77.	Engine Fuel Flow Schedule.	138
78.	E ³ Double-Annular Combustor Predicted Emission Characteristics.	140
79.	Machined-Ring and Shingle Combustors.	145
80.	E ³ Combustor Axial Liner Temperature Distribution, Inner Liner - Panel 1.	148
81.	Typical Thermal-Stress Distribution.	149
82.	E ³ Combustor - Alternate Design.	153
83.	E ³ Combustor - Alternate Design Test Configuration.	155

LIST OF ILLUSTRATIONS (Continued)

<u>Figure</u>		<u>Page</u>
34.	E ³ Single-Annular-Combustor Emission Characteristics.	156
35.	E ³ High Pressure Turbine.	158
36.	E ³ Turbine Rotor Cooling Source.	164
37.	E ³ High Pressure Turbine Cooling-Flow Distribution.	164
38.	High Pressure Turbine Stage 1 Nozzle Diaphragm Design Features.	
89.	E ³ High Pressure Turbine Stage 1 Vane Airfoil Cooling.	
90.	E ³ High Pressure Turbine Stage 1 Vane Band Cooling.	
91.	E ³ High Pressure Turbine Stage 1 Blade.	168
92.	E ³ High Pressure Turbine Stage 2 Nozzle Vane.	169
93.	High Pressure Turbine Stage 2 Blade.	171
94.	E ³ HPT Materials - Rotor Components.	173
95.	E ³ HPT Components - Static Components.	174
96.	High Pressure Turbine Active Clearance Control.	176
97.	E ³ High Pressure Turbine Stage 1 Disk Stresses.	178
98.	E ³ Low Pressure Turbine - Five Stages.	179
99.	Low Pressure Turbine Materials.	182
100.	Cooling System - E ³ Low Pressure Turbine.	184
101.	E ³ Low Pressure Turbine Active Clearance Control.	185
102.	E ³ LP Turbine Aerodynamic Design Features.	186
103.	LPT Vane Features.	188
104.	LPT Blades: Stages 1-5.	189
105.	FPS Turbine Frame and Mixer.	193

LIST OF ILLUSTRATIONS (Continued)

<u>Figure</u>		<u>Page</u>
106.	Turbine Frame End View.	194
107.	Turbine Frame - Mixer Flow Field STC Analysis.	198
108.	E ³ Mixed-Flow Thrust Gains.	200
109.	FPS Engine.	202
110.	FPS Sumps and Drive System.	205
111.	FPS Forward Sumps.	206
112.	FPS No. 3 Bearing Spring/Damper Housing.	207
113.	FPS Aft Sump.	209
114.	FPS Rotor Thrust Summary.	210
115.	FPS Sump Labyrinth Seals - Typical.	212
116.	FPS Engine Side View.	214
117.	FPS Accessory Gearbox.	215
118.	FPS Accessory Drive System.	216
119.	E ³ Accessory Drive Gear Schematic.	217
120.	FPS Lube System.	218
121.	Full Authority Digital Control (FADEC).	221
122.	Control System Inputs.	223
123.	Control System Outputs.	224
124.	Hybrid Electronics.	226
125.	Fuel System.	227
126.	Fuel Heater/Regenerator Schematic.	228
127.	Compressor Stator Vane Control.	230
128.	Compressor Clearance Control System.	232

LIST OF ILLUSTRATIONS (Concluded)

<u>Figure</u>		<u>Page</u>
129.	Turbine Clearance-Control Systems.	233
130.	Nacelle General Arrangement.	238
131.	Front View, Reverser Cross Section.	239
132.	Side View of Reverser Translating Sleeve and Blocker Door.	240
133.	Thrust Reverser Actuation.	240
134.	Overall Engine Reverse Thrust Comparison.	242
135.	Engine Mount System.	244
136.	Mount Reactions Schematic.	245
137.	Preliminary E ³ Ovalization.	246
138.	Accessory Package.	249
139.	Accessory Package.	250

LIST OF TABLES

<u>Table</u>		<u>Page</u>
1.	FPS Engine Design Requirements.	15
2.	Typical Optimization Studies and Results.	17
3.	Aircraft Trade Derivatives Used in Studies.	17
4.	HPT Stage 1 Blade-Clearance Calculation.	22
5.	Preliminary Stability Assessment.	25
6.	Preliminary Material Cost Estimate/Flight Hour.	32
7.	Weight Comparison.	32
8.	FPS Cost Estimate.	34
9.	Maintenance Comparison (1977 Dollars).	34
10.	Comparison of Engine Performance Δ sfc % (Reference CF6-50 at Mx Cr).	35
11.	Comparison of Mission-Based Economic Benefits, Δ DOC and Δ Block Fuel (Based on Lockheed Trijet Performance).	35
12.	E ³ FPS Cycle Definition.	49
13.	FPS Cycle - Maximum Cruise Component Performance.	50
14.	E ³ FPS and CF6-50C Reference Engine Maximum Cruise sfc Comparison.	51
15.	E ³ Growth Capability.	53
16.	Growth Component Changes.	53
17.	Performance-Retention Features.	54
18.	Estimated In-Service Performance Losses.	55
19.	Bulk Absorber Treatment Development Highlights.	72
20.	Bulk Absorber Testing Experience.	72
21.	Acoustic Prediction Methodology.	77

LIST OF TABLES (Continued)

<u>Table</u>	<u>Page</u>
22. E ³ System Noise-Reduction Studies.	77
23. E ³ LPT Noise-Reduction Options.	78
24. Flight Noise Estimates for E ³ Advanced Aircraft.	81
25. Advanced Technology Features (Boeing).	88
26. Resulting Domestic Airplane Characteristics (Boeing).	89
27. McDonnell-Douglas Advanced Features.	90
28. McDonnell-Douglas Comparison of Characteristics.	91
29. Airframe Advanced Technologies (Lockheed).	92
30. Lockheed Study Parameters.	92
31. Economic Benefits, Block Fuel.	93
32. Airplane Pricing Functions.	95
33. Major Engine Input to DOC Analysis.	96
34. Economic Benefits, Direct Operating Cost (NASA-Coordinated Rules).	97
35. Summary of Alternate Fan Study.	111
36. FPS Fan Module Weight Summary.	115
37. Compressor Mechanical Design Criteria.	120
38. Compressor Radial Blade/Casing-Clearance Adders.	128
39. Compressor Weight Summary.	130
40. Broad Specification Fuels (BSF).	143
41. Summary of Heat Transfer Analysis.	147
42. Liner Maximum Temperature Predictions.	147
43. Predicted Liner Life.	147

LIST OF TABLES (Continued)

<u>Table</u>		<u>Page</u>
44.	E ³ Combustor - Emission Goals (EPA 1981 Standards for Newly Certified Engines).	151
45.	E ³ Combustor - Parts Life Goals.	151
46.	E ³ Combustor - Key Performance/Operating Requirements.	152
47.	E ³ Combustors - Aerodynamic Design Parameter Comparison.	154
48.	E ³ Double-Annular Combustion System Weight Estimate (Baseline Engine).	157
49.	High Pressure Turbine Major Technology Features.	158
50.	High Pressure Turbine FPS Goals.	159
51.	Estimated HPT Efficiency.	159
52.	HPT Energy Distribution	160
53.	HPT Aerodynamic Description.	160
54.	HPT Aerodynamic Design Requirements.	162
55.	HPT Weight Summary.	163
56.	HPT Stages 1 and 2 Blades and Vanes.	172
57.	HPT Active Clearance Control.	177
58.	HPT Stage 1 Disk - LCF Life with Mission Mix.	177
59.	Estimated LPT Efficiency.	181
60.	LPT Aerodynamic Description.	181
61.	Low Pressure Turbine FPS Goals.	181
62.	LPT Aerodynamic-Design Selection Study Made for ICLS.	187
63.	Low Pressure Turbine Stage 1 Vane.	190
64.	Low Pressure Turbine Stage 1 Blade.	190

LIST OF TABLES (Concluded)

<u>Table</u>		<u>Page</u>
65.	Low Pressure Turbine Acoustic Study: 156 Fourth-Stage Blades.	192
66.	Low Pressure Turbine Weight Summary.	192
67.	Direct Operating Cost and Maintainability Features.	196
68.	Turbine Frame Assembly Material Summary.	196
69.	Mixer Design Goals.	199
70.	Turbine Frame/Mixer Status Weight Summary.	199
71.	FPS Major Design Goals.	202
72.	FPS Comparison to Baseline (CF6-50).	203
73.	Major Areas of Study.	203
74.	FPS Main-Shaft Bearing Description.	211
75.	FPS Bearing Loads and Life.	211
76.	FPS Sump Labyrinth Seals.	211
77.	Accessory Gearbox Location Trade Study Results.	248
78.	Nonquantitative Factors in Accessory Package Selection.	248

LIST OF SYMBOLS AND ABBREVIATIONS

ACC	Active Clearance Control
A/F	Airframe
AGB	Accessory Gearbox
AMAC	Advanced, Multistage, Axial-Flow Compressor
APU	Auxiliary Power Unit
AR	Aspect Ratio
As-HIP	As Hot Isostatic Pressed
BPR	Bypass Ratio
B/U	Buildup
CD&I	Component Development and Integration
CDP	Compressor Discharge Pressure or Compressor Discharge Plane
D _{HL}	Highlight Diameter
D _{max}	Maximum Diameter
DN	Bearing Bore Diameter (mm) x Shaft rpm or (Fan Speed - Core Speed) (rpm)
DOC	Direct Operating Cost
DS	Directionally Solidified
DVM	Double Vacuum Melted
E	Modulus of Elasticity
E ³	Energy Efficient Engine
EAS	Equivalent Airspeed
ECCP	Experimental Clean Combustor
ECS	Environmental Control System
EPA	Environmental Protection Agency
EPNdB	Effective Perceived Noise in Decibels
EPNL	Effective Perceived Noise Level
ERBS	Experimental Referee Broad Specification
FADEC	Full Authority Digital Electronic Control
FAR	Federal Airworthiness Regulation
FBP	Final Boiling Point
F _n or F _n	Net Thrust

LIST OF SYMBOLS AND ABBREVIATIONS (Continued)

FOD	Foreign Object Damage
FPR	Fan Pressure Ratio
FPS	Flight Propulsion System
g	Acceleration of Gravity
G/B	Gearbox
h	Enthalpy
Hast X	Hastelloy X
HIP	Hot Isostatic Pressed
HP	High Pressure
HPC	High Pressure Compressor
HPT	High Pressure Turbine
HPX	High Pressure Compressor Stage No. "X"
IBP	Initial Boiling Point
ICA	Initial Cruise Altitude
ICLS	Integrated Core/Low Spool
I.D.	Inner Diameter
IGB	Inlet Gearbox
IGV	Inlet Guide Vane
Inco	Inconel
ITMA	Inlet Turbulence Modification Apparatus
j	Constant Equal to: 778 ft-lb/Btu
K	Spring Constant
K ₁	Constant Dependent on HPT Disk Bore Geometry, Range: 0.15 to 0.25
K ₂	Constant Dependent on HPT Disk Bore Ring Geometry
K\$	Kilodollars (\$1000)
l/c	Length/Chord
LCF	Low Cycle Fatigue
LP	Low Pressure
LPT	Low Pressure Turbine
L _t /D	Treated Length/Fan Diameter (Acoustic Parameter)
M	Mach Number

LIST OF SYMBOLS AND ABBREVIATIONS (Continued)

M&PTL	Materials and Processes Technology Laboratory
MEW	Manufacturers Empty Weight
MTOW	Maximum Takeoff Weight
M_x Cl	Maximum Climb Power
M_x Cr	Maximum Cruise Power
N	Rotational Speed
N_0	Speed Corrected to Standard Conditions
ODS	Oxide-Dispersion Strengthened
OEW	Operating Empty Weight
OGV	Outlet Guide Vane
O _{WE}	Operating Weight Empty
P	Pressure
PD&I	Preliminary Design and Integration
PDR	Preliminary Design Review
PM	Powder Metallurgy
P/P	Pressure Ratio
P_S	Static Pressure
P_T	Total Pressure
PTO	Power Takeoff
QCSEE	Quiet Clean Short-Haul Experimental Engine
R	Radius or Radial Dimension
rms	Root Mean Square
SAE	Society of Automotive Engineers
sfc	Specific Fuel Consumption
SLS	Sea Level Static
SLTO	Sea Level Takeoff
SN	SAE Smoke Number
SS	Steady State
S.S.	Stainless Steel
STC	Streamtube Curvature
STEDLEC	Study of Turbofan Engines Designed for Low Energy Consumption
Stg	Stage

LIST OF SYMBOLS AND ABBREVIATIONS (Continued)

T	Temperature
TBC	Thermal-Barrier Coating
t/c	Thickness/Chord
TCS	Turbulence-Control Structure
TGB	Transfer Gearbox
T/O	Takeoff
TOGW	Takeoff Gross Weight
T/R	Thrust Reverser
U	Velocity
UHC	Unburned Hydrocarbons
USTEDLEC	Unconventional STEDLEC
V/B	Number of Vanes/Number of Blades
VSCF	Variable-Speed/Constant-Frequency (Generator)
VSV	Variable Stator Vane
W	Airflow or Gas Flow
W _{af}	Weight of Airframe
W/O	Without
α	Coefficient of Thermal Expansion
δ	Deflection
Δ	Prefix Indicating a Differential Increment
η	Efficiency
σ	Stress
σ_{eff}	Effective Stress: $\sqrt{\sigma_1^2 - \sigma_1 \sigma_2 + \sigma_2^2}$
σ_1	Hoop Stress
σ_2	$-K_1 \sigma_1 - E \alpha (\Delta T/2) K_2$
ψ	Loading

Subscripts

0	Free Stream or Ambient
1	Fan Hub
2	Core Hub
3	Combustor Discharge

LIST OF SYMBOLS AND ABBREVIATIONS (Concluded)

4.1	HPT Inlet
12	Fan Inlet (at Tip)
25	Compressor Inlet
49	LPT Inlet
b	Bending
B	Blade
C	Coolant; or Centrifugal
eff	Effective
f	Fuel
g	Gas
P	Pitch Line
R	Radial
S	Static
T	Total
θ	Tangential; or Corrected to Standard Conditions

1.0 SUMMARY

The Energy Efficient Engine (E³) Project is being conducted as part of the NASA Aircraft Energy Efficiency (ACEE) Program. An objective of this project is to develop the technology base for a new generation of fuel-efficient propulsion systems for future subsonic commercial-transport aircraft.

This report contains the results of the preliminary analysis and design of an advanced Flight Propulsion System (FPS) done by the General Electric Company. The advanced FPS would be more fuel efficient than current commercial turbofans while at the same time, being more attractive economically and environmentally. This preliminary analysis and design was performed to more fully define and verify the system characteristics of an FPS that could be introduced into commercial service in the late 1980's to early 1990's. Preliminary analysis and design also established the technology needs and provided the basis for the design of component development hardware and the integration effort to follow in the E³ project.

In the report, all aspects of the FPS are addressed including component design, engine system integration (including nacelle), and aircraft integration results. Results of the FPS preliminary design indicate that all of the NASA E³ Project goals, with the possible exception of the emission goal for nitrous oxides (NO_x), should be met or exceeded.

The following is a comparison of the original NASA E³ goals with the current FPS status.

<u>FPS Characteristic</u>	<u>NASA Goal</u>	<u>FPS Status</u>
● Installed Specific Fuel Consumption (sfc)	Minimum 12% Reduction from CF6-50C*	14.2% Reduction
● Direct Operating Cost (DOC)	Minimum 5% Reduction from CF6-50C on equivalent aircraft	5 to 11.6% Reduction depending on mission and aircraft
● Noise	Meet FAR36 (1978) Provision for Growth	Meets with Margin
● Emissions	Meet EPA Proposed 1981 Standards	Meets with Margin except for NO _x
● Performance Retention	Minimum 50% Reduction from CF6-50C Levels	Projected to Meet

An illustration of the installed FPS is given in Figure 1.

*Measured at maximum cruise thrust at M = 0.8, 10,668 m (35,000 ft).

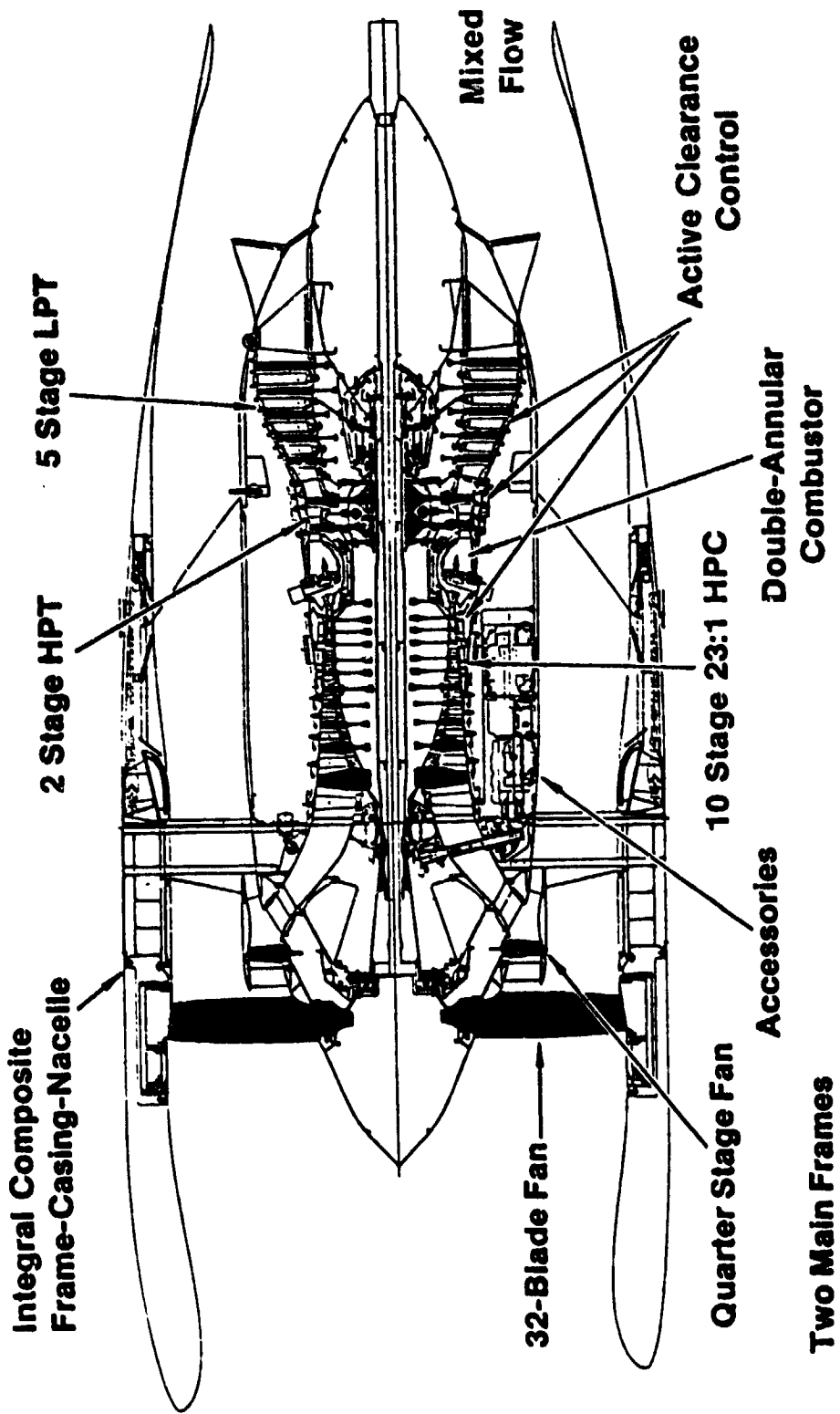


Figure 1. FPS Features.

The FPS incorporates a long-duct nacelle composed primarily of advanced composite construction with extensive use of acoustic absorbers on the inner surface. The wide-chord, titanium, 32-blade fan features a lowered midspan shroud and low tip speed to enhance efficiency and reduce noise. A quarter-stage booster provides additional core supercharging and centrifuges foreign objects from the core air to help prevent foreign object damage (FOD). A moderately loaded, five-stage, low pressure turbine drives the fan and booster. Selective aerodynamic loading and stage blade number are used to reduce low pressure turbine noise. A mixer is used to mix the hot core-exhaust gas with the cooler fan air to improve the sfc of the engine and reduce exhaust noise. The mixer also spoils core thrust in the reverse mode - allowing the weight and cost of a core reverser to be eliminated from the installed FPS.

An active clearance-control system is employed on the aft portion of the High Pressure Compressor (HPC), the High Pressure Turbine (HPT), and the Low Pressure Turbine (LPT). Active clearance control enables minimum clearances to be maintained and permits larger clearances during transients when current engines would ordinarily experience performance-deteriorating tip wear.

A 10-stage, highly loaded, high pressure compressor is driven by a two-stage turbine. The compressor produces a 23:1 pressure ratio at the maximum-climb-power design point. The combustor is a double-annular design with two combustion zones to reduce emissions for all power settings. A shingled liner design is utilized in the combustor for longer life and reduced maintenance cost. Accessories are driven by a core-mounted accessory gearbox. Core mounting reduces nacelle frontal area and consequent aerodynamic drag. Two main frames with special mounting designs are utilized to minimize engine cas. distortion and consequent blade-tip and seal wear.

Some of the cycle/performance characteristics of the E³ are given below:

Overall Pressure Ratio, Max. Climb	38
Bypass Ratio, Max. Climb	6.8
Fan Pressure Ratio, Max. Climb	1.65
Turbine Inlet Temperature, ° C (~ F)	
Takeoff, 30° C (86° F) Day	1343 (2450)
Altitude, Max. Cruise, Std. Day	1188 (2170)
Max. Cruise sfc, Std. Day, kg/N-hr (lbm/lbf-hr)	
Uninstalled	0.0553 (0.542)
Installed	0.0583 (0.571)
Max. Cruise Δsfc (Relative to CF6-50C), % (Isolated Installed Nacelle Drag)	-14.2

In the design size, the following system characteristics have been estimated for the E³:

Takeoff Thrust, kN (lbf)	162.36 (36,500)
Weight, kg (lbm)	
Uninstalled Engine	3,288 (7,250)
Installed Engine	4,082 (9,000)
Cost, K\$ (1977 Dollars)	
Uninstalled Engine	1,955
Installed Engine	2,533
Maintenance Cost, \$/Flight-Hour (1977 Dollars) Bare Engine and Thrust Reverser	66.25

These results were supplied to three aircraft company subcontractors (The Boeing Company, McDonnell Douglas Corporation, and the Lockheed-California Company) for use in the aircraft-integration portion of the study. Each subcontractor evaluated the projected FPS installed on appropriate advanced-transport designs and compared the results against a properly scaled CF6-50C installed on a transport of the same advanced technology. The results project block fuel savings of from 15 to 23% and reductions in Direct Operating Costs (DOC) of from 5 to 12% depending upon the aircraft and mission studied. These results clearly indicate that the major goals set by NASA for the Energy Efficient Engine Project should be met with this engine configuration.

2.0 INTRODUCTION

The NASA Energy Efficient Engine (E³) Component Development and Integration Project under contract NAS3-20643 with the General Electric Company was initiated January 2, 1978. The initial-study concepts for the current engine program were largely derived from a previous NASA-sponsored study (NAS3-20627) "E³ Preliminary Design and Integration Studies" (Reference 1). In addition, several of the advanced material, cycle, and configuration concepts came from other earlier NASA-sponsored studies (References 2, 3, 4, and 5).

The objective of the E³ program is the development of technology to improve the energy efficiency of propulsion systems for subsonic commercial aircraft of the late 1980's and early 1990's. The need for the development of more fuel-efficient engines has become apparent in view of the expected continuing shortage of petroleum-based fuels. The E³ Project is a major element of the NASA Aircraft Energy Efficiency (ACEE) Program.

The following technical goals were established for the fully developed FPS by NASA:

- Fuel Consumption - Minimum 12% reduction in installed sfc compared to a CF6-50C at maximum cruise thrust, M = 0.8 at 10,668 m (35,000 ft) altitude on a standard day.
- Noise - Comply with FAR36 (1978) with provisions for growth.
- Emissions - Comply with EPA (1981) Standards for new engines.
- Performance Retention - A 50% reduction in the rate of performance deterioration in service as compared to the CF6-50C.

To meet and demonstrate the NASA Aircraft Project goals, the E³ Project has four major technical tasks structured as follows: Task 1 addresses the design and evaluation of the E³ Flight Propulsion System (FPS); this is the propulsion system designed to meet the requirements for commercial service and includes a flight nacelle. The Task 1 results establish the requirements for the experimental test hardware including the components, core, and integrated core/low-spool. Task 2 consists of the design, fabrication, and testing of the components and includes supporting technology efforts. These supporting technology efforts are performed where required to provide verification of advanced concepts included in the propulsion system design. In addition, more advanced technologies, not specifically included in the propulsion system design (but which provide the potential for further performance improvements), are also explored. Task 3 involves the design, fabrication, and test evaluation of a core engine consisting of the compressor, combustor, and high

pressure turbine. Integration of the core with the low-spool components and test evaluation of the integrated core/low spool (ICLS) comprise Task 4. At the conclusion of the program, the latest performance of the experimental hardware (integrated core/low-spool and parallel core and component efforts) will be factored into a final propulsion system/aircraft evaluation (as part of continual ongoing evaluations in Task 1) to determine achievable performance as compared to the program goals.

The status of the preliminary analysis and designs of the Task 1 Flight Propulsion System as of November 1978 is presented in this report. Section 3 describes the design and performance of the Flight Propulsion System, as currently envisioned, and Section 4 describes the preliminary design of each of the major components in the engine. These designs will be modified during the remainder of the E³ Project as more information is gained from the experimental technology efforts.

3.0 FLIGHT PROPULSION SYSTEM PRELIMINARY DESIGN AND PERFORMANCE

3.1 FLIGHT PROPULSION SYSTEM (FPS) DESIGN

3.1.1 FPS Features

The uninstalled FPS, shown in Figure 2, has many advanced design features. A wide-chord, 32-blade fan with lowered shroud is utilized to obtain good climb and cruise performance while retaining the FOD resistance needed for ground operation and low level flight. Containment is accomplished by means of a hybrid system, steel and Kevlar, to enhance safety while reducing weight relative to current armor-steel systems. By integrating the fan case structurally with the composite fan frame, case stiffness and roundness control is improved, and thus reduced fan-tip-to-case clearance is permitted.

A quarter-stage booster has been employed to increase the core supercharge so that the overall pressure ratio of 38:1 at the maximum climb design point can be achieved. The configuration tends to centrifuge foreign objects into the fan dust and away from the core inlet. It also permits flow-matching of the booster and the core compressor to be achieved through varying operating conditions with no variable-bypass-flow devices such as valves or bypass doors.

The 10-stage compressor is an aerodynamically advanced feature of the FPS. Through high tip speed and the low-aspect-ratio blading, a 23:1 compression ratio is developed at the maximum climb design point. This permits the use of a short, stiff, core configuration with two main frames and only two core engine bearings. The compressor has four variable-vane stages and a variable Inlet Guide Vane (IGV). In addition, a seventh-stage-bleed system is used during subidle operation to improve the available stall margin. To reduce operating tip clearances, fifth-stage air is modulated such that the aft inner compressor casing is cooled at appropriate times. Besides reducing tip clearance at climb and cruise, the active clearance control is able to open clearances during periods of large potential engine deflections such that inadvertent rubs that contribute to performance deterioration are prevented.

A double-annular combustor has been employed to reduce emissions both at low power and high power. Proper fuel/air mixtures are maintained by burning in the primary annulus only at low power and switching to both annuli during higher power operation. A shingled liner design has been employed to achieve long combustor life and, thus, to reduce maintenance costs in a traditionally very high-cost section of the engine.

Two high-tip-speed turbine stages provide power for the core compressor. High efficiency is attained by maintaining a low level of work loading, by advanced aerodynamics design, and by the use of active clearance control based on fan-air cooling of the casing. Cooling-air needs have been reduced by using directionally solidified, higher temperature alloys in the first- and second-stage blades and the second-stage vane. The cooling-air circuit has

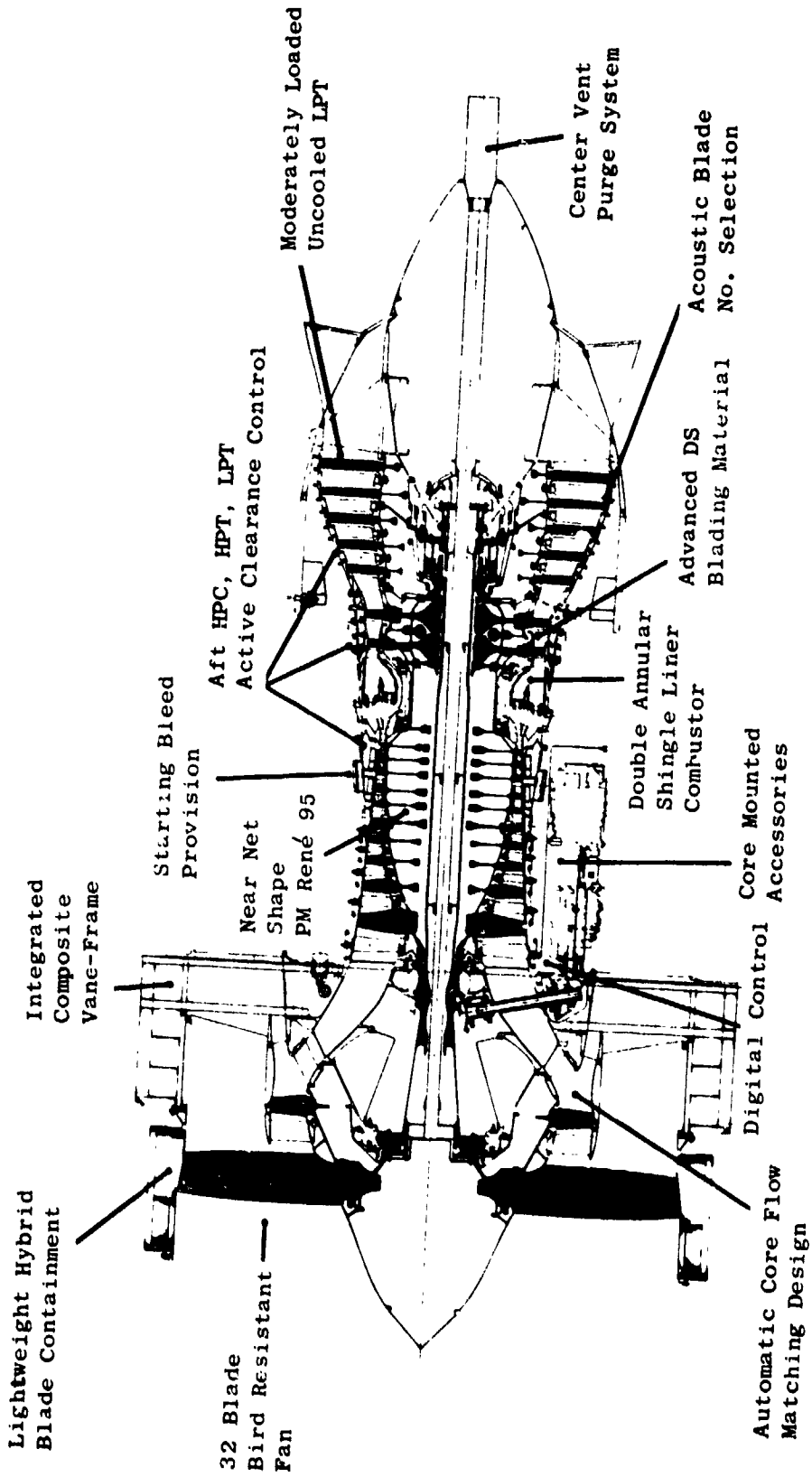


Figure 2. Uninstalled FPS Features.

been designed to take cooler, pitch-line air from the compressor exit and accelerate it to the rotational velocity of the core shaft. This causes minimum losses and allows the shafting to be covered by the coolest possible air. The cooling air is then pumped up to the required blade-cooling pressure by a side-plate compressor on the front of the first-stage disk. Both turbine disks are constructed of powdered René 95 compacted into a near-net shape, to reduce the usage of powder, before machining. This results in a reduction in the cost of the disks. Both turbine disks are designed with no bolt holes through the main load-carrying portion of the disk; this feature helps to achieve the long design-life goals.

The fan and quarter-stage are driven by a five-stage LPT of moderate aerodynamic loading. A short transition duct is used between the HPT and LPT to permit higher blade velocities for the initial stages. This permits a lower overall average loading and (coupled with advanced aerodynamic design, active clearance control, and careful flowpath construction) results in a high level of turbine efficiency.

Core exhaust gases pass into a mixer that collects the flow and injects it into the cooler fan-air stream to mix before expansion through the mixed-flow exhaust nozzle. The configuration of the mixer has been chosen to allow the greatest possible mixing while keeping core and fan stream pressure losses as low as possible.

The following tabulation is a summary of the major operating cycle parameters achieved by the uninstalled engine.

<u>Parameter</u>	<u>Takeoff</u>	<u>Max. Climb</u>	<u>Max. Cruise</u>
Bypass Ratio	7.3	6.8	6.9
Fan Pressure Ratio	1.5	1.65	1.61
Compressor Pressure Ratio	20.0	23.0	22.6
Overall Pressure Ratio	29.7	37.7	36.1
Turbine Inlet Temp ° C (° F)	1343 (2450)	1282 (2340)	1244 (2272)
Uninstalled sfc (standard day)	0.294	0.546	0.542

The maximum cruise performance was achieved with the following FPS component performance goals. The status levels are given with the changes that have occurred since the initial-study FPS.

<u>Component</u>	<u>Status Performance</u>	<u>Δ From Initial Study</u>
Fan Bypass η	0.887	+0.005
Fan Hub η	0.892	
Compressor η	0.861	-0.001
Combustor η	0.995	
HPT η	0.924	-0.001
LPT η	0.917	
Mixing Effectiveness (%)	75	+10

Although the FPS thrust level is scalable, the design-size thrust at takeoff was set at 40.2 kN (36,500 lbf). This thrust size was selected to be representative of a likely thrust requirement for the type of subsonic transport aircraft envisioned for the 1990's.

Control of the FPS would be through a Full Authority Digital Electronic Control (FADEC) that would accurately provide all current-generation engine-control functions plus others such as active clearance control. The control will be described more fully in Section 4.8.

Core-mounted accessories have been chosen for the FPS primarily to avoid the nacelle "bump" that occurs when fan-core-mounted accessories are used. This choice allows a slender nacelle and thus reduced nacelle drag. In the initial study FPS the accessories were located in the pylon, but maintenance considerations resulted in the selection of the core-mounted locations. As shown in Figure 2, the accessories are isolated from the core engine by a thermal-isolation compartment. By providing a thermal barrier and separate cooling air, reliability and safety are both enhanced.

Installation features of the FPS are shown in Figure 3. Extensive use of composites has been assumed for the nacelle to reduce both weight and installed cost. The nacelle is slender, relative to current practice, with a highlight diameter (diameter of inlet lip) to maximum nacelle diameter ratio of 0.86. This results from the use of core-mounted accessories and a more efficient (thinner) integrated engine frame and nacelle. A slender nacelle provides the benefit of relatively low installed drag. The long-duct, mixed-flow configuration also enhances installed performance with the thermodynamic benefit of mixing.

The mixer also eliminates the need for a core thrust reverser since deployment of the fan-stream thrust reverser results in a sudden core-jet expansion and consequent core-thrust spoiling. The feature permits a considerable weight and cost reduction over current engines which require core-thrust spoilers.

Acoustic suppression is provided by a combination of suppression material and design configuration. Advanced Kevlar bulk absorbers are utilized throughout the cooler portions of the installation such as the inlet and fan-duct regions. Turbine acoustic treatment is provided by a similar high temperature bulk absorber. Source noise is reduced by such features as increased fan-blade-to-vane spacing and selection of appropriate numbers of turbine blades. The mixed-flow design also results in reduced jet-exhaust noise. This will be covered in more detail in Section 3.4.

Freedom of the compression portion of the engine from FOD has been enhanced by the use of the quarter-stage configuration. A significant portion of outer booster air (about 40%) is bled into the fan duct; thus, the air most likely to have dust particles bypasses the core compressor. In addition, the long-chord fan will be more resistant to accidental damage from rocks or birds.

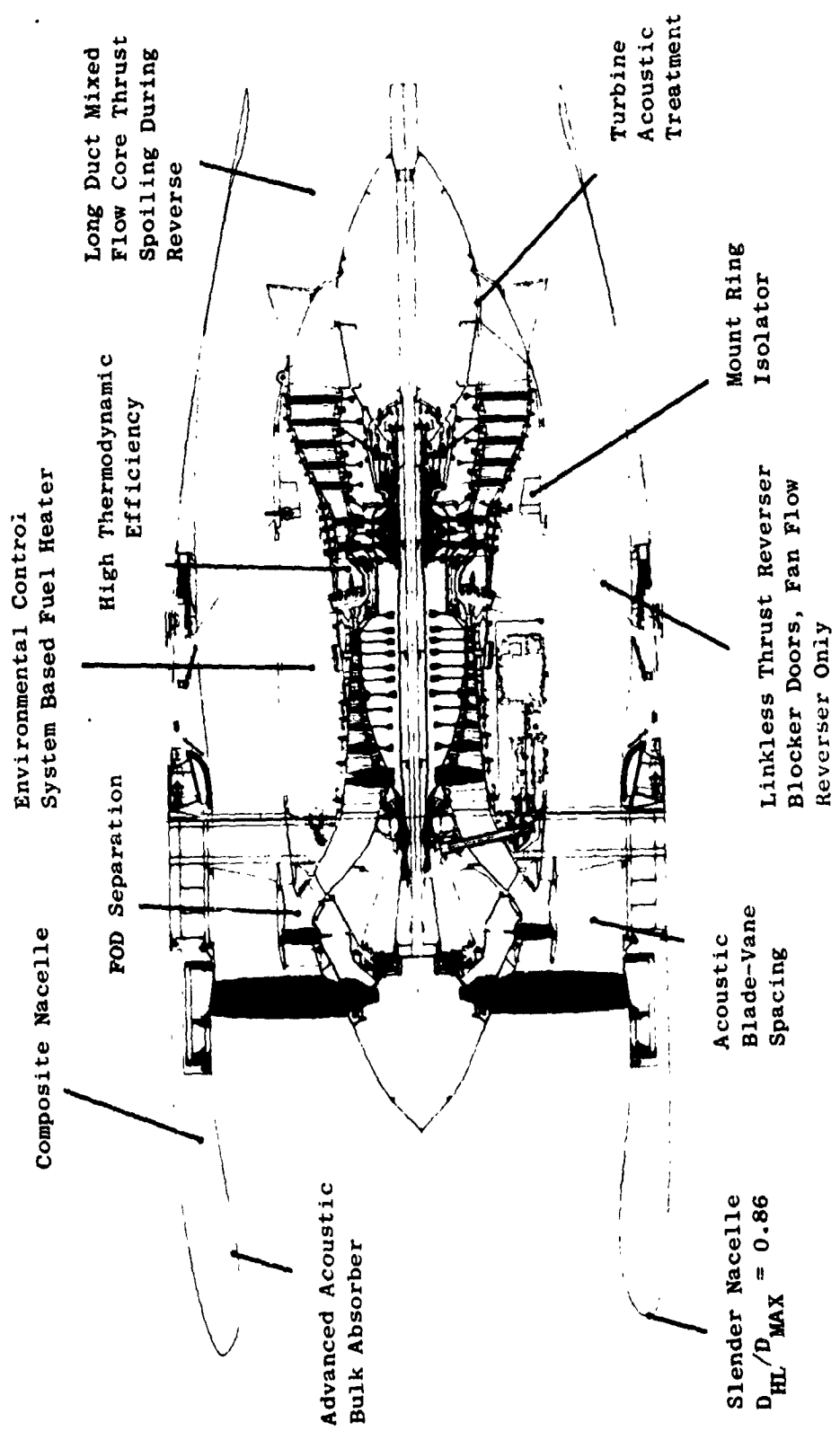


Figure 3. Installed FPS Features.

Another advanced feature of the installed FPS is the proposed use of customer Environmental Control System (ECS) air as an integral part of the engine thermodynamics. This system, which will be more fully described in Section 4.8, makes use of the waste heat of the ECS air by reinjecting it into the engine in the form of heated fuel. The proposed system also has the potential of eliminating current ECS fan-air coolers and fuel anti-icing heaters.

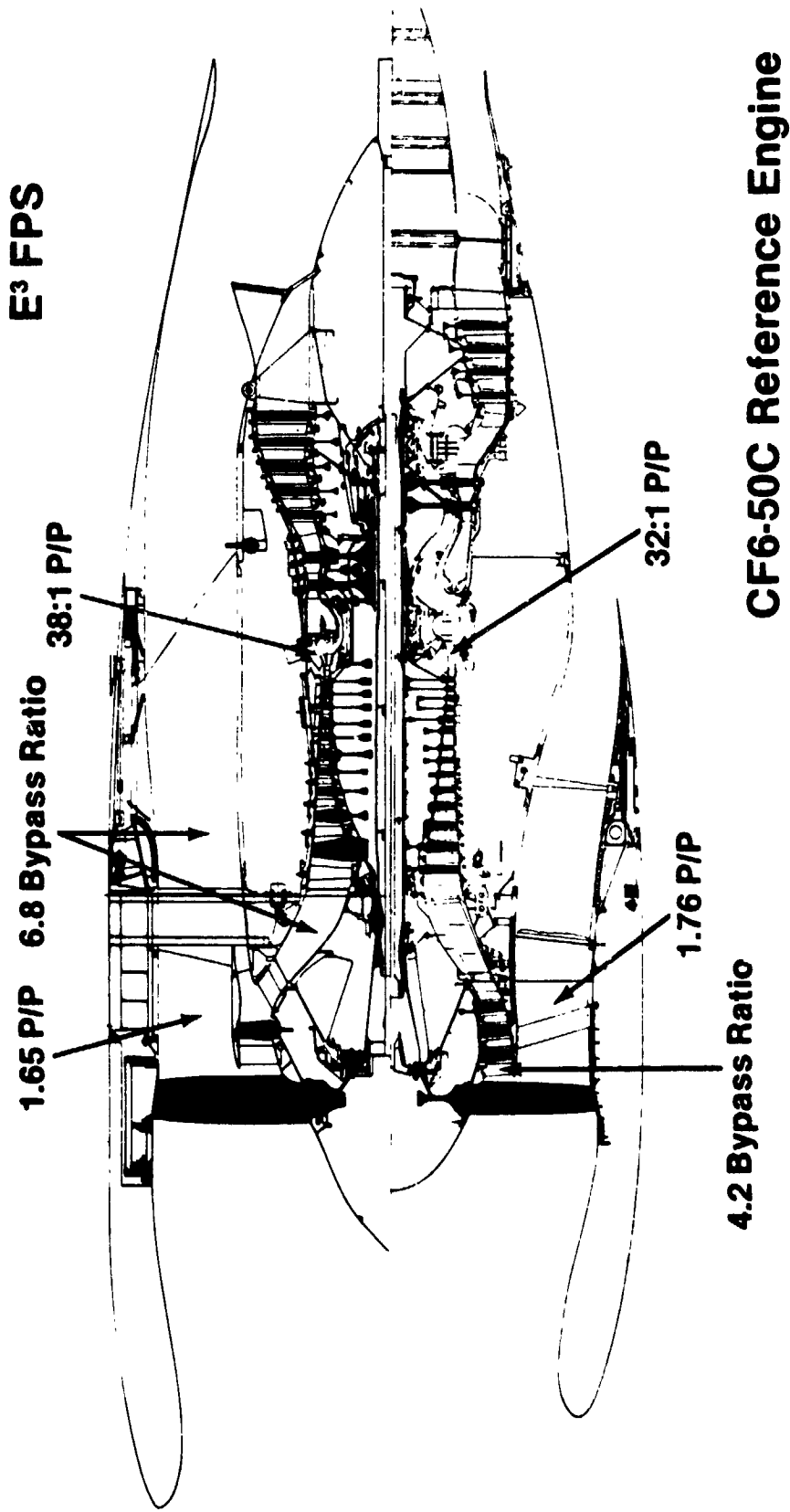
To determine if the FPS was meeting the benefit goals established by NASA, the CF6-50C was used as a baseline comparison engine. When used by the airframe subcontractors to evaluate the differences, both the installed FPS and the CF6-50C were scaled to proper thrust sizes and analytically installed on the equivalent advanced-technology aircraft. Figure 4 compares the status installed FPS with an installed CF6-50C. In this case, both engines have been scaled to provide equivalent maximum climb thrust at 10,668 m (35,000 ft) altitude at $M = 0.8$.

A comparison of the major cycle parameters of the FPS and the baseline CF6-50C is given in Figure 4. The major difference between the two engine cycles is the reduced specific thrust of the FPS as reflected in the differences in fan size, fan pressure ratio, and fan bypass ratio. This produces increased propulsive efficiency. Thermodynamic engine efficiency has been improved through use of more efficient components, a higher overall engine pressure ratio, a significantly higher cruise turbine-inlet temperature, and the mixed exhaust flow. On a comparable basis, a fully installed cruise sfc reduction of 14.6% has been projected for a fully developed FPS over the referenced CF6-50C engine (including the effects of customer bleed and power extraction).

Figure 5 illustrates what the engine would look like hung from the pylon with some of the required piping exposed. Use is made of the mounting ring to conduct air around the engine to the starter. Mounting of the engine is at three axial locations. The forward point takes thrust, side, and vertical loads; the middle mount point supplies roll reaction only, while the aft mount point takes vertical and side loads. The mount is essentially nonredundant under normal flight loads. This mount arrangement has been analyzed in a preliminary manner and results in low levels of casing ovalization and bending. Analyses of this and other mount configurations are continuing to determine the optimum configuration for the FPS.

3.1.2 Design Requirements

The design of the FPS has been conducted in accordance with General Electric's commercial engine practices. In some areas, the design requirements have been revised in response to General Electric commercial engine field experience. In particular, longer life is required in the combustor and turbine hot section in order to reduce maintenance expenditures. Table 1 presents the principal mechanical design requirements. These are consistent with the weight and maintenance estimates used for the FPS economic evaluations.



For Equivalent Max. Climb Thrust

Figure 4. Engine Cycle Comparison.

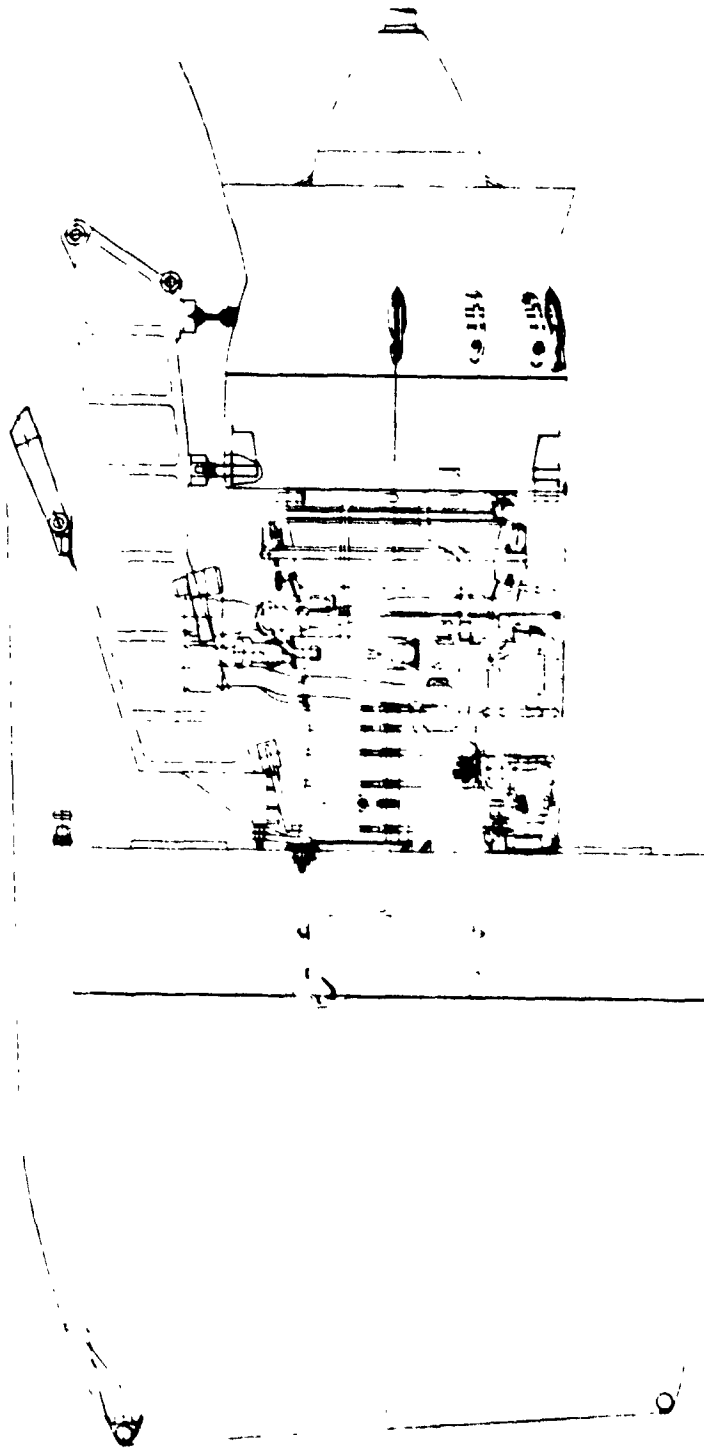


Figure 5. Installed Engine Piping and Mount Details.

Table 1. FPS Engine Design Requirements.

Parameter	Requirement
Life	36,000 hours
Cyclic Life	36,000 flight cycles - cold parts 18,000 flight cycles - hot parts
Cost	Competitive with current engines
Deterioration	Half the rate of current high bypass engines
Safety	Complies with all FAA requirements
Maintainability	On-condition with modularized construction Repair allowance (such as thickened flanges to allow flatness and bolt-hole rework)

The growth requirements for the FPS were accommodated in the following manner. Provisions were made for anticipated growth in the rotor and stator structures; however, the materials, cooling, and aerodynamic designs were optimized for the FPS size and cycle. When evaluating FPS weight and cost, all provisions for growth (e.g., extra rotor and stator structural weight) are subtracted.

3.1.3 Design Studies and Results

Many changes have been made in the FPS design and configuration since contract initiation. Figure 6 shows the initial FPS cross section over the current FPS cross section.

Table 2 is a listing of some of the more important studies and design changes. A more efficient, 32-blade fan has replaced the original 38-blade design, and the regeneration heat source for the heated-fuel system has changed from the seventh-stage compressor air to the more system-efficient ECS air. Active clearance control has been expanded forward two stages in the compressor and aft into the LPT, and the HPT clearance-control air system has been changed from a variable convection system to an external fan-air-impingement arrangement.

Design life considerations led to the selection of a shingle-liner combustor over the original, one-piece, film- and impingement-cooled liner. The accessory location was changed from the original pylon mount to a core mount due to considerations of maintenance ease and a general preference for a non-pylon arrangement by aircraft and airline companies.

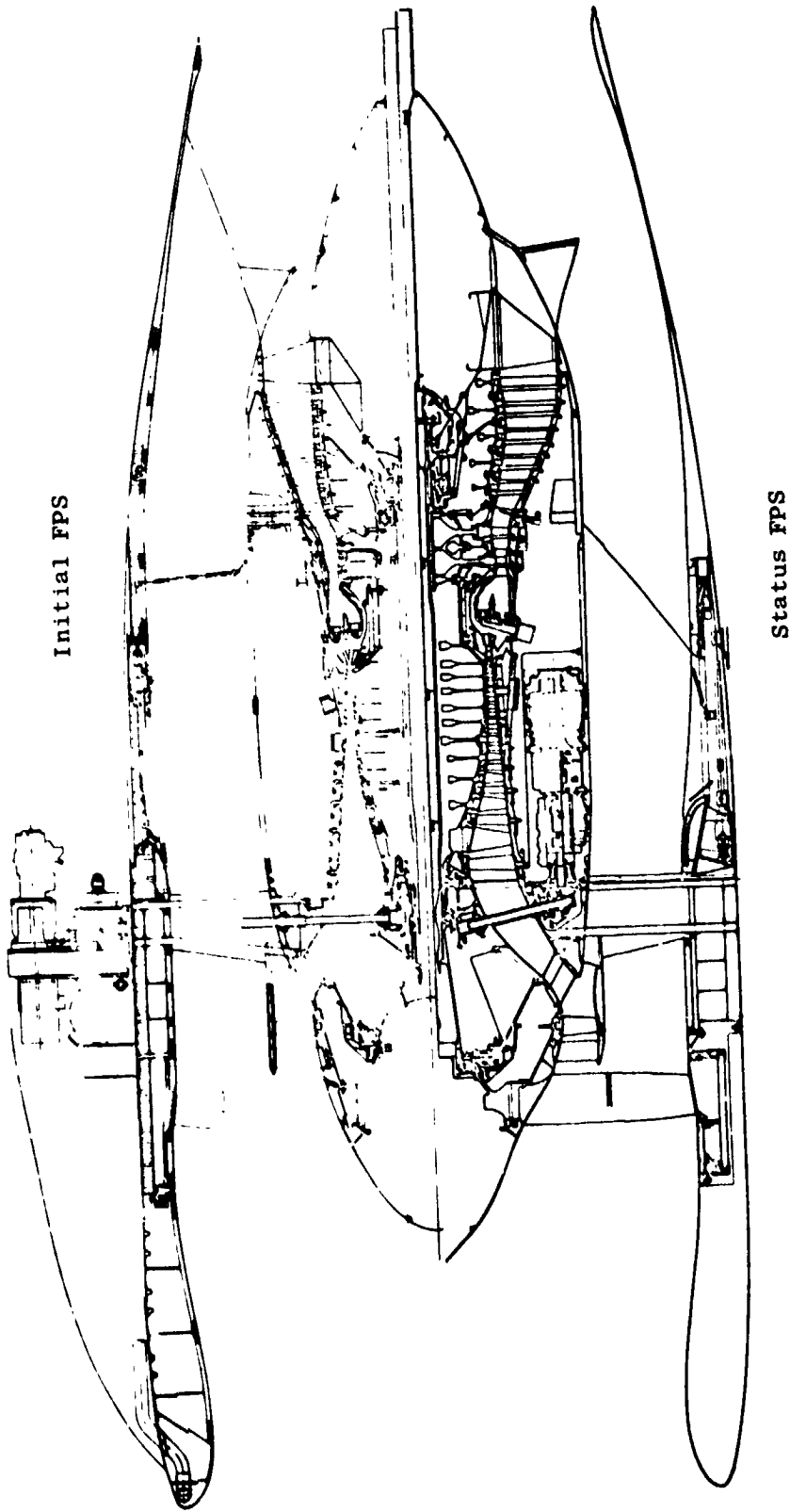


Figure 6. FPS Comparison.

Table 2. Typical Optimization Studies and Results.

Area of Study	Results	Section
LPT Staging	Current 5-Stage LPT Retained as Optimum	4.5.5
Alternate Fan Configuration	32-Blade, Low-Shroud Design Adopted	4.1.2
Fuel Heater Studies	New ECS Based System Adopted	4.8.8
Accessory Gearbox Location	Core-Mounted System Selected	4.9.3
Clearance Control Studies	Fan-Air Control Selected for HPT, LPT	4.2.2
Combustor Liner Studies	Shingle Liner Design Selected for Long Life	4.3.4
Dirt Separation Studies	50-60% Separation Efficiency Predicted	4.1.1
Thrust Mount System	Forward Links and Spread Vertical-Pickup Links Adopted	4.9.2

Table 3. Aircraft Trade Derivatives Used in Studies.

$F_n = 162,352 \text{ N (36,500 lbf)}$ SLTO, Domestic Mission 1,296 km (700 mi),
Average Cost of Fuel = 9¢/liter (35¢/gal)

- For Constant Fuel Burned (W_f)
1% sfc = 1.3% W_f = 340.2 kg (750 lbm)
- For constant Direct Operating Cost (DOC)
1% sfc = 0.5% DOC = 181.4 kg (400 lbm) =
\$4.34/hr Maintenance Cost = K\$155.5 Price
- For Constant Takeoff Gross Weight (TOGW)
1% sfc = 0.6% TOGW = 122.5 kg (270 lbm)

While performing these and other trade studies, a set of aircraft trade derivatives was used to evaluate the effect of possible design changes. These are shown in Table 3 and were the derivatives developed in the previous NASA-sponsored Energy Efficient Engine studies (Reference 1).

3.1.4 Active Clearance Control

Extensive use of an active clearance-control (ACC) system has been made on the FPS in order to improve efficiency and delay engine deterioration due to inadvertent rubs. Although each component has a somewhat different ACC configuration, they all depend on controlled cooling of the casing structure to modify running clearances. Figures 7 and 8 illustrate schematically the configuration and operation of the FPS ACC systems.

Figure 9 shows the effect on tip-clearance behavior of ACC for a typical stage. Without an ACC system, the tip-clearance operating line is shown as the upper, uncooled-stator, steady-state tip clearance. This operating line usually results from a worst-case interference situation, depicted by the dotted line. Generally, it is not desirable to operate with tip clearances of less than a minimum operating clearance that is determined by operating conditions such as maneuver loads or stage buildup tolerances. With an ACC system, it is possible to operate along the cooled-stator tip-clearance line. This produces an excess-clearance situation (more than the minimum operating clearance) for just a small, low-power portion of the engine operating regime. For all the more significant operating regions, a minimum operating clearance can be obtained and held for maximum efficiency.

By selectively cooling or not cooling the casing, transient clearance mismatch is avoided by temporarily opening up the tip clearances to the upper uncooled-clearance operating line. After the transient condition is past, the clearance can be pulled back down to the cooled-stator levels to avoid accidental rubbing and the resulting performance deterioration.

Attainable clearance levels were determined analytically by taking the engine through a simulated flight with very severe transient conditions imposed. The mission profile used is shown in Figure 10; it begins with stabilized idle and continues through a thrust increase to sea level takeoff (SLTO) power and then climb, cruise, descent, etc.

By analytically evaluating the required clearance that results from the worst-case mismatch and the other operating factors that determine clearance, a set of minimum achievable tip clearances at cruise power for selected stages was developed. An example of how this was accomplished for Stage 1 of the HPT is given in Table 4 where a breakdown of the clearance effects for the operating conditions at cruise and the resulting minimum required clearance are presented. In Table 4, the clearance effects due to g loads, vibrations, tolerance stack, and rub allowance are summed in both vertical and horizontal planes. The most extreme amount, -0.254 mm (-0.010 in.) occurs in the horizontal plane and sets minimum clearance for cruise. During takeoff, an additional ovalization term must be included. This makes the most extreme amount -0.483 mm (-0.019 in.) and sets minimum clearance for takeoff which is larger than the clearance required for cruise. Fortunately, the ACC system permitted the additional clearance at takeoff and then was able to reduce the HPT Stage 1 clearance to the minimum required cruise clearance.

OPERATION

- Modulating Valve Varies Proportion of Case-Cooling and Bypass Air
- Minimum Clearance is Maintained at Cruise/Climb
- Full-Authority Digital Electronic Control
- Cooling/Heating Occur at Proper Times During Accel and Decel to Minimize Buildup and Running Clearances

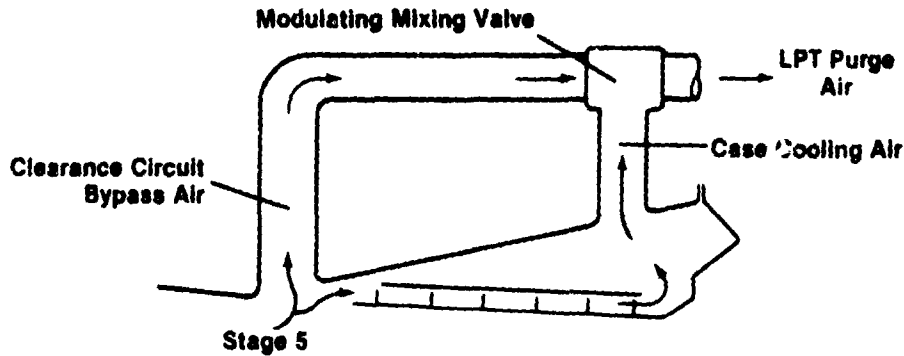


Figure 7. High Pressure Compressor ACC System.

OPERATION

- Separate Fan-Air-Modulating Valves (2) for HPT and LPT
- Some Opening of Clearance at Sea Level Takeoff
- Full-Authority Digital Electronic Control

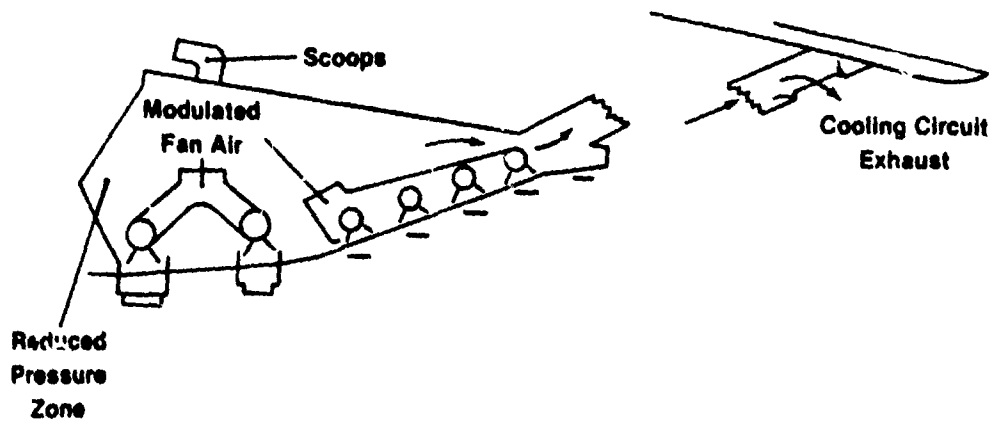


Figure 8. High/Low Pressure Turbine ACC System.

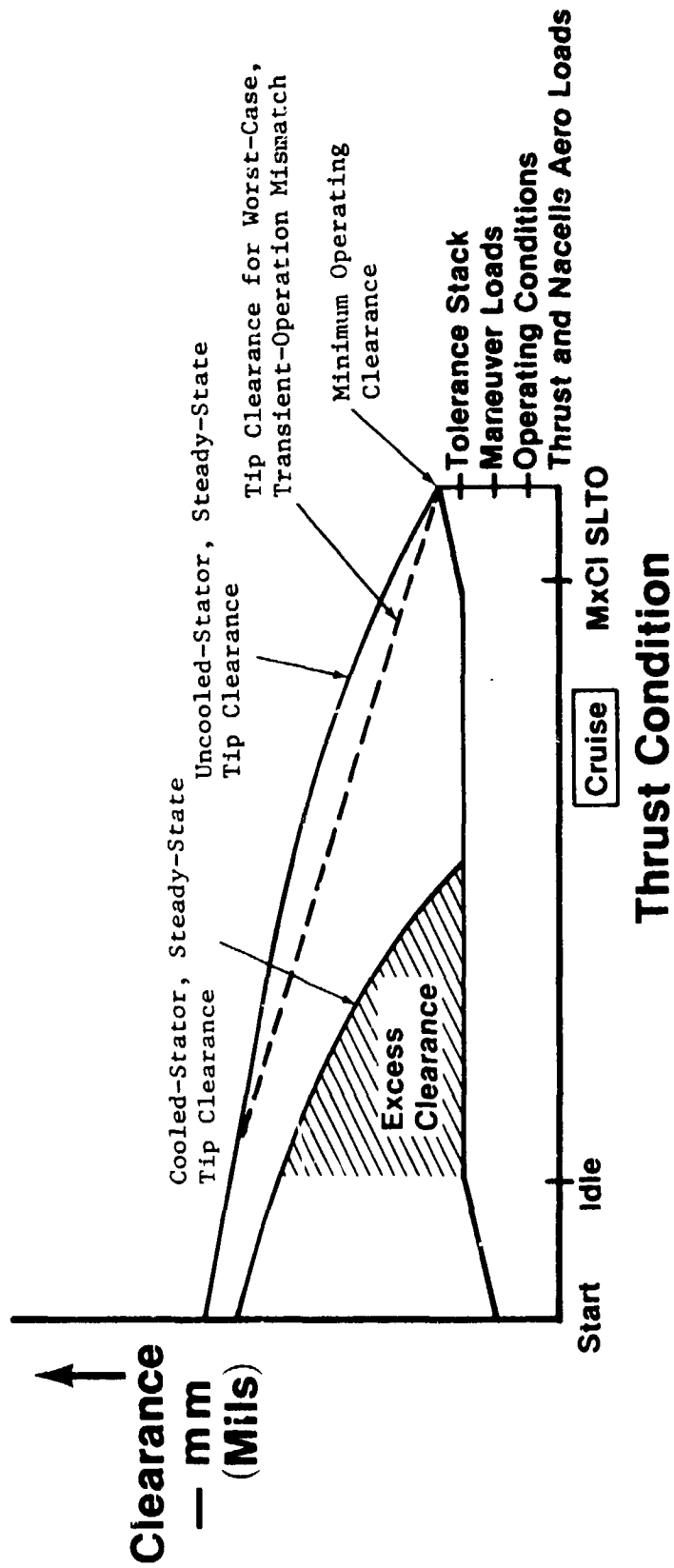
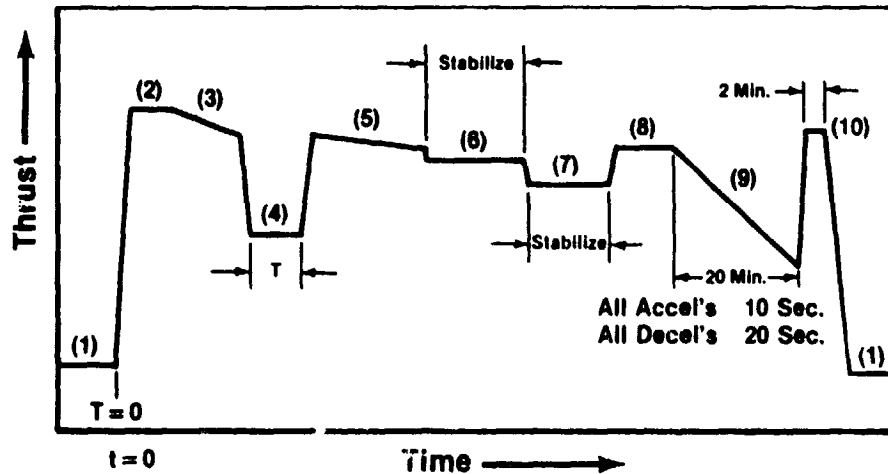


Figure 9. Typical Tip Clearance Behavior.



- | | |
|---------------------|--------------------------|
| (1) Stabilized Idle | (6) Max. Cruise |
| (2) SLTO Power | (7) 60% Cruise |
| (3) Max. Climb | (8) Max. Climb |
| (4) Flight Idle | (9) Flight Idle/Approach |
| (5) Max. Climb | (10) Thrust Reverse |

Figure 10. Typical Mission Profile.

Table 4. HPT Stage 1 Blade-Clearance Calculation.

Clearance Effect*	Vertical ΔR mm (in.)	Horizontal ΔR mm (in.)
g Loads	-0.127 (-0.005)	-0.127 (-0.005)
Vibration, 381 g-cm (150 g-in.)	-0.025 (-0.001)	-0.025 (-0.001)
Maneuver (Yaw, Pitch)	-0.076 (-0.003)	-0.102 (-0.004)
Tolerance Stack (rms)	±0.102 (+0.004)	±0.102 (±0.004)
Rub Allowance (High Blade/Shroud)	+0.102 (+0.004)	+0.102 (+0.004)
Total for Cruise	-0.024 (-0.001) -0.228 (-0.009)	-0.050 (-0.002) <u>-0.254 (-0.010)</u>
Required Cruise Clearance	+0.254 (+0.010)	+0.254 (+0.010)
Ovalization (SLTO Thrust/Airloads)	+0.178 (+0.007)	-0.229 (-0.009)
Total for SLTO	+0.154 (+0.006) -0.050 (-0.002)	-0.279 (-0.011) <u>-0.483 (-0.019)</u>
Required SLTO Clearance	+0.483 (+0.019)	+0.483 (+0.019)
*Positive (opening) clearance effect indicated by "+"; negative (closing) effect indicated by "-".		

Figure 11 presents a short transient history of the HPT Stage 1 tip clearance at the worst-mismatch point and at 100% and 50% cruise power at altitude. Starting with required cold-buildup (B/U) average clearances, the worst shroud-to-rotor-tip mismatch occurs 15 seconds after increasing the thrust from idle to SLTO - as on a takeoff roll. At the cruise condition, it can be seen that the clearance can be varied from that shown with an uncooled shroud to that shown for a cooled shroud.

Figure 12 presents the average cruise tip clearance assumed for the FPS cruise performance projection and the current projected clearances that can be achieved through ACC. The large clearance shown for Stage 5 of the LPT is due to a large, gyroscopically induced deflection of the LPT aft stages caused by pitch and yaw rotation of the aircraft.

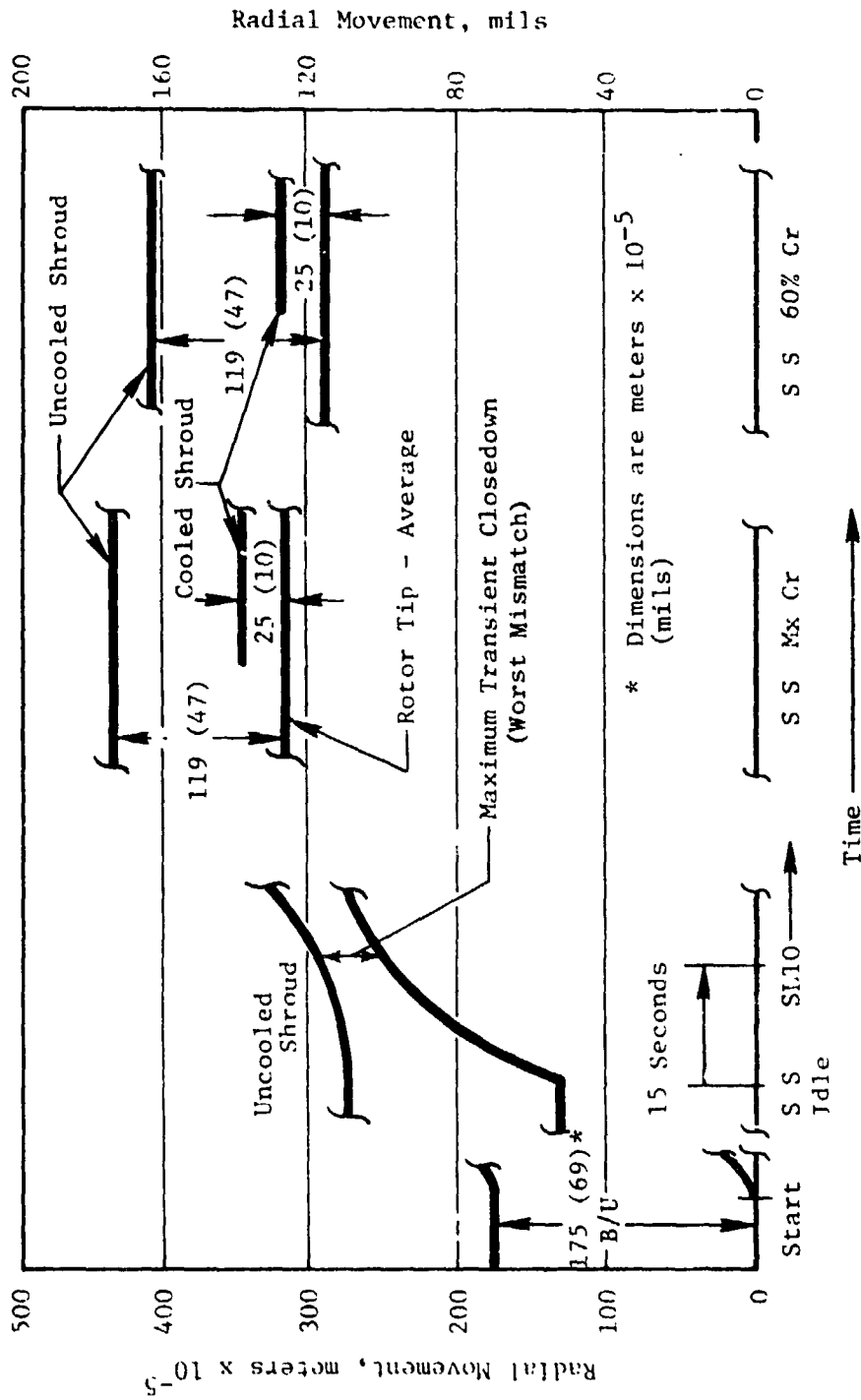


Figure 11. HPT Stage 1 Rotor Stator Transient Clearances.

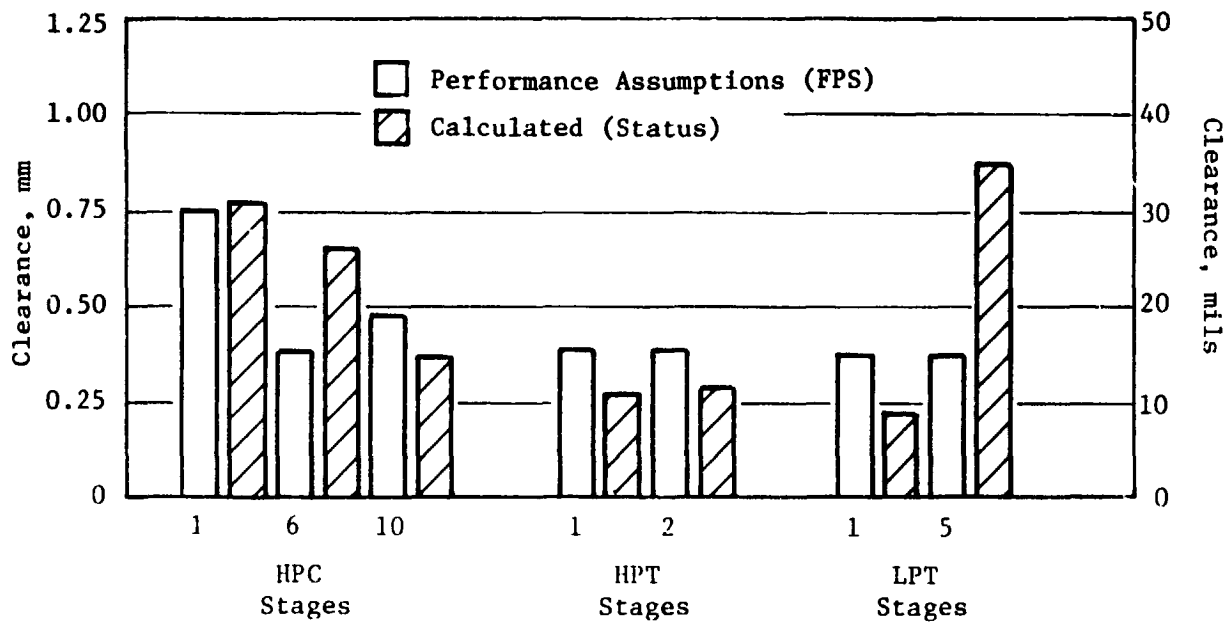


Figure 12. Average Stage Clearance at Max Cruise.

The ACC analyses accomplished so far indicate that projected FPS performance should not be affected significantly by achievable clearances, and the ACC should help reduce engine deterioration.

3.1.5 System Compatibility

Evaluation of the compatibility of the FPS fan and HPC includes determining the requirements for stall surge margin, deterioration sensitivity, and distortion tolerance. In addition, it includes a stability analysis consisting of a surge-line estimation and performance/stability trades.

A preliminary stability assessment for the HPC and fan indicates more than adequate stall margin for the more critical operating points investigated in Table 5. On a percentage basis, the least surplus margin occurs for the fan at the SLTO thrust condition; the HPC has the least surplus margin at the altitude climb condition.

Table 5. Preliminary Stability Assessment.

Component	CLS Ground Idle	SLS Takeoff	M 0.8/10.7 km (35,000 ft) Mx Cl	M 0.8/10.7 km (35,000 ft) Mx Cr
Fan Margin Available, %	3.5	15.8	15.5	16.6
Excess	>150	>25	>400	>500
HPC Margin Available, %	34.4	29.2	25.2	27.2
Excess	>50	>40	>25	>30

Figures 13 and 14 illustrate the makeup of the required surge margin for the fan and HPC at the SLTO thrust condition. For the fan, distortion is the largest single contributor to the stall margin requirement. For the HPC, the thermal effects on clearance produce the largest single contributor to the margin requirement.

In conclusion, the preliminary compatibility effort has analytically predicted more than adequate stall margin for expected operational conditions. It will remain for the component and engine testing to verify these results.

3.1.6 Maintainability

An important aspect of commercial engine operation is the maintainability of the engine as related both to maintenance costs and to aircraft utilization.

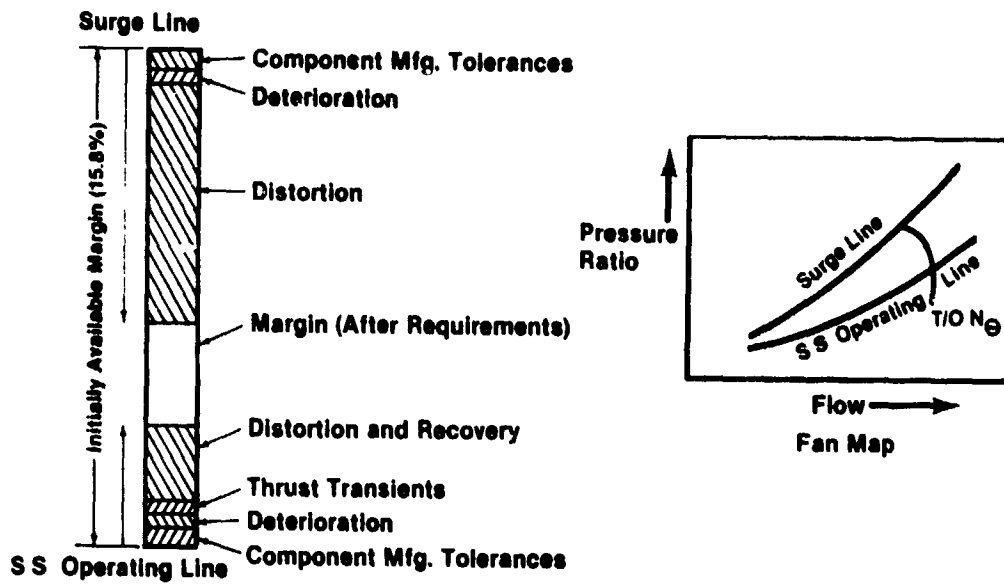


Figure 13. Sample Stability Stack Crosswind - Fan at T/O Thrust.

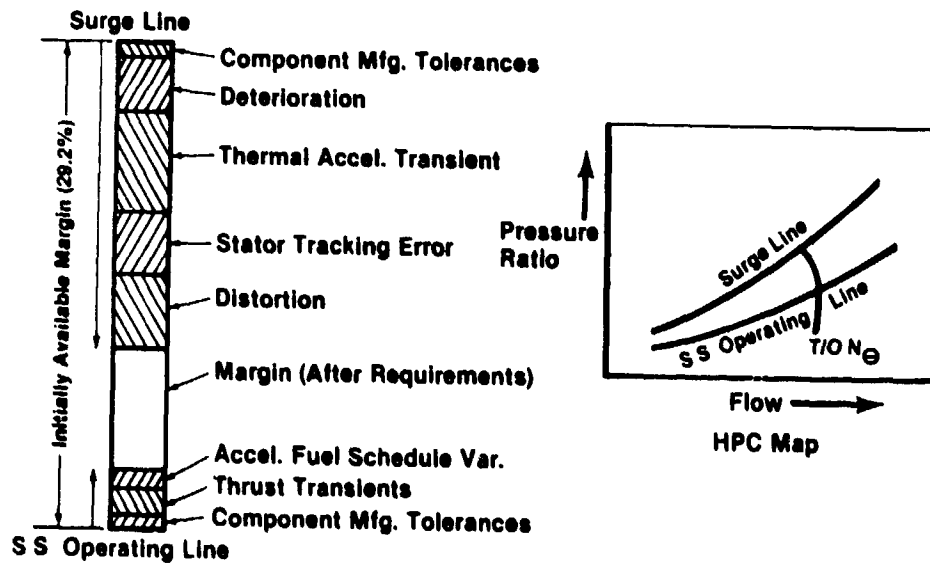


Figure 14. Sample Stability Stack Crosswind - HPC at T/O Thrust.

Maintainability has continued to be a prime design and configuration consideration for the FPS.

Figure 15 illustrates the access feature of the FPS. Both the outer fan-cowl/reverser and inner cowl cover are swung up to permit access to the core engine. Since the current configuration includes core mounting of the accessories, this quick access is even more important than on some current commercial engines. The oil tank is located on the outer fan case to permit quick inspection and servicing when required.

Maintenance of the FPS bare engine is based on the module concept. Separable modules containing the major engine components can be built-up and stored separately for quick replacement and consequent quick engine returns to service. Figure 16 illustrates the major modules as they could exist in a maintenance facility. The engine design has also tried to preserve the ability to remove the LPT module without seriously disturbing the rest of the built-up engine.

Some of the important maintainability features of the FPS are illustrated in Figure 17. These features have been retained because General Electric experience in the commercial engine business has proven that they enhance the serviceability of commercial engines and reduce maintenance costs.

Another aspect of the maintainability effort was the estimation of expected maintenance costs for the fully developed FPS. The estimate was based on the CF6-50C commercial-engine-service data base with scaling factors applied for thrust, mission, and part design life. In addition, such parameters as operating temperatures and speeds, configuration differences, and parts costs were considered.

A preliminary part-cost estimate per flight hour is listed in Table 6 by major module. The total part cost per hour is for a fully developed, mature engine flown on an average two-hour domestic mission.

Reliability also impacts the maintainability of an engine in a very direct way. The configuration of the FPS has been in the direction of simplifying or reducing the number of parts wherever possible. Figure 18 illustrates some of the features that are believed to enhance reliability and also provides a comparison of some classes of engine parts with the CF6-50C. As can be seen, there has been a considerable decrease in the number of blades and vanes and especially frames, sumps, and main shaft bearings.

It is believed that the FPS design will produce a system superior to current commercial engines in reliability and maintainability.

3.1.7 Weight, Cost, Maintenance Cost, Engine Performance, and Economic Benefits

A current-status weight for the FPS versus the initial-study FPS weight estimate is given in Table 7. As can be seen, the bare-engine weight estimates have increased significantly while there has been a decrease in the

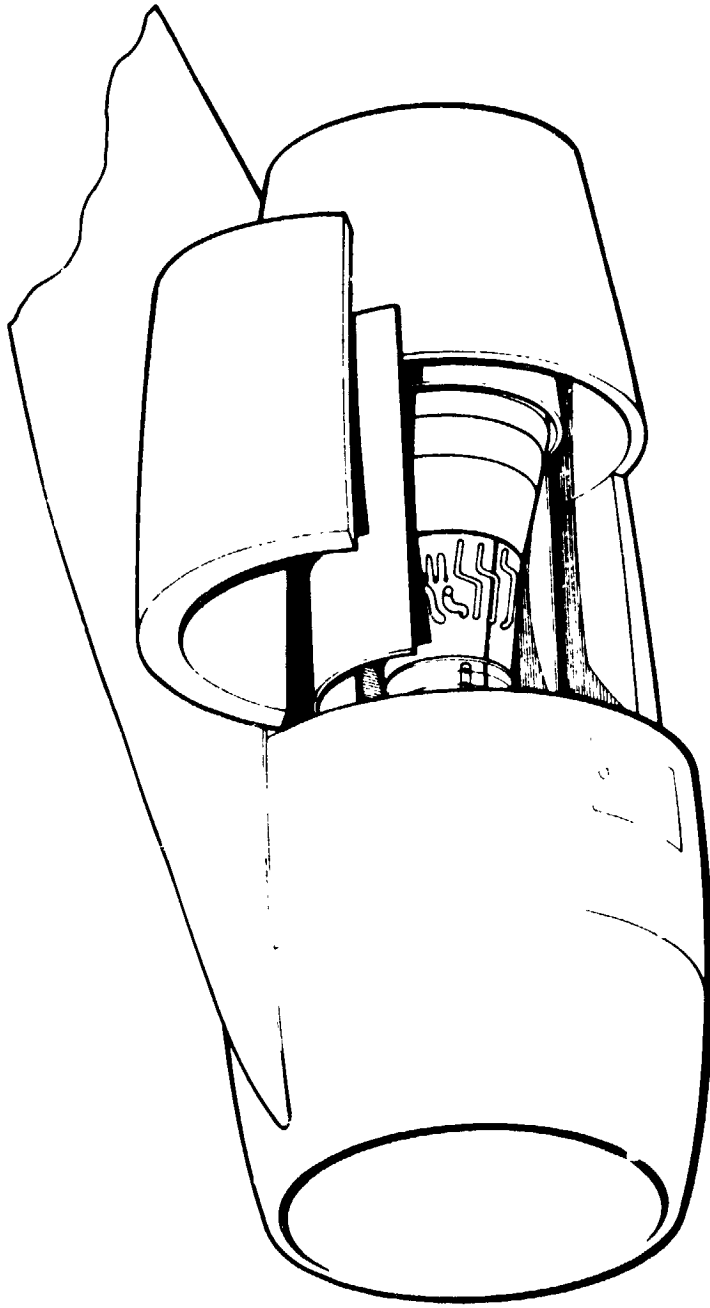
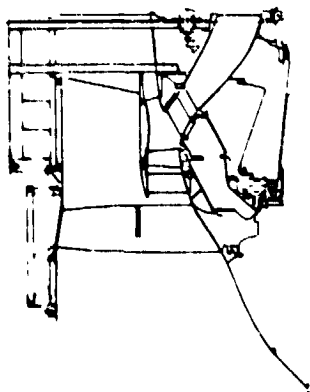
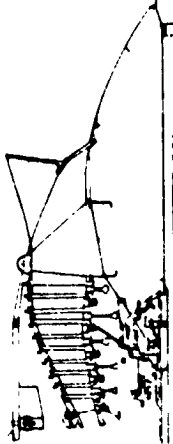


Figure 15. FPS On-Wing Access Provisions.



**Fan & IGB
Module**

Core Module

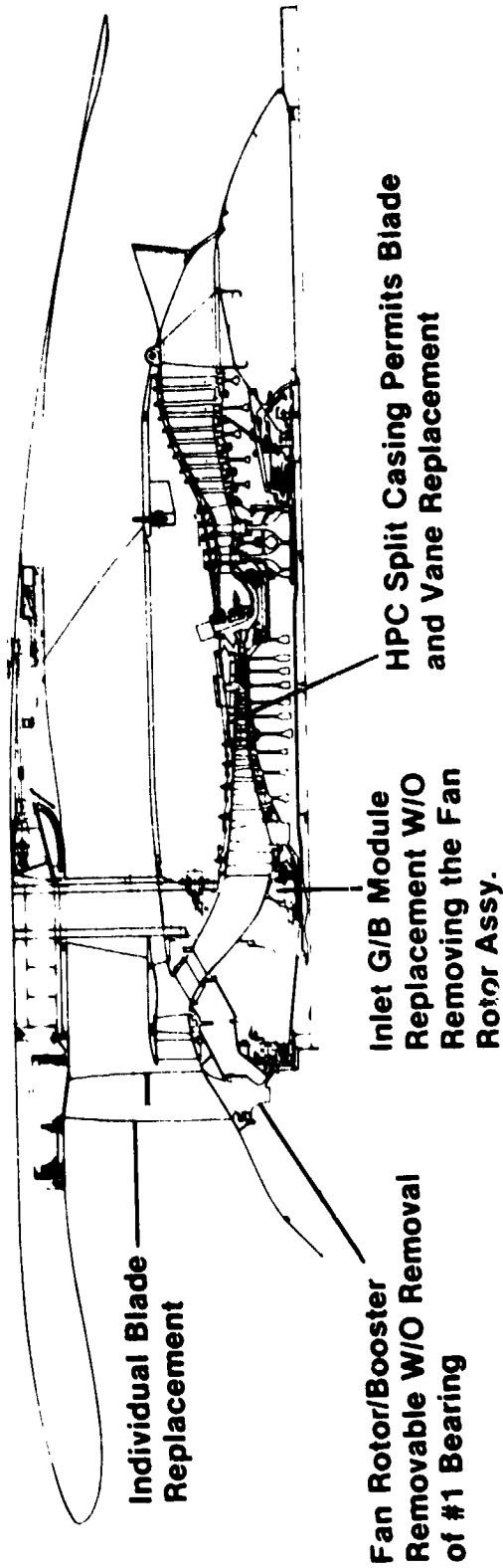


LPT Module



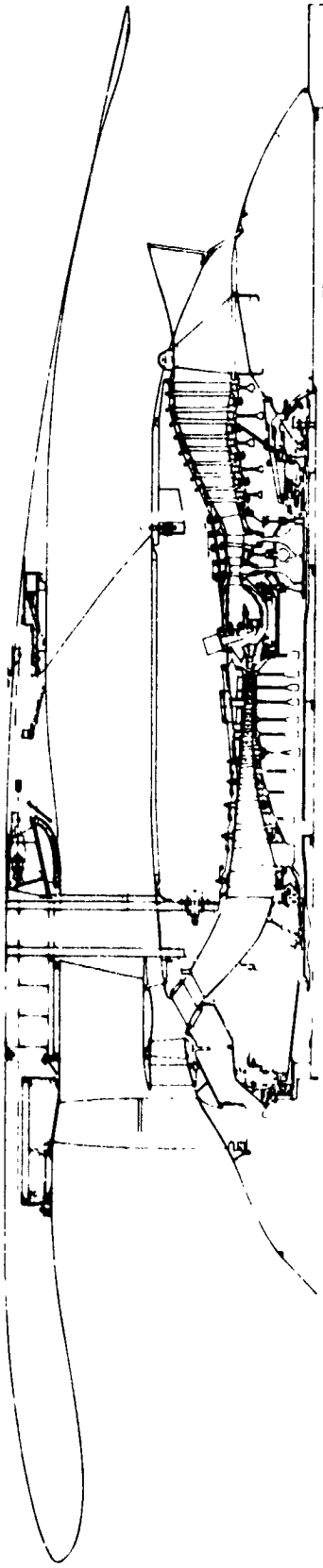
**Accessory Gearbox
Module**

Figure 16. Energy Efficient Engine Modules.



- Borescope & Radiographic Inspection Capability
- Soap Sampling, Chip Detectors and Filter Bypass Compatibility on the Lube System
- Fan Module Can be Removed Without Removing Any Other Modules

Figure 17. FPS Maintainability Features.



FPS CF6-50C

Blades	1456	1673	Comburtor	—	Shingle Design has Lower Thermal Stresses Mechanical Loads Carried in Shell
Vanes	1554	1750		—	Have <u>NO</u> Bolt Holes thru the Disk
Frames	2	4	HPT & LPT	—	Built-In FOD Separation
Sumps	2	4	Fan Booster	—	
Main Shaft Bearings	5	7			

Figure 18. FPS Reliability Features.

Table 6. Preliminary Material Cost Estimate/Flight Hour.

Module	\$/EFH
Fan	1.45
LPT	3.20
HPC	4.69
Combustor	4.01
HPT	4.70
Mixer	0.20
Other	8.00
Total Engine	26.25

Table 7. Weight Comparison.

Component	Initial kg (lbm)	Status (No Margin) kg (lbm)	Change kg (lbm)
Fan Module	1091 (2405)	1066 (2350)	-25 (-55)
LPT Module	579 (1275)	731 (1610)	+152 (+335)
HPC	429 (945)	481 (1060)	+52 (+115)
Combustor	86 (190)	122 (270)	+36 (+80)
HPT	356 (785)	404 (890)	+48 (+105)
Mixer	18 (40)	23 (50)	+5 (+10)
Miscellaneous	340 (750)	463 (1020)	+122 (+270)
Subtotal	2899 (6390)	3290 (7250)	+390 (+860)
Inlet	175 (385)	161 (355)	-14 (-30)
Fan Reverser and Duct	415 (915)	304 (670)	-111 (-245)
Core Cowl, Tailpipe	134 (295)	125 (275)	-9 (-20)
Engine Buildup	245 (540)	204 (450)	-41 (-90)
Subtotal	969 (2135)	794 (1750)	-175 (-385)
Total Installed Engine Weight	3868 (8525)	4084 (9000)	+216 (+475)

estimated installation weight. In total, however, the installed FRS weight estimate is now greater than it was initially.

The cost estimates for the engine, shown in Table 8, have not been changed from the initial-study because not enough detail design has been accomplished to significantly alter the previous estimates. However, as the design proceeds, these estimates will be updated.

A comparison of the estimated total maintenance cost is given in Table 9. For the same two-hour domestic mission, it is estimated that the current FPS total maintenance cost per engine would be \$8.75 per flight hour less than the initial estimate. This revision is due primarily to a refinement in the maintenance cost estimates.

A comparison of the projected FPS performance using the CF6-50C as a reference is given in Table 10. On an installed basis, with no customer bleed or power extraction, the projected performance is 0.2% less than initially. However, if the bleed and power extraction are considered, along with the new ECS fuel heater that replaces the initial seventh-stage-air fuel heater, the FPS performance projection is now 0.6% better at the cruise rating point.

The overall economic and fuel-consumption comparison of the initial- and current-status FPS is given in Table 11. Using Direct Operating Cost (DOC) and block fuel burned (W_f) derivatives based on the domestic Lockheed tri-jet transport, all the changes in weight, cost, maintenance, and specific fuel consumption (sfc) are evaluated in terms of a change from the initial status. The evaluation indicates the DOC is better by 0.7% than initially, and the block fuel consumption is the same.

3.1.8 Engine System Vibration

The dynamic-response characteristic of the overall engine system is an important consideration in the design process. The complex, lightweight, high-speed, engine structural system has numerous critical speeds which can be excited by rotor imbalance.

For a hard-mounted core rotor, the dynamic loads in the bearings and supporting structures are high for the core rotor unbalance levels expected in normal commercial service. These high loads are associated with bending modes of the low pressure (LP) shaft and core rotor and with core rotor "bounce" modes involving mass coupling of the core rotor with core bearing-support-structure activity.

Relative to smaller levels of rotor unbalance, three design goals were established that are derived from a base of experience obtained with engines in commercial airline service. The first design goal is to provide the ability to maintain clearance with a HPC unbalance level of 3.81 g-m (150 g-in.). It is expected that this level of unbalance could exist, in engines with long service time, due to minor FOD, erosion, slipped bolt joints, etc. The second design goal is to provide an 18,000-hour bearing life with a HPC

Table 8. FPS Cost Estimate.

Component	Cost Status*
Fan Module	520
LPT Module	472
HPC	296
Combustor	96
HPT	323
Mixer	11
Miscellaneous	237
Subtotal	1955
Inlet	95
Fan Reverser and Duct	240
Core Cowl, Tailpipe	71
Engine Buildup	172
Subtotal	578
Total Installed Engine Cost	2533

*K\$, 1977 dollars.

Table 9. Maintenance Comparison.

- 1977 Dollars
- 162,352 N (36,500 lbf) Takeoff Thrust
- Mature Engine, No Derate
- Two-Hour Mission

\$ Per Engine Flight Hour	Initial Estimate	Status
Material	\$36.80	\$28.05*
Direct Labor and Burden	38.20	38.20
Total Maintenance Cost	\$75.00	\$66.25
= \$8.75 Less for Equivalent Utilization		

*Includes Bare Engine and Thrust Reverser Maintenance.

Table 10. Comparison of Engine Performance Δ sfc %
(Reference CF6-50 at Mx Cr).

Configuration	Initial	Status
Bare engine	-13.7	-13.3*
Reduced Nacelle Drag	-0.7	- 0.6
Generator Oil Cooler Loss	**	- 0.3
Installed, No Customer Bleed/HPX	-14.4	-14.2
Customer Bleed/HPX Effect	+ 0.4	+ 0.4
ECS Based on Fuel Heater	**	- 0.8
Fully Installed, Customer Bleed/HPX	-14.0	-14.6
Change, sfc		-0.6

*Due to Removal of Seventh-Stage Fuel Heater

**Not Included in Initial Benefit Analysis

Table 11. Comparison of Mission-Based Economic Benefits,
 Δ DOC and Δ Block Fuel (Based on Lockheed Trijet
Performance).

	Initial	Status		
		Item	Change	Δ DOC
Δ DOC (Reference Scaled CF6-50)	Base	Δ Weight	+215 kg (+475 lb)	-0.6
		Δ Maintenance	\$ -8.75	-1.0
		Δ sfc Installed	-0.6	-0.3
		Δ Cost	0\$	+ 0
		Net		-0.7
Δ Block Fuel - % (Reference Scaled CF6-50C)	Base	Δ Weight	+215 kg (+475 lb)	Δ Wf +0.8
		Δ sfc Installed	-0.6	-0.8
		Net		0

unbalance level of 7.62 g-m (300 g-in.). This level of unbalance could result from moderate FOD. The third goal was to establish an acceptable (10-hour) bearing life under a heavy unbalance level, 38,1 g-m (1500 g-in.), that would be associated with blade loss.

In order to meet the design objectives for bearing life and clearance control, the design concept was changed from the initial configuration to include a tuned core-rotor-bearing support arrangement combined with multiple squeeze-film dampers. However, the general bearing arrangement is unchanged; the Nos. 1 and 2 bearings support the forward fan shaft, the Nos. 3 and 4 bearings support the core rotor, and the No. 5 bearing supports the aft LP shaft off the rear turbine frame. Figure 19 shows the tuned bearing-support system for the E³ FPS core rotor. Also shown is a static-housing squeeze-film damper at the No. 3 bearing location and a rotating-housing damper at the No. 4 bearing location. Note that the current design approach is to use only the single, static-housing damper at the No. 3 bearing and to make provisions for the later inclusion of an additional damper at the No. 4 bearing if it proves necessary.

The damper bearing design concept reduces the dynamic-response levels by driving the bending-strain energy associated with rotor bending into the tuned bearing supports. This allows the single squeeze-film damper that is in parallel with the forward tuned bearing support to provide an efficient energy sink to dissipate vibration energy by viscous damping. The damper is the closed-end or "no end flow" type and functions as a nonrotating or nutating hydrodynamic bearing. As a result of the core rotor whirl motion transmitted by the No. 3 ball bearing, a hydrodynamic squeeze action occurs on the oil film in the damper annulus. The subsequent viscous shear results in damping action that reduces the transmitted forces.

In order to determine engine critical speeds and the resulting frequency response, a finite-element model of the total engine system was constructed. Because the engine system has planes of symmetry, a planar model was formulated that describes the vibratory response characteristics in a single plane. This model includes all rotating and static structural components and mathematically represents the engine system with discrete masses connected by flexible beam, core, and spring elements. The spring rates used to represent the flexibility of the complex engine frames were determined by separate, three-dimensional, finite-element analyses. In these analyses, the frames were modeled with plate and beam elements. The engine system-vibration model includes deformations due both to bending and to shear effects and loadings due to imbalance forces, translational and rotary inertia, and gyroscopic forces associated with synchronous and asynchronous rotor whirl. The effects of linear structural damping in static and rotating components are included. For the rotating components, the effects of both synchronous and asynchronous precession on the structural damping are addressed.

Figure 20 shows a schematic of the E³ FPS vibration model. This model has 1074 degrees of freedom and is an assemblage of substructure and generalized, spring-type elements. The former element type, represented by solid lines, is called a span and includes both stiffness and mass properties. The

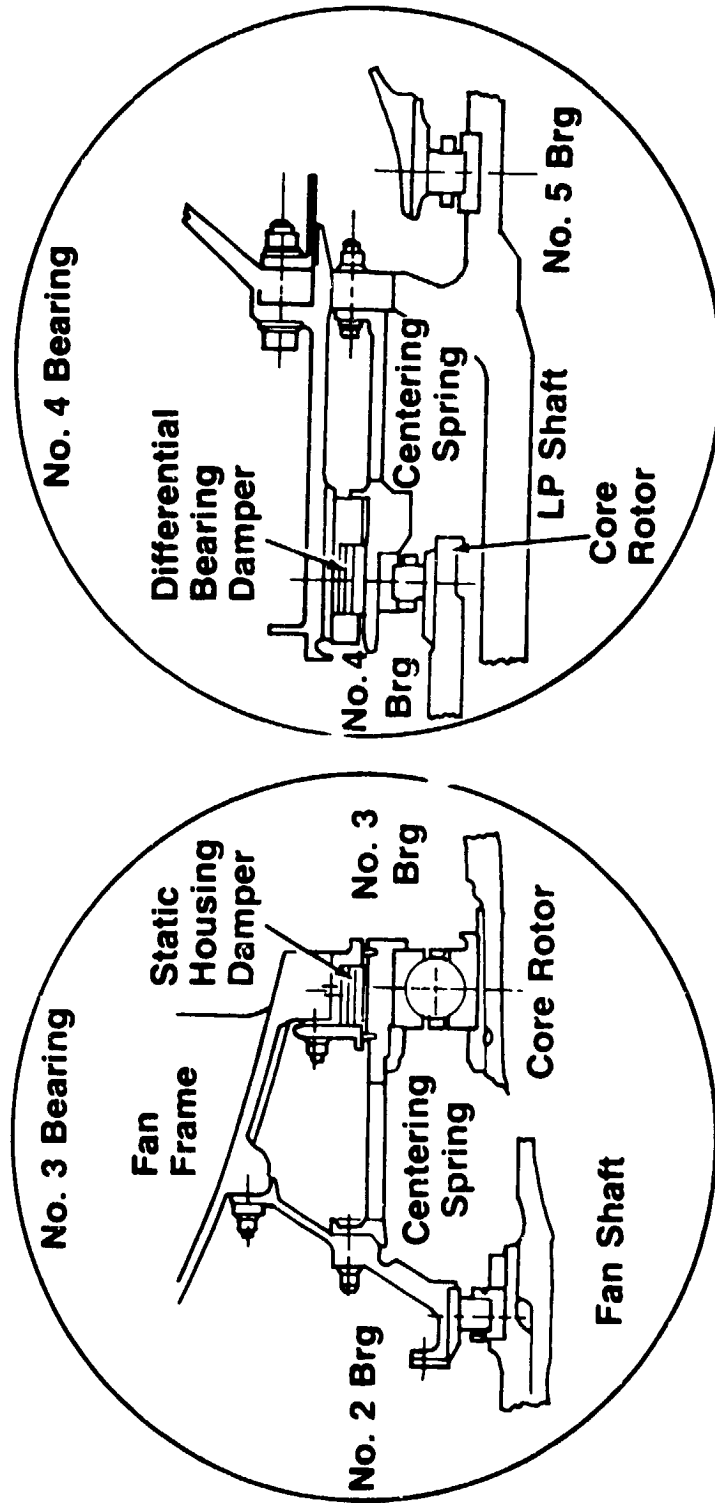


Figure 19. Combined Tuned Bearing Support and Damper Arrangement for the E3 FPS Core Rotor.

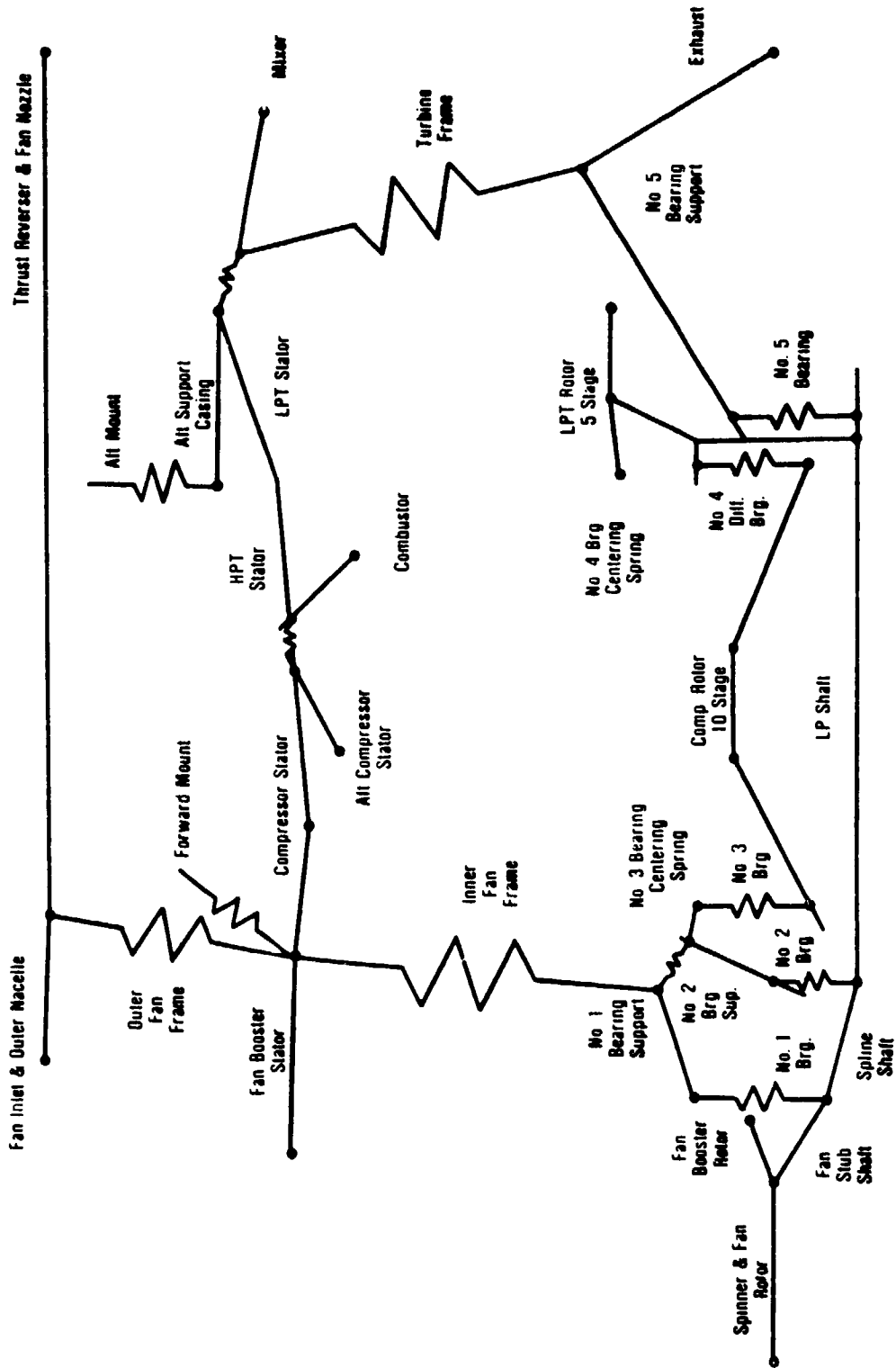


Figure 20. FPS Engine Dynamics Model with Component Descriptions.

latter element, represented pictorially by the "springs" in Figure 20, models strain energy load paths and includes fully coupled action.

The engine system natural frequencies, displacements, and loads were computed for each mode, together with the potential (strain) energy and kinetic energy distributions in the various components. The potential and kinetic energy distributions pinpoint the sensitivity of a mode to flexibility and mass effects in each component, thus, indicating the most profitable areas for adjustment to obtain the desired dynamic characteristics.

A modal formulation, using inputs calculated with the system vibration model, was used to determine the combined-modes frequency response of the engine. This modal formulation includes the effects of lumped, nonlinear, spring-viscous damping contributed by a squeeze-film damper. The solution for the nonlinear system response obtained with a squeeze-film damper was established through an iterative approach whereby assumed damper displacements were used to calculate the oil-film stiffness and damping; the resulting engine system solution was then used to calculate the damper displacements. This process continued until convergence was achieved for the damper displacements.

Analysis of the dynamic characteristics of the total engine structure goes considerably beyond methods that address only to rotor models mounted on simplified, spring representations of bearing/support systems. Hence, the coupled vibration between the rotors and static structures or between the high and low pressure rotor of the E³ FPS is accurately predicted by the analysis.

It was determined that the core rotor-mounting configuration had a significant effect on the response characteristics of the engine system. The tuned bearing supports consist of "squirrel cage" structural systems. These "squirrel cage" structures provide relatively soft load paths via spring elements, usually of rectangular section, that are machined integral with the cylindrical structural portions. It was established that a 52.54 MN/in. (3×10^5 lbf/in.) spring rate for each "squirrel cage" would provide the required rotor centering and permit the squeeze-film damper to provide the desired vibration control.

Sleeves or shims are inserted into the annulus of the damper to increase the damping and decrease the spring rate produced by the hydrodynamic squeeze action. These sleeves are continuous, 360° rings that promote self-equilibrating forces between the annuli. In order to determine the number of shims that would optimize the damper performance, the Nos. 3 and 4 bearing forces were computed for different numbers of shims for 38.1 g-m (1500 g-in.) HPT unbalance. This high level of unbalance approximately corresponds to the loss of two HPT Stage 2 airfoils. Figures 21 and 22 show the peak No. 3 and No. 4 bearing loads as a function of the number of shims. The lowest bearing force at the No. 3 bearing is achieved with anywhere from five to eight shims; the minimum force at the No. 4 bearing is achieved with five shims.

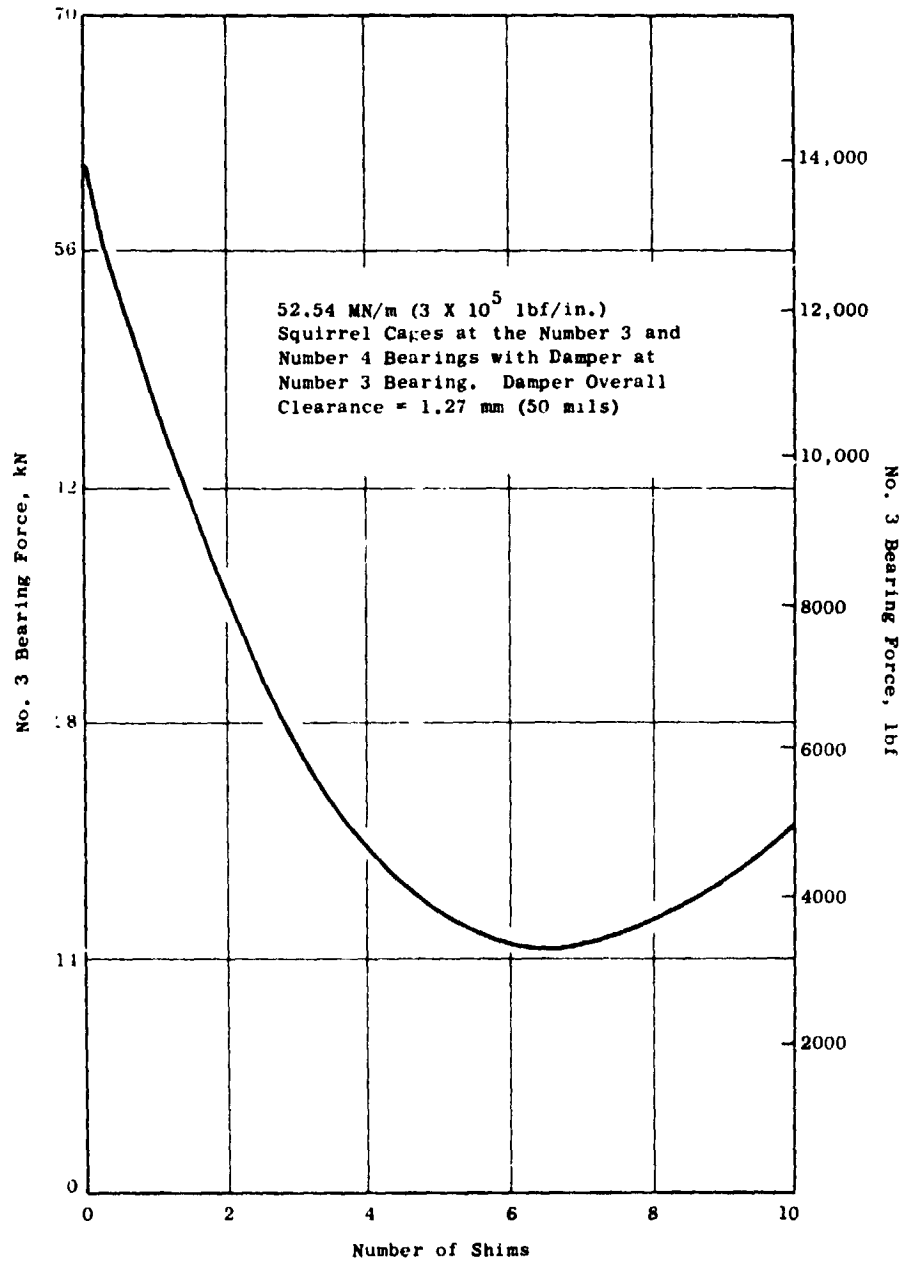


Figure 21. Maximum Value of No. 3 Bearing Force Versus Number of Shims for 0.0381 kg-m (1500 g-in) HPT Unbalance.

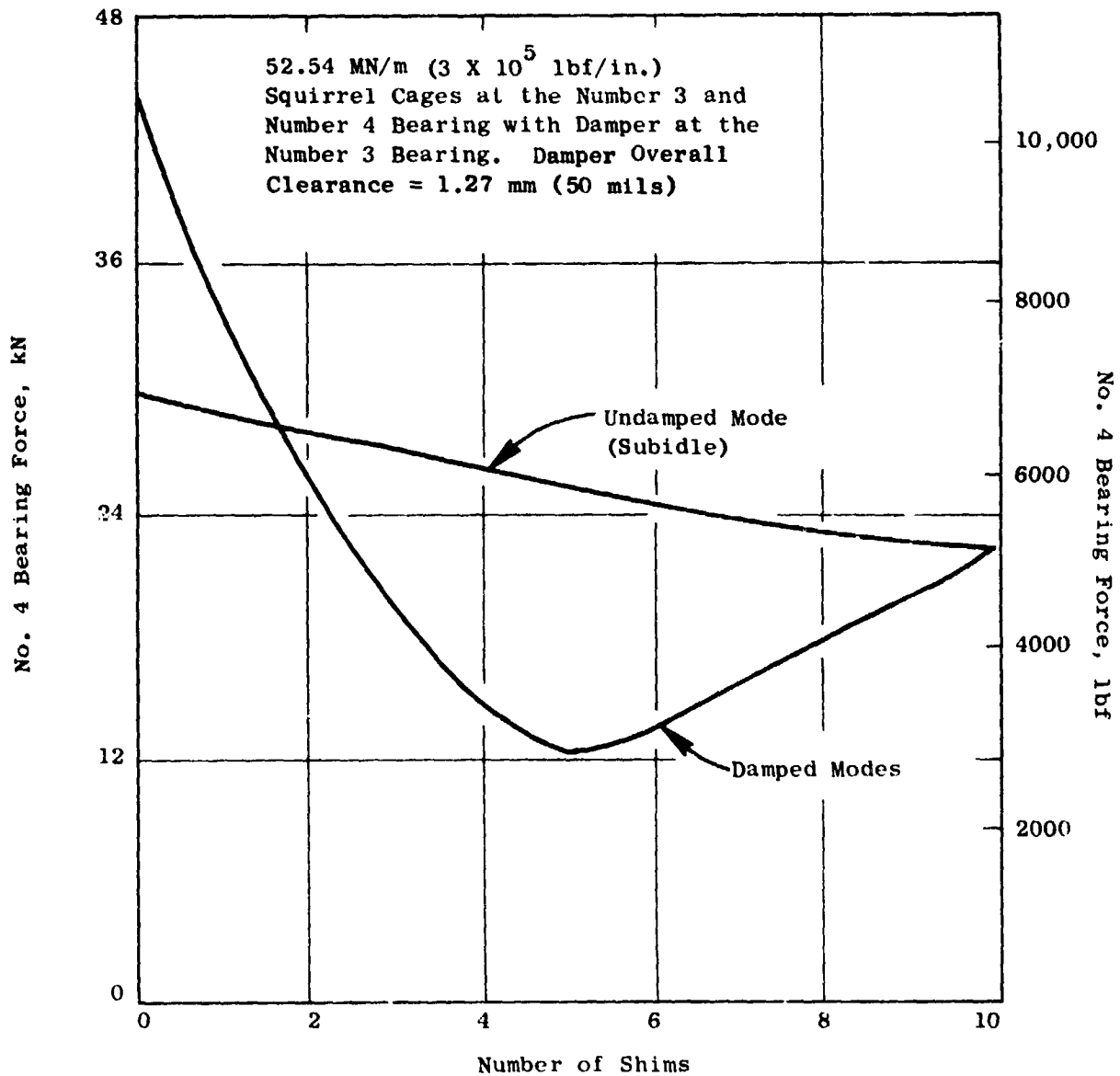


Figure 22. Maximum Value of Number 4 Bearing Force Versus Number of Shims for 0.0381 kg-m (1500 g-in.) HPT Unbalance.

Clarification is required in interpreting the results presented in Figure 22 relative to the terms damped and undamped modes. The curve labeled damped modes corresponds to those modes which involve activity at the No. 3 bearing and, hence, modes for which the damper provides effective vibration control. These modes cover the design speed range and most of the subidle speed range. The undamped-mode curve corresponds to the response of a mode in the low subidle speed region which involves some activity at the No. 4 bearing but very little at the No. 3 bearing. Hence, this mode is basically independent of the number of damper shims used.

Figures 23 and 24 show the combined-mode response of radial force versus core rpm for the No. 3 and No. 4 bearings for the large unbalance level corresponding to HPT airfoil loss. There are several modes that cause concern for a hard-mounted core rotor because bearing loads are excessive and could result in structural damage to the bearing or support structures. The tuned bearing-support/damper system has a very flat response characteristic that provides a bearing life exceeding the design objective of 10 hours for the abnormal unbalance levels associated with blade loss. Note that the response peak at approximately 2500 rpm in Figure 24 for the damped support system corresponds to the undamped mode discussed previously.

Figures 25 and 26 show the response at the No. 3 and No. 4 bearings with 7.62 g-m (300 g-in.) imbalance in the HPC. The very significant reduction in bearing load obtained with the tuned bearing-support/damper system achieves the goal of approximately 18,000 hours of bearing life. Analysis of the response characteristics with 3.81 g-m (150 g-in.) also shows that the core-rotor stage clearances are maintainable at the desired values; for the HPC, the maximum clearance change is less than 0.076 mm (3 mils) at Stage 1, and for the HPT the maximum clearance change is less than 0.0254 mm (1 mil) at Stage 2.

3.2 CYCLE AND PERFORMANCE

3.2.1 Cycle History and Selection Criteria

The E³ FPS preliminary design cycle is based on the results of a number of NASA programs involving component and cycle technology studies. As shown in Figure 27, the development of the E³ cycle began in 1974 with the study known as STEDLEC (Study of Turbofan Engines Designed for Low Energy Consumption), Reference 2. This was an extensive cycle and technology study of turbofan engines and considered separate- and mixed-flow exhaust systems, boosted and nonboosted single-stage HP turbines, and direct-drive and geared fan configurations. All engines were studied as installed on advanced transport aircraft for evaluation against the NASA performance and economic goals.

This was followed by the USTEDLEC (Unconventional STEDLEC) program, Reference 3, which continued the turbofan studies along with turboprop engines and regenerative cycles. This study narrowed the candidates to four engine types with separate- and mixed-flow-exhaust versions of direct-drive and geared fan configurations. Concurrently the Preliminary Design Study of

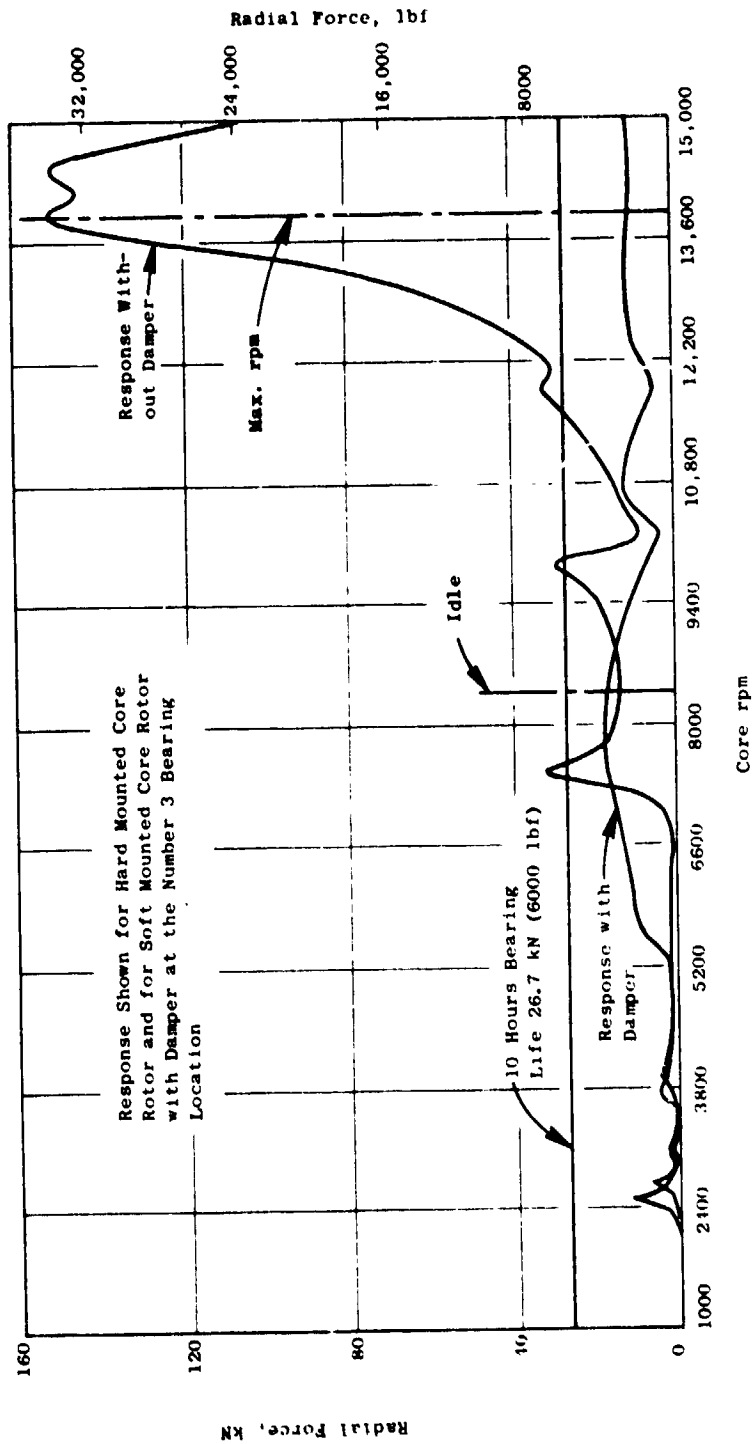


Figure 23. E³ FPS No. 3 Bearing Load Versus Core Speed for Combined Mode Response with 0.0381 kg-m (1500 g-in) HPT Unbalance.

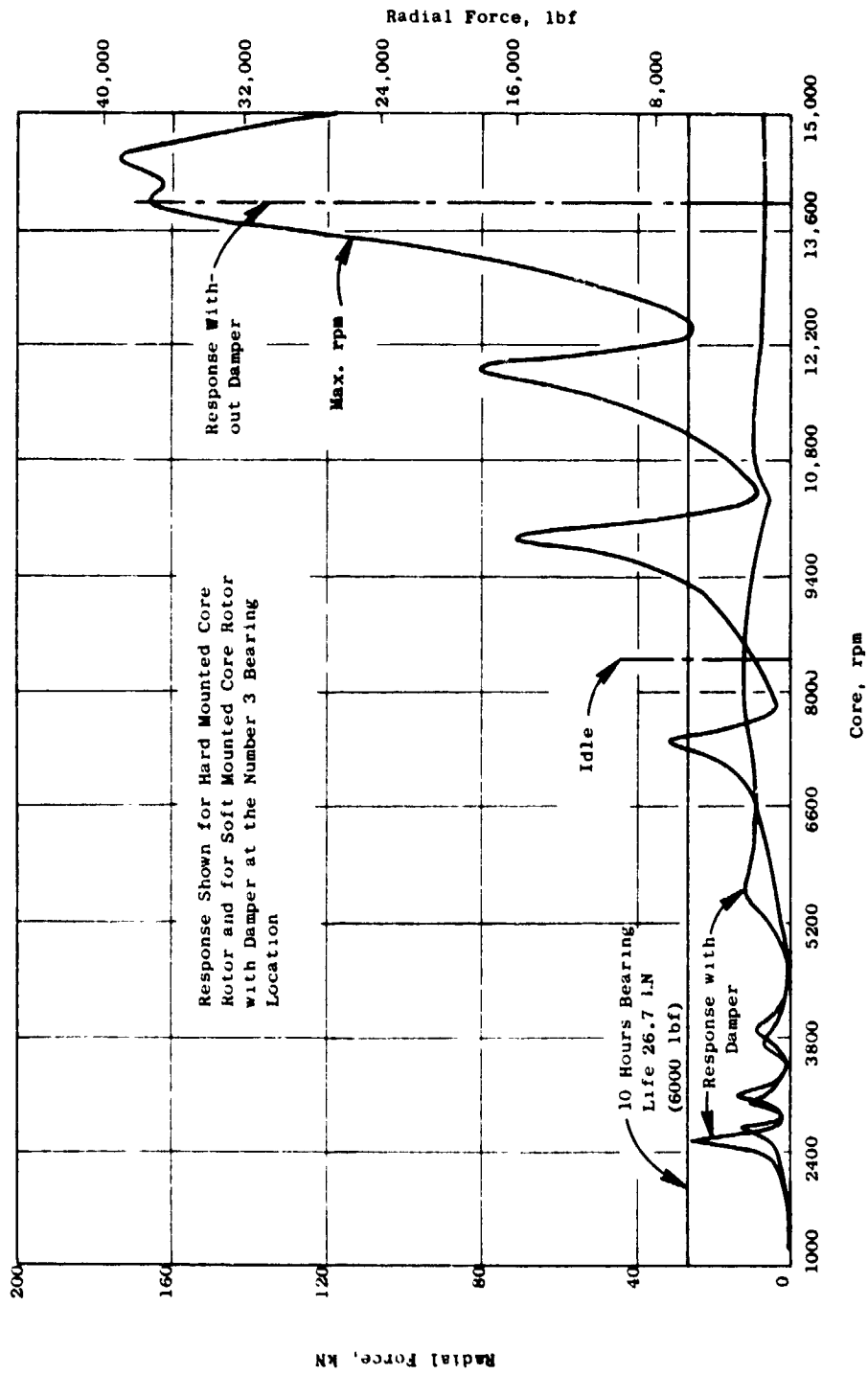


Figure 24. E³ FPS No. 4 Bearing Load Versus Core Speed for Combined Mode Response with 0.0381 kg-m (1500 g-in) HPT Unbalance.

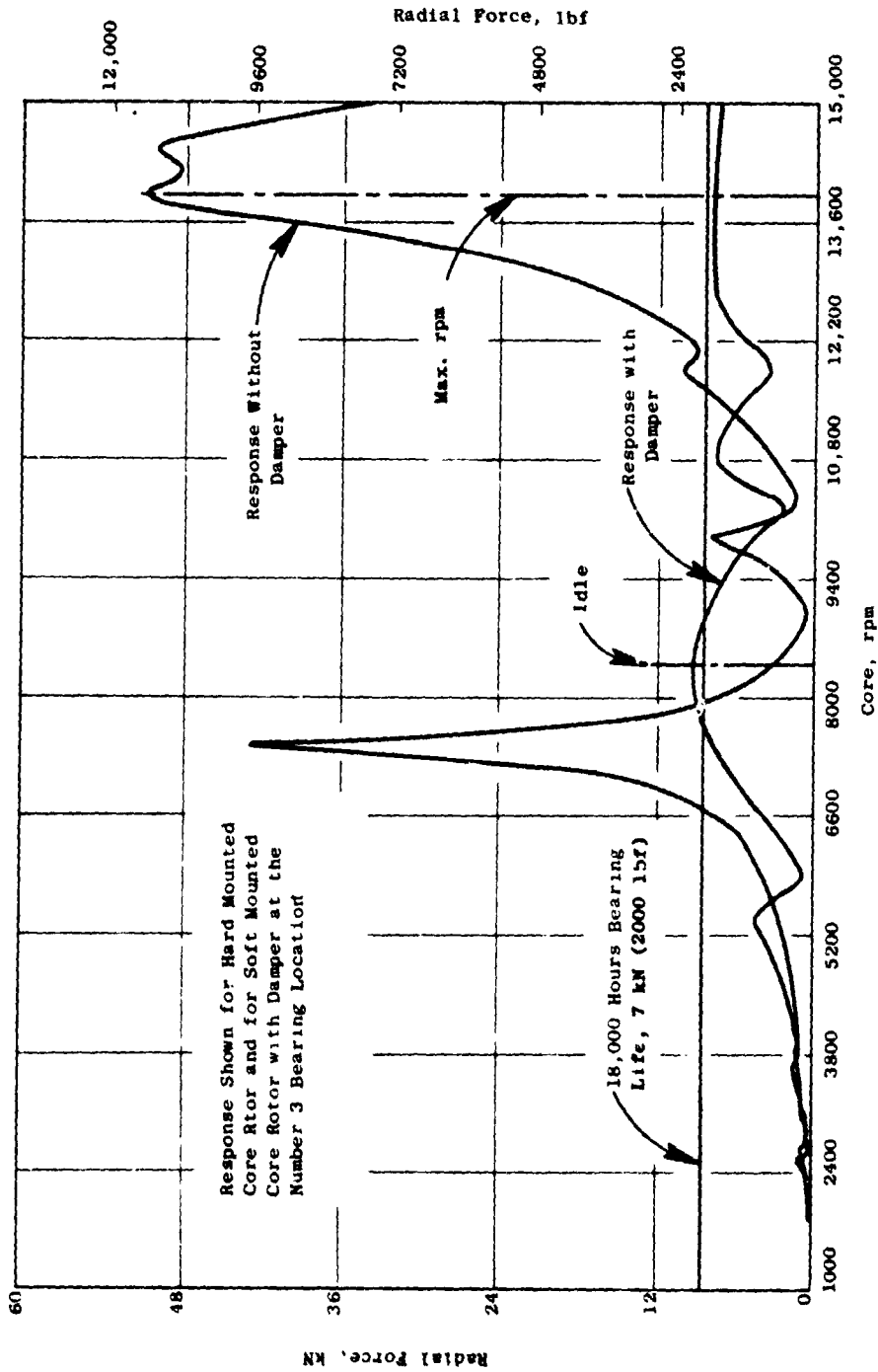


Figure 25. E³ FFS No. 3 Bearing Load Versus Core Speed for Combined Mode Response with 0.00762 kg-m (300 g-in) HPC Unbalance.

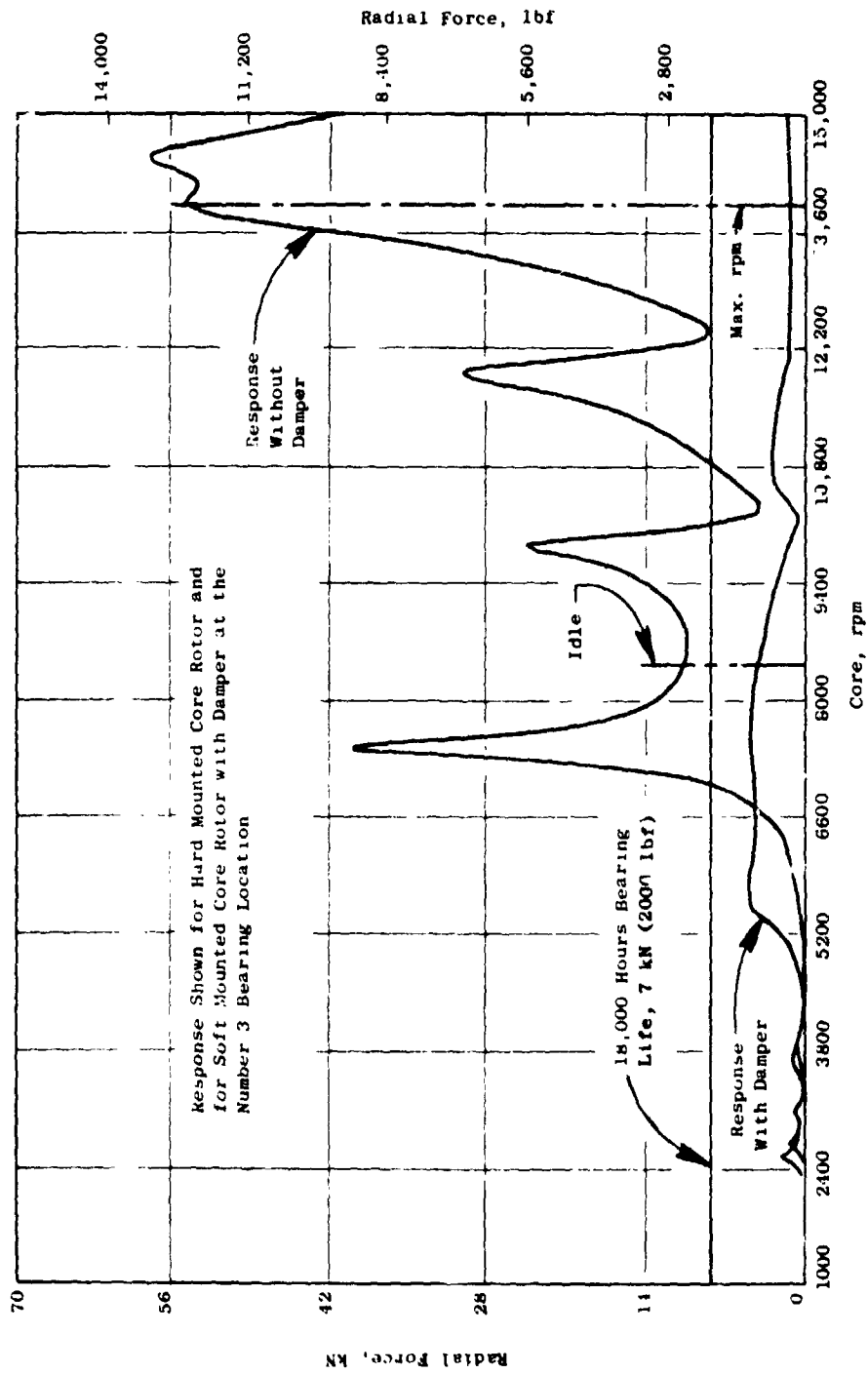


Figure 26. E³ FPS Number 4 Bearing Load Versus Core Speed for Combined Mode Response with 0.00762 kg-m (300 g-in) HPC Unbalance.

NASA Program	1974	1975	1976	1977	1978
STEDLEC	[] Cycle and Technology				
USTEDLEC		[] Unconventional Engines			
AMAC		[] 10-Stage 23:1 Compressor			
E ³ PD&I				[] Initial FPS Study Cycle	
E ³ CD&I					[] Minor Changes - FPS Cycle

Figure 27. E³ Cycle Selection.

Advanced Mult stage Axial Flow Core Compressors (AMAC) defined an advanced, 10-stage, 23: pressure ratio compressor (Reference 6). This compressor was to be used with a two-stage HPT in a nonboosted, direct-drive, turbofan engine.

The E³ Preliminary Design and Integration (PD&I) program studies (Reference 1) evaluated four engine types using advanced components, cycles, and material technologies against the NASA goals on operating economics, fuel efficiency, and environmental factors. Mission studies were conducted by airframe contractors based on advanced transport-aircraft designs. The final cycle from this study was selected as the cycle for the E³ Component Development and Integration Program (CD&I).

3.2.2 Cycle Selection Process

The cycle selection process involved two phases. The first phase developed a family of engines which provided performance for a range of values of the significant cycle parameters. These were fan pressure ratio, bypass ratio, cycle pressure, HPT inlet temperature, and exhaust system type. These engines were evaluated in the second phase, by airframe subcontractors, on a variety of missions which incorporated advanced concepts in transport-aircraft designs. The aircraft designs included twin-jet, trijet, and quadjet configurations. The mission studies were evaluated against the NASA goals on: economics (DOC), specific fuel consumption (sfc), fuel burned (W_f), emissions, and acoustics. The engines were scaled to meet specific thrust requirements.

The thrust size for the E³ FPS design was selected by General Electric based on these mission studies and corporate evaluation of market requirements for the 1990's.

3.2.3 Cycle Definition

The E³ cycle parameters are shown in Table 12 for the three key rating points: maximum climb, maximum cruise, and sea level takeoff. The climb and cruise points are shown for 10,668 m (35,000 ft), Mach 0.8 flight conditions. All points are defined for dry air, zero bleed and power extraction, and 100% inlet-ram recovery.

The cycle design point (for component matching) is at the maximum climb flight condition which was established in the initial-study cycle. As the cycle was refined for changes in component performance and cooling-flow requirements, the parameters for the match point (see Table 12) were maintained - resulting in a revision in the HPT rotor inlet temperature. The cycle parameters for the maximum cruise and takeoff thrust ratings then result from the component off-design characteristics as the engine is throttled to lower fan speeds.

Table 12. E³ FPS Cycle Definition.

Parameter	Max. Climb*	Max. Cruise	Takeoff
Uninstalled sfc (Std. Day), kg/N/hr (lbm/lbf/hr)	0.0557 (0.546)	0.0553 (0.542)	0.0300 (0.294)
Overall Pressure Ratio	37.7	36.1	29.7
Bypass Ratio	6.8	6.9	7.3
Fan Bypass Pressure Ratio	1.65	1.61	1.50
Fan Hub Pressure Ratio	1.67	1.63	1.51
Compressor Pressure Ratio	23.0	22.6	20.0
HPT Rotor Inlet Temperature,** ° C (° F)	1282 (2340)	1244 (2272)	1343 (2450)

*Cycle Match Point.

**Temperature at the ambient flat-rating temperature.

The engine thrust is constant (flat-rated) over a range of ambient temperatures up to the flat-rating temperature, subject to a maximum HPT rotor inlet temperature, as shown below:

- Standard Day +15° C (+27° F) for the takeoff rating.
- Standard Day +10° C (+18° F) for the climb and cruise ratings.

The HPT rotor inlet temperatures shown in Table 12 for each rating are at the flat-rating temperature condition.

The uninstalled sfc values in Table 12 are for a standard day ambient temperature. The uninstalled maximum cruise sfc is adjusted for isolated nacelle drag to determine the installed sfc goal of the E³ program.

The cycle data in Table 12 are calculated from the General Electric cycle deck computer program system used on all engine programs. These are large scale computer programs that contain mathematical models of the engine components including: maps, cooling and parasitic flows, pressure losses, Reynolds number effects, and exhaust system characteristics. Steady-state performance is calculated with momentum balance, energy, and flow continuity maintained from station to station in the engine. The deck also contains models of the 1962 U.S. Standard Atmosphere and thermodynamics using real gas effects including dissociation.

Table 13 shows the component efficiencies and cooling-flow levels at the maximum cruise condition. The cooling-flow levels are shown as a percent of compressor inlet flow.

Table 13. FPS Cycle - Max Cruise Component Performance.

Component	Predicted Performance	% Δ sfc*
Fan Bypass	$\eta = 0.887$	-2.2
Fan Hub	$\eta = 0.892$	-0.7
Compressor	$\eta = 0.861$	-0.4
Combustor	$\eta = 0.995$	0
HPT	$\eta = 0.924$	-0.6
LPT	$\eta = 0.917$	-0.2
Mixing Effectiveness	0.75	--
Total Cooling Flow - % Compressor Inlet Flow	20.5	---
Total		-4.1

*Relative to CF6-50C, component only.

3.2.4 Reference Engine Comparison

The E³ sfc improvement goal of 12% is evaluated against a General Electric CF6-50C engine. The comparison is made for maximum cruise thrust at 10,668 m (35,000 ft), Mach 0.8, at standard day ambient temperature with zero bleed and power extraction and 100% inlet-ram recovery.

Table 14 shows that the E³ sfc improvement is -13.3% uninstalled and -14.2% installed as an isolated nacelle. The data identifies the source of the sfc improvement based on a cycle parameter comparison of the two engines.

Initial evaluation of the data shown could lead to misinterpretation of how the E³ design is providing the sfc improvement. For example, of the -4.1% improvement attributed to adiabatic efficiencies, more than 2% results from an improved fan. However, when considering a comparison of the two compressors, the E³ has a much higher pressure ratio (23:1 versus 13:1) and represents an improvement in polytropic efficiency. With a higher pressure ratio compressor and advanced cooling-flow technology, a higher thermal-efficiency cycle can be obtained as evidenced by the improvements due to cycle pressure ratio and HPT inlet temperatures. The propulsive efficiency improvement results from the lower fan pressure ratio and higher bypass ratio. The

mixed-flow improvement results from the fact that the CF6-50C has a separated-flow exhaust system.

A more realistic comparison of the E³ and the CF6-50C reference engine can be made on a fully installed basis since all aircraft fly with some nominal bleed and power extraction in normal operation. The following data show the effect of applying 1.22 kg/sec (2.7 lb/sec) compressor bleed, 238.6 kW (320 hp) of power extraction, and a 0.995 inlet ram recovery. The E³ sfc penalty for a fixed compressor-bleed rate is greater than the penalty for a CF6-50C because the core is smaller; therefore, a larger percentage of the compressor total flow is required. As shown in Table 14, combining the isolated installed Δ sfc and the Δ sfc due to bleed and power extraction and the customer air fuel-heater/regenerator results in a 14.6% sfc advantage over the CF6-50C. The bleed sfc penalty can be recovered with a net sfc improvement by the addition of a fuel-heater system added external to the engine cycle and integrated with the customer bleed-air system. The customer bleed air is cooled by the fuel heater, providing additional heat for the engine cycle and eliminating the need to bleed fan air for coolant as is currently done on the CF6-50C.

Table 14. E3 FPS and CF6-50C Reference Engine Max. Cruise Sfc Comparison.

Parameter	FPS % Δ sfc from CF6-50C
Component Efficiencies	- 4.1
Mixed-Flow Exhaust	- 3.1
Propulsive Efficiency (FPR-BPR)	- 2.5
Increased Cycle Pressure Ratio (+20%)	- 1.0
Increased HPT Inlet Temperature, 96° C (+175° F)	- 1.5
Cooling and Parasitic Flows	- 1.0
Flowpath Pressure Losses	- 0.1
Uninstalled Δ sfc Improvement	-13.3%
Reduced Isolated Nacelle Drag	- 0.6
Integrated Aircraft Generator Cooler	- 0.3
Installed Δ sfc Improvement	-14.2%
Bleed, Power Extraction	+ 0.4
Fuel Heater, Customer Air	- 0.8
Fully Installed Δ sfc Improvement	-14.6%

3.2.5 Growth Capability

In the design of a new engine, the impact of thrust-growth requirements on component design changes should be assessed prior to finalizing the baseline design. This will identify the areas where the baseline design must allow provision for component change. On this program, studies were conducted for balanced growth up to 20% in thrust with the constraint that the engine flowpath would remain unchanged. Flexibility for growth in steps is provided by the fan hub quarter-stage that can be modified to increase core engine boost.

Thrust-growth levels of +5%, +10%, and +20% were evaluated and are summarized in Tables 15 and 16. Table 15 presents a summary of the major cycle parameters for the maximum climb and sea level takeoff conditions. A +5% "throttle push" point is shown as a reference for sfc and HPT inlet temperature changes without benefit of a fan hub quarter-stage change. Table 16 identifies the components which require modification. Note that all the thrust-growth points show a cooling-flow modification to maintain turbine blade life.

The +20% growth engine requires changes to most of the components in the engine but not to the flowpath. The major items are: a new fan blade with higher flow, tip speed, and pressure ratio; a high-flow compressor that will require some reblading and a new stator schedule; and some turbine aerodynamic changes. The interim growth steps will overspeed the same fan blade to attain the required engine airflow. The higher fan speed will permit a significant increase in hub boost (about 23%). These changes to the front of the engine, of course, require changes in the turbine stator vanes and in the mixer area split. The HPT flow function will increase only about 3%, but the LPT will increase about 13%. The mixer total area will remain unchanged in order to maintain the same nacelle size. The exhaust-nozzle area will decrease by only 2%.

3.3 PERFORMANCE RETENTION

A major NASA goal for the E³ is to find ways of reducing in-service performance deterioration of the FPS to half the value experienced in current high bypass engines. To accomplish this, the FPS has many features designed to reduce performance deterioration. In general, these design features fall into three major categories:

- Prevention of engine deterioration,
- Tip-clearance retention,
- FOD and erosion prevention.

Typical performance-retention features are listed in Table 17 and discussed individually in this report.

Table 15. E³ Growth Capability.

Max. Climb - 10,668 m (35,000 ft)/0.80 M

Parameters		Throttle Push +5%	+5%	+10%	+20%
Net Thrust	FPS				
Uninstalled sfc (Std Day) kg/N/hr (lbm/lbf/hr)	0.0556 (0.546)	0.0564 (0.553)	0.0562 (0.551)	0.0570 (0.559)	0.0577 (0.566)
Overall Pressure Ratio	37.7	39.0	42.3	42.7	47.0
Bypass Ratio	6.8	6.7	6.1	6.1	5.4
Fan Bypass Pressure Ratio	1.65	1.68	1.70	1.70	1.75
Fan Hub Pressure Ratio	1.67	1.70	1.90	1.87	2.05

Takeoff - SLS/30° C (86° F)

Net Thrust, kN (lb)	162.36 (36500)	170.50 (38330)	170.50 (38330)	178.60 (40150)	194.83 (43800)
HPT Rotor Inlet Temp., ° C (° F)	1343 (24500)	1367 (2493)	1353 (2467)	1394 (2541)	1443 (2630)

Table 16. Growth Component Changes*.

Component Change Required	Throttle Push +5%	+5%	+10%	+20%
New Fan Blade				X
New Booster Blading		X	X	X
High-Flowed Compressor				X
Larger HPT Nozzle Area				X
Increased Cooling Flows	X	X	X	X
Larger LPT Flow Function		X	X	X
New Mixer - Same Total Area				X
Smaller Exhaust Nozzle				X

*Engine Flowpath Unchanged.

Table 17. Performance-Retention Features.

- Active Clearance Control (ACC) - Rear Half of HPC, HPT, and LPT
- Selection of Materials/Control of Stator Temperature-Response Rate to Match Rotor
- Provision for Transiently Larger Actively Controlled Clearances When Engine Bending Loads are High
- Engine Mounting and Structure Designed to Minimize Aerodynamic, Maneuver, and Thrust-Induced Deflections
- Stiff, Strong, Static Structure
- Short, Stiff, HP Rotor
- Abradable Materials to Minimize Stackup and Transient Penalties
- Booster Separator to Reduce Core Erosion
- Low-Aspect-Ratio (Long-Chord) Blading

Figure 28 shows a curve of typical CF6-50C deterioration with time, in this case 6000 hours, and the projected deterioration rate required to satisfy the NASA goal for the FPS. These curves do not necessarily represent any particular engine; they are representative of an average for a fleet of engines. To determine if the FPS could be projected to reduce in-service performance deterioration, a survey was made of causes of deterioration in current high bypass engines.

Table 18 presents a summary of the factors, and the estimated deterioration due to each factor, for a typical long-service CF6-50C. Along with each CF6-50C deterioration factor, an estimate is made of what the deterioration effect on an FPS would be for a comparable period of time.

Table 18 indicates that the major improvement of the FPS over the CF6-50C is expected to be the retention of clearance and reduction in erosion. A major improvement in leakage of the HPC will also be achieved. Clearance retention will be improved by the ACC system and the improved mounting and engine-roundness control. The major effect of this will be seen in the aft part of the HPC and throughout the HPT and LPT. Improved, abradable shrouds will be used in the HPC and HPT in conjunction with the ACC system.

Fan-erosion effects should be reduced by a combination of slower tip speeds and the long-chord fan blade and vane designs. The longer chords will result in large leading- and trailing-edge radii that will be less susceptible aerodynamically to the erosion that does occur. The quarter-stage debris-separator feature, coupled with the long-chord HPC blade and vane designs, should also serve to reduce core erosion. Although this improvement will be felt primarily in the compression section of the engine, some benefit should be seen in the turbine sections.

Leakage improvement of the FPS will be seen primarily in the HPC and reflect the more rigid rotor/stator structure and the improved, high-boss, variable-vane-trunnion construction. The longer and wider vane-bearing structure should exhibit significantly less vane-trunnion leakage. Some beneficial effect in the HP and LP turbine vane shroud seals should also be seen because the ACC system will maintain better shroud-to-rotating-seal clearances with less seal wear.

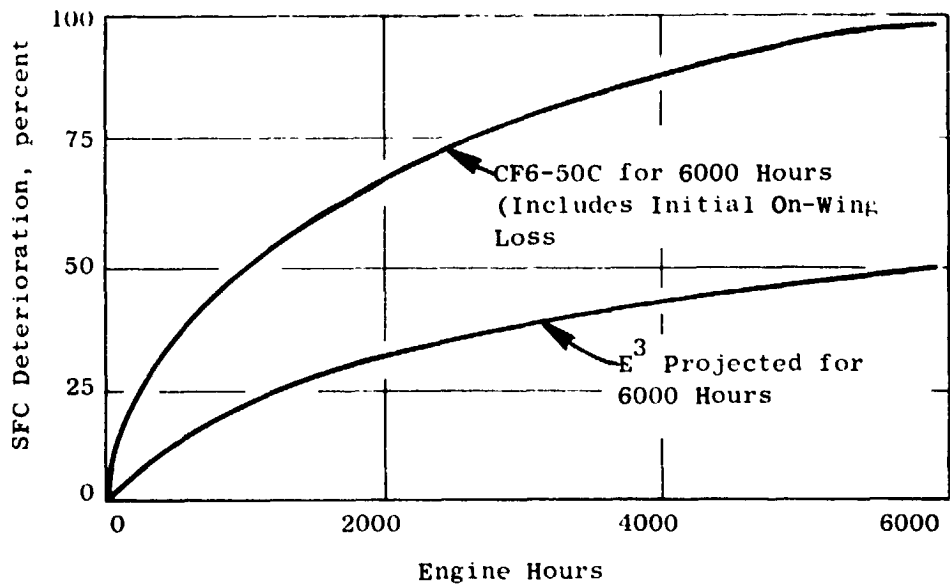


Figure 28. Long-Term Performance Retention.

Table 18. Estimated In-Service Performance Losses.

Causes	Estimated Losses - %		Reduction
	CF6-50C	FPS (Estimate)	
Clearances			
Fan	3	1	
HPC	13	3	
HPT	29	9	
LPT	4	2	
Subtotal	49	15	-34
Leakages			
HPC	10	4	
HPT	6	5	
LPT	3	2	
Subtotal	19	11	- 8
Erosion			
Fan	7	4	
HPC	8	3	
HPT	2	1	
LPT	5	4	
Subtotal	22	12	-10
Miscellaneous	10	10	0
Total	100	48	-52

In conclusion, it is estimated that the FPS in-service deterioration should be reduced by at least 50% from the current CF6-50C (as indicated in Table 18).

3.4 MATERIALS AND PROCESSES

The materials and processes to be utilized on the E³ FPS are divided into three basic categories:

- Advanced or Development
- Recently Introduced and Flight Tested
- Proven in Commercial Service

Examples of each of these categories are discussed in this report along with descriptions of the experience, supporting technology programs, and engine tests planned. E³ supporting technology programs are discussed which describe the work being done in the areas of thermal-barrier coatings, variable stator-vane bushings, ceramic shrouds, disk alloy support, and alloy mechanical behavior.

The selection of materials and processes for the FPS includes several developed under other engine or government-sponsored programs. Included in this category are AF115, inertia-welded hardware, the directional-solidification process for blades and vanes, Genaseal shroud material, and containment material.

Advanced/development materials and processes are listed and described briefly below:

As Hot Isostatic Pressed (As-HIP) AF115 - This material is a recently developed, high-strength alloy specifically designed for powder-metal processing for operating at temperatures up to 760° C (1400° F). It is to be used in areas where elevated temperature capabilities (above René 95) can be utilized.

Directionally Solidified René 150 - This material is a nickel-base turbine blade and vane alloy developed by General Electric's Material and Process Technology Laboratories (M&PTL) for directional solidification with a goal of achieving a 69° C (125° F) advantage over René 80 in terms of creep and rupture strength.

René 80 +df - This is a nickel-base turbine blade and vane alloy developed by M&PTL for directional solidification with thin-wall creep and rupture advantages, thermal fatigue properties greatly improved over conventional alloys, and better castability than René 150.

Ceramic Shrouds - A supporting technology program, described later in this report, is underway to identify a viable, long-life, ceramic-shroud system for use on the FPS HPT.

Composite Nacelle/Frame Technology - Building on the technology developed in the QCSEE program, a lightweight, integrated nacelle using graphite and Kevlar, adhesively bonded with epoxy in low temperature applications and PMR in higher temperature areas, offers a weight reduction over conventional techniques.

Containment Materials - These are being developed under a current NASA contract in TF34 size; development work is also being carried on for the CF6 family of engines. Thin steel sheet at the flowpath bonded with lightweight epoxy honeycomb to form a stiff box structure that is wrapped with dry Kevlar cloth covered with a fiberglass skin.

CTX-2 - This is an alloy developed to have a controlled coefficient of thermal expansion such that over the room temperature to 427° C (800° F) range expansion is significantly lower than conventional alloys, and above 427° C (800° F) expansion parallels conventional alloys. It will also have improved notch sensitivity and eliminate the Stress-Accelerated, Grain-Boundary Oxidation (SAGBO) phenomenon seen in Inconel 903.

Thermal-Barrier-Coating Systems - A supporting technology program, defined later in this report, is underway to identify a thermal-barrier-coating system that will act as an insulating blanket between the hot gas stream and component substrate material in high-heat-flux regions of turbine blades and vanes. As such, these coatings offer the potential to reduce metal temperatures, cooling flow requirements, and cooling-system complexity while increasing hot section component life and system efficiency.

EA-Ni-Cr-Al-Hf Coatings - In order to meet the higher temperature/longer life requirements of advanced turbine engines, coatings are needed with improved capabilities over the conventionally used pack-aluminide coatings. EA-Ni-Cr-Al-Hf is a development "add on" coating that is implemented by electroplating and aluminiding and will meet the stringent goals of this engine.

Near-Net Shapes - Emphasis on as-HIP processing to near-net shapes has evolved from General Electric's determination of the cost-reduction potential of decreasing process steps and increasing materials utilization.

Genaseal Shrouds - This is sintered material, for turbine shrouds, with improved abrasability over Bradelloy. It has oxidation resistance to 1177° C (2150° F) and has good erosion resistance.

Recently introduced and flight-tested materials and processes are listed below:

René 95	Inconel 903
Titanium 17	Inertia Welding
Inconel Alloy MA754	Aluminum-Bronze/Nickel-Graphite
René 125	Compressor Clearance Coating
Double Vacuum Melted (DVM) M50	Metco 443/Nickel-Graphite Com- pressor Clearance Coating

Some materials and processes that fit into the category of being well-tested in commercial service are listed below:

<u>Materials</u>	<u>Processes</u>
Inconel 718	Conventional Casting
René 80	Welding Brazing
X 40	Codep Coating
A 286	Forging
Ti-6Al-4V	Carburizing
Marage 250	Shot Peening
7075 Aluminum	Plasma Spraying
Hastelloy X	
AISI 9310	
M152	

The actual materials selections are shown in the engine and components cross sections in Figures 29 through 38. In conjunction with several of the advanced-technology areas, there are major supporting technology programs underway to define, develop, and/or test systems to meet FPS needs. Brief descriptions of the aim and status of several of these programs are given below:

Ceramic-Shroud Program - The program objective is to identify, by screening tests, a long-life candidate ceramic system for turbine shroud applications. In Phase I there are two approaches:

1. Hot-pressed silicon carbide blocks with a boron nitride rub layer.
2. Zirconia overlays on conventional metal shrouds.

In Phase II, a single shroud process will be developed in laboratory and subscale-rig tests by iteratively refining the process. During Phases III and IV, full-scale shrouds will be fabricated for component tests along with three sets of shrouds for engine test.

Thermal-Barrier Process Program - The aim of this program is to develop a thermal-barrier-coating system and demonstrate its adequacy for the E³. This is being accomplished by screening tests of various potential coating materials. Three candidate materials will be selected for further process development and evaluation. One of these will be applied to HPT blades and vanes and tested in a CF6-50 factory endurance test of 1000 "C" cycles (simulated commercial-service cycles on an accelerated basis).

Variable Stator Vane (VSV) Bushing Application Program - This is to identify VSV bushing materials and configurations with temperature capabilities up to 482° C (900° F) for long-life service for the E³. To date, the bushing requirements have been defined, specimens have been obtained, and the test equipment has been adapted for testing.

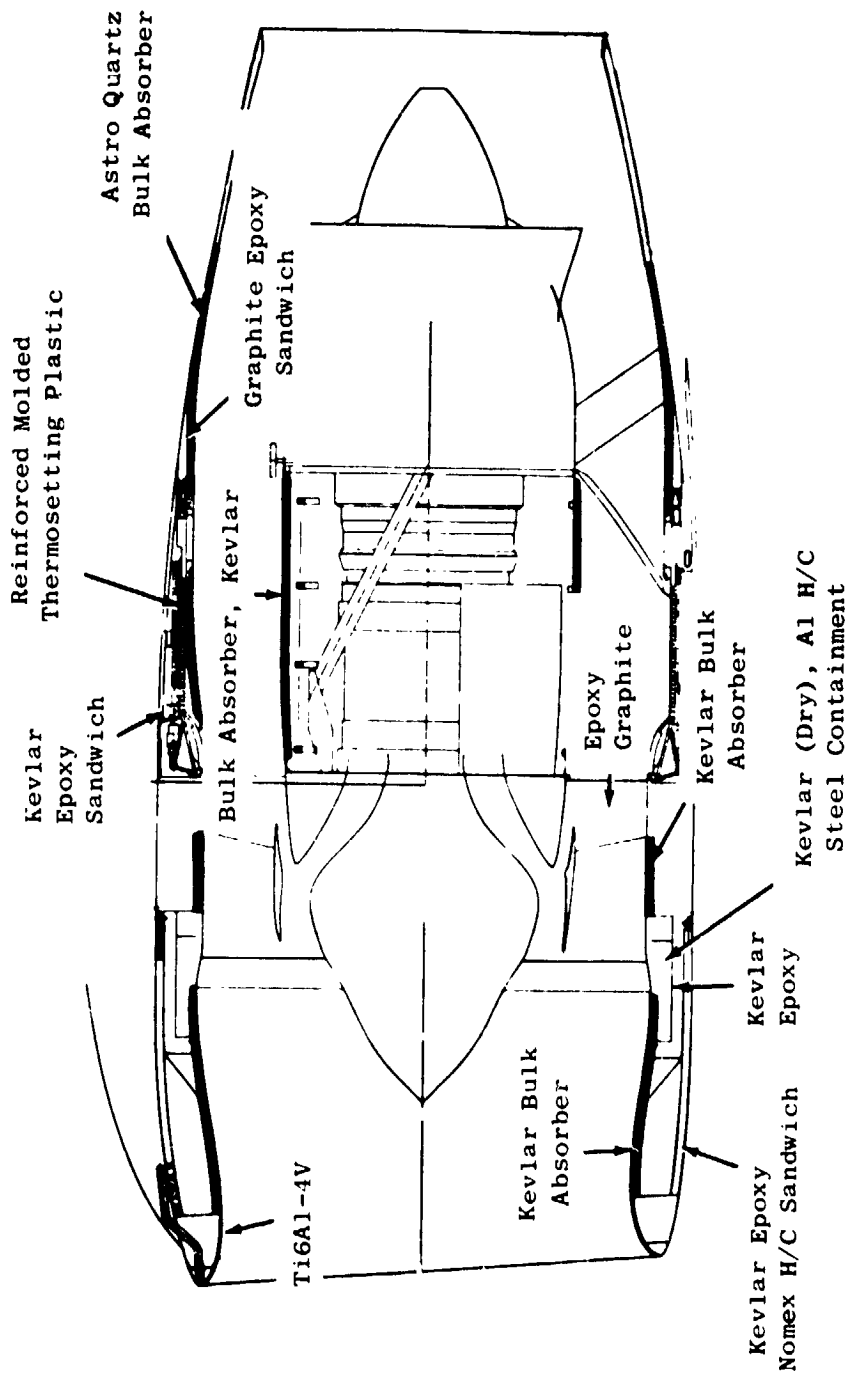


Figure 29. Fan Frame and Nacelle.

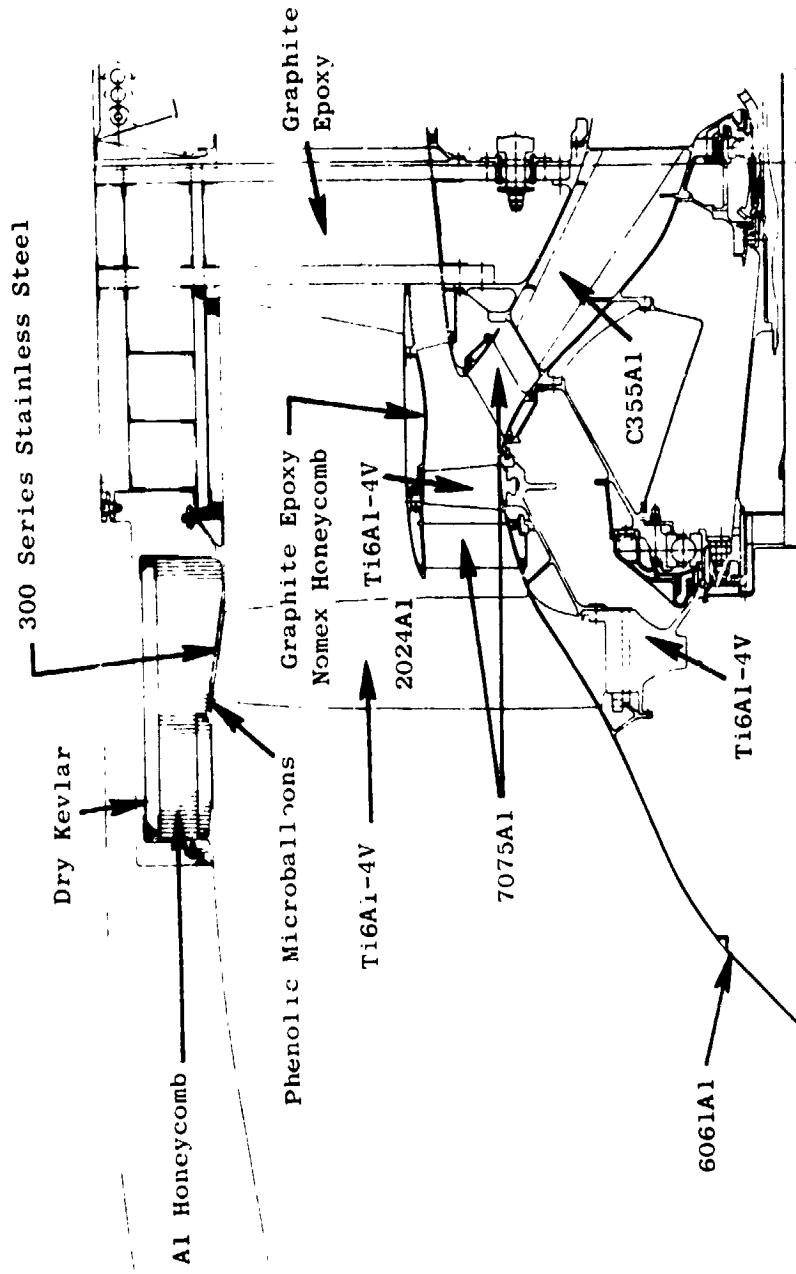


Figure 30. Fan Rotor and Stator.

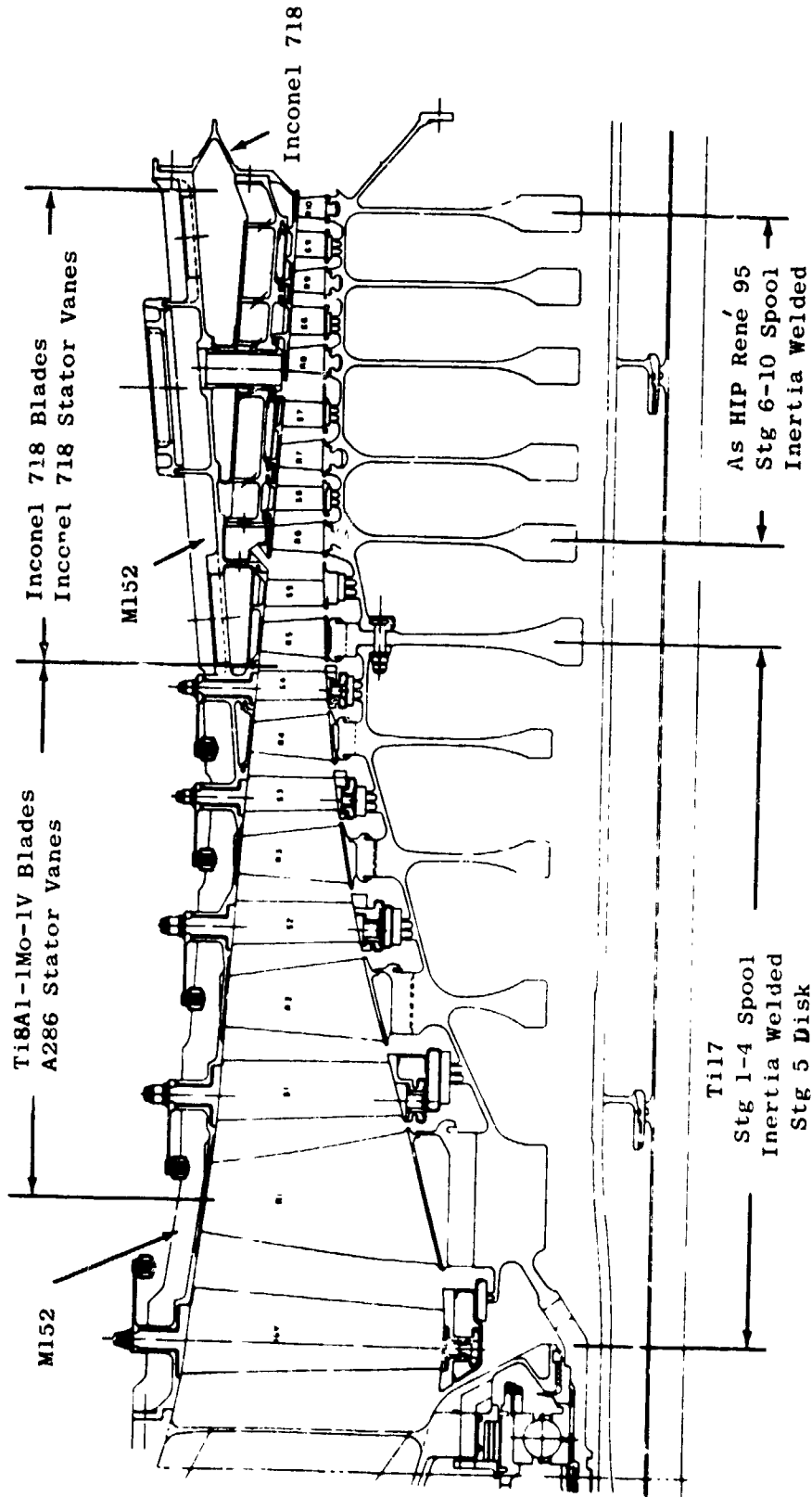


Figure 31. hP Compressor Rotor and Stator.

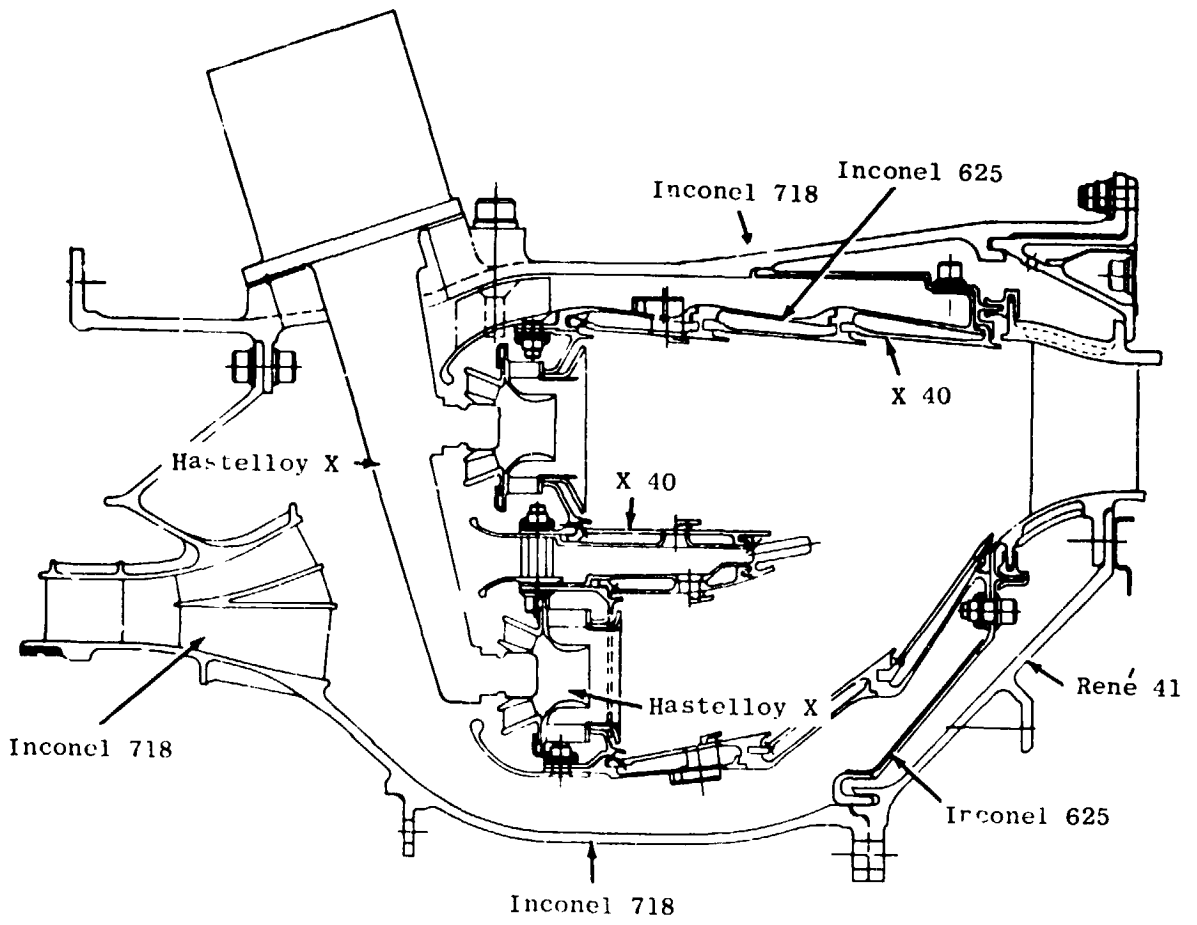


Figure 32. FPS Combustor.

Zirconia Filled



Hot-Pressed SiC + BN/Si-SiC

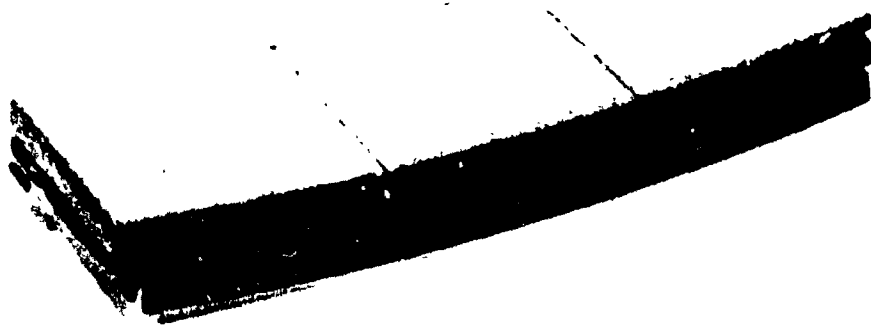


Figure 33. Turbine Shroud Concepts.

● Engine Demonstrated Advanced Materials

- René 95 PM - HIP
- René 150 DS - Blade Airfoil

● Engine Development Alloys

- AF 115 PM - HIP

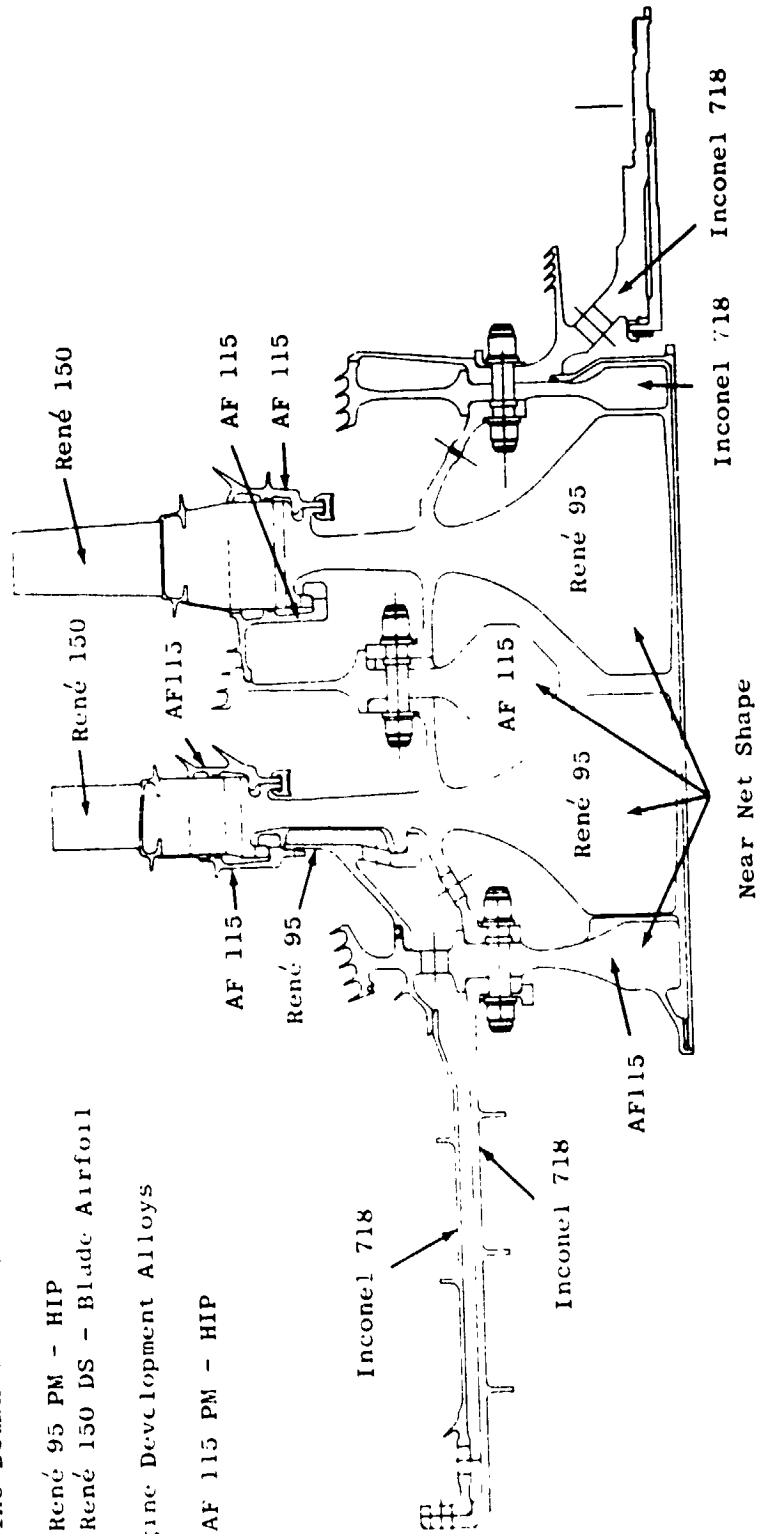
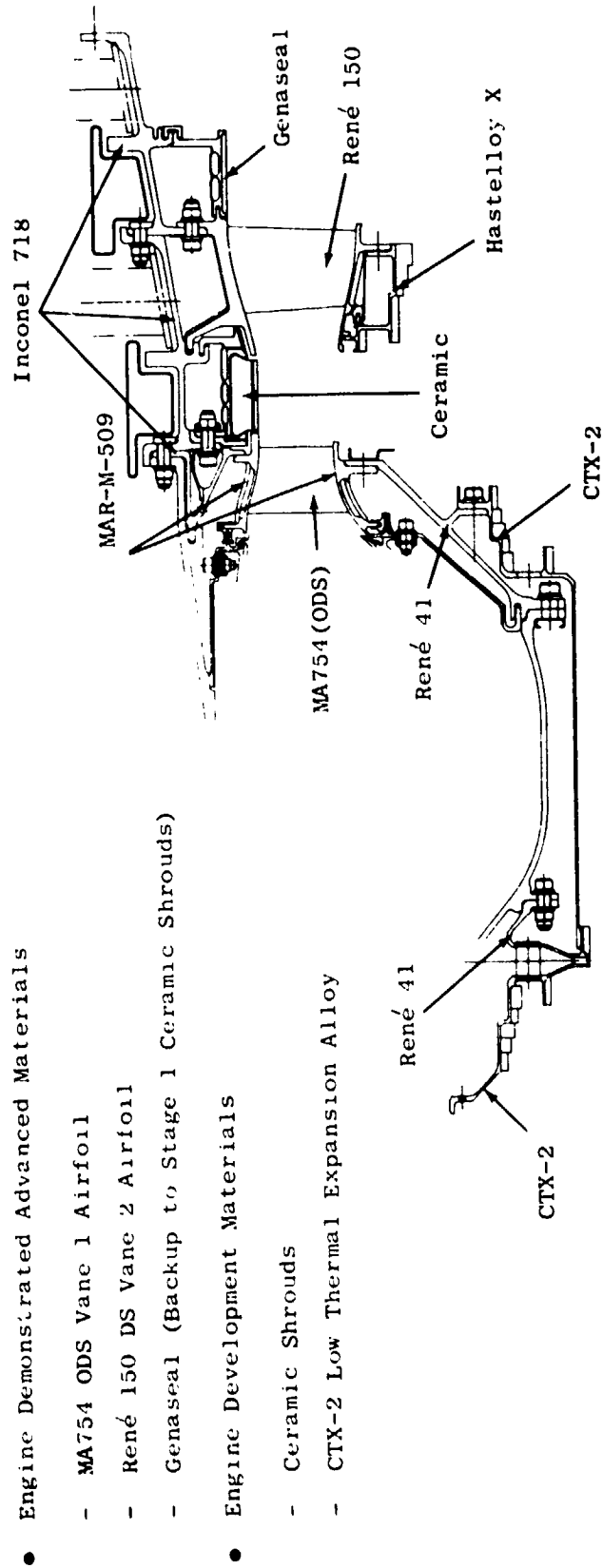


Figure 34. E³ HF Turbine Materials, Rotating Components.



- Engine Demonstrated Advanced Materials
 - MA754 ODS Vane 1 Airfoil
 - René 150 DS Vane 2 Airfoil
 - Genaseal (Backup to Stage 1 Ceramic Shrouds)
- Engine Development Materials
 - Ceramic Shrouds
 - CTX-2 Low Thermal Expansion Alloy

Figure 35. E³ HPT Materials - Static Components.

Hastelloy X Honeycomb Stations and Seals, Typical

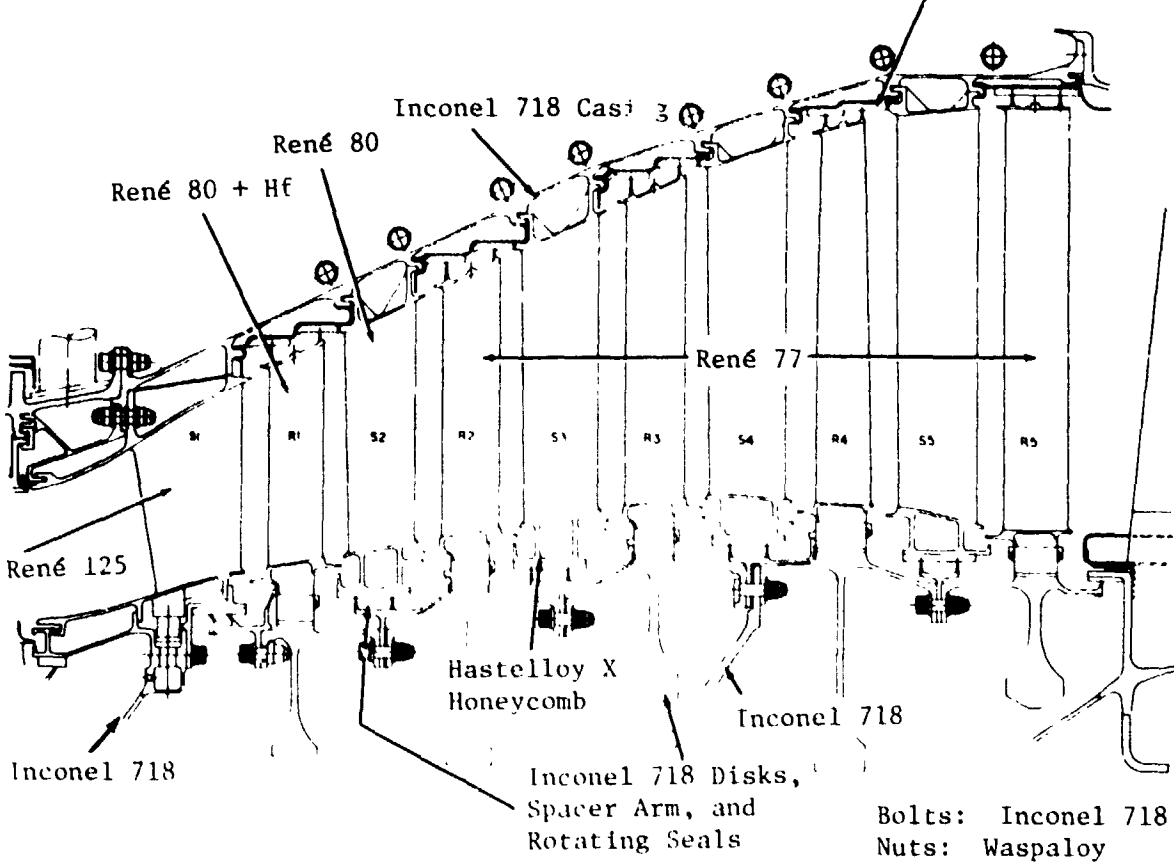


Figure 36. Low Pressure Turbine Materials.

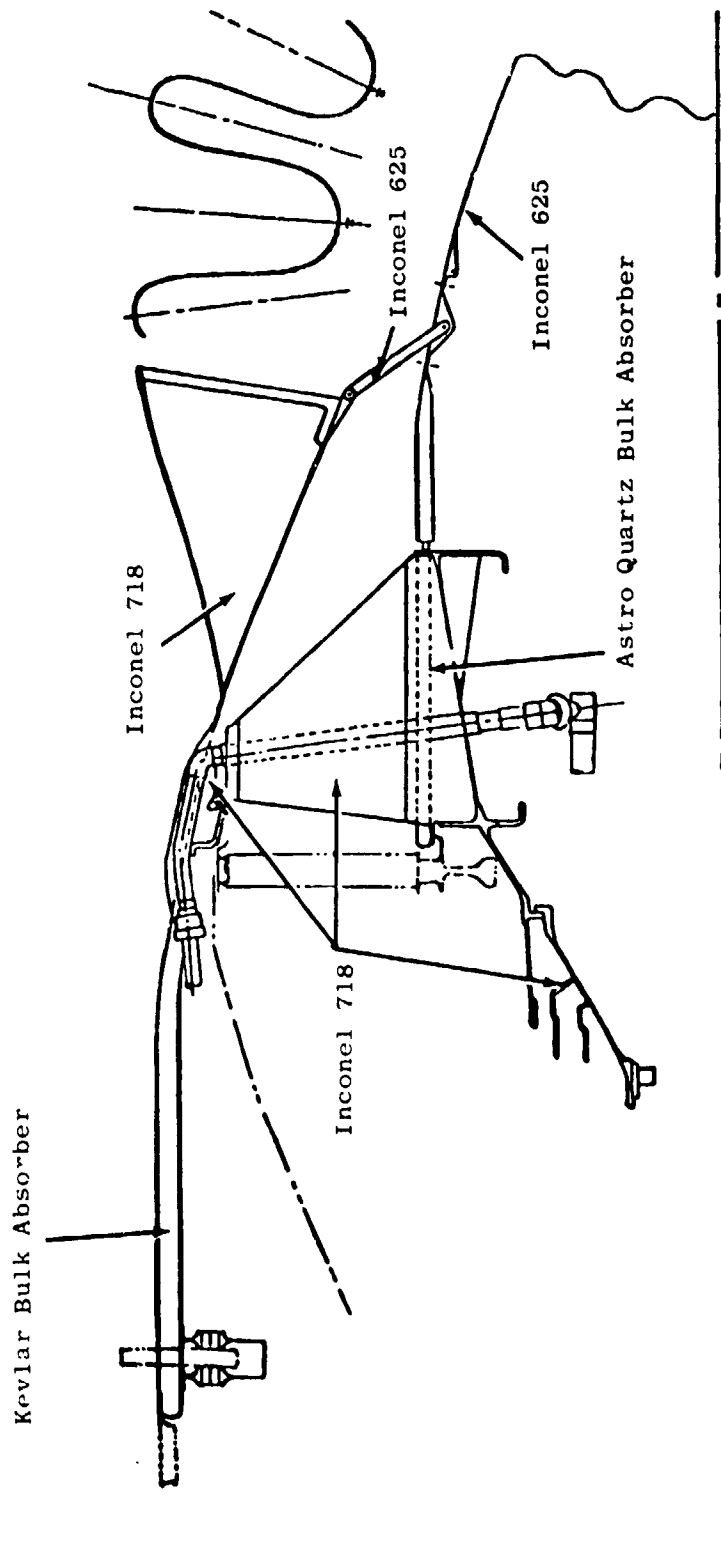


Figure 37. Mixer and Turbine Frame.

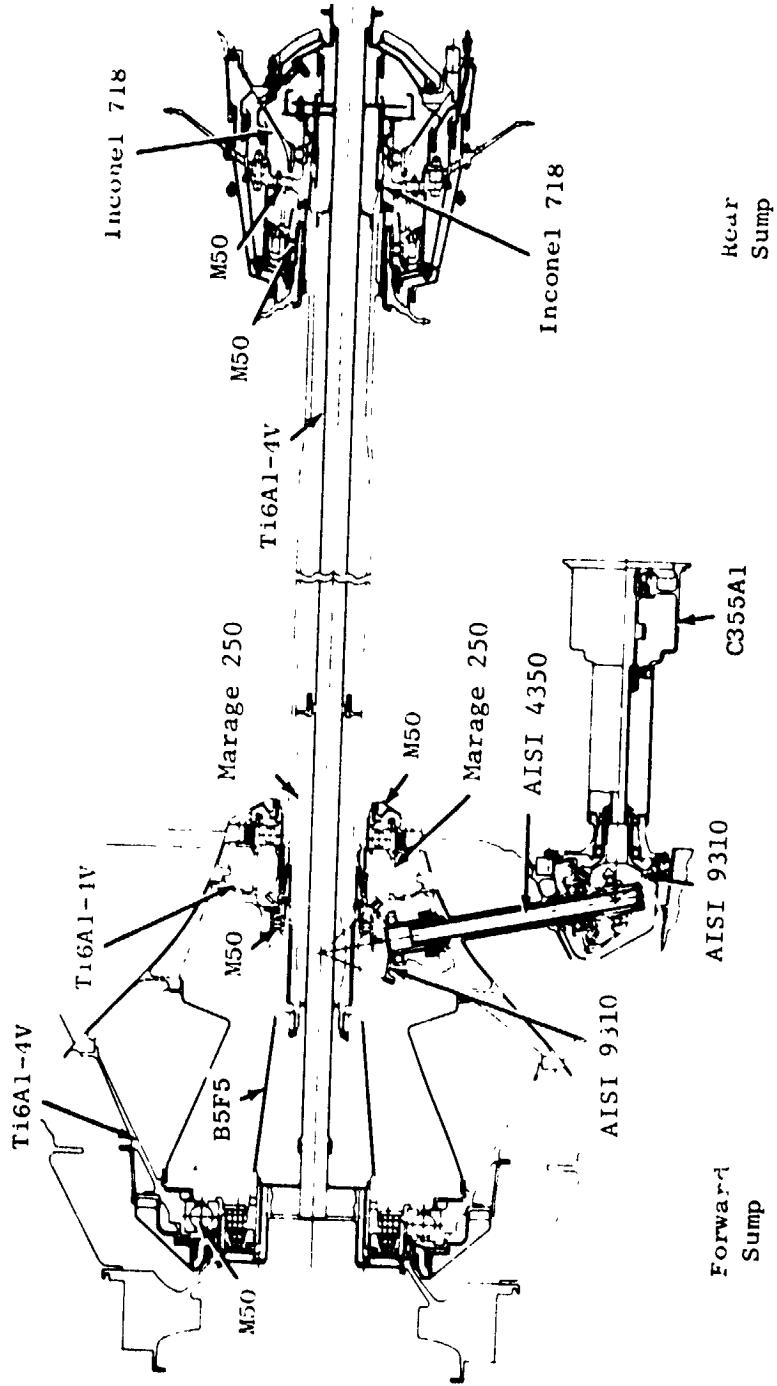


Figure 38. Bearings, Seals, Drives and Shafting.

Alloy Mechanical Behavior Program - This program defines and evaluates critical material behavior needed for the successful application of René 150 and Inconel Alloy MA754 to E³ blades and vanes. Rupture testing will be carried out to determine thin-wall and coating effects on René 150 under E³ conditions, and complex fatigue effects covering hold times, coatings, combined thermal and mechanical cycling, and cooling-hole geometries will be done on Inconel Alloy MA754 and René 150.

Disk Alloy Mechanical Behavior Program - This program is to evaluate as-HIP René 95 and AF115 fatigue and cyclic crack-growth rate behavior for engine conditions and compare to existing data for these and other disk alloys. Variables include temperatures, processing imperfections, hold-time effects, notch sensitivity, and strain ratio.

These supporting technology programs are primarily intended to evaluate the materials/processes in those areas of high risk in materials and processing technology. These areas include:

- Ceramic Shrouds
- Powder Metals (René 95, AF115) LCF Capabilities
- Thermal-Barrier Coatings
- High Temperature VSV Applications

The overall breakdown into specific alloy families is as follows:

<u>Alloy Base</u>	<u>% Installed Engine Weight</u>
Composites	20
Aluminum	10
Titanium	16
Iron	17
Nickel	36
Cobalt	1

In comparison with current engines, the FPS will replace a significant amount of aluminum with lightweight composites.

3.5 ACOUSTICS

3.5.1 Acoustic Considerations

Recent modifications by the FAA to the FAR Part 36 noise regulations have significantly reduced the current noise limits for the next generation of commercial aircraft. In light of such changes, engines must be designed employing advanced acoustic technology for these new-generation aircraft.

The primary objectives of the E³ acoustics program are the acoustic design and demonstration of an advanced engine which will meet FAR Part 36 (1978) with a minimum margin of three Effective Perceived Noise decibels (EPNdB) at each monitoring condition on an advanced aircraft. To ensure that this objective is achieved, the acoustics program will monitor the design and development of each major engine component and incorporate advanced, low-noise, design features consistent with program performance goals. In addition, supporting component-test programs are in place to evaluate the integral vane-frame design and the mixer from an acoustic point of view.

Results to date indicate that, based on the scale-model vane-frame test, the integral vane-frame design will not cause increased forward-radiated fan tone levels due to the near-unity blade/vane ratio source (Reference 7). This result is particularly significant since it allows the use of the light-weight integral vane-frame, rather than the heavier conventional rotor-OGV-strut design, with no penalty to total system noise.

Estimates of the flight system noise levels for typical twin-jets, tri-jets, and quadjets, powered by the advanced energy efficient engine, show that all aircraft achieve the program objective of FAR36 (1978) with a 3-EPNdB margin at each measurement point.

The acoustic design of the Energy Efficient Engine is summarized in Figure 39; pertinent low noise design features include:

- High Bypass Ratio
- Low-Velocity, Mixed-Flow Jet
- Moderate Tip-Speed Fan
- Integral Vane-Frame with Long Blade-to-Vane Spacing
- Long-Duct Nacelle
- Reduced Turbine Source Noise
- Advanced Bulk Absorber Acoustic Treatment

The acoustic design evolved as the detailed characteristics of the advanced study aircraft became better defined (References 1 and 3). System noise studies were carried out in such areas as fan inlet and LPT to evaluate various methods of reducing total system noise and permit the various advanced engine aircraft systems to meet the program objective.

3.5.2 Component Design Features

The bulk absorber acoustic treatment was chosen because the suppression characteristics are superior to conventional, resonator designs. The extensive General Electric experience in this field, as shown in Tables 19 and 20, permitted the bulk absorber to be selected with confidence. Table 19 shows

- **Advanced Bulk Absorber Treatment**

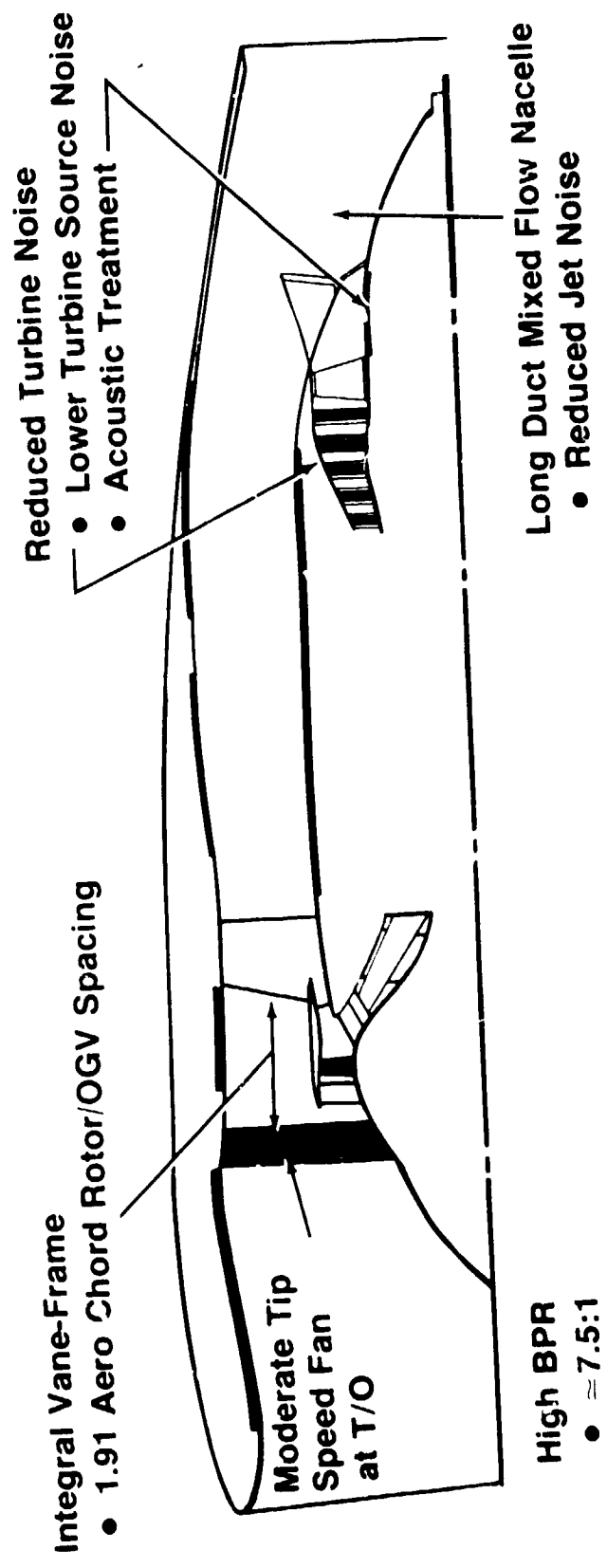


Figure 39. Energy Efficient Engine - Low Noise Design Features.

engine test experience and planned testing with bulk absorbers. In support of the engine tests, special laboratory testing has been conducted to evaluate the mechanical acceptability of both low and high temperature bulk absorber material. Table 20 lists some of the tests conducted during previous programs.

Table 19. Bulk Absorber Treatment Development Highlights.

1974	Bulk Absorber Development Initiated at General Electric for Inlet Environment
1975	Bulk Absorber Development Initiated for Fan and Core Exhaust Applications
1976	Engine Endurance Testing Initiated
1977	Additional Component Tests and Continuation of Engine Endurance Testing
1982	Demonstrate Flight-Weight Astroquartz and Kevlar Acoustic Treatment Panels During E ³ Integrated-Core/Low-Spool (ICLS) Testing

Table 20. Bulk Absorber Testing Experience.

Component Test	Low Temperature	High Temperature
Freeze-Thaw	X	X
Panel Damping	X	X
Mechanical Vibration	X	X
Contamination	X	
Engine Exhaust	X	X
Acoustic Fatigue	X	
Braze Contamination		X
Hot Start		X
Liquid Repellancy/Retention	X	
Engine Test		
Test Panel Construction	X	X
Engine Environment	X	X

Figure 40 shows a comparison of the integral vane-frame design and a conventional fan frame design. Due to the near-unity vane-blade ratio of the integral vane-frame, the rotor-stator wake-interaction source is cut-on; that is, the source will propagate. It was necessary, therefore, to evaluate the impact on fan-radiated noise under simulated flight conditions of the integral vane-frame relative to a conventional OGV-strut design. A series of tests, using a scale-model rotor, was conducted to evaluate the contribution due to the cut-on rotor-stator noise source. The rotor-turbulence source, that controls the fan fundamental tone under static conditions, was removed by using a Turbulence Control Structure (TCS), shown in Figure 41. This device reduces the in-flow turbulence levels and the resulting rotor-turbulence noise. Figure 42 shows results of these tests at two typical fan speeds. The E³ vane-frame was shown to be essentially equivalent, on a PNdB basis, to the conventional frame in terms of forward-radiated fan noise. Aft-radiated fan noise will be evaluated at a later date by comparing acoustic-probe data for the two configurations.

Initial flight-noise estimates for advanced aircraft powered by the FPS were made using the methodology outlined in Table 21. Specifically, the flight effects accounted for include:

- Atmospheric absorption
- Inverse square law
- Jet relative-velocity effects
- Dynamic effect
- Flight "cleanup" of fan tones
- Turbulence scattering
- Ground-reflection corrections

The resultant system Effective Perceived Noise Level (EPNL) levels, including the effects listed above, indicated that at approach the system goal of FAR 6 (1978) minus 3 EPNdB could not be achieved without reducing fan-inlet and turbine-related noise. Figure 43 shows a breakdown of component noise contributions for a typical trijet at approach power. Several studies were undertaken to evaluate ways of reducing fan-inlet and turbine noise, as well as jet noise and fan-exhaust noise. Table 22 lists these studies.

Results showed that the system goal of FAR36 (1978) minus 3 EPNdB is achievable with a slight improvement in inlet-treatment effectiveness and a 6-PNdB reduction in turbine noise.

Several approaches to turbine-noise reduction were evaluated (Table 23). These included using a higher number of blades to drive the tone frequency into a less annoying region, increased rotor-stator spacing, acoustic treatment, and reduced loading on the dominant stage. Evaluation of each concept

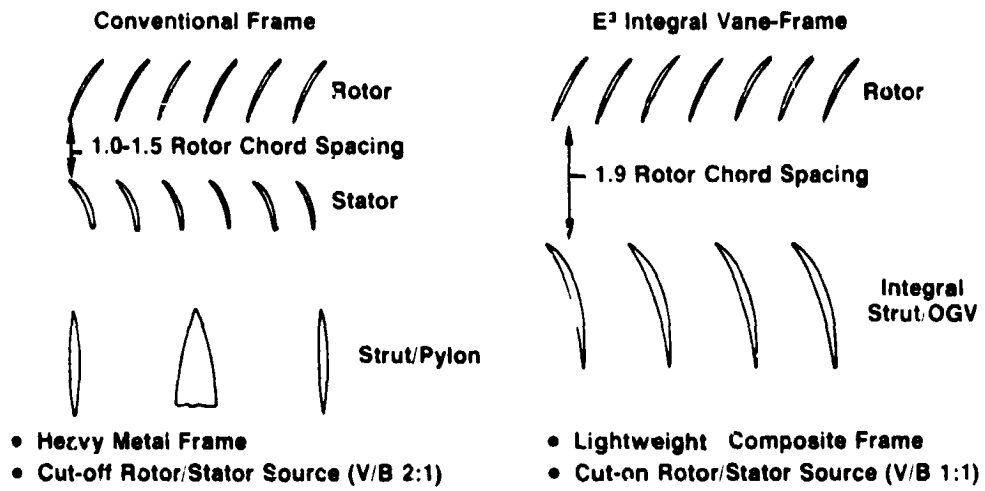


Figure 40. Fan Frame Acoustic Evaluation.

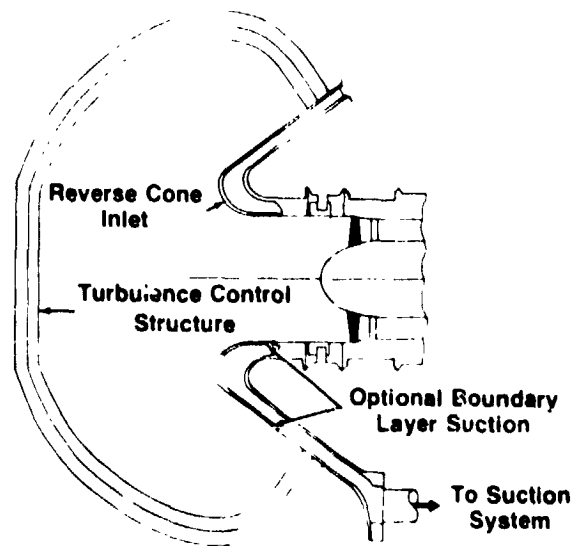


Figure 41. Turbulene Control Structure and Test Setup.

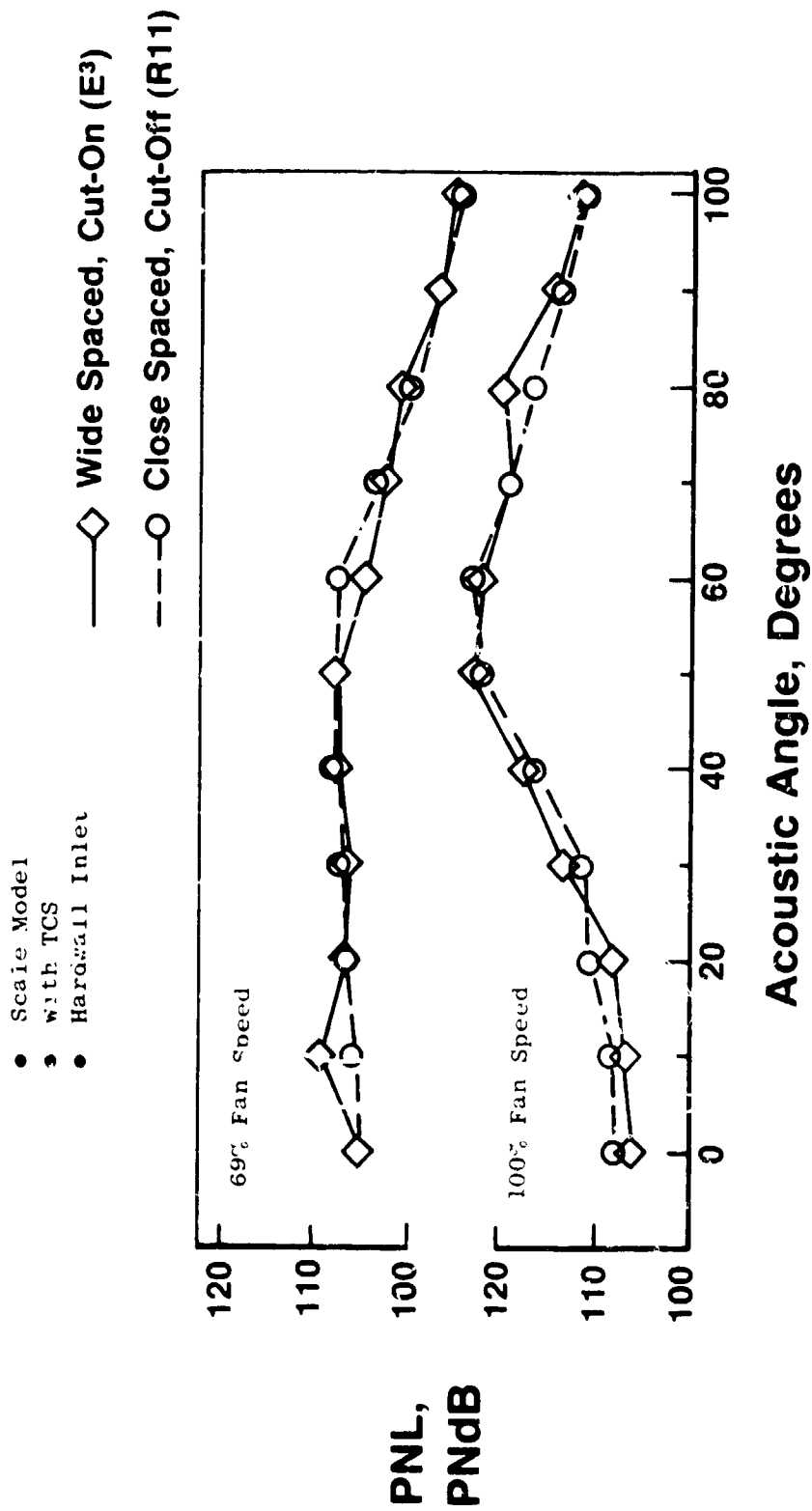


Figure 12. Effect of Cut-On Vane-Frame at Wide Spacing.

- Initial FPS Design
- Approach Power
- Lockheed Trijet

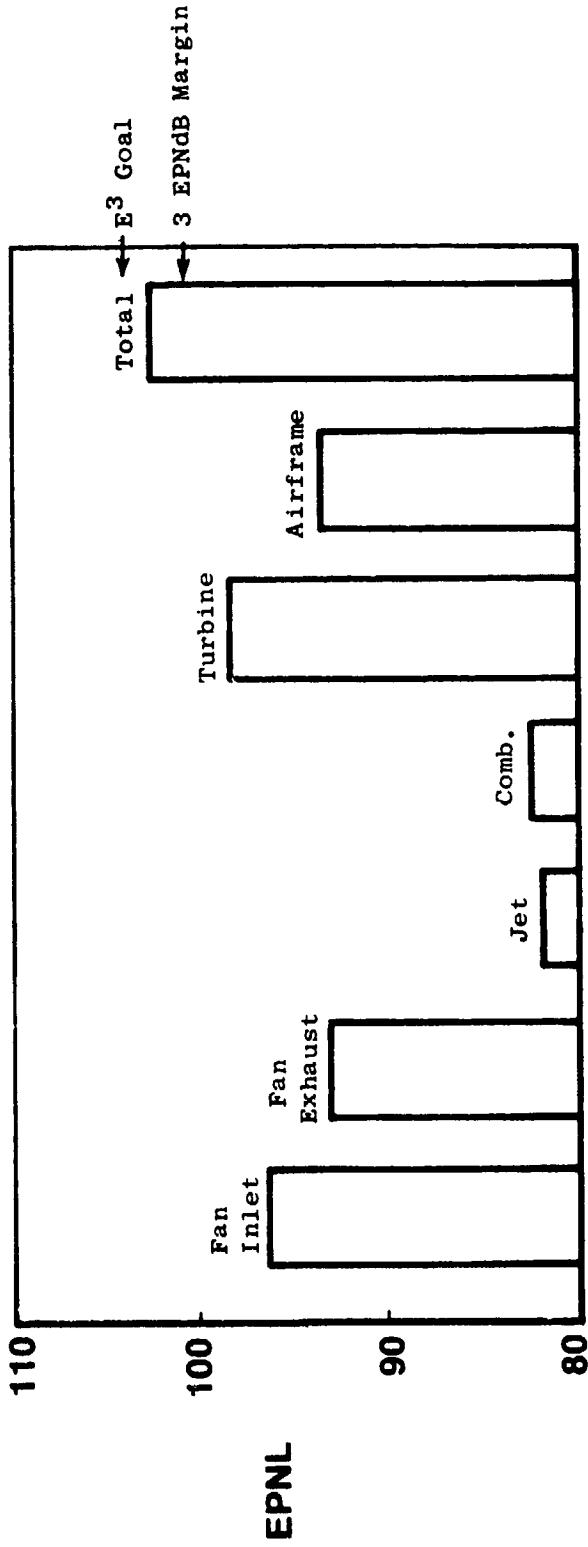


Figure 43. E³ Component Noise Levels.

C-2

Table 21. Acoustic Prediction Methodology.

Static Component Sources Predicted by Scaling Existing Data or Using Semiempirical Prediction Method



Extrapolate Static Components to Flight; Adjust for Flight Effects



Acoustic Treatment Effects Applied to Appropriate Source



Components Summed to Produce Total Spectra at Each Angle



System EPNL Calculated Using Resultant PNL Vs. Time History

Table 22. E³ System Noise-Reduction Studies.

Fan Inlet	Longer Inlet, ($L_T/D \approx 1.0$) Improved Inlet Suppression Hybrid Inlet (Takeoff Power Only)
Fan Exhaust	Common Nozzle Outer Wall Acoustic Treatment (Approach Only)
Turbine	Turbine Noise Reduction
Jet Noise	Variable-Area Nozzle

Table 23. E3 LPT Noise-Reduction Options.

• Six-PNdB Reduction Required

Option	Potential Noise Reduction Δ PNdB	Design Effects	ADOC, [*] %
1. 20% Aerodynamic Loading Reduction on 4th Stage	1.0 - 1.5	-0.17 Points in LPT Efficiency	+0.05
2. Increased Spacing Between 4th Stage Stator and Rotor, =2.5 cm (1 in.)	2.5 - 4.0	+18.1 kg (+40 lb) Weight \$1000 Cost	+0.06
3. Increased Blade Number** in 4th Stage (112 → 156)	5.0	\$2300 Cost	+0.01
4. Added Acoustic Treatment	1.0 - 1.5	Selected Approach 6.0 - 6.5 PNdB Reduction +2.3 kg (+5 lb) Weight \$6000 Cost	+0.04

*A System Benefit Results when ADOC is Negative.

**Includes Benefit for Improved Spacing Due to Reduced Chord.

and various combinations led to the final design choice: a combination of high blade number and acoustic treatment. This design produces the desired 6-PNdB reduction with no performance penalty and the smallest DOC penalty to the system. Figure 44 shows the improvement in total system noise, at approach, due to the reduced fan-inlet and turbine noise components. These improvements provided the required 3-EPNdB margin at each measuring point of FAR36 (1978).

Using the results of the various component-noise-reduction studies, the flight-noise levels for various advanced aircraft powered by the FPS were estimated. The aircraft performance characteristics, including airframe noise at approach, were provided by the Boeing Commercial Aircraft Company, the Lockheed Aircraft Company, and the McDonnell-Douglas Aircraft Company as part of subcontracts to the overall E³ Program (Reference 1). These aircraft therefore represent a wide spectrum of design philosophies and a cross section of the anticipated future needs of the commercial aircraft market. Table 24 shows the resultant system-noise levels for each aircraft and the associated margin relative to FAR36 (1978); all aircraft meet FAR36 (1978) with at least 3-EPNdB margin at each point.

In conclusion, incorporation of advanced, low-noise-design features (including bulk absorber acoustic treatment, reduced turbine noise, and integral vane-frame) permit advanced aircraft powered by the NASA/General Electric Energy Efficient Engine to meet the FAR36 (1978) noise-regulation goal with a 3-EPNdB margin.

3.6 PROPULSION-SYSTEM/AIRCRAFT INTEGRATION

A significant portion of the FPS preliminary analysis design was the evaluation of the benefits of the installed system in an advanced aircraft. Assessments were made in terms of acoustic, fuel burn, and economic advantages relative to a suitably scaled CF6-50C reference engine installed in the same aircraft. This section presents a summary of the results of the aircraft-integration studies; more detailed discussion will be presented in the Aircraft Integration report (Reference 8). The subcontractor's (airframe companies) reports will be included as appendixes to the Aircraft Integration report.

Aircraft integration effort was intended to ensure consistency of the E³ FPS design with the anticipated requirements of advanced commercial aircraft in the late 1980's to early 1990's. For this purpose, subcontracts were established with the Boeing, McDonnell-Douglas, and Lockheed Aircraft Companies. Using appropriate projections of their advanced-transport designs, the aircraft companies evaluated the E³ FPS against the baseline CF6-50C current-technology engine to determine the advantage offered by E³ technology in mission fuel consumption. The advantage in DOC due to E³ technology was then evaluated by General Electric, using calculation procedures coordinated by NASA, to ensure a consistent evaluation for all the aircraft that were studied.

- FPS Baseline
- Δ EPNdB

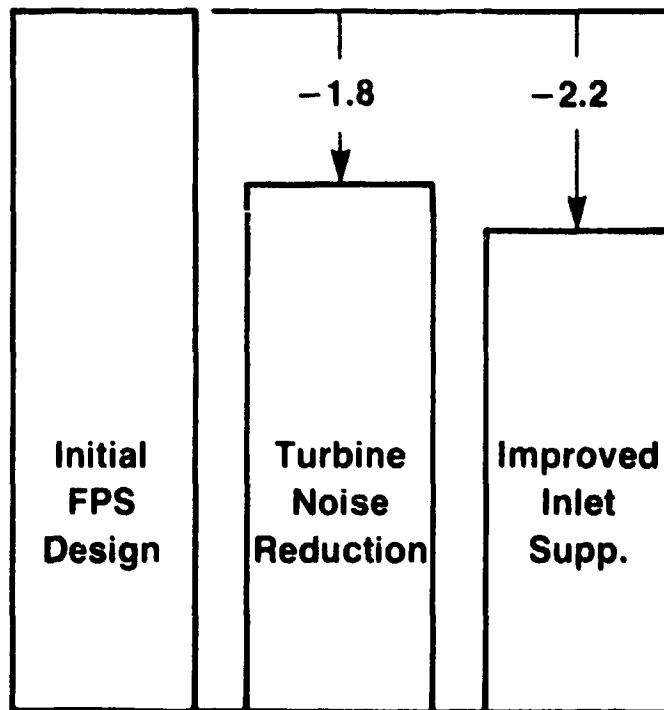


Figure 44. E³ System Noise Reduction Studies - Approach.

Table 24. Flight Noise Estimates for E³ Advanced Aircraft.

	Boeing Twin Jet	Lockheed Trijet	Lockheed Quadjet	Douglas Trijet
TOGW, kg (1bm)	110,524 (243,660)	205,416 (452,857)	284,335 (626,841)	225,370 (496,850)
SLS F _n , N (lbf)	167,734 (37,710)	181,287 (40,757)	167,988 (37,767)	183,391 (41,230)
<u>Takeoff</u>				
Level, EPNdB	88.7	93.7	98.3	94.4
Margin Re: FAR 36 (1978)	-5.0	-6.7	-5.9	-6.5
<u>Sideline</u>				
Level, EPNdB	89.0	91.6	92.8	92.2
Margin Re: FAR 36 (1978)	-9.2	-8.9	-8.9	-8.7
<u>Approach (With A/F Noise)</u>				
Level, EPNdB	98.9	100.1	100.4	97.2
Margin Re: FAR 36 (1978)	-3.0	-3.9	-4.6	-7.3
<u>Airframe Supplied (Aircraft Noise)</u>				
Level, EPNdB	93.2	95.9	96.0	92.3

In addition to the direct mission economic evaluations that were performed, the aircraft company subcontracts provided for review and critique of the nacelle design including inlet and afterbody aerodynamics, engine mounting, accessory gearbox arrangement, and thrust reverser and cowling mechanical design. Results of this effort will be discussed in Section 4.9, Nacelle Design.

As part of the aircraft integration evaluation, it is planned to conduct a series of coupled wing/nacelle-drag tests at the NASA Langley wind tunnel under the direction of Dr. Richard Whitcomb. Testing is planned for a series of CF6-50C nacelle configurations (including the reference configuration) and a representation of the FPS long-duct, mixed-flow nacelle. Various wing-to-nacelle spacings will be tested to obtain the lowest possible interference-drag penalties. As mentioned in Section 3.2, part of the anticipated installed sfc advantage of the FPS over the CF6-50C is attributed to an estimated 0.6% drag reduction. The Langley testing should verify if this reduction is attainable.

3.6.1 Aircraft Company Subcontracts

The subcontracts with Boeing, McDonnell-Douglas, and Lockheed called for the evaluation of the E³ FPS and the baseline CF6-50C, appropriately scaled in thrust size, on advanced commercial-transport designs representative of each company's projections into the late 1980's - early 1990's. Boeing studied a twin-engine, 196-passenger airplane with a design range of 3704 km (2000 nmi). Douglas evaluated a three-engine, 458-passenger, advanced derivative of their DC-10 aircraft with a 5556-km (3000-nmi) design range. Lockheed studied two aircraft: a three-engine, 500-passenger aircraft with a 5556-km (3000-nmi) design range, and a four-engine, 500-passenger aircraft with a 12,038-km (6500-nmi) design range, both advanced derivatives of the L-1011 aircraft. All of the study aircraft incorporated advanced-technology features projected by the respective aircraft companies for commercial-transport studies in the late 1980's and early 1990's. Summary descriptions of the aircraft and advanced-technology features are shown in Figures 45 through 48 and Tables 25 through 30.

The aircraft companies were provided with engine performance, weight, dimensions, price, and maintenance-cost data for the baseline CF6-50C and the E³ along with data to permit scaling both engines to match the different power requirements of the aircraft. They performed sizing and mission evaluations for each aircraft at design payload/range and for off-design payload/range combinations selected as typical by each aircraft company. These results in turn were used as input to the economic analysis performed by General Electric. The E³ FPS evaluations were made with and without the 1% improvement in long-term average sfc due to improved performance retention. This 1% improvement is based on the reduced deterioration schedule for the FPS (Figure 28). Results of the aircraft company evaluations are shown in Table 31 and Figure 49. These show an improvement in mission block fuel consumption of 14.5% to 22.9%, depending on range and credit for improved performance retention.

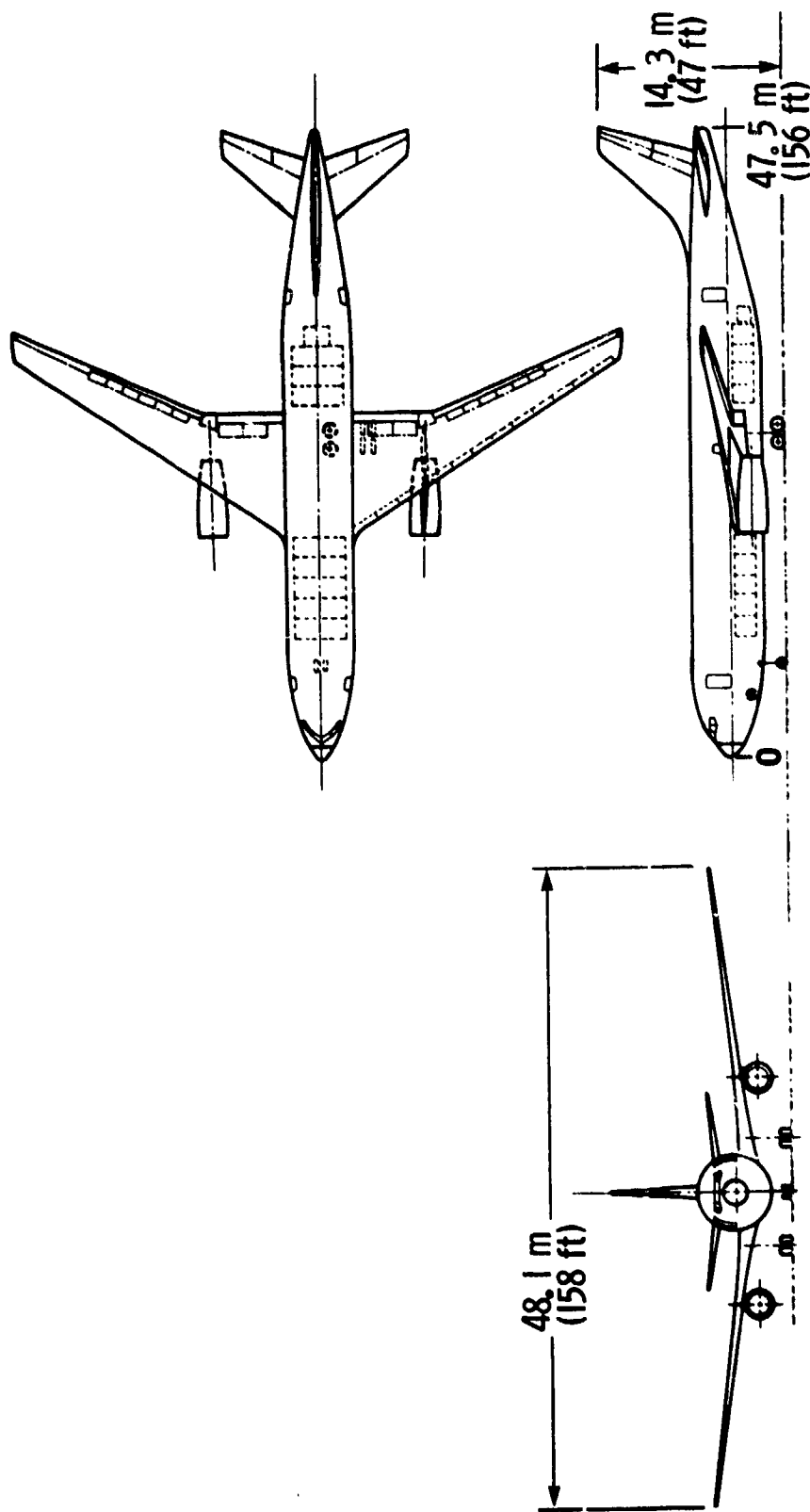


Figure 45. Energy Efficient Engine, Model 768-868 Domestic Airplane (Boeing).

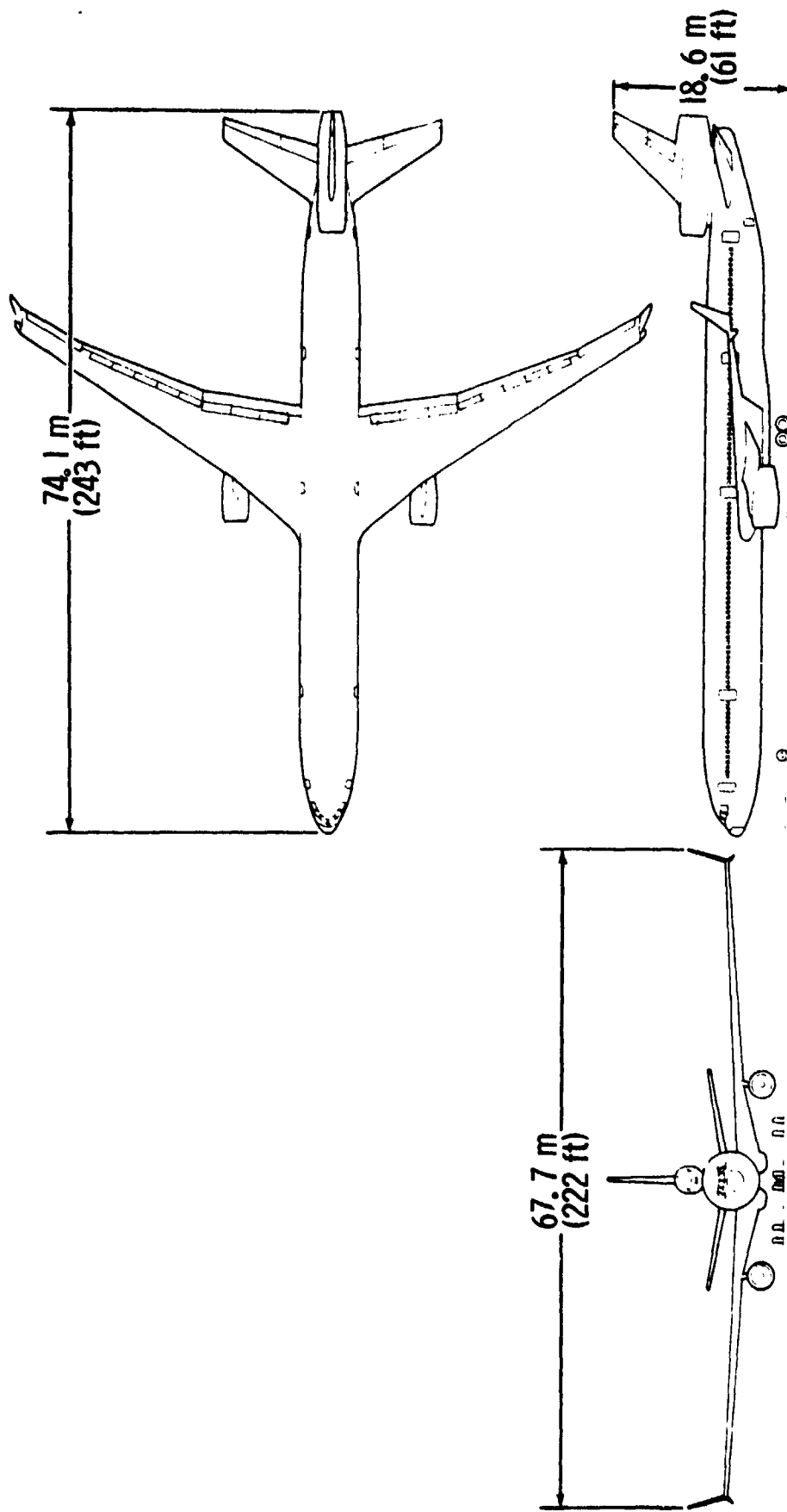


Figure 46. General Arrangement, Domestic Transcontinental Pange Version (McDonnell-Douglas).

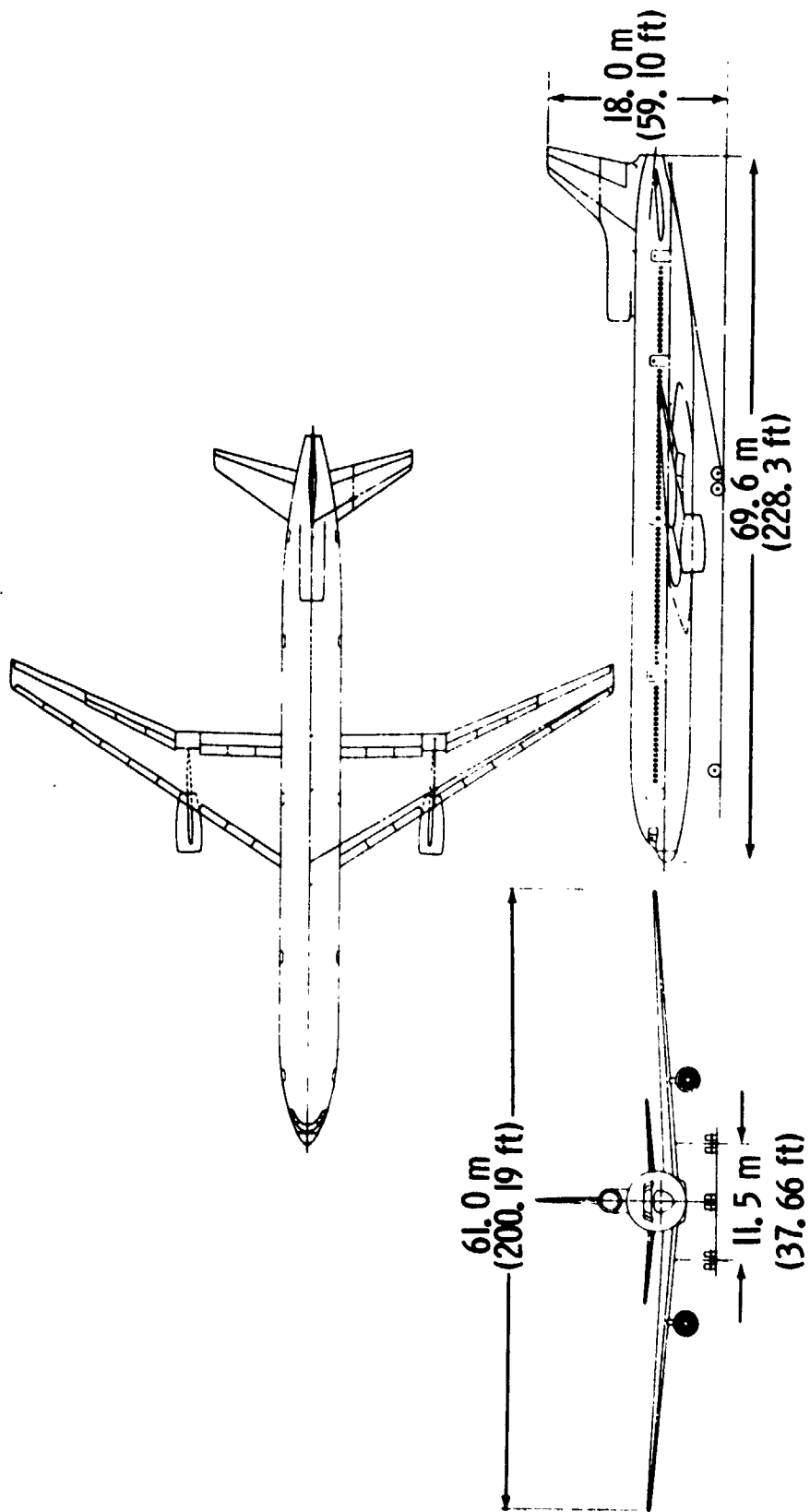


Figure 47. General Arrangement, Domestic Aircraft (Lockheed).

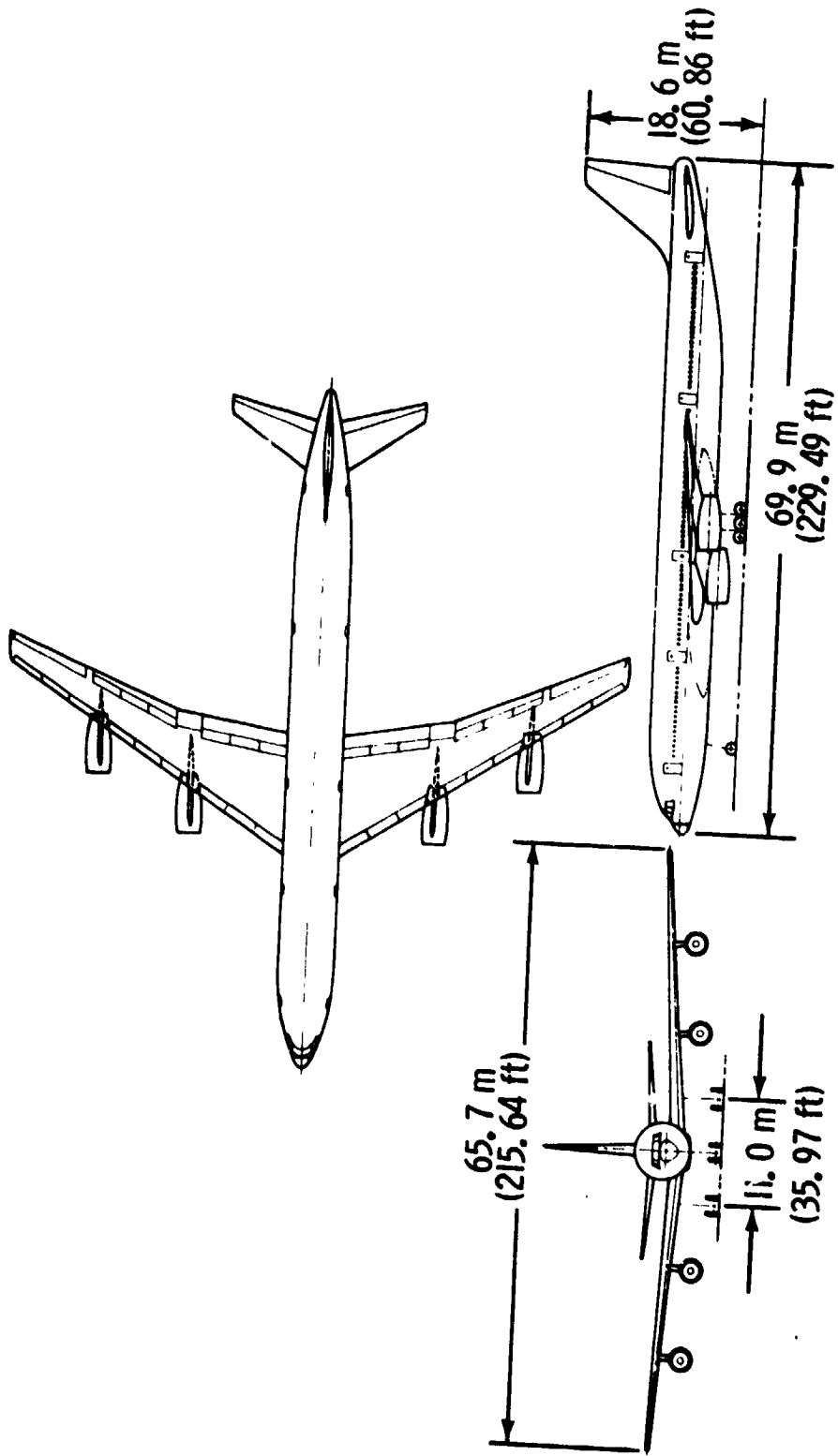


Figure 48. General Arrangement, Intercontinental Aircraft (Lockheed).

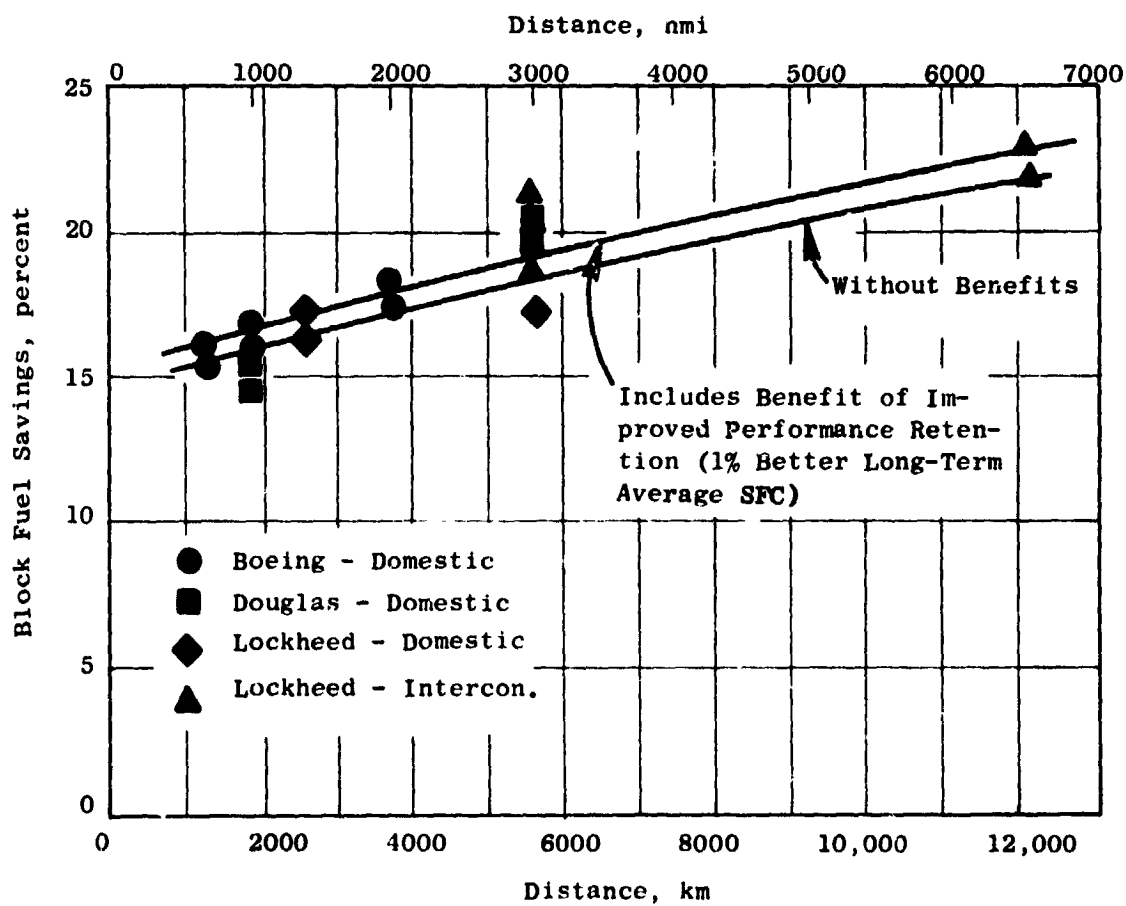


Figure 49. Block Fuel Savings (E^3 Engine Vs. CF6-50C).

Table 25. Advanced Technology Features (Boeing).

- **AERODYNAMIC TECHNOLOGY**
 - Advanced Airfoil/Wing Design
 - Wing/Strut/Nacelle Design for Favorable Interference between Wing, Nacelle, and Nozzle Pressure Field
 - Empennage Designed to Operate Efficiently in Complex Wing/Body Flow Field, Interference Free
 - Three-Position, Variable-Camber, Leading-Edge Flaps
 - Double-Slotted, Trailing-Edge Flaps
 - Aileron Droop
- **FLIGHT CONTROLS TECHNOLOGY**
 - All Axes Handling Qualities SAS
 - All Flying Tail
 - Double-Hinged Control Surfaces
- **SYSTEM TECHNOLOGY**
 - Conventional APU
 - Air-Cycle Cooling System
 - Cabin Air Reconstituted and Recirculated
 - Integrate TAI with ECS
 - Carbon Brakes and Limited-Slip Braking

NEW STRUCTURES TECHNOLOGY

- **ADVANCED COMPOSITE STRUCTURES**
 - All Control Surfaces
 - Landing Gear Doors
- **HIGH STRENGTH TITANIUM FITTINGS**
 - Landing Gear Support
 - Wing/Body Attachments
 - Empennage/Body Attachments
 - Engine and Strut Support Structure
 - Flap Support Fittings
- **ADVANCED ALUMINUM ALLOYS**
 - Wing Upper Surface
 - Wing Lower Surface
 - Wing Spars and Ribs
 - Wing Leading and Trailing Edges
 - Fuselage
 - Empennage

Table 26. Resulting Domestic Airplane Characteristics (Boeing).

Characteristic	Model 768-869 with Scaled CF6-50C Engine	Model 768-868 with Scaled FPS
Design Range, km (nmi)	3,704 (2,000)	3,704 (2,000)
Design Payload, Passengers/kg (lbm)	196/18,225 (40,180)	196/18,225 (40,180)
Number of Crew	3	3
Cruise Mach Number	0.80	0.80
Number of Engines	2	2
Performance	Base	-1.0
Retention Allowance, % Tsfc	168.9 (37,970)	168.3 (37,840)
Takeoff Thrust/Engine, kN (lbf) (Sea Level Static Without Bleed or HPX)	116,732 (257,350)	110,885 (244,460)
TOGW, kg (lbm)	73,001 (160,940)	71,786 (158,260)
Operating Weight Empty, kg (. lbm)	67,830 (149,540)	66,596 (146,820)
Manufacturer's Empty Weight, kg (lbm)	104,621 (230,650)	99,378 (219,090)
Maximum Landing Weight, kg (lbm)		
Block Fuel, kg (lbm)		
• At Design Range and Payload	18,928 (41,730)	15,463 (34,090)
• At 1852 km (1000 nmi), 108 Passengers	8,677 (19,130)	7,208 (15,890)
• At 1232 km (665 nmi), 108 Passengers	6,015 (13,260)	5,035 (11,100)
		168.7 (37,930)
		111,171 (245,090)
		71,885 (158,430)
		66,692 (147,030)
		99,636 (219,660)
		15,604 (34,400)
		7,276 (16,040)
		5,083 (11,205)

Table 27. McDonnell-Douglas Advanced Features.

Wing

- Supercritical Airfoils - Reduced Weight and Drag, Increased Lift Capability
- High Aspect Ratio - Reduced Induced Drag Decreases Both Fuel Burned and Thrust Required
- Winglets - Reduced Induced Drag Decreases Fuel Burned While Minimizing Span and Weight Increase

High-Lift System

- Variable-Camber Krueger - High Maximum Lift Capability With Modest Flap Deflections
- Two-Segment Flap - High Lift-to-Drag Ratio With Limited Flap Deflection Minimizes Thrust Required and Approach Noise

Composites

- Wing and Empennage Primary and Secondary Structure
 - Control Surfaces
 - Floor Beams
 - Landing Gear Doors
 - Fairings
 - Carbon Brakes
- } - Less Weight

Metals

- Bonded Structure
 - Improved Alloys
- } - Less Weight

Other

- Longitudinal-Stability - Smaller Empennage Results in Less Drag and Reduced Weight
- Wing Load Alleviation - Reduced Wing Bending Loads Result in Reduced Weight
- Digital Avionics - Reduced Weight and Improved Reliability
- Flight Performance - Reduced Operational Fuel Consumption Management
- Advanced Cockpit Displays - Reduced Weight, Improved Performance
- Air Conditioning - Less Engine Bleed
- APU - Reduced Weight and Fuel Consumption

Table 28. McDonnell-Douglas Comparison of Characteristics.

Engine	Scaled CF6-50C	Advanced
Engine Thrust Size, kN/Engine (lbf/Engine)	198.5 (44,630)	184.7 (41,520)
Wing Area, m ² (ft ²)	482.2 (5,190)	436.6 (4,700)
Weights - Maximum Takeoff, kg (lbm)	244,486 (539,000)	227,703 (502,000)
- Operator's Empty, kg (lbm)	137,547 (303,240)	132,531 (292,180)
Cruise Mach Number	0.80	0.80
Takeoff Field Length, m (ft) MTOW, SL 29° C (84° F)	2130 (6,900)	2256 (7,400)
Approach Speed, km/hr-EAS (knots-EAS) Passengers, Baggage, Reserves	222 (120)	230 (124)
Thrust-Limited Initial Cruise Altitude, km (ft)	10.1 (33,000)	10.1 (33,000)
Buffet-Limited Initial Cruise Altitude, km (ft)	11.3 (37,100)	11.1 (36,500)

- Engines Sized by Thrust-Limited ICA = 10.1 km (33,000 ft)
- Wing Sized by 9.4 km (31,000 ft) Buffet-Limited ICA of Intercontinental Aircraft

Table 29. Airframe Advanced Technologies (Lockheed).

Supercritical Wing

- 2% Reduction in Wing Weight with AR = 10, t/c = 13%

Active Controls (Load Relief, Relaxed Stability)

- -5.5% Wing Height
- -1.0% Body Weight
- -28% Tail Size

Advanced Composites (Primary and Secondary)

- -8.7% MEW - Domestic
- -9.2% MEW - Intercontinental

Net Benefit

- -10% MEW - Domestic
- -10.5% MEW - Intercontinental

Table 30. 1990's Aircraft (Lockheed).

Mission	Domestic		Intercontinental	
Design Range, km (nmi)	5,556	(3,000)	12,038	(6,500)
Cruise Mach Number	0.8		0.8	
Initial Cruise Altitude, km (ft)	11.3	(37,000)	10.4	(34,000)
Field Length, m (ft)	2,121	(6,958)	2,883	(9,459)
No. Pax	500		500	
Gross Weight, kg (lbm)	206,529	(455,319)	285,511	(629,443)
Empty Weight, kg (lbm)	116,895	(257,710)	129,622	(285,767)
Engine Thrust (SLTO), kN (lbf)	182.3	(40,978)	168.7	(37,925)
Typical Range, km (nmi)	2,593	(1,400)	5,556	(3,000)
Typical Load Factor, %	55		55	

Table 31. Economic Benefits, Block Fuel.

Aircraft	Mission	Range km (nmi)	Without Performance Retention % Δ Block Fuel	With Performance Retention % Δ block Fuel
Boeing Twin Fan	Design	3704 (2000)	-17.6	-18.3
	Typical	1852 (1000)	-16.2	-16.9
	Typical	1232 (665)	-15.5	-16.3
Douglas Trifan	Design	5556 (3000)	-19.5	-20.5
	Typical	1852 (1000)	-14.5	-15.4
Lockheed Trifan	Design	5556 (3000)	-17.3	-18.3
	Typical	2593 (1400)	-16.3	-17.3
Lockheed Quadfan	Design	12038 (6500)	-21.7	-22.9
	Typical	5556 (3000)	-20.1	-21.2

3.6.2 Economic Studies

The results of the aircraft company mission evaluations were used as input to a DOC analysis. The ground rules were established under NASA coordination to provide a consistent comparison of E³ versus CF6-50C technology for all the different aircraft that were studied. The study groundrules, which drew heavily from the Boeing Company economic method for evaluating operating costs, are summarized on the following page:

<u>Element</u>	<u>Calculation Method</u>
Price Escalation	All costs in 1977 dollars.
Flight Crew Cost	Boeing 1977 method. Three-man crew for all flights.
Fuel	\$105.68/m ³ (40 ¢ per gallon) Domestic, \$118.79/m ³ (45 ¢ per gallon) International.
Aircraft Price	Table 32.
Block Time	Boeing 1977 method.
Insurance	0.5%.
Aircraft Maintenance	Boeing 1977 method. Include nacelle in airframe maintenance.
Maintenance Burden	200% on labor only, airframe and engine.
Engine Maintenance	General Electric methods based upon mature engine - no derates. Includes bare engine, engine accessories and reverser.
Depreciation	Straight line, 15 years to 10%.
Spares	Airframe 6%, engine 30% (total propulsion system including nacelle and reverser).
Utilization	Boeing 1977 method, as modified in December 1977, provides a constant number of trips per year as a function of range.
Ground Time	Domestic Trunk - 15 Minutes U.S. International - 20 Minutes
Fuel	Weight 802.7 kg/m ³ (6.71 lbm/gal).
Oil	Include oil cost at \$2,642/m ³ (\$10/gal), 970.4 kg/m ³ (8.1 lbm/gal) usage, 0.061 kg/hr/engine (0.135 lbm/hr/engine).
Airframe Weight	W _{AF} = O _{WE} - (bare engine + rev. + engine access. + nacelle).
Engine Maturity	All engines are mature.
Labor Rate	\$9.70/hr in 1977 \$.
Landing Fees	Not included in DOC.
Average Range	Typical mission range supplied by the airframe companies.
Average Load Factor	Load factor supplied by airframe companies.
Depreciation	Straight line, 15 years to 10% residual.
Interest	There are no borrowed funds.

NOTE: A 2% nonrevenue flight time shall apply to fuel and maintenance costs.

Major engine inputs to the DOC calculations included sfc, weight, engine price, and maintenance cost. Table 33 compares these parameters for the CF6-50C baseline engine and the E³. The E³ values are shown for the design size of 16,556 kg (36,500 lbm) takeoff thrust and scaled to the same max. climb thrust as the CF6-50C at 10, 668 m (35,000 ft)/Mach 0.8. In order to calculate mission DOC, these inputs were scaled to the thrust size required for each study aircraft.

The results of applying these rules to the aircraft mission evaluations are shown in Table 34 and Figure 50. These show DOC improvements of from 5.0% to 12.3% for the E³ technology over the current technology, depending on range and credit for improved performance retention.

Table 32. Airplane Pricing Functions.

Airplane Price = Bare Airframe + Furnishing + Avionics + Engines

BARE AIRFRAME PRICE

Current, New, and Derivative Wide Body = $0.5 (W_{af}/1000)^{0.7}$

$W_{af} = \text{OEW} - (\text{Bare Engine} + \text{Reverser} + \text{Engine Accessories} + \text{Nacelle})$

FURNISHING PRICE

Domestic Aircraft = $0.0080 N_{\text{seat}} - 0.284$

International Aircraft = $0.0089 N_{\text{seat}} - 0.315$

AVIONICS PRICE

Derivative and Wide Body Domestic = $0.0022 N_{\text{seat}} + 1.54$

Derivative and Wide Body Over Water = $0.0022 N_{\text{seat}} + 1.81$

Above Values in Millions 1977 \$

Table 33. Major Engine Input to DOC Analysis.

Engine	CF6-50	E3
Takeoff Thrust Size, kN (lbf)	223.5 (50,250)	162.4 (36,500)
Bare Engine Weight, kg (lbm)	3,946 (8,700)	3,289 (7,250)
Engine + Nacelle Weight, kg (lbm)	5,761 (12,700)	4,082 (9,000)
Engine Price, 1977 Dollars	2,281,000	2,533,000
Maintenance Materials, \$/EF hr*	51.00	28.05
Maintenance Labor, \$/EF hr*	15.50	12.73
Labor Burden (200%), \$/EF hr*	31.00	25.47
Total Maintenance, \$/EF hr*	97.50	66.25
		208.6 (46,000) (Scaled)**
		4,504 (9,930)
		5,511 (12,150)
		2,951,000
		31.70
		14.38
		28.78
		74.86

*Two-hour Mission, no Derate.

**Same Max. Climb Thrust at 10.7 km (35,000 ft) M 0.8, Installed as CF6-50C

Table 34. Economic Benefits, Direct Operating Cost (NASA-Coordinated Rules).

Aircraft	Mission	Range km (nmi)	Without Performance Retention Benefit % DOC	With Performance Retention Benefit % DOC
Boeing Twin Fan	Design	3704 (2000)	- 6.6	- 6.9
	Typical	1852 (1000)	- 5.4	- 5.7
	Typical	1232 (665)	- 5.0	- 5.3
Douglas Trifan	Design	5556 (3000)	- 9.0	- 9.5
	Typical	1852 (1000)	- 7.6	- 7.2
Lockheed Trifan	Design	5556 (3000)	- 7.4	- 8.0
	Typical	2593 (1400)	- 6.2	- 6.8
Lockheed Quadfan	Design	12038 (6500)	-11.6	-12.3
	Typical	5556 (3000)	- 9.9	-10.5

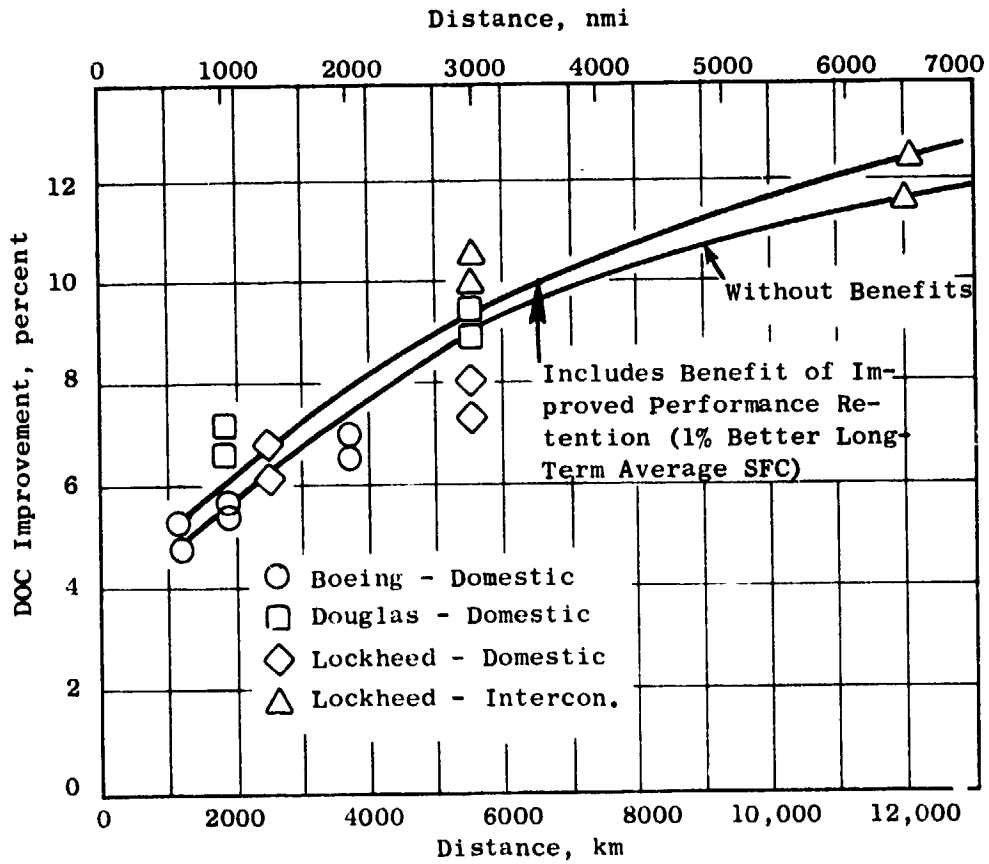


Figure 50. Direct Operating Cost (DOC) Improvement (E^3 Vs. CF6-50C).

4.0 COMPONENT PRELIMINARY ANALYSIS AND DESIGN

4.1 FAN

4.1.1 FPS Configuration

Figure 51 shows a cross section of the FPS fan configuration and a operating map. Changes in the fan configuration since the initial study (Reference 1) are primarily reducing the number of blades from 38 to 32 and lowering the radius of the part-span shroud from 70% span to approximately 55% span. This reduced-aspect-ratio blade provides improvements in blade ruggedness and aerodynamic efficiency that offset the increased weight of the fan.

The fan has an inlet-radius ratio of 0.342 and an average aspect ratio of 2.60. The flow is split by a quarter-stage island; 22.2% of the total fan flow passes under the island and is supercharged by the quarter-stage rotor. Before entering the core, the flow is further split with approximately 43% of the quarter-stage flow entering into the bypass stream. The flow that enters the core compressor has a pressure ratio of 1.67. The airflow that passes over the outer surface of the island mixes with the flow that is spilled from the quarter-stage to give an average total-pressure ratio of 1.65 at the bypass vane-frame exit.

The aerodynamic design point is maximum climb, but efficiency goals are referenced to the maximum cruise point: Mach No. = 0.8, Altitude = 10,688 m (35,000 ft). Fan parameters are as follows for maximum climb, maximum cruise, and takeoff power conditions:

Parameter	MxC1	MxCr	Takeoff
Corrected Speed, %	100	97.1	88.7
Bypass Stream Pressure Ratio	1.65	1.61	1.50
Core Stream Pressure Ratio	1.67	1.63	1.51
Bypass Ratio	6.8	6.9	7.3

Starting with the efficiency for a current technology fan in the E³ application and applying advancements incorporated into the E³ fan, an efficiency of 88.7 is projected as follows:

Current Technology Level	84.7
Improved Tip Clearance	+0.5
Improved Aero Design	+3.3
Booster Boundary Layer	-0.3
Lowered Part Span Shroud	+0.5
E ³ Fan Bypass Efficiency at Max. Cruise	88.7

Core stream efficiency is 0.892 at maximum cruise.

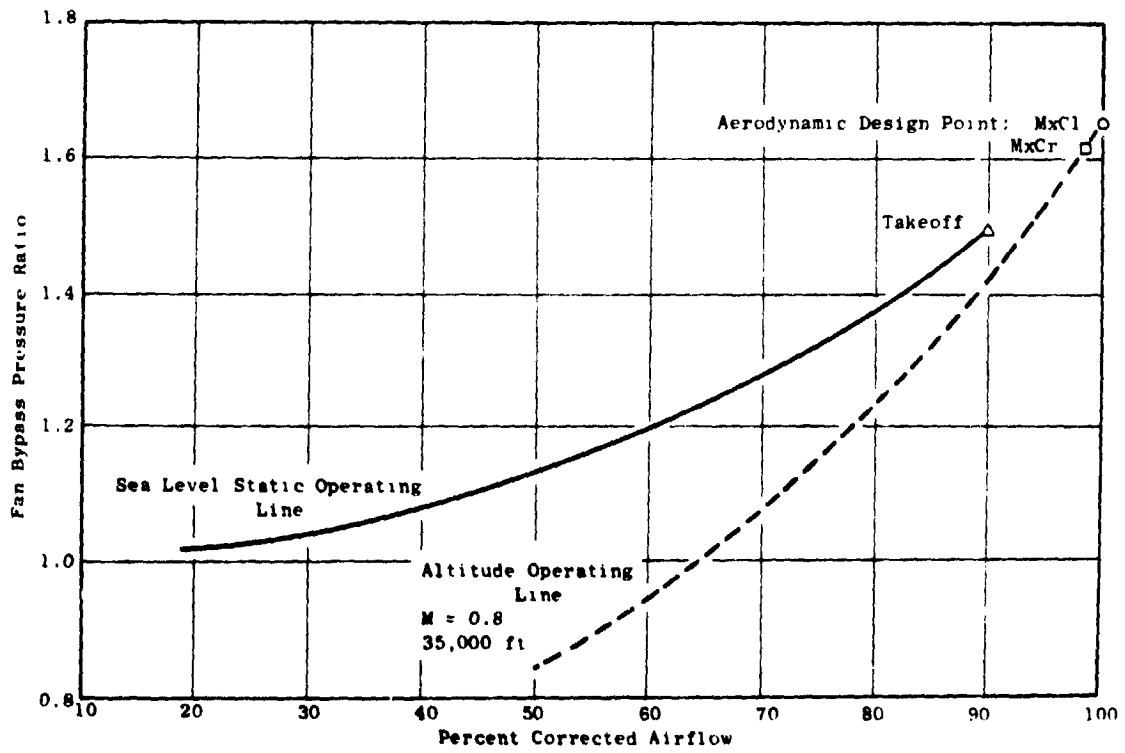
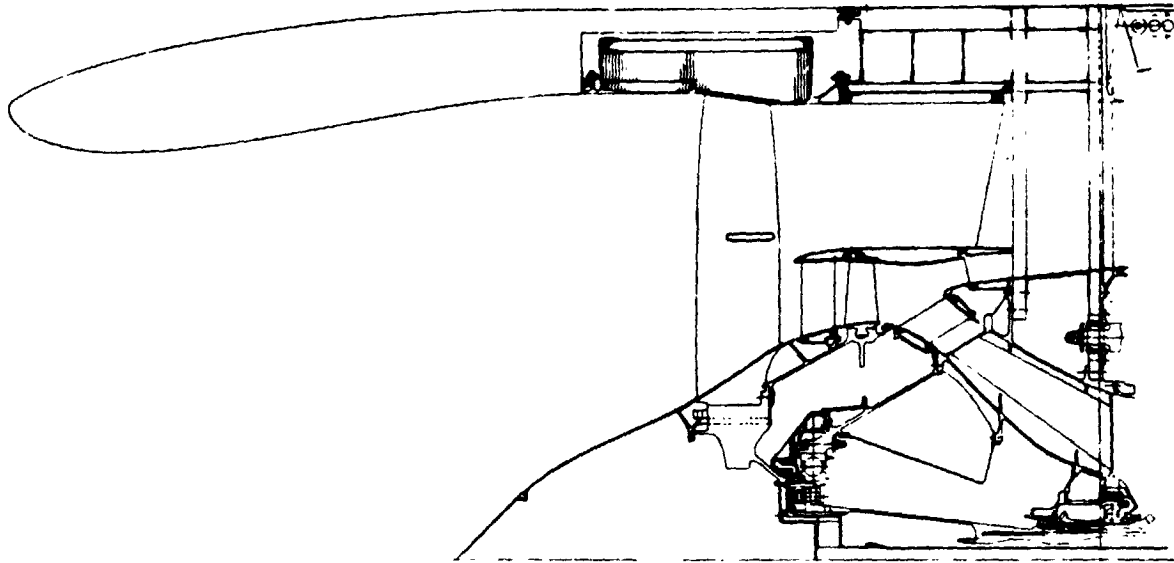


Figure 51. Fan Module Cross Section and Preliminary Operating Map.

All the significant aerodynamic parameters remain unchanged from the initial-study values except that the bypass-stream efficiency has increased by 0.005. This was primarily the result of changing to the 32-blade design which allowed a thinner part-span shroud to be placed at a lower radius.

Also, the lower aspect-ratio blade resulted in improved stall margin and is estimated to be able to meet bird-ingestion design criteria. The quarter-stage configuration is expected to reduce erosion and FOD to the core compressor. Engine test experience shows that bird-ingestion debris in the hub region tends to be centrifuged to the outer span of the booster blades and pass into the fan bypass duct. Figure 52 shows two examples of calculated particle trajectories for 25- and 100- μm dust particles. In all, eight particle sizes ranging from 10- μm to 1000- μm were evaluated at different radial locations on the inlet. Figure 53 shows the particle size distribution of AC Coarse, AC Fine, and C-Spec. dusts. The analytic results indicate that from one-half to two-thirds of AC Coarse and C-Spec. dust that enters the fan inlet within the core air capture area would be separated from the core air. This verifies the performance-retention benefit of cleaner air into the HPC from the quarter-stage configuration.

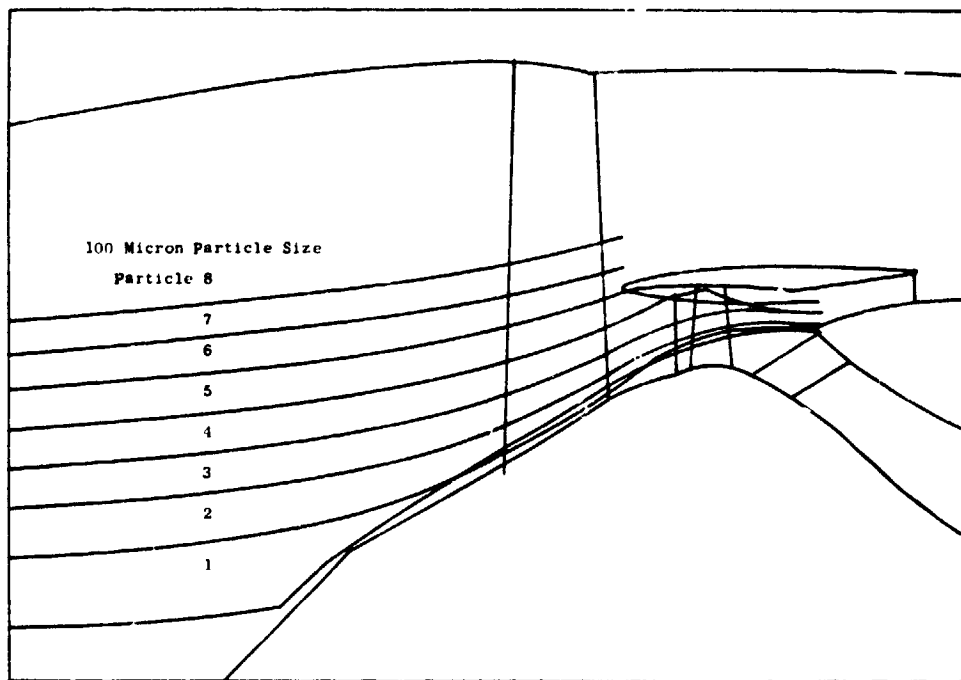
The rotor structure will feature a nonstructural spinner with the latest ice-resistant configuration, a high-bore ring disk for coupled blade-disk mode stiffness and internal fan-structure accessibility, a one-piece quarter-stage spool, and a fan shaft arrangement that allows for disassembly of either the shaft, the entire fan rotor, or the fan module (rotor and stator) from the high pressure compressor forward face.

The containment ring for the FPS fan is an advanced technology design consisting of a metal-face Kevlar belt. The design also includes an aluminum honeycomb nesting area to hold blade fragments outside the flowpath. The containment ring is supported by a lightweight integral vane-frame and nacelle structure utilizing advanced composite materials. During the evolution of the aerodynamic design, it was determined that the solidity of the vane-frame was higher than desirable. This resulted in a reduction in the number of integral vanes in the frame from 40 to 36 with no change in the chordal dimension.

The airfoils and structure are designed for the FPS baseline engine cycle (Table 12). Service life is assumed to be 36,000 missions with two stress cycles per mission. The fan structure will be designed to be capable of sustaining stall events with no mechanical damage, and there will be no coupled-mode resonances in the operating-speed range between the rotor and fan case. The FPS material selection features a Ti 6-4 fan and booster rotor and an Al 6061 spinner. The stator structure features a graphite/epoxy frame with a cast-aluminum C355 hub structure. All material-properties data in the fan design will be based on average minus three standard deviations properties, including section size considerations.

4.1.2 Alternate Fan Study

A major design effort was devoted to the alternate fan study. The study compared numerous configurations with the initial-study fan. Tradeoffs of sfc, DOC, initial cost, weight, and durability were used to establish an optimum fan configuration for commercial service. For the purposes of this study, the 38-blade initial fan design was used as a baseline reference for



• E³ Sea Level Takeoff

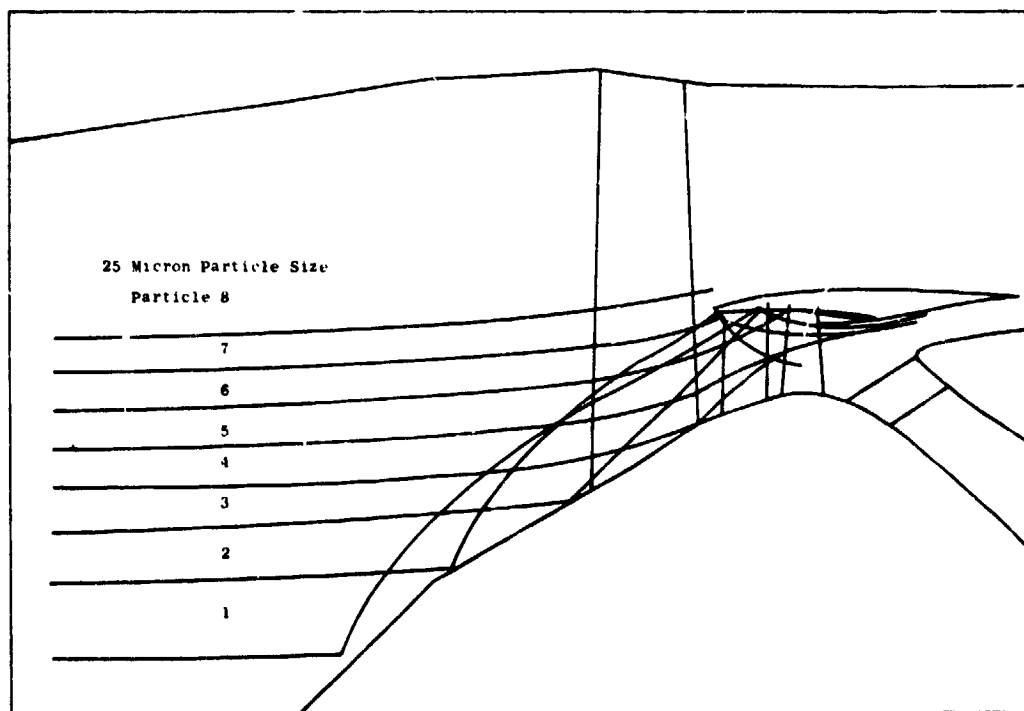


Figure 52. Particle Trajectories.

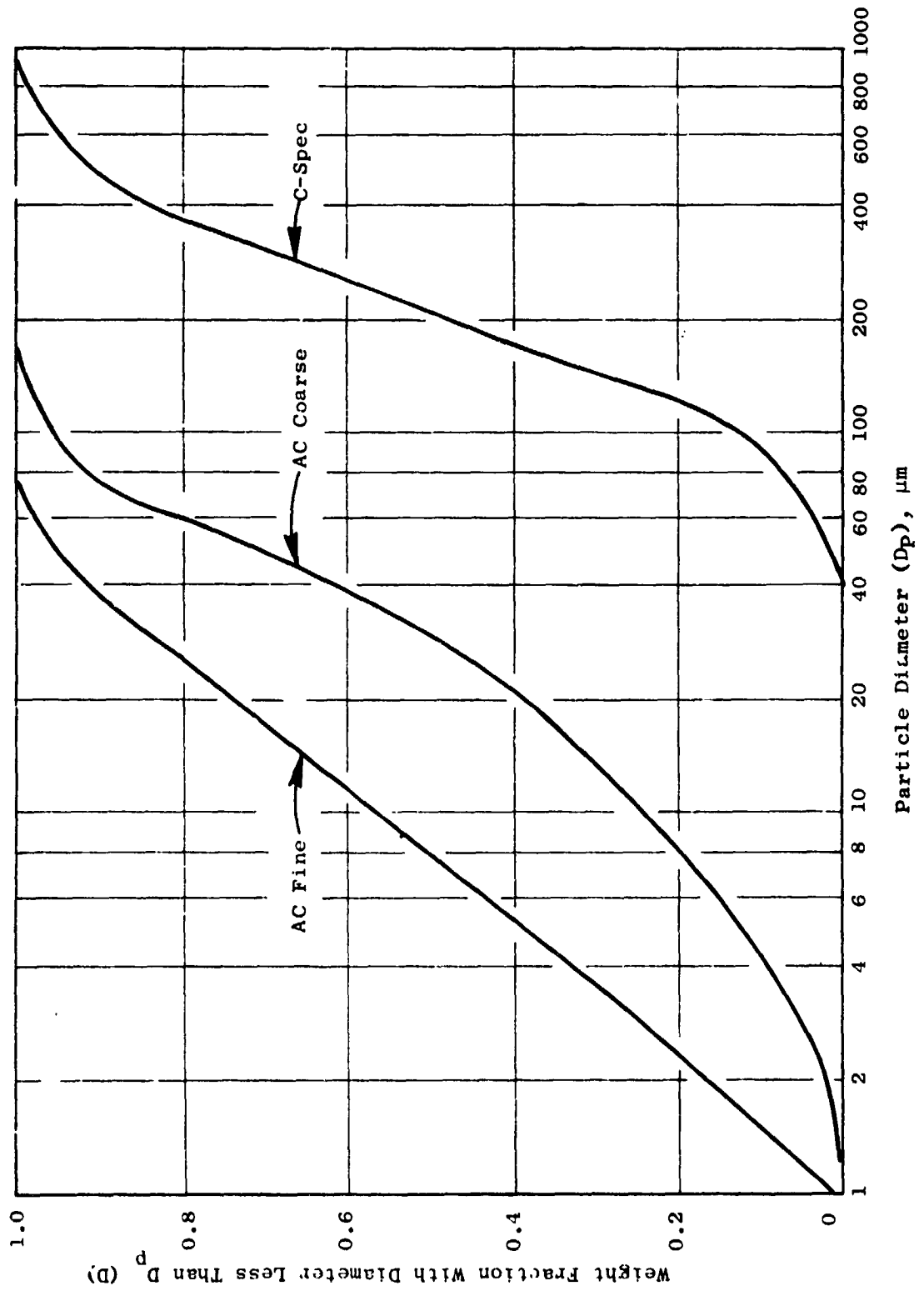


Figure 53. Typical Tests and Particle Size Distribution.

the alternate designs. While the baseline fan met the design objectives of the FPS, it was expected that a comprehensive study might indicate further improvements that would be suitable for future commercial engine service.

It was assumed that the relatively small variations in fan diameters for this study could be accommodated within the current nacelle. Also, based on prior experience, the costs of hollow titanium blade designs were assumed to be twice those of comparable, solid-blade designs. All comparisons in performance were made at the same maximum cruise operating point.

Six basic fan configurations were studied during these alternate fan studies. The 38-blade, initial-study configuration shown in Figure 54 was used as a baseline for comparing the five other configurations shown in Figures 55 through 59. A summary comparison of all the alternate fans, including hollow-fan variations, is presented in Table 35. Tradeoffs are summarized on the basis of cost, weight, sfc, DOC, and fuel burned using the trade derivatives given in Section 3.1.

For the studies, the following component efficiency effects were assumed:

- +1% Δ Fan Bypass Efficiency = -0.65% Δ Cruise Efficiency
- +1% Δ Fan Core Flow Efficiency = -0.11% Δ Cruise Efficiency
- +1% Δ Turbine Efficiency = -0.7% Δ Cruise Efficiency

On the basis of the tradeoffs, the 32-blade design with solid titanium airfoils and a booster stage was selected for the FPS fan configurations. This choice provides significant improvements in sfc and fuel burned in spite of the 45 kg (100 lb) weight penalty of the solid titanium blade. The choice of a larger blade also provides greater potential for future improvements through the development of a lightweight composite or hollow-outer-panel titanium blades. The latter approach would offset the weight penalty of the solid 32-blade design, but current increased manufacturing costs would introduce a slightly unfavorable change in DOC.

In addition to the performance benefits of the selected 32-blade design, the lower aspect-ratio blade yields a projected 3% increase in stall margin. The larger blade also provides improved tolerance to bird ingestion and FOD without introducing performance penalties. Because of the lower blade-passing frequency of the 32-blade design, it is expected that the system noise level will be increased slightly (0.5 EPNdB).

Another fan configuration that offered some improvement in sfc was the unshrouded, 28-blade design shown in Figure 56. The relatively high-aspect-ratio, unshrouded, 28-blade design raised concerns that are important in the context of long-life, commercial fans. A blade of this design would cross

- 38 Blades
- 70% Span Shroud
- Booster
- 0.35 Radius Ratio
- 88.2% Bypass Efficiency
- 89.2% Core Efficiency

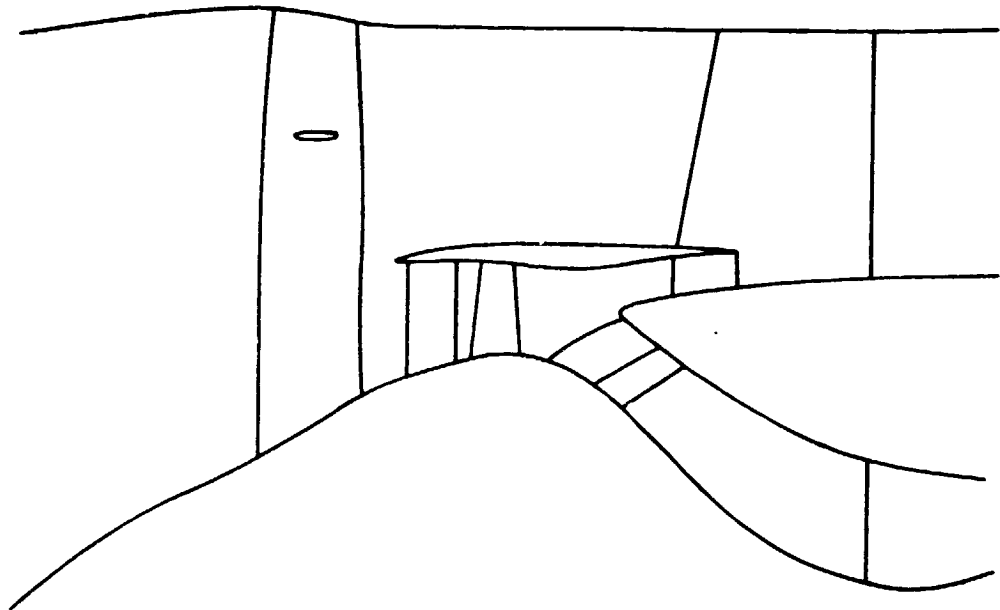


Figure 54. E³ Initial-Study Fan - Baseline.

- 70% Span Shroud
- 0.3996 Radius Ratio

Change From Baseline

- 0.4% Bypass Efficiency
- 4.5% Core Efficiency
- +0.1% LPT Efficiency
- +3 cm (1.2 in.) Fan Diameter
- \$18K 250th Engine Cost
- 34 kg (75 lb) Weight
- +0.69 Sfc

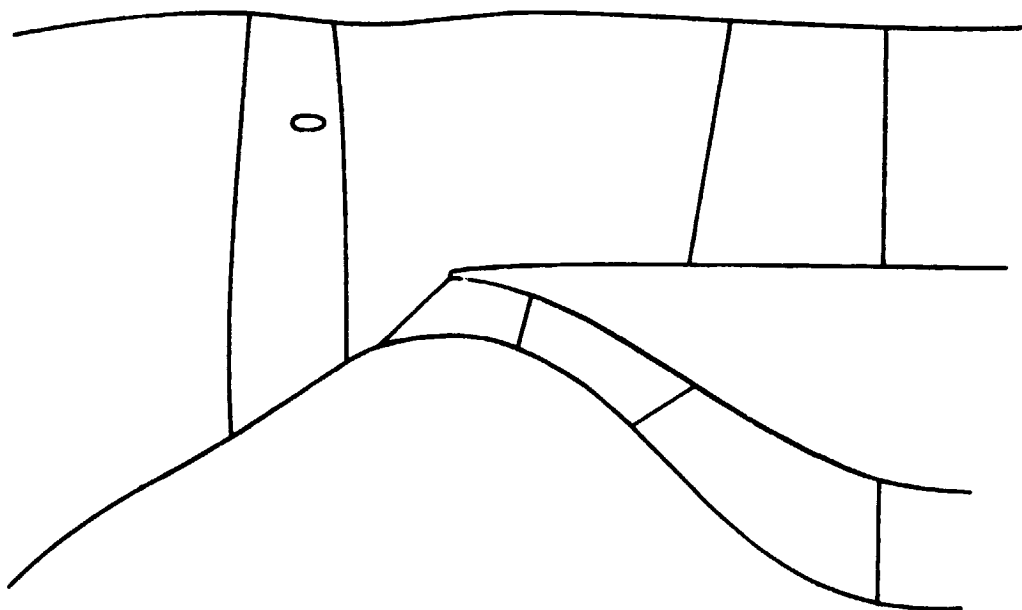


Figure 55. Thirty-Eight-Blade Design - No Booster.

- No Shroud
 - No Booster
 - 0.42 Radius Ratio
- Single Blade Cost
 Solid = \$1500
 Hollow = \$3000
 (1978 \$'s/250th Engine)

Change From Baseline

- +1.3% Bypass Efficiency
- 3.6% Core Efficiency
- 0.4% LPT Efficiency
- +7 cm (2.7 in.) Fan Diameter
- Cost (250th Engine): -\$28K (Solid Blades)
+\$14K (Hollow Blades)
- Weight: +67.1 kg (148 lb) (Solid Blades)
=0 (Hollow Blades)
- 0.17 Sfc

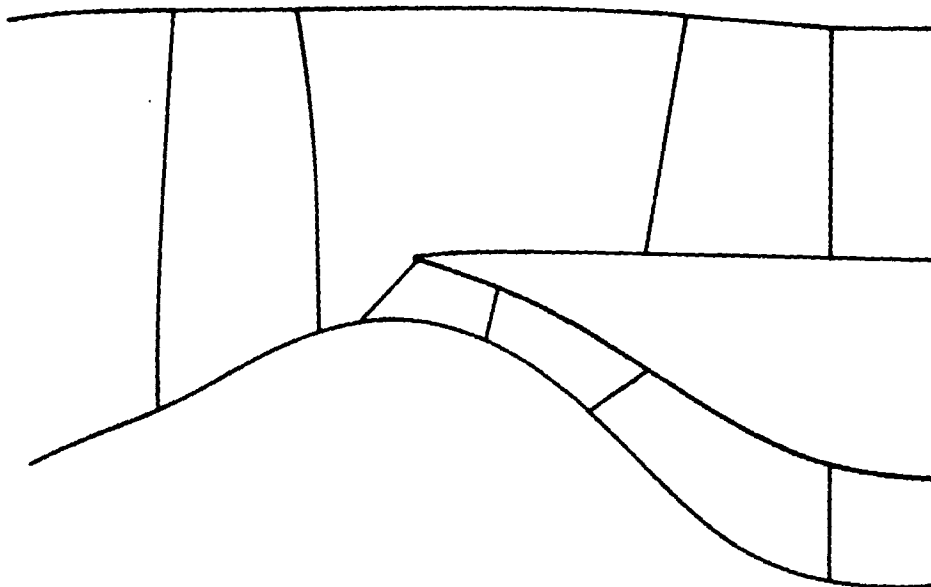


Figure 56. Twenty-Eight-Blade Design - Pin Root.

- 50% Span Shroud
- 0.40 Radius Ratio

Change From Baseline

+0.2% Bypass Efficiency
-4.0% Core Efficiency
0% LPT Efficiency
+5 cm (1.9 in.) Fan Diameter
-\$22K 250th Engine Cost
+51.3 kg (113 lb) Weight
+0.31 Sfc

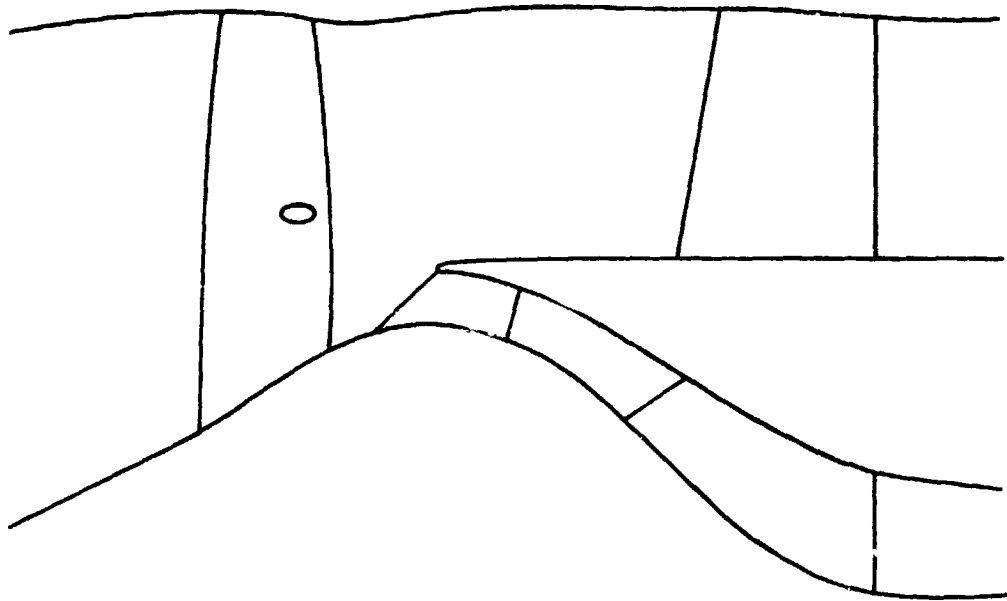


Figure 57. Thirty-Two-Blade Design - No Booster.

- 0.31 Radius Ratio
- Hollow Airfoils

Change From Baseline

- +0.8% Bypass Efficiency
- +0.3% Core Efficiency
- +0.1% LPT Efficiency
- 3 cm (1.1 in.) Fan Diameter
- +\$23K 250th Engine Cost
- +133.4 kg (294 lb) Weight
- 0.62 Sfc

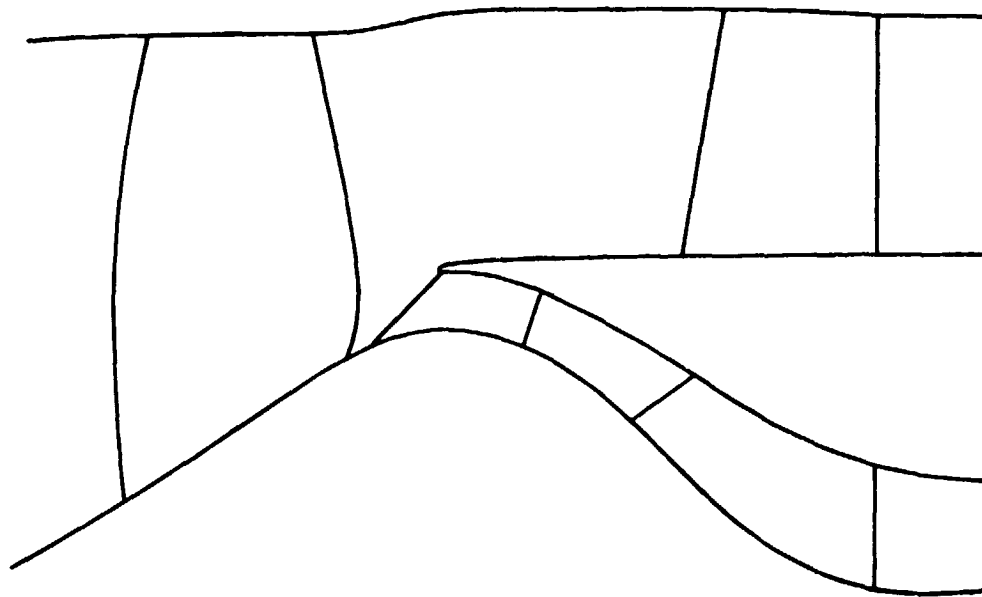


Figure 58. Twenty-Blade Design - No Shroud or Booster.

- 50% Span Shroud
- 0.35 Radius Ratio

Change From Baseline

+0.5% Bypass Efficiency

0% Core Efficiency

0% LPT Efficiency

0 cm Fan Diameter

Cost (250th Engine): -\$4K
(+\$43K, Hollow Outer Panel)

Weight: +45.4 kg (100 lb)
[-1.4 kg (3 lb), Hollow
Outer Panel]

-0.33 Sfc

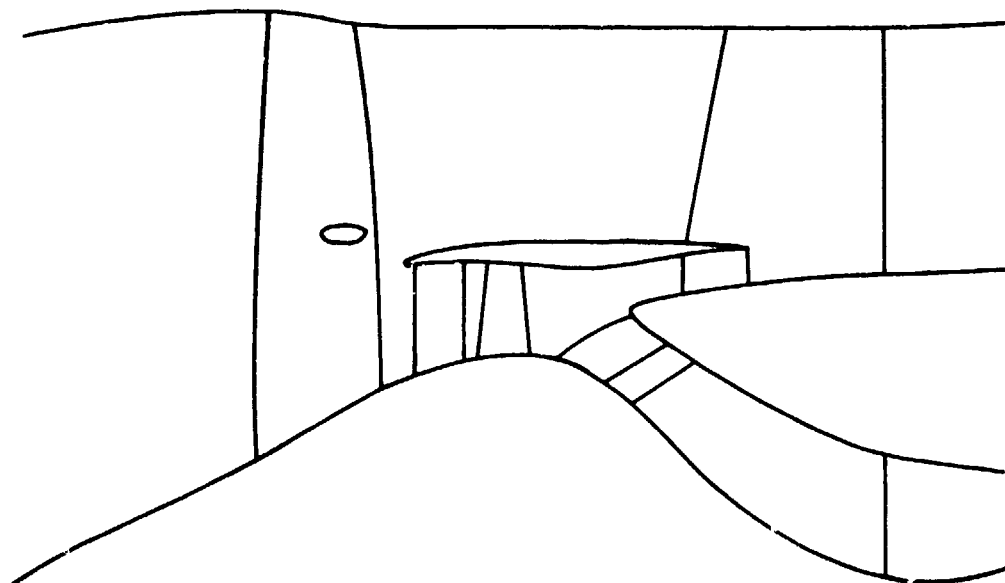


Figure 59. Thirty-Two-Blade Design - With Booster.

Table 35. Summary of Alternate Fan Study.

• Comparisons with Baseline Configuration

Configuration	ΔCost K\$	ΔWeight kg (lb)	ΔInstalled sfc	Δ% Fuel Burned	Δ% DOC
38 Blades - No Booster, Part-Span Shroud	-18	-34.02 (-75)	+0.69	+0.77	+0.15
28 Blades - Pinned Root, Solid Blades	-28	+67.13 (+148)	-0.17	+0.04	-0.06
28 Blades - Pinned Root, Hollow Blades	+14	-24.49 (-54)	-0.17	-0.31	-0.07
32 Blades - Booster, Part-Span Shroud	-4	+45.36 (+100)	-0.33	-0.33	-0.06
32 Blades - Booster, Part-Span Shroud, Hollow Outer Panel	+43	-1.36 (-3)	-0.33	-0.25	+0.07
32 Blades - No Booster, Part-Span Shroud	-22	+51.26 (+113)	+0.31	+0.60	+0.17
20 Blades - No Booster, Hollow Blades	+23	+133.36 (+294)	-0.62	-0.30	+0.19

the 2/rev excitation line in the middle of the operating-speed range. Experience has shown that fans with this property can be operated with no special problems as demonstrator components in test cells but could be vulnerable to the excitation sources of crosswind and thrust-reverse distortion in commercial service. The 2/rev crossing can be avoided by using a pinned-root design, but the pin would encounter a wear problem in long commercial service. A pinned-root design would also require a fan hub inlet-radius ratio of approximately 0.42 to provide sufficient space in the disk rim to accommodate the pins and the disk.

In the case of the low-aspect-ratio, 20-blade, unshrouded design (shown in Figure 58) a hollow airfoil would be required since a solid blade could not be supported by a dovetail at the desired radius ratio. While this design shows attractive efficiency improvements, the additional weight and cost have an unfavorable impact on the direct operating costs. The hollow-blade design would represent a high technical risk for the E³ program since a comparable solid-blade design could not be used as a backup.

Preliminary frequency analysis of the 32-blade fan rotor indicates that a shroud will be required at 55% span. The Campbell diagram of Figure 60 shows that with the shroud at 50% span the two-nodal-diameter mode has a relatively small 8% margin from the 2/rev stimulus at the maximum fan speed. When the shroud is moved to 55% span, the frequency margin is increased to an acceptable value, and the three-diameter mode crosses the 3/rev line at a comfortably low, 60% speed.

A Campbell diagram of the lower modes of the quarter-stage rotor blade is presented in Figure 61. These preliminary frequency analyses show no resonant conditions of concern in the quarter-stage design. Frequency analysis of the fan stator vanes likewise shows favorable characteristics, free of major resonances.

The total projected weight of the FPS fan module is shown in Table 36 by component.

4.2 COMPRESSOR

4.2.1 Configuration and Design

The core compressor for the E³ FPS, shown in Figure 62, has evolved from a configuration selected during the earlier NASA AMAC study (Reference 6). This configuration has design parameters favoring both high efficiency and compactness in order to minimize overall engine-system installed fuel consumption and direct operating cost.

Design parameters favoring high efficiency incorporated into the E³ core compressor were:

- Medium aspect ratio blading - 1.48 average
- Medium pitch-line solidity - 1.38 average

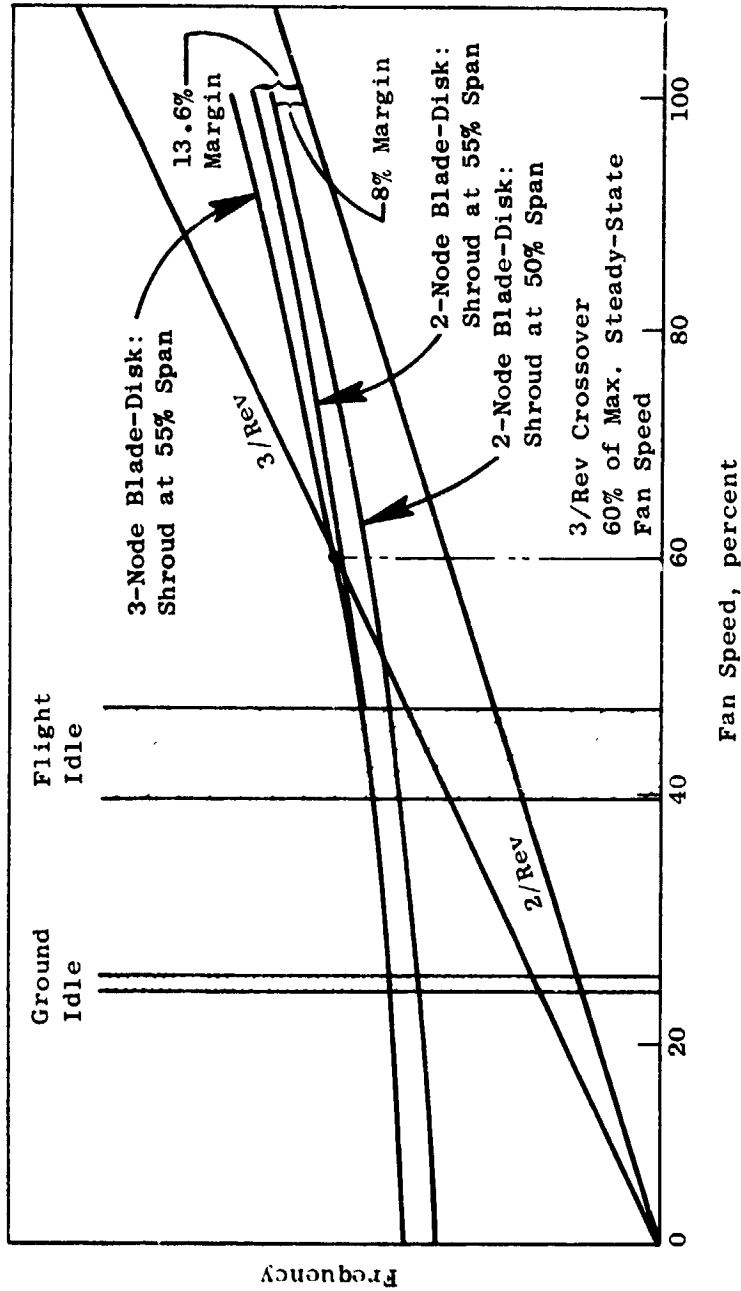


Figure 60. E³ 32-Blade Fan, Preliminary Coupled-Blade-Disk Campbell Diagram.

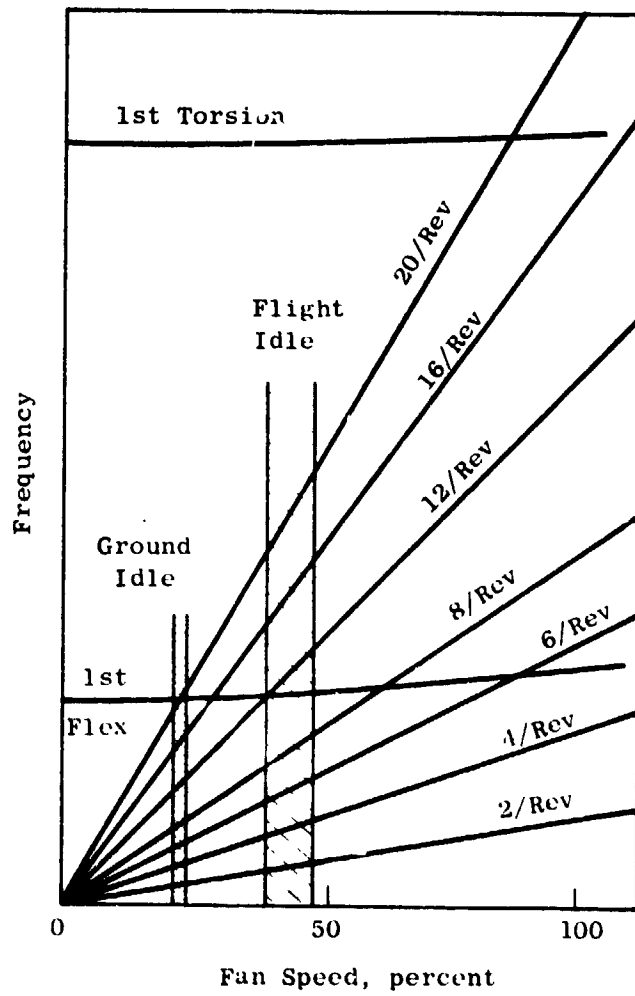


Figure 61. E³ Quarter-Stage Preliminary Blade Campbell Diagram.

Table 36. FPS Fan Module Weight Summary.

Component	Weight	
	kg	(lbm)
Rotor		
Fan Blades	230.1	(507.2)
Disk	121.2	(267.2)
Quarter-Stage Blades	17.2	(38.0)
Quarter-Stage Spool	51.0	(112.5)
Forward Shaft	25.8	(56.8)
Spinner	9.4	(20.8)
Blade Retention	5.0	(11.0)
Hardware	<u>8.8</u>	<u>(19.5)</u>
Total Rotor	468.5	(1033.0)
Stator		
Bypass Frame	245.0	(540.0)
Containment	151.5	(334.0)
Core Frame	111.6	(246.0)
Core Stators	<u>89.4</u>	<u>(197.0)</u>
Total Stator	597.5	(1317.0)
Total Fan Module Weight	1066.0	(2350.0)

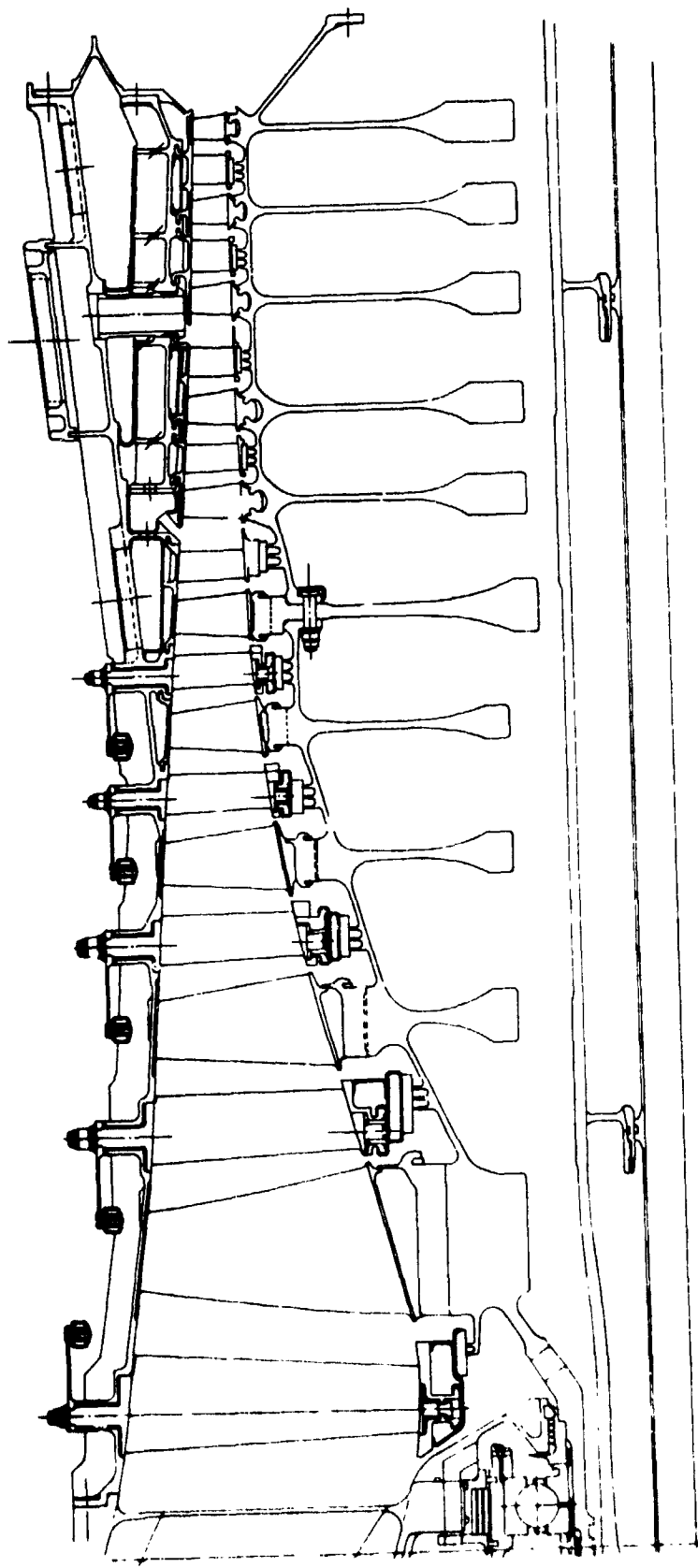


Figure 62. E³ High Pressure Compressor.

- Moderate through-flow Mach numbers

Design parameters favoring compactness were:

- Ten stages, for a pressure ratio of 23:1
- High inlet corrected tip speed
- High exit radius ratio

Compared to current-technology turbofan engines, the core compressor for the E³ has higher speeds, higher rear radius ratios, lower aspect ratios, fewer stages and airfoils, and produces nearly double the pressure rise.

Performance goals for this design are quite high despite the advances in loading, speed, and compactness. Advanced-technology airfoil shapes, developed under the current NASA-sponsored Core Compressor Exit Stage Study (Contract NAS3-20070), have been incorporated to reduce end-wall losses below current levels and thereby achieve the challenging efficiency levels established for the fully developed E³ FPS. The core compressor characteristics at the principal engine-operating conditions of maximum climb, maximum cruise, takeoff, and idle are listed below, and an estimated compressor performance map is shown in Figure 63; adiabatic efficiency at maximum cruise power is 0.861.

Parameter	Mx Cl	Mx Cr	Takeoff	Idle
Corrected Speed, % design	100.00	99.5	97.7	76.8
Total Pressure Ratio	23.0	22.4	20.1	4.2
Inlet Temperature, K (° R)	304.4 (547.9)	301.4 (542.5)	327.8 (590.1)	292.0 (525.6)
Inlet Pressure, kPa (lbf/in. ²)	59.64 (8.65)	58.06 (8.42)	105.59 (21.84)	104.80 (15.2)

The peak efficiency goal was set to be consistent with the General Electric preliminary design procedure used during the AMAC compressor studies. The efficiency prediction model (Reference 9) that was used forecasts the potential peak efficiency of a well-designed, fully developed compressor. It accounts for all sources of loss present at the minimum-loss operating condition: blade surface-profile drag, shocks in the blading, part-span-shroud

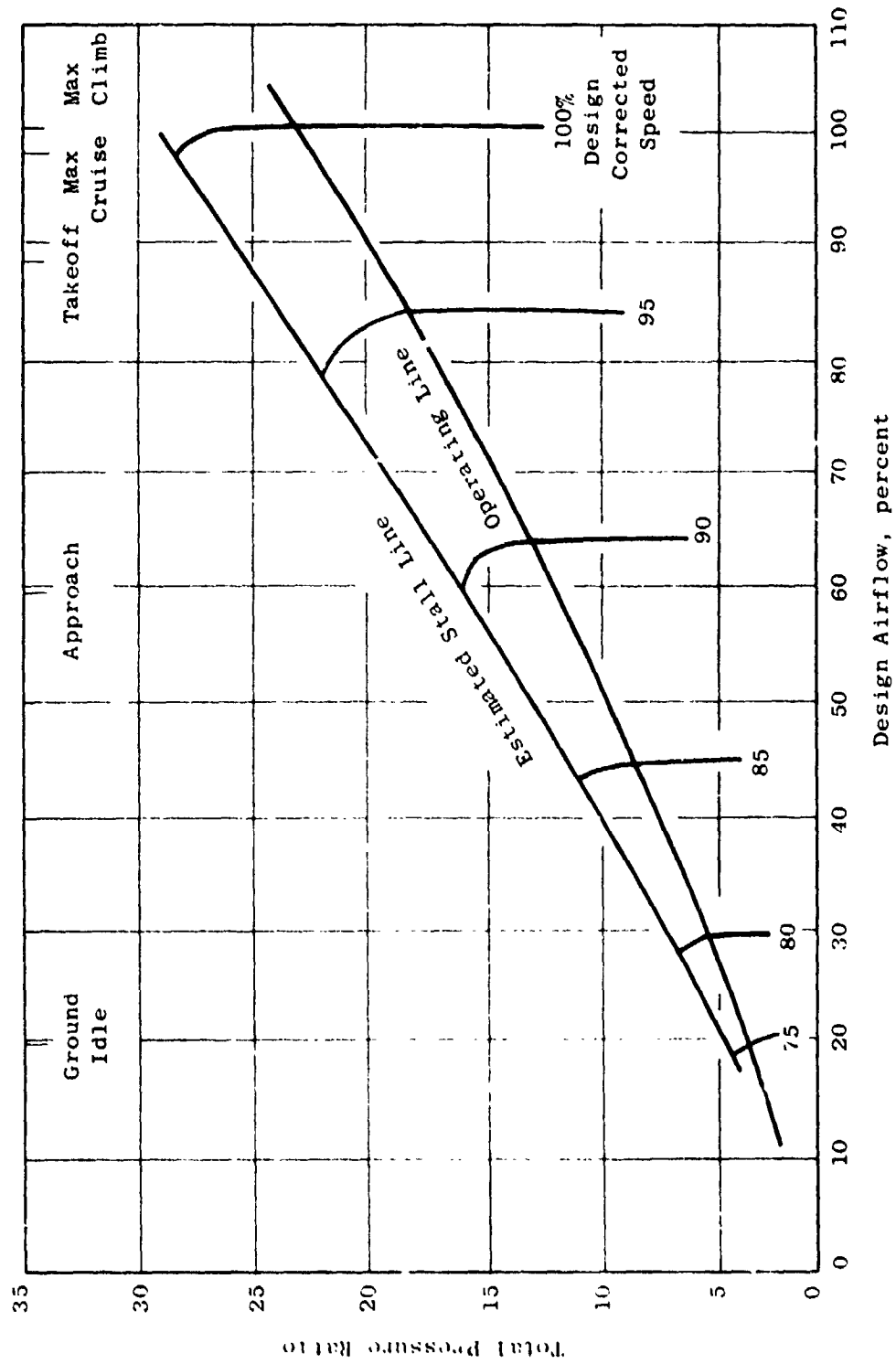


Figure 63. Core Compressor Performance Map Estimated from Stage Characteristics, Without Starting Bleed.

losses, and end-wall region losses due to wall boundary layers, secondary flows, and leakage. It does not predict losses caused by off-design operation, inappropriate blade shapes, or poor hardware quality. All important design parameters are accounted for, however. Blade-profile losses, for example, are related to suction-surface diffusion, blade maximum and trailing-edge thicknesses, Reynolds number, surface roughness, Mach number, and streamtube contraction. Passage shock losses are dependent upon both inlet and exit Mach number; leading-edge bow-shock losses depend on inlet Mach number, leading-edge thickness, solidity, and stagger. The model for part-span-shroud loss, although not a factor in the proposed compressor configuration, is based both on analytical formulations for drag coefficient and on experimental data. Finally, measured end-wall boundary layer thicknesses have been correlated versus aspect ratio, solidity, stagger, tip clearance, blade-row axial spacing, and aerodynamic loading level to determine end-wall losses.

The model-predicted peak efficiency has been compared to test data from numerous high speed and low speed multistage compressors. These comparisons indicate that, in most cases, the model agrees with the experimental data within one point in efficiency. For the AMAC study, and for predicting the potential peak efficiency of the E³ core compressor, certain advancements in aerodynamic and mechanical technology were assumed. Aerodynamic technology advancements were assumed to consist primarily of reductions in end-wall losses; it was assumed that a 15% reduction in these losses, below that predicted by the model, would result from research efforts now in progress.

Achievement of in-service, tip-clearance levels equal to those in recent demonstrator engines was also assumed. Finally, it was assumed that the fan for the E³ would be designed to minimize ingestion of foreign objects, such as sand and bird fragments, into the core engine. This permits retention of the very smooth blade-surface finishes that are possible using advanced manufacturing methods and allows the use of relatively sharp leading edges. These mechanical technology assumptions contributed a further one point to the predicted efficiency compared to that given by the model for clearances and surface finishes found in current production engines.

Starting with an efficiency projection based on the aerodynamic-loading parameters of the E³ HPC but utilizing current-state-of-the-art performance, E³ projected performance and improvement are as follows for maximum cruise at altitude:

Current-Technology Projected Performance:	84.1%
Reduced End-Wall Losses:	+1.0%
Improved Airfoil Surface and Sharp Leading Edges:	+0.3%
Improved Clearance Control:	<u>+0.7%</u>
Estimated E ³ Adiabatic Efficiency:	86.1%

Configuration evolution to the current FPS compressor is illustrated in Figure 64. The rotor structure for the FPS compressor includes 10 stages of low-aspect-ratio, highly loaded airfoils mounted in two inertia-welded spools joined by a single, rabbeted bolt joint at the Stage 5 disk.

Inner Diameter (I.D.) bleed extraction on the initial-study engine for rotor cooling and sump pressurization has been replaced by a system that extracts air from the booster discharge. The air is introduced to the rotor through holes in the forward shaft from the flowpath-exposed cavity below the IGV shroud and is circulated through the rotor and into the rear sump.

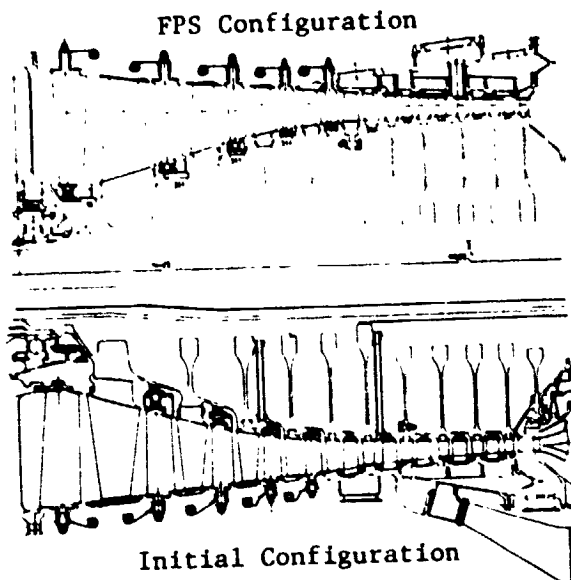
Axial dovetails have been extended from the first two stages throughout the front spool and Stage 5 disk. The single rotor-bolt joint has been moved forward from Stage 7 to Stage 5. An individual disk has been added at Stage 5 to achieve a symmetrical bolt-joint configuration.

Several significant changes have been made to the compressor stator. The steel-lined titanium casing, using Stage 7 bleed air for active clearance control over the last three stages, was changed to an unlined steel casing over the first three stages with steel liners over the remaining stages. The bleed air used for clearance control is now taken from Stage 5 to gain control over an additional two stages and to increase the amount of control over the latter stages by using cooler Stage 5 bleed air.

Mechanical-design features and goals are listed in Table 37. The airfoils and structures are designed for the FPS engine cycle. Service life is 36,000 missions with two stress cycle each. The compressor will be designed to be capable of sustaining stall events with no mechanical damage, and there will be no aeromechanical instabilities in the operating-speed range. Active airfoil resonances will be detuned to eliminate any high response at steady-state operating points.

Table 37. Compressor Mechanical Design Criteria.

- 36,000 Flight Cycles
- Burst Speed: 120% Maximum Physical Speed
- Active Airfoil-Mode Resonances Detuned
- No Aeromechanical Instabilities
- Repeated Stall Capability



- **Booster Discharge Rotor Cooling Air**
- **No ID Air Extraction**
- **Steel Compressor Case**
- **Improved Active Clearance Control, Stages 6-10**
- **Axial Dovetails in Forward Rotor Spool**
- **Rotor Bolt Joint at Stage 5**

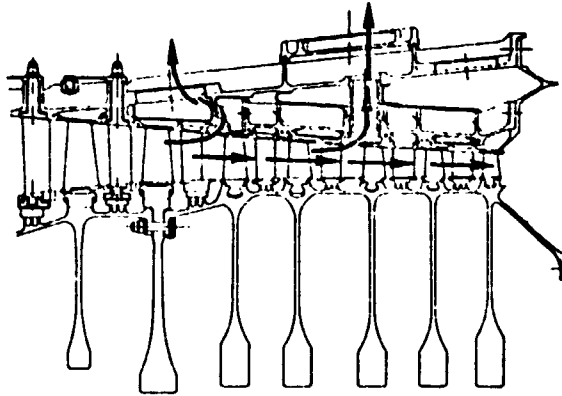
Figure 64. Configuration Changes from the Initial to Current FPS Compressor.

Some of the more important mechanical-design features are as follows:

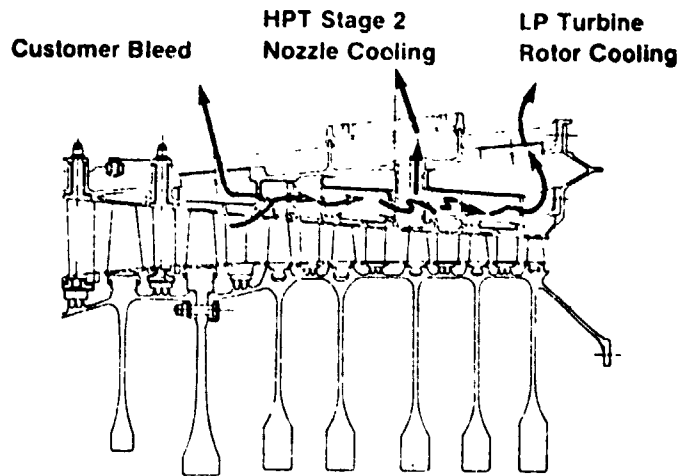
- An unlined steel casing over the first three stages to reduce compressor weight, reduce cost by eliminating separate removable liners, and reduce the amount of machining required to incorporate the liners.
- Abradable rub strips over each rotor stage to accommodate blade tip rubs without incurring damage to the blades.
- A steel casing of M152 material for the forward and rear casings. Circumferential rings are located in the plane of each row of variable-stator-vane bosses on the forward casing and over the flowpath mounting points on the rear casing to help maintain casing roundness.
- The high-boss, variable-stator-vane design provides stiff mounting in the casing and minimizes casing deflection due to vane applied loads. This design also reduces the rate of bushing wear and leakage because bushing loads are reduced.
- The outer platform of the vane covers the entire leading edge of the airfoil to prevent cross-circulation between vane passages due to tip clearance normally encountered in this region. Tip clearances at the trailing edge are at the minimum required for vane actuation; however, this area is not as sensitive to cross-circulation as the leading edge since the majority of rotor-induced swirl has been removed at this point.
- Rub liners are integral with the fixed stator vanes for Stages 5 through 10. This feature greatly reduces the number of parts and the amount of machining required on the casings.
- Bleed manifolds are integral with the casing configuration. All manifolds are 360° to minimize casing distortions that could result from interruptions in the manifold.
- Honeycomb interstage seals are used on all stages for control of recirculation around the stator shrouds.
- An active clearance-control system provides controlled amounts of Stage 5 bleed air over the aft inner case on Stages 6 through 10 as illustrated in Figure 65. Cooling is accomplished by directing bleed air through impingement rings onto the rear case for increased cooling effectiveness. The air is then collected in the manifold over Stage 10 and routed to the LPT rotor for cooling purge and reintroduction to the cycle.

- S5 Bleed**
- Customer
 - LP Turbine Rotor Cooling

- S7 Bleed**
- Starting
 - HPT Stage 2 Nozzle Cooling



(a) Without Active Clearance Control



(b) With Active Clearance Control

Figure 65. Compressor Case Cooling Flow.

- Crossover transfer tubes direct Stage 7 bleed air across the Stage 5 clearance-control-air environment into the Stage 7 manifold. These tubes are installed after the casing halves are mated and prior to the assembly of the manifold cover.

The forward and aft compressor rotor spools will be inertia-welded. Seven-inch bores will be used in the aft spool to achieve a lightweight, highly efficient, structural design. As previously mentioned, axial dovetails will be used on Stages 1 through 5, and circumferential dovetails will be used on Stages 6 through 10.

The FPS material selection for the compressor stator includes A286 for vanes. The compressor cases, both outer and inner, will be M152. The fixed-vane sectors and rub liners will be Inconel 718. All the rotor blades for Stage 5 aft will be Inconel 718. The rotor blades for Stages 1 through 4 will be titanium 8-1-1 to provide high strength in the dovetail area. The forward spool and the Stage 5 disk are Titanium 17, and the aft spool is as-HIP PM René 95.

Major design studies pursued to date include the rotor-cooling scheme, the compressor-case material selection, blade and vane frequency tradeoffs, and the active-clearance-control study.

The purpose of the rotor-cooling study was to determine a scheme that would maintain low temperatures in the disk bores, aid in shaft temperature control, avoid stress concentrations in the spacers, and avoid pressure loads across the disk webs. This led to the design shown in Figure 66. Compressor flow is brought through the compressor rotor back to the aft sump. The net result is that the bore temperatures in the back end of the rotor are in the range of 100° C (380° F) at takeoff speed, down to 110° C (230° F) at idle. However, the range of temperatures in the rim area is much greater and results in high thermal transient stresses.

As shown in Figure 67, during a 10-second acceleration from a stabilized idle condition the temperature difference between the rim and the bore increases quickly. Mechanical stress comes up very quickly; thermal stress responds somewhat slower, and the net result is that the rim stress peaks out somewhere in the 1 or 1.5-minute range with an unconcentrated peak compressive stress of 414 kPa (60 ksi). A loading-slot geometry has been developed that reduces the stress concentration to an acceptable value to meet design life.

Selection of M152 as the casing material was based on a comparison of weight, cost, and rotor tip clearance changes for both a lined titanium and an unlined steel version. The lined version features a titanium forward casing with a change to Inconel 718 aft of the variable stages. This is necessary to provide fire safety in the bleed manifolds and to accommodate the high temperatures reached at maximum operating conditions. The unlined version features a M152 steel casing for the full length of the compressor. This simplifies the design by eliminating the liners and the bolted joint required for a material

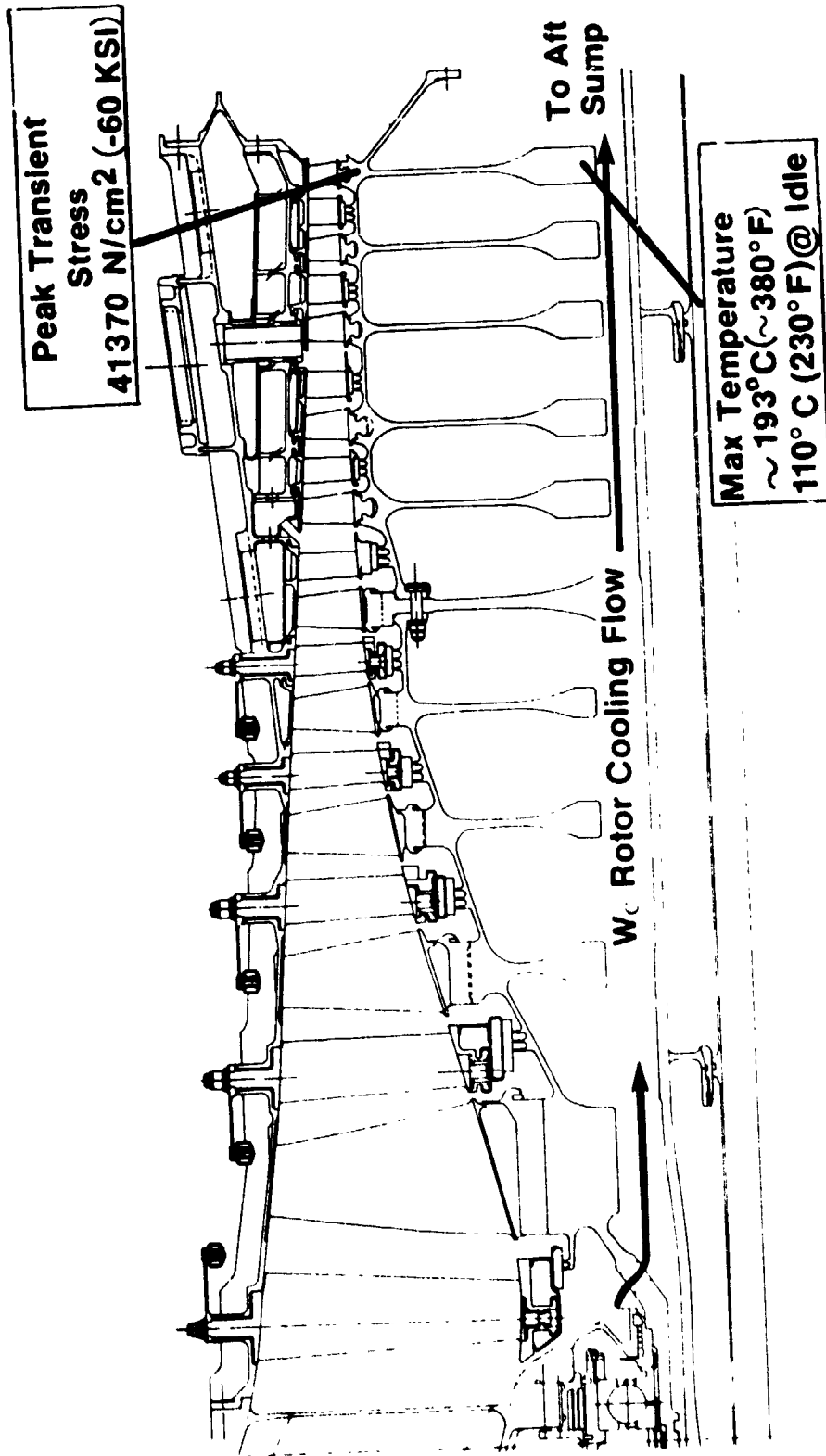


Figure 66. Compressor Rotor Cooling.

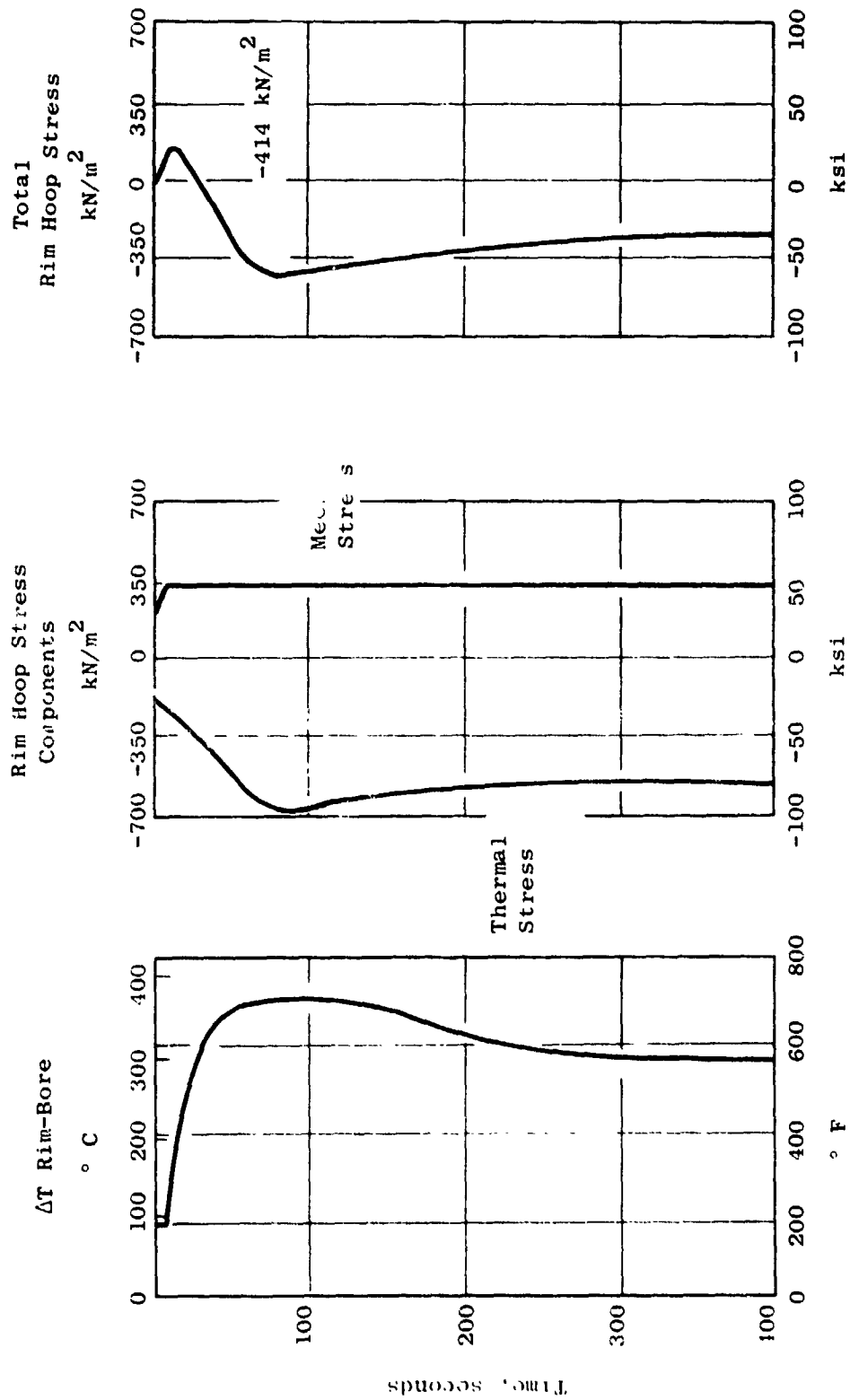


Figure 57. HP Compressor Aft Rotor Spool Stresses.

change on the lined version. This simplification offsets the weight advantage of titanium, and the cost of both versions is nearly the same.

Rotor-blade/stator-vane airfoil geometry has been selected to avoid active-mode resonances, in the compressor operating range, which may be stimulated by rotor-blade/stator-vane passing frequencies from nearby blade rows. Airfoil-geometry modifications were made by adjustments to chord, thickness, and location of the stacking axis to avoid strong resonances in the operating-speed range while maintaining aerodynamically acceptable airfoils.

It is also desirable to avoid any potential airfoil or dovetail fatigue failures in long-term service. Figure 68 shows a typical Campbell diagram for a rotor blade with some of the modes tuned to avoid strong lower per/revs in the high-speed operating range. The stripe modes avoid crossing the stator-vane-passing frequency within the operating range. Similar frequency analyses were completed on all the blades and stator vanes in the compressor.

4.2.2 Active Clearance Control

Active clearance-control studies concentrated on arriving at a configuration providing the best clearance match with the rotor at all operating conditions. Particular emphasis was placed on achieving tight clearance at the cruise condition. During typical transient operation of a commercial aircraft engine, differential growths of the rotor and stator normally develop. As a result, the clearance between rotor and stator will pass through a minimum point, usually during a rapid throttle movement from a stabilized idle condition or during a thrust-reverser operation. Ideally, it would be possible to have a zero clearance during this transient minimum. However, the practical considerations of manufacturing tolerances, maneuver loads, rotor vibration, etc. require some clearance at the minimum point. Table 38 lists the clearance adders for three representative stages through the compressor. A root-sum-square (RSS) approach is used to establish an appropriate manufacturing tolerance stackup. The adders of Table 38 assume that the small ovalization of the compressor can be accommodated with an "elliptic grind" and that high-speed stalls would result in modest rubs.

Figure 69 shows the results of the transient analysis of the compressor clearances at Stages 1, 6, and 10. The cold-buildup clearance was selected such that the minimum clearances during transient operation at takeoff or thrust reverse satisfy the limits established in Table 38. This, in turn, establishes the operating clearances at cruise as shown in Figure 69. Active clearance control has the ability to reduce the cruise clearance for improved performance as indicated. Figure 69 represents the current status of the design analysis. It is anticipated that cruise clearance will be further reduced as the design is refined and improved transient heat-transfer characteristics are established from the component test program.

The total weight of the high pressure compressor module is projected to be 481 kg (1060 lbm); of this, 222 kg (490 lbm) is in the rotor structure and 259 kg (570 lbm) in the stator structure. The weight breakdown is summarized in Table 39.

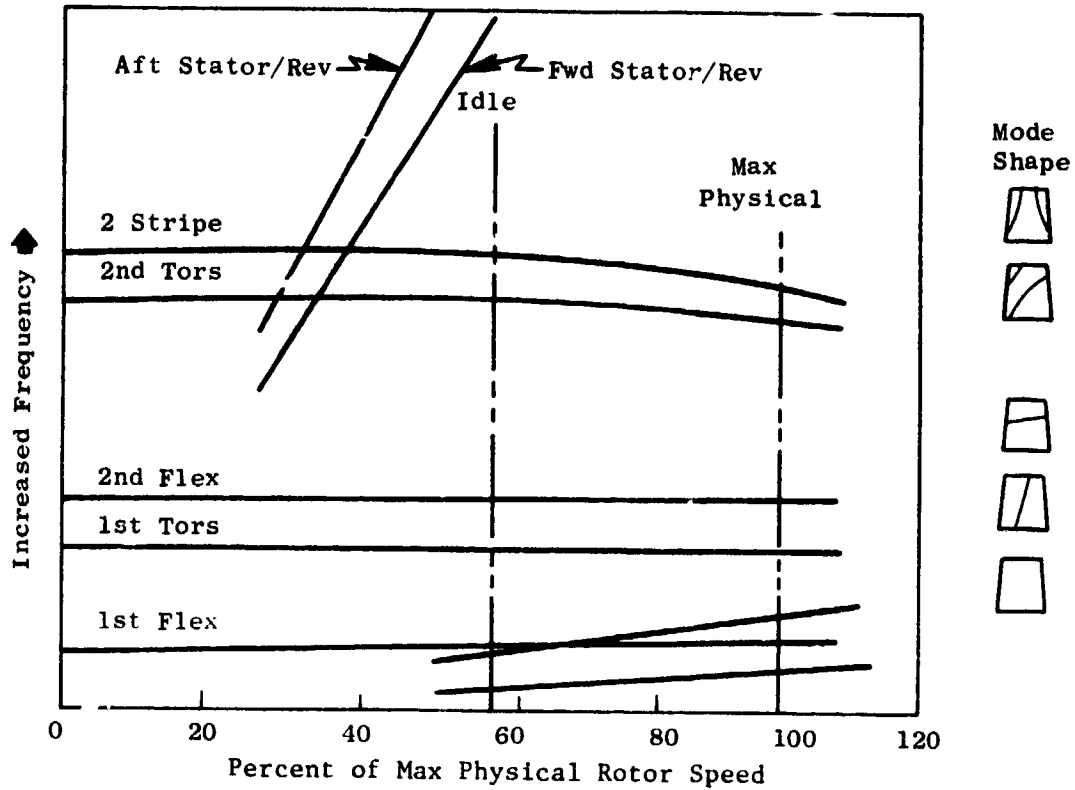


Figure 68. Compressor Rotor Blade; Typical Campbell Diagram.

Table 38. Compressor Radial Blade/Casing-Clearance Adders.

Adder	Stage 1 mm (mils)	Stage 6 mm (mils)	Stage 10 mm (mils)
Stackup (RSS)	0.127 (5.4)	0.127 (5.4)	0.127 (5.4)
Maneuver	0.051 (2.0)	0	0.025 (1.0)
Bearing Shift (Stall)	0.152 (6.0)	0.076 (3.0)	0.051 (2.0)
Blade Stall Deflection (100%, First Flex)	0.376 (14.8)	0.025 (1.0)	0
Rotor Vibration 38.1 g-m (150 g-in)	0.071 (2.8)	0.053 (2.1)	0.036 (1.4)
Ovalization (Elliptic Grind)	0	0	0
Rub at Stall	0.254 (10.0)	0.127 (5.0)	0.127 (5.0)
Rotor "g" Load	0.102 (4.0)	0.102 (4.0)	0.102 (4.0)
Minimum Operating Clearance	0.635 (25.0)	0.267 (10.5)	0.224 (8.8)

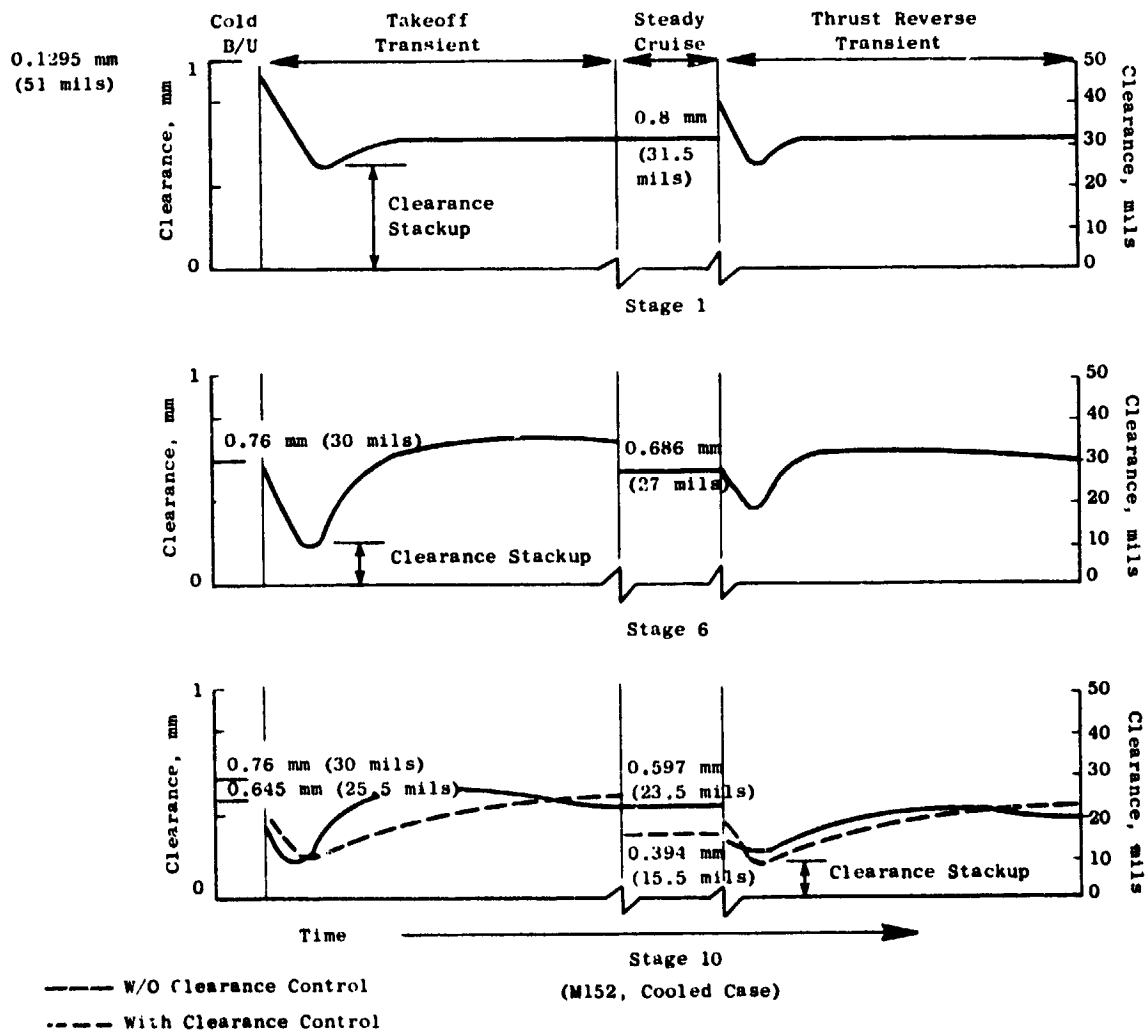


Figure 69. Compressor Clearance Study.

Table 39. Compressor Weight Summary.

Component	Weight	
	kg	(lbm)
Blades	39.5	(87)
Forward Spool	52.2	(115)
Stage 5 Disk	11.8	(26)
Aft Spool	94.9	(209)
CDP Disk	19.5	(43)
Hardware and Retainers	<u>4.5</u>	<u>(10)</u>
Total Rotor	222.4	(490)
Vanes, Snrouds, and Seals	100.8	(222)
Forward Case	79.9	(176)
Rear Case	25.9	(57)
Stage 7 Manifold	12.7	(28)
Actuation Rings and Lever Arms	15.9	(35)
Wishbone	6.4	(14)
Stages 3 and 4 Liners	3.6	(8)
Nuts, Bolts, and Hardware	<u>13.6</u>	<u>(30)</u>
Total Stator	258.8	(570)
Total Compressor	<u>481.2</u>	<u>(1060)</u>

4.3 COMBUSTOR

4.3.1 Component Description

Meeting the emissions goals of the E³ Program, as well as satisfying the combustion performance requirements, required the selection of an advanced combustor design concept. A double-annular-dome design was selected for the E³ combustion system because of previous successful development experience in the NASA/GE Experimental Clean Combustor Program (ECCP, Reference 10) and NASA/GE QCSEE Clean Combustor Program (Reference 11). A cross section of the E³ combustion system, showing key design features, is presented in Figure 70. The major components of the combustion system are a short-length, split-duct diffuser; a pressure-atomizing fuel-nozzle assembly; parallel and independently staged domes separated by a centerbody; counter-rotating swirl cups in each dome; and segmented, impingement-plus-film-cooled liners.

One of the key advanced-technology features in this combustion system is the split-duct diffuser shown in Figure 71. This design approach was selected because its short length and low pressure loss result in a substantial reduction in engine weight and length compared to a conventional, single-passage design.

The diffuser design features two parallel passages that direct the combustor airflow to the outer and inner flow passages of the combustor. The diffuser passages are separated by a splitter located and supported by 30 hollow radial struts. These radial struts provide the load-carrying structure for the combustor inner flowpath. A novel aspect of this diffuser design is the turbine rotor cooling-air-extraction feature. Turbine rotor cooling air is extracted at the trailing edge of the splitter and ducted through the hollow support struts inward to the turbine rotor cooling-air circuit.

The dome assembly features are shown in Figure 72. The dome structure contains the combustor mounting and load-carrying features. The combustor is supported by 30 radial pins located in line with the fuel nozzle and swirl cups. The inner and outer domes are connected and supported by 30 cowl struts located between swirl cups that provide the load-carrying path from the inner combustor flowpath to the outer case. The 30 counterrotating swirl cups in each dome have a stationary, concentric venturi and secondary swirler. The primary swirler is attached to the venturi with a slip joint to permit thermal growth and to accommodate dimensional tolerances. The dome surfaces exposed to the hot combustion gases are fully shielded by splash plates to provide maximum protection of the dome structure from the combustion-gas heat loads. The swirl cup barrel extension is a design feature incorporated to reduce emissions. These extensions prevent fuel from accumulating on the splash plate surfaces and becoming entrained in the liner cooling air.

The fuel nozzle design, shown in Figure 73, features two pressure-atomizing nozzles mounted on a single stem to which fuel is independently supplied by the two scheduling valves contained in the inlet of each nozzle assembly. The fuel nozzle stem is encased in a heat shield to insulate the

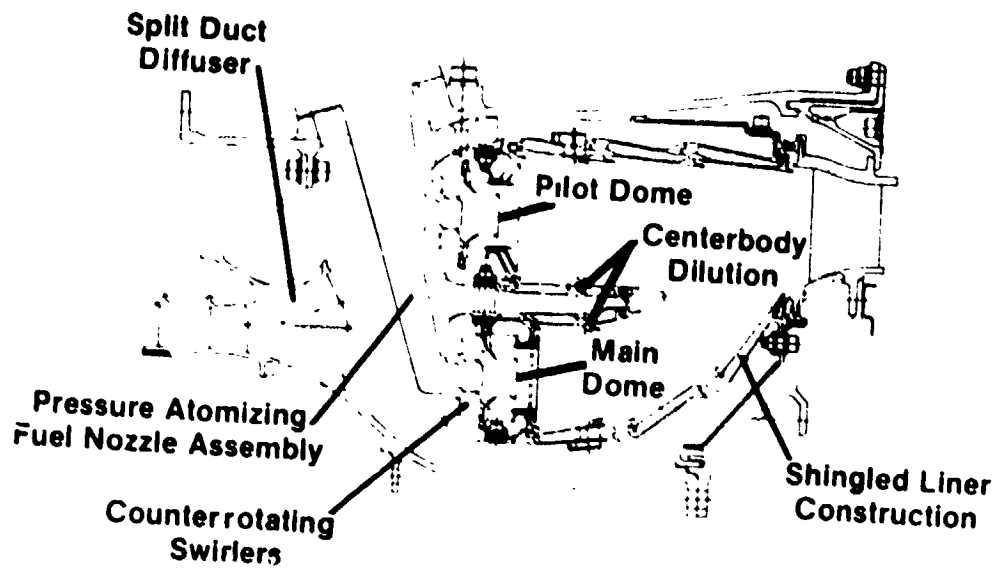


Figure 70. E³ Combustor - Selected Design.

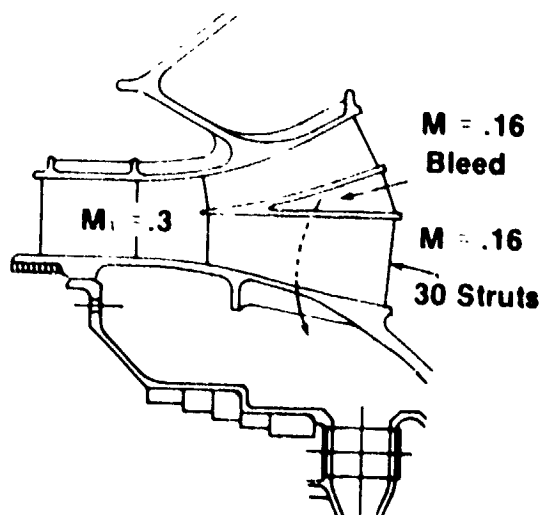


Figure 71. Split Duct Diffuser Design.

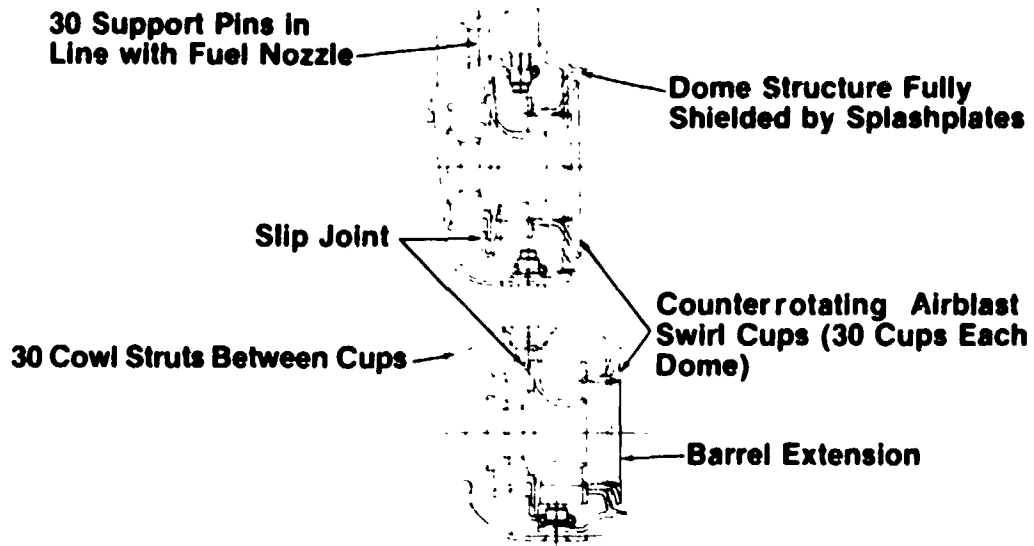


Figure 72. Dome/Swirl-Cup Design.

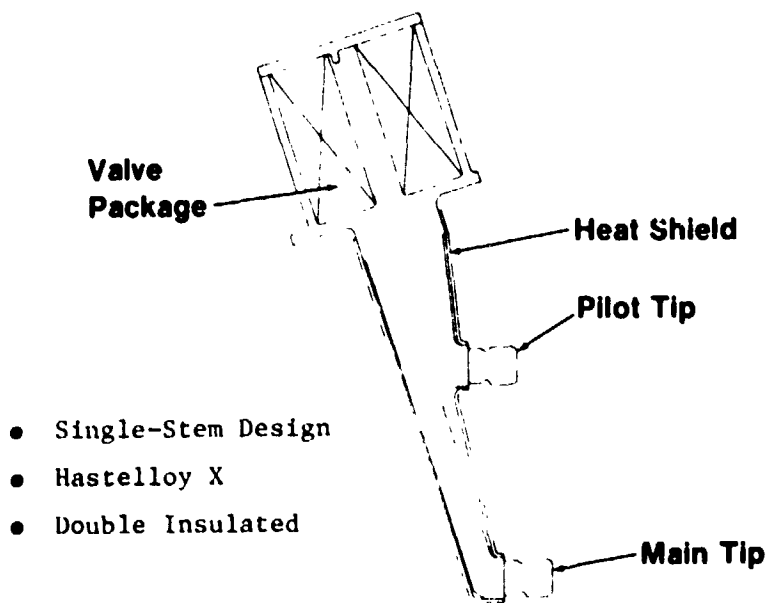


Figure 73. Fuel Nozzle Design.

fuel from the hot compressor-discharge air. This insulation feature prevents coking of the fuel in the flow passage and enhances fuel nozzle life.

The incorporation of an axially and circumferentially segmented combustor liner with impingement-plus-film cooling is another important advanced-design feature. This feature was included to meet the life goals of the FPS Program. The individual segments are supported by a 360° impingement liner that serves as the mechanical-load-carrying structure. The hot-film liner, because it is segmented, has low thermal stresses and can be fabricated with high temperature alloy available in cast ring form. A photograph of a typical shingle liner design is shown in Figure 74. This particular liner was designed for an advanced-engine program. The excellent durability of this combustor liner approach has been demonstrated on advanced-engine vehicles and in combustor component cyclic-endurance tests. The shingle liner design has been tested at combustor-inlet conditions approaching those for the E³ combustor.

The materials selected for the E combustor components are shown in Figure 75; they are generally the same as those currently used in conventional combustion systems. However, with the selection of the shingle liner design approach, it is possible to use a castable, high-temperature alloy such as X-40 in place of the Hastelloy X normally used for the combustor cooling liners.

4.3.2 Aerodynamic Design

Two programs have been conducted at General Electric, under the sponsorship of NASA, to design and develop double-annular-dome combustors similar to the E³ design. The first was the NASA/GE ECCP (Contract NAS3-19736) which involved the design and development of a CF6-50-sized double-annular-dome combustor. This program was directed at developing a large combustor with very low CO, HC, and NO_x emissions levels, compared to those of a conventional CF6-50C combustor, over the range of operating conditions of a modern, high-pressure-ratio, turbofan engine. The second of these programs involved the design and development of a double-annular-dome combustor conducted as part of the NASA/GE Quiet Clean Short-Haul Experimental Engine (QCSEE) Program (Contract NAS3-18021). This program was similar to the NASA/GE ECCP except that the QCSEE combustor is much smaller and more compact than the CF6-50C design, as shown in Figure 76.

Obtaining very low CO and HC emissions levels at ground idle, and low NO_x emissions levels at high power conditions, requires a staged combustion process. In the double-annular-dome concept, only the outer dome is fueled at low power settings, providing a rich combustion zone for rapid consumption of the CO and HC emissions; at high power settings, both domes are fueled and are designed for very lean operation of the combustion zone. This lean combustion is accomplished for the most part by introducing large quantities of airflow into the inner dome annulus. The introduction of these large quantities of airflow in the combustion zone severely limits the availability of air to perform the other aerodynamic functions such as liner cooling and exit gas temperature control. Therefore, careful consideration must be given to the

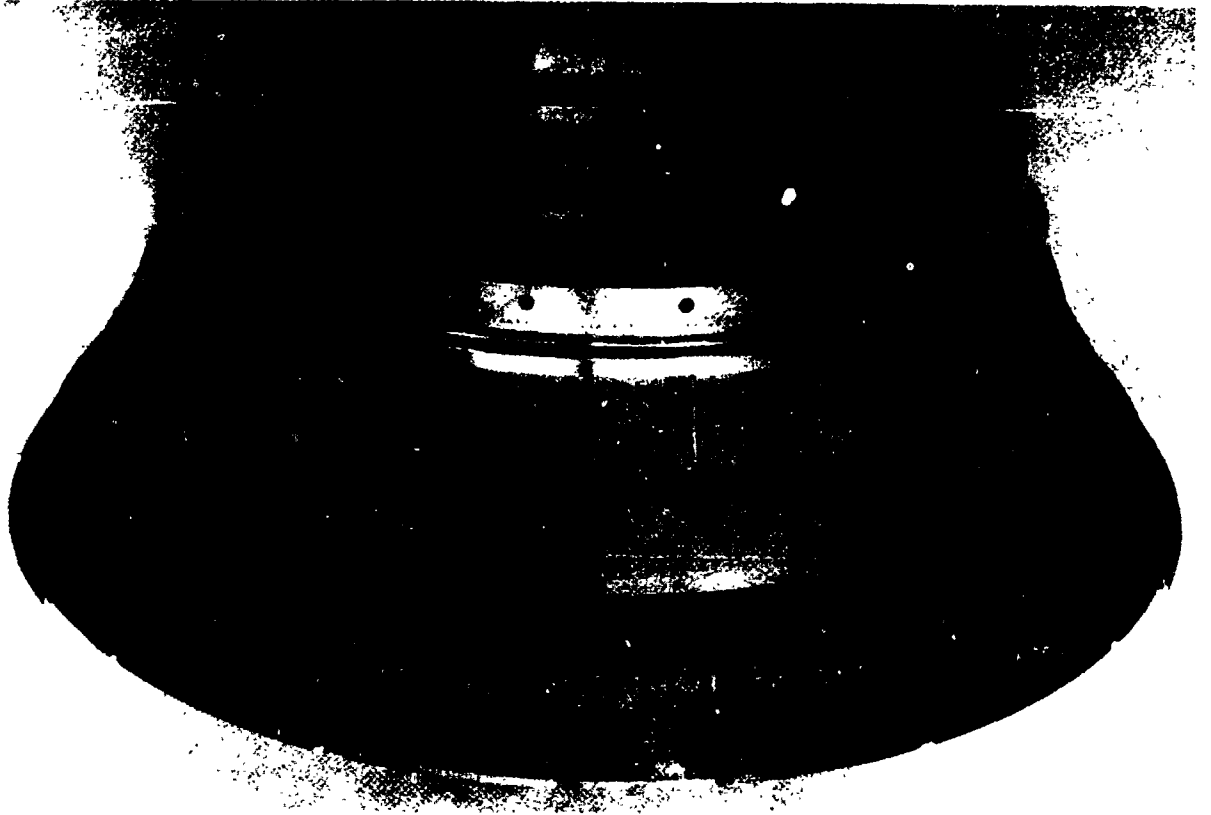


Figure 74. Shingle Liner Design.

ORIGINAL PAGE IS
OF POOR QUALITY

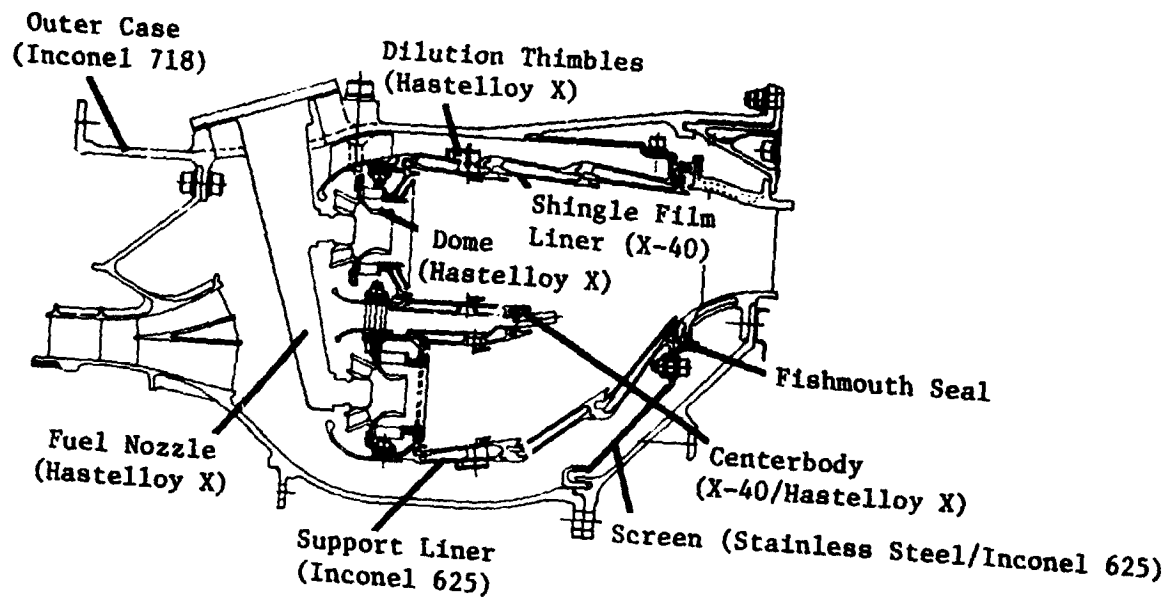


Figure 75. E³ Combustor Materials Selection.

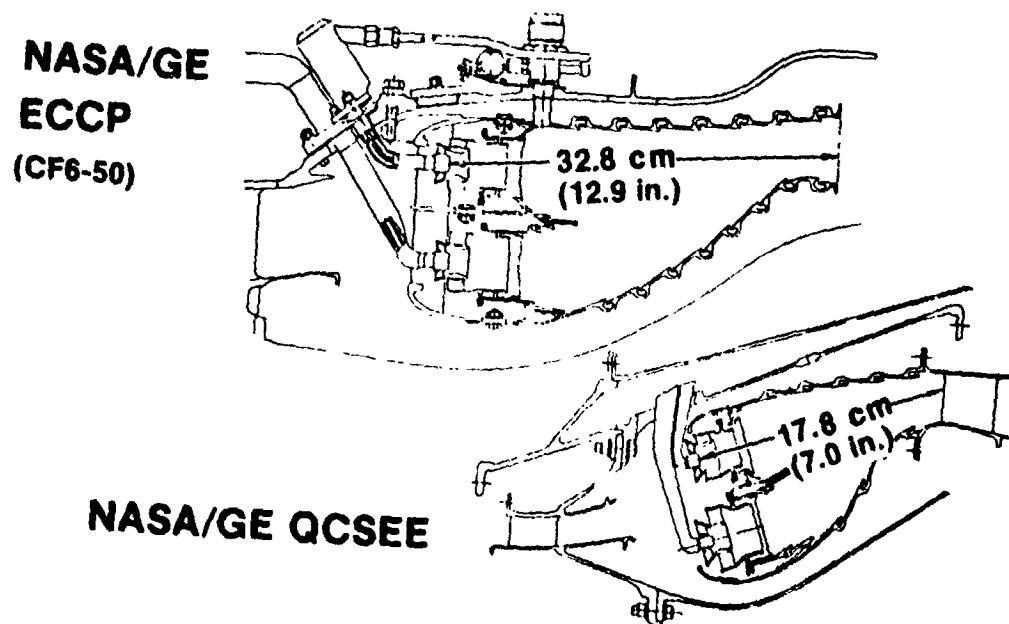


Figure 76. E³ Combustor Design Technology.

selection of the combustor flowpath to minimize system pressure losses, maintain the shortest possible length, and provide a practical mechanical design, as well as to satisfy the combustor emissions and performance requirements of the FPS.

The split-duct-diffuser approach was selected primarily for the features of positive flow distribution, short length, and low diffuser pressure losses. The key prediffuser-passage dimensions were selected to assure stable and predictable flow regimes at all E³ operating conditions. The prediffuser design was selected to provide a reasonable pressure loss for the diffuser system without excessive prediffuser length. Since prediffuser length affects engine length and weight directly, it is desirable to keep the prediffuser as short as possible without jeopardizing the overall combustion system performance. The E³ prediffuser design is less than 7.6 cm (3 inches) long with a pressure loss of only 1.5%. The split-duct diffuser also provides positive direction to the airflow supplied to the two annular regions of the combustor.

The airflow supplied to the outer region of the combustor is distributed to the pilot dome, outer liner, and part of the centerbody. The airflow supplied to the inner region of the combustor is distributed to the main dome, inner liner, and centerbody. The prescribed airflow quantities are specified based on established design guidelines. The pilot-stage swirl cup flow level is selected to provide a combustion-zone stoichiometry of about one at ground idle operating conditions, when only the pilot stage is operating. The main-stage swirl cup is sized to pass the maximum amount of airflow within the geometry constraints of the dome. The primary-combustion-zone dilution holes are sized to provide complete combustion and adequate mixing within the combustion zone. The cooling-air quantities have been determined, using heat transfer analysis, aimed at providing adequate metal strength and cyclic life. The remaining airflow is allocated to trim dilution for controlling the combustor-exit temperature profile and peak temperature. After the key flowpath dimensions were selected and the combustor airflow distribution was established, estimates of the emissions levels of the E³ double-annular combustor design were made based on the emissions characteristics of the CF6-50C and the QCSEE double-annular designs. In making these estimates, it was assumed that, with appropriate development, the pilot stage can reach the minimum CO emissions level when operating at idle conditions.

In order to obtain the required CO and HC emissions levels at low power and the required NO_x emissions levels at high power, a fuel-distribution schedule similar to that shown in Figure 77 is required. A very high combustion efficiency, greater than 99.5%, is required at all operating conditions to meet the E³ goals for CO and HC emissions. Therefore, it is expected that it will be necessary to operate the pilot stage alone, both at idle and at approach conditions, to obtain the required low CO and HC emissions levels. Thus, at sea level thrust conditions up to 35% power, the pilot stage is operated alone to provide the near-stoichiometric combustion zone needed to minimize CO and HC emissions levels at these severe combustor-operating conditions. At higher power conditions, the fuel flow to the pilot stage is

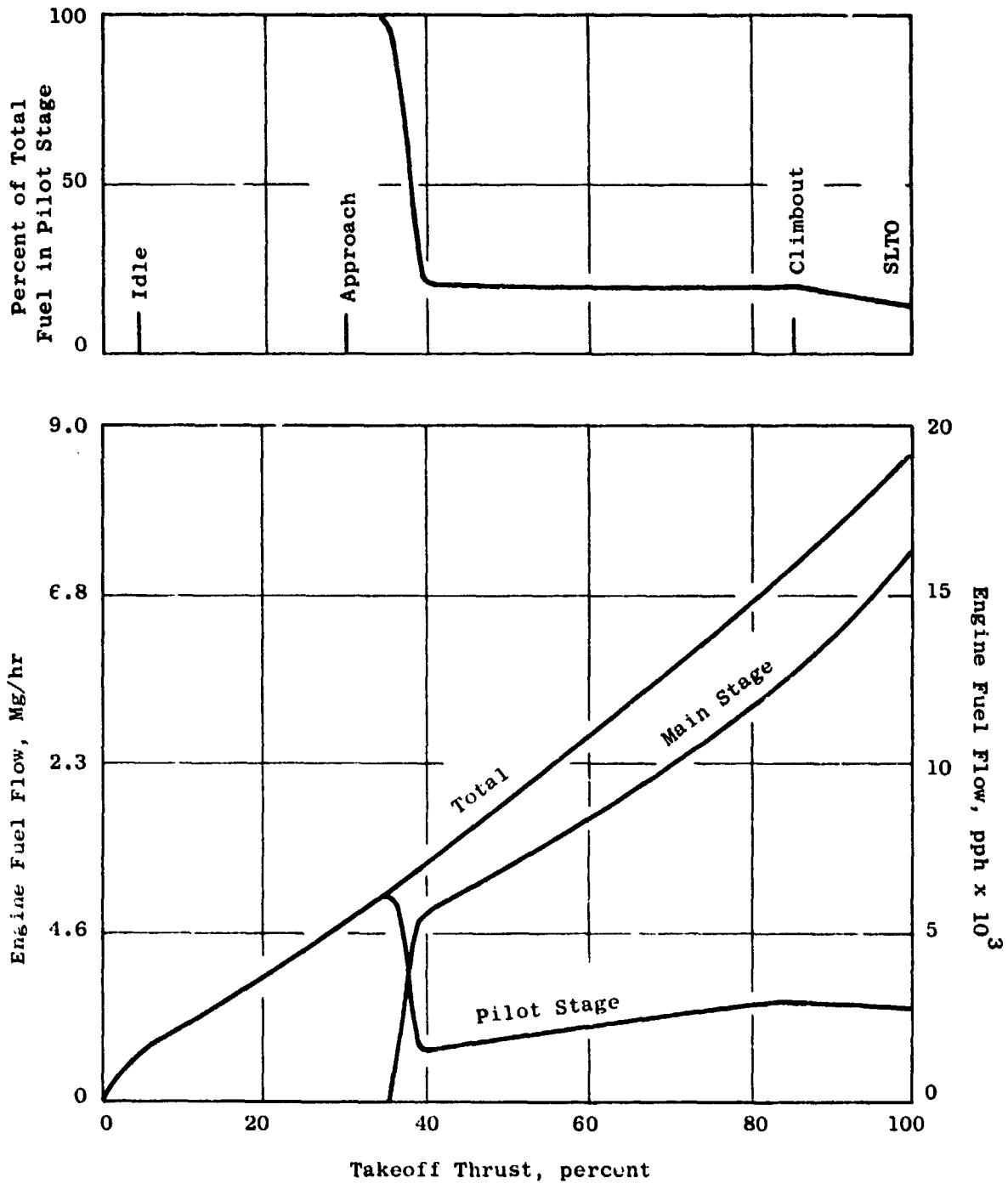


Figure 77. Engine Fuel Flow Schedule.

reduced, and the remaining fuel flow is supplied to the high-airflow, high-velocity, main-stage dome to provide a low-residence-time, lean-combustion zone for low NO_x emissions.

The predicted emissions levels for this double-annular-dome combustor are shown in Figure 78. These predictions are based on data developed in the NASA/GE ECCP and NASA/GE QCSEE double-annular-dome combustor programs with appropriate adjustments to account for differences in combustor size and inlet conditions for the different engine cycle.

These estimates were based primarily on data from combustor-component-development tests where dimensional tolerances and combustor-inlet conditions can be controlled to the prescribed cycle conditions. For the case of a production engine, some added margin is required to account for engine-to-engine variation as well as measurement variations. Based on data obtained at General Electric, a variability margin of about 20% is considered necessary for CO emissions; however, a much larger variability margin (about 40%) is considered necessary for HC emissions. The emissions of NO_x are somewhat more repeatable and are expected to vary only about 10% from the average level. Even after applying these variability factors to the E^3 emissions estimates, based on previous development-test results, it is expected that, at the completion of the initial E^3 combustor-development program, the CO and HC emissions levels will meet or closely approach the E^3 emissions goals with a prescribed ground idle thrust of 4% takeoff thrust. For ground idle operation with 6% takeoff thrust, ample margin would be available for both CO and HC emissions compared to the program goals. However, in the case of NO_x emissions, although the average engine would be expected to meet the goals, there would be a small percentage of engines that would not meet the program goals under adverse conditions. Smoke is expected to meet the standard even when the large variability in smoke levels is taken into consideration.

During the preliminary design phase, several design and tradeoff studies were conducted to arrive at the current E^3 combustor design. Some of the major studies conducted are outlined below and described in detail:

- Combustor Length
- Combustor Orientation
- Pilot Dome Annulus Location
- Swirl Cup Quantity
- Prediffuser Bleed-Air Extraction Location

Combustor length is one of the key parameters to be selected; it has a strong influence on engine length, weight, and combustor performance. The combustor should be as short as possible; however, a combustion length that is too short will provide insufficient residence time to permit completion

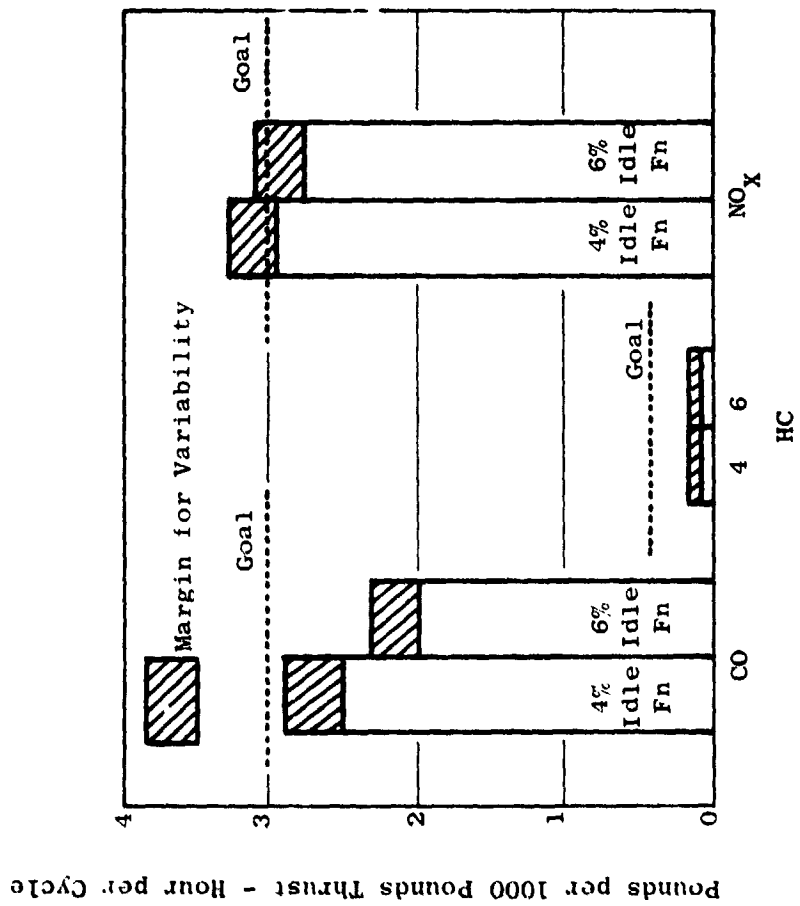
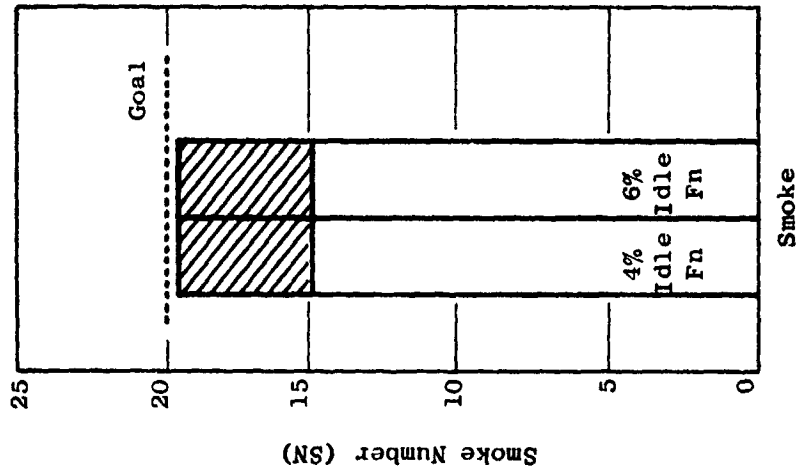


Figure 78. E³ Double-Annular Combustor Predicted Emission Characteristics.

of the combustion process and result in combustion inefficiency and/or combustion-gas mixing inadequate to provide a satisfactory exit-temperature distribution. The E³ combustor zone is about 20% shorter than that of a scaled conventional design. It should be noted that the length selected for the E³ double-annular-dome combustor design is nearly identical to that of the QCSEE double-annular-dome combustor. Based on the excellent combustion efficiency and performance obtained with the QCSEE double-annular design, the length selected for the E³ design will provide high combustion efficiency at the key operating conditions.

Orientation of the combustor in the engine flowpath is largely dictated by the radius ratio between the compressor exit and the first-stage vanes of the turbine. The larger this radius ratio, the more canting of the combustor is required to connect the two flow areas. As an example, the F101 combustor is canted at 20° to the engine centerline and has a radius ratio of about 1.5 between the turbine and compressor. The E³ has a radius ratio of 1.2. With this relatively small radius ratio, the E³ double-annular combustor configuration was selected to be parallel to the engine centerline, thus, providing a more cylindrical design. One of the key reasons for selecting this cylindrical-design approach is the improved installation and attachment associated with cylindrical machine features compared to conical machine features. With a canted design, the fuel nozzle tips are parallel to the swirl cup ferrules, but not aligned, and must ride on the swirler face to permit engagement. This feature requires provisions for more radial travel of the swirler to engage the fuel nozzle tip and is an order of magnitude more difficult to install. The cylindrical design is not expected to create any additional adverse effects with respect to installation or combustor performance.

Two important decisions were the selection of the radial location of the pilot-stage dome annulus and the quantity of swirl cups. The CF6-50C double-annular-dome combustor design featured the pilot-stage dome located in the outer annulus. To meet the emissions goals of the QCSEE double-annular-dome combustor program, it was necessary to locate the pilot stage in the inner annulus dome. In the QCSEE double-annular-combustor design, it was concluded that the swirl cup spacing in the outer annulus dome location was too large and that a more desirable spacing could be obtained with the swirl cups located in the inner annulus dome. There are many advantages to locating the pilot stage in the outer annulus. First, the location of the igniter makes it much simpler to install and maintain. Second, at operating conditions where only the pilot stage is operating, it is more desirable mechanically for the turbine to have a temperature profile that is peaked outboard. In addition, the required main-dome dimensions to maintain the proper dome velocity and combustion-gas residence times are more favorable. With the main dome located on the inner annulus, the main-dome height is 5.1 cm (2.0 inches). However, if the main dome were located on the outer annulus, the main dome height would be only 3.6 cm (1.4 inches).

As an integral part of the dome-location studies, it was necessary to select the quantity of swirl cups to be used in each dome. The initial quantity of swirl cups proposed for each dome was 28; however, 30 swirl cups

per dome provides several desirable design features. With 30 swirl cups in the pilot dome, the cup spacing is identical to that of the QCSEE combustor which demonstrated very low CO and HC emissions levels at QCSEE ground idle operating conditions. In addition, with 30 swirl cups located in each dome, the ratio of swirl cup width to dome height is nearly one for both the pilot and the main dome locations. A width-to-height ratio of about one is desirable from the standpoint that the fuel-spray discharge is conical and would lend itself to a more uniform distribution of fuel in the dome. Also, the 30-swirl-cup array provides an even number of degrees spacing per cup (mechanical symmetry) which is desirable from a design and fabrication standpoint.

During the design of the split-duct diffuser, two approaches were considered for extracting turbine rotor cooling air. The first approach extracts bleed air from the base of the splitter and routes the airflow through hollow struts. This approach offers the advantages of enhancing the diffuser airflow stability at the trailing edge of the pre-diffuser, providing positive dirt separation for the turbine cooling-air circuit, and providing easy modification of cooling-flow levels. The second approach extracts bleed air at the leading edge of the splitter. This approach offers the advantages of a positive pressure feed and slightly cooler bleed air since the compressor discharge air is coolest at the center. The main disadvantages to this approach are the dimensional sensitivity of the cooling-air-feed slot to meter the bleed flow and the difficulty expected in reworking the hardware if the bleed-flow levels were off-design. Because of the high risk associated with obtaining off-design bleed-airflow levels with the leading-edge design, the trailing-edge bleed-air-extraction design was selected as the preferred approach.

4.3.3 Impact of Broad-Specification Fuels

It is expected that aircraft will be obliged to operate with broad-specification fuels in the future. In addition to the basic combustor-design studies, the impact of broad-specification fuels on combustor operation was briefly evaluated. Shown in Table 40 is a comparison of properties of a typical broad-specification fuel evolved at NASA called Experimental Referee Broad Specification (ERBS), a typical Jet A fuel, and the Jet A fuel specification limits. In general, broad-specification fuels will have higher aromatics content, viscosity, and freezing point and lower hydrogen content.

These fuel-property changes represent more of a problem to the airframe, in terms of storage and pumping, than to the engine. However, there are several areas of combustor operation that are expected to be affected by the use of fuels typified by ERBS. Smoke is expected to increase slightly because of the lower hydrogen content; however, it is expected that the smoke levels will still be below the program goal. Accompanying the higher smoke levels would be higher flame-radiation levels - producing a small increase in liner skin temperatures. With the shingle liner design, these small increases in temperature are not expected to limit the combustor in meeting the life goals.

Table 40. Broad Specification Fuels (BSF).

Property	Jet A Typical	Jet A Specification	ERBS*
Freezing Point, ° C (° F)	-46 (-50)	-40 (-40) Max.	-29 (-20) Max.
Viscosity at -23° C (-10° F), Centistokes	6.0	9.0 Max.	12.0 Max.
Aromatics Content, %	18.0	25.0 Max.	≈35.0
Hydrogen Content, %	13.6	≈13.4	13.0 Min.

*Experimental Referee Broad Specification; typical ERBS properties are undefined as yet.

Slightly higher flame temperatures are associated with the expected lower hydrogen content of broad-specification fuels. This will tend to increase NO_x emissions levels. Additional margin in the NO_x emissions levels obtained with the Jet A fuel would have to be developed to accommodate this increase. Also, the increased viscosities and higher boiling points of broad-specification fuels are expected to make the fuel more difficult to atomize and to result in poorer thermal stability.

The impact of broad-specification fuel on ignition was assessed qualitatively based on available test data. In the case of conventional, single-annular combustors it has been determined that changes in key fuel properties such as flashpoint, initial boiling point (IBP), viscosity, surface tension, and other properties which affect the atomization, volatility, and flammability characteristics of the fuel can result in some deterioration of combustor ignition performance.

In the case of ERBS, the two fuel properties expected to adversely affect ignition to the greatest degree are viscosity and volatility. The viscosity requirement for ERBS at -23° C (-10° F) will permit about 35% more viscosity than the Jet A specification. In the case of volatility, there is no specific requirement for ERBS or Jet A. However, several fuel-distillation parameters such as flashpoint, vapor pressure, initial boiling point (IBP), 10% recovery, and final boiling point (FBP) are indicators of the degree of volatility. It would be expected, in general, that broad-specification fuels like ERBS would be less volatile than Jet A and therefore be more difficult to ignite. Tests conducted on existing single-annular-combustor designs show a definite correlation for cold-day ground starting with volatility and viscosity (atomization); the less volatile, more viscous fuels require higher fuel/air

ratios and higher combustor-inlet temperatures to obtain ignition. Altitude-relight testing demonstrated similar effects. For low-volatility/high-viscosity fuels at low flight Mach number, a need for starter-assist was clearly indicated. In both ignition evaluations, no effect from fuel hydrogen content or aromatic type was evident.

Ignition performance in the case of the E³ double-annular combustor is also expected to be affected with a broad-specification fuel such as ERBS. However, the pilot-stage dome in which the ignition source is located is designed for low ground-idle emissions. To obtain these low ground-idle emissions requires a high-volume, long-residence-time dome design which also provides very favorable airflow conditions for altitude and ground-start ignition. Therefore, the use of broad-specification fuels might result in poorer ignition performance than Jet A fuel, but the impact would be expected to be less than for a conventional combustor design. In general, it is expected that the use of broad-specification fuels will result in only a slight degradation of combustor performance compared to Jet A fuels now in use.

4.3.4 Mechanical Design

During the preliminary design phase of the E³ double-annular combustor, two major areas were studied in depth as part of the selection process for the mechanical-design approach. The initial efforts were centered around heat-transfer studies to select the preferred cooling-ring configuration for the combustor liners. Subsequent design studies focused on selection of a liner construction approach that would meet the E³ life goals. Two cooling-liner structural concepts were considered. The first was a two-piece, double-wall approach with a full 360° circumferential machined cooling-ring supported by an impingement-cooling liner. The second approach used circumferentially and axially segmented cooling rings supported in a 360° impingement-cooling liner. This assembly is called the shingle liner design. These two approaches are illustrated in Figure 19.

E³ life goals could not be met with the two-piece-construction, machined-ring liner, even with the application of thermal-barrier coatings. A shingle liner design approach was then evaluated.

The shingle liner design approach is highly desirable for long-life applications. The hot-film liner is segmented to reduce the thermal stresses in the liner material, thus, producing longer life both through the low-stress design and the ability to use higher temperature alloys. Based on careful consideration of all of the alternatives, the shingle liner approach was selected for the E³. The shingle combustor design will satisfy both the life and minimum-cooling-flow goals for the E³ program. The following paragraphs summarize the various liner mechanical-design studies.

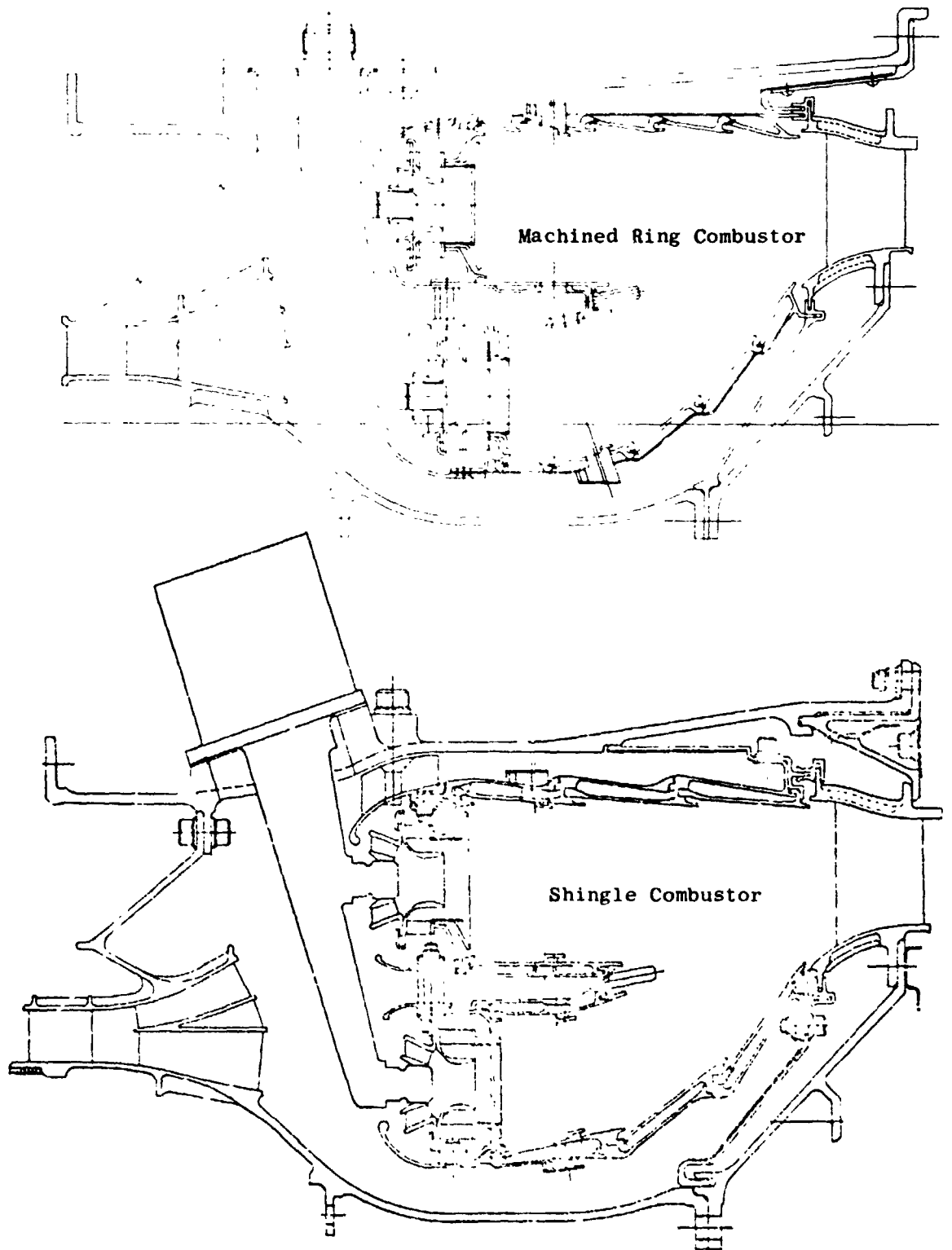


Figure 79. Machined Ring and Shingle Combustors.

ORIGINAL PAGE IS
OF POOR QUALITY

Initial design studies were devoted to heat-transfer analysis of the double-wall, machined-ring, liner configuration. A summary of the E³ combustor-liner configurations and engine operating conditions analyzed is shown in Table 41. Three basic cooling-ring approaches were analyzed. The preferred cooling-ring configuration selected, from a mechanical-design standpoint, was the short overhang. Preliminary estimates of the effects of thermal-barrier coatings were made with this configuration. The heat-transfer analysis was extended to evaluate hot-day and engine-usage deterioration effects on liner temperatures. Temperature levels for the growth engine also were investigated. Because of the high degree of similarity between the machined ring and the shingle cooling systems, temperature predictions are applicable to both designs.

A typical temperature distribution for standard day takeoff is illustrated in Figure 80. Both the average temperatures and the hot-streak values are illustrated. The most severe local temperature gradient occurs between the overhang (C) and the cooling ring nugget (D). This high gradient is the source of considerable mechanical stress in combustors.

Table 42 summarizes the current estimates of the liner temperatures at various conditions. The overhang peak temperature, combustor-inlet temperature (T₃), and the temperature differences are given. The difference, ΔT , is used in the mechanical design to characterize the life capabilities of the liner at various conditions. It is recognized that circumferential variations in the combustor temperature distribution do occur and have a significant effect on the life of the liner. Hence, the peak temperature shown is the estimated hot-streak maximum temperature. The hot streak was estimated by assuming a local region of hot, high-velocity gas at the liner boundary.

Liner stress analyses were conducted for the double-wall, machined-ring-liner design for the three selected cooling-ring configurations. A typical stress distribution for a machined-ring liner is given in Figure 81. The short overhang was preferred mechanically because of reduced overhang length, cooling-ring stiffness, and highest panel life. It is believed that the short-overhang configuration will produce the most stable overhang design.

Combustor life estimates were generated for the machined-ring, film/impingement-liner system using the results of the heat transfer and stress studies. Predicted liner lives for the machined ring did not meet the combustor life goals for the E³ program. Additional analyses were conducted incorporating a ceramic, thermal-barrier coating applied to the liner. However, the combustor cyclic-life estimates even with the coating, although significantly better than an uncoated design, were still well below the life goals.

Similar analyses conducted for the shingle design approach, with associated low thermal stresses, resulted in cyclic-life estimates substantially better than those for the nonshingled cooling-liner design and will meet the E³ life goals. A comparison of the predicted E³ combustor liner life for the shingled and nonshingled design approaches is shown in Table 43. Based on the results of these design studies, the shingled liner approach was selected for the E³ combustor.

Table 41. Summary of Heat Transfer Analysis.

- Evaluated Three Cooling-Ring Designs
 - Super Slot
 - Long Overhang
 - Short Overhang (Selected Mechanical Design)
- Evaluated Thermal-Barrier Coating Effects
- Evaluated Hot Day and Deterioration Effects
- Evaluated Growth-Engine Temperatures.

Table 42. Liner Maximum Temperature Predictions.

Condition	° C (° F)	T _{Overhang} *	Δ _T
		° C (° F)	° C (° F)
Standard Day SLTO (Baseline)	541 (1005)	816 (1550)	275 (545)
Hot Day	578 (1072)	899 (1650)	321 (578)
Standard Day Deteriorated	557 (1037)	893 (1639)	336 (602)
Hot Day Deteriorated	596 (1104)	948 (1739)	352 (635)
Standard Day SLTO (Growth)	586 (1087)	910 (1670)	324 (583)

*Max. Metal Temperature Based on Hot-Streak Levels.

Table 43. Predicted Liner Life.

Impingement-Plus-Film-Cooled Liner Configuration	Predicted Life - Cycles		
	Uncoated	Coated	Program Goal
Nonshingled	1,600	4,000	9,000
Shingled	>9,000	>9,000	9,000

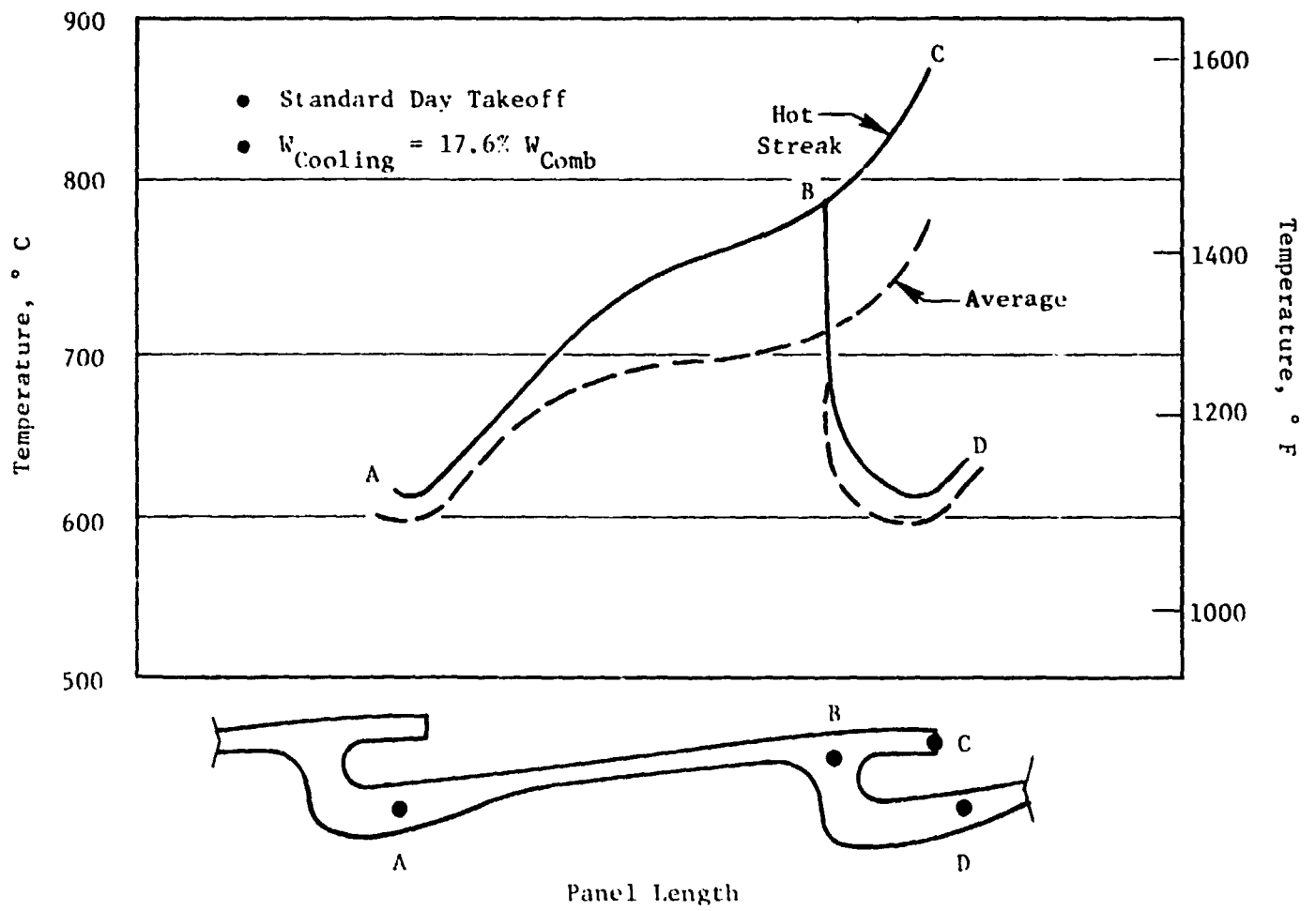


Figure 80. E³ Combustor Axial Liner Temperature Distribution, Inner Liner - Panel I.

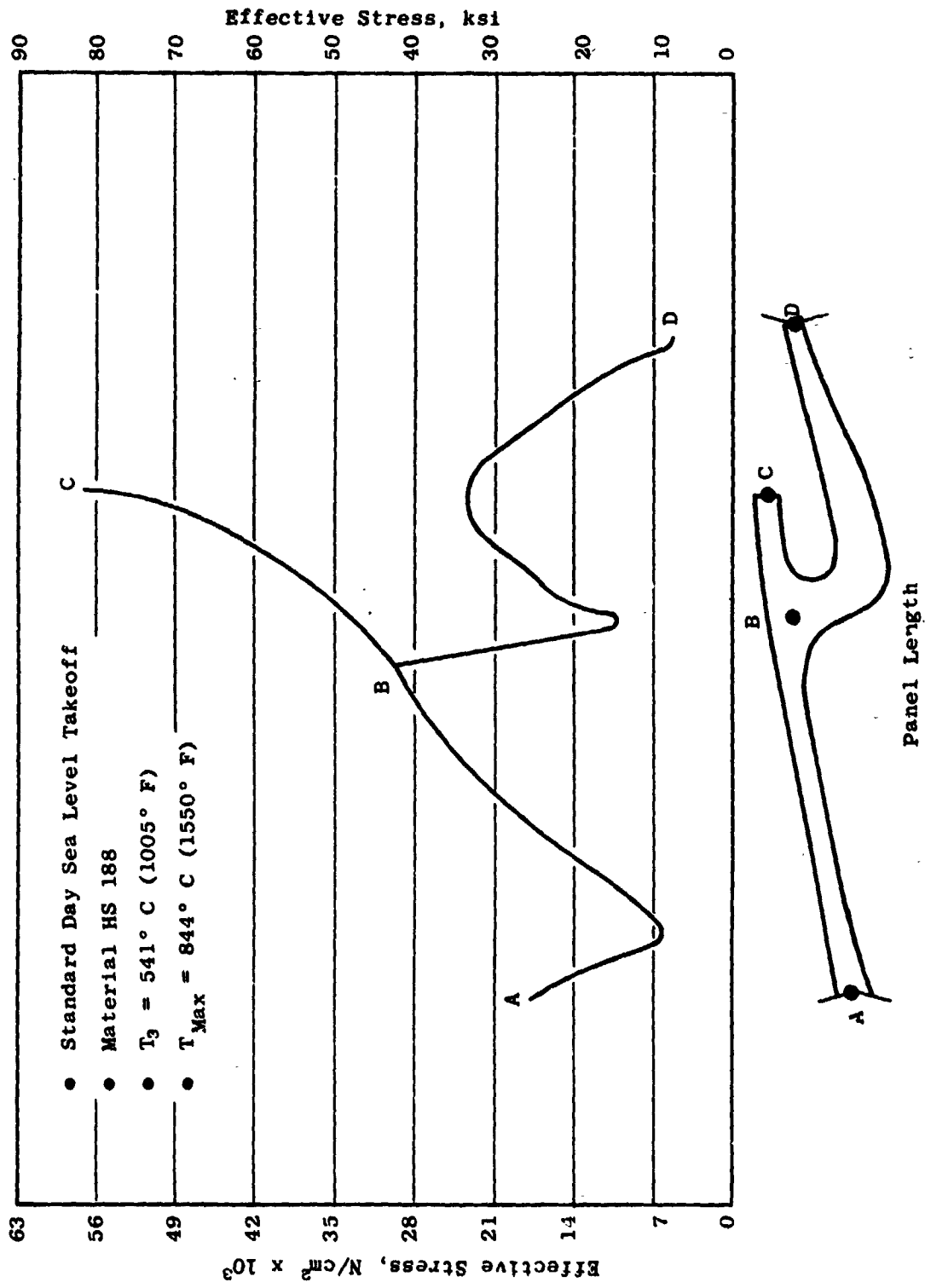


Figure 81. Typical Thermal Stress Distribution.

The overall objectives and goals of the combustion system for the E³ are to design and develop an advanced combustor configuration to meet the E³ Program goals for CO, HC, and NO_x emissions - which are equivalent to the current requirements specified by the Environmental Protection Agency (EPA) for Class T2 aircraft engines newly certified after 1981. These requirements are shown in Table 44. In addition to meeting these very stringent emissions goals for the E³ Program, the combustion system also must be designed for long life as shown in Table 45.

The major emphasis in the combustion system design is directed at meeting the very technically challenging emissions and life goals of the program; however, the combustion system also must provide the performance characteristics required for operation of a typical modern turbofan engine. The performance parameters generally considered most important in a combustion system are shown in Table 46. It should be noted that not only is high combustion efficiency required at SLTO conditions for this design, but efficiency must be maintained at a level greater than 99.5% at idle in order to meet the CO and HC emissions goals of the program.

The design condition generally selected for evaluating combustor performance is the sea level takeoff condition. However, in the case of emissions, the definition of design conditions is much more complicated. The EPA requirements are based on a prescribed landing/takeoff cycle consisting of specific operating times at idle, approach, climbout, and takeoff power settings. The emissions, as specified by the EPA, are based on the total mass of pollutants emitted per unit of thrust per hour over the prescribed cycle. Therefore, the design conditions selected for evaluating emissions are directly related to the cycle conditions which exist at each of the prescribed power settings.

The design conditions selected for conducting the mechanical analyses are predicated on meeting two program goals: combustor life and mechanical integrity. The design condition selected for conducting life analysis is sea level takeoff. However, as part of the heat transfer analysis to define metal-temperature distribution, a hot-streak condition is imposed to represent a more severe but realistic operating condition. Analyses to determine adequate structural integrity are conducted at the maximum pressure-load condition. For the structural analysis, operating conditions for a growth version of the engine were also evaluated.

4.3.5 Alternate Combustor Design

Extensive research and development efforts (Reference 12) conducted by NASA, General Electric, and other organizations have shown that the stringent EPA standards for CO, HC, and NO_x emissions necessitate the use of advanced combustor technology, including such provisions as combustion-process staging or variable-geometry features. As expected, combustor designs incorporating these advanced-technology features are considerably more complex and sophisticated than conventional combustor designs. Because of the advantages of related experience, reduced complexity, and lower costs that are attendant with

Table 44. E³ Combustor - Emission Goals (EPA 1981 Standards for Newly Certified Engines).

Carbon Monoxide (CO)	} 1bm/1000 lbf/hr Per Cycle	3.0
Hydrocarbons (HC)		0.4
Nitrogen Oxides (NO _x)		3.0
Smoke	SAE Smoke Number	20.0

Table 45. E³ Combustor - Parts Life Goals.

Item	Hours	Average Flight Cycles
Hot Parts		
First Repair	18,000	9,000
Total	36,000	18,000
Cold Parts		
Total	72,000	36,000

Table 46. E³ Combustor - Key Performance/Operating Requirements.

Parameter	Requirement
Combustion Efficiency at SLTO, %	99.5 (Min.)
Total Pressure Drop at SLTO, %	5.0 (Max.)
Exit Temperature Pattern Factor at SLTO	0.250 (Max.)
Exit Temperature Profile Factor at SLTO	0.125 (Max.)
Altitude Relight Capability, km (ft)	9.1 (30,000) (Min.)
Ground Idle Thrust, % of SLTO	6.0 (Max.)

a conventional combustor design approach, a design and development program to define a single-annular combustor, shown in Figure 82, was conducted in parallel with the efforts on the double-annular-dome combustor design of the E³ Program. This single-annular design was intended to be a possible alternate E³ combustor design. A comparison of the aerodynamic design parameters is shown in Table 47. The purpose of this program was to establish the feasibility of meeting the E³ Program emissions goals in addition to the other combustion-system requirements with an advanced, single-annular-combustor design.

To provide the low combustion-residence time required in a single-annular combustor (to minimize NO_x emissions levels), high air loading and short length are needed. These two design features in a fixed-geometry, single-annular combustor are expected to moderately compromise other important performance features such as altitude relight and exit-temperature pattern factor.

As shown in Table 47, the single-annular concept would require a very short length and high space rate. This single-annular design would contain many of the features proposed for the double-annular-dome design, such as a split-duct diffuser and shingle liners.

To provide the low combustion-residence time required to minimize NO_x emissions, a much shorter and higher space-rate combustor is required than other General Electric designs of this size category. It also should be noted that combustion-residence time at idle, relative to the residence time at sea level takeoff, is constant. Therefore, a shorter combustion-residence time at high power results in shorter residence times at ground idle. Contrary to the combustion-zone conditions desirable for low NO_x emissions, long combustion-residence times are desirable at ground idle to permit the consumption of CO and HC emissions. Therefore, with a single-annular combustor, highly loaded at high power conditions, low CO and HC emissions at ground idle conditions should be more difficult to obtain.

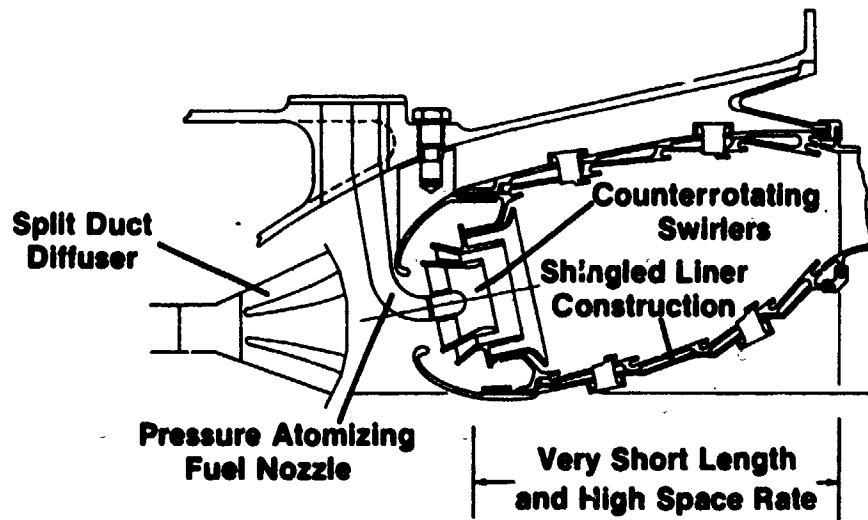


Figure 82. E³ Combustor - Alternate Design.

Table 47. E³ Combustors - Aerodynamic Design Parameter Comparison.

Parameter	Double-Annular Combustor	Single-Annular Combustor
Burning Length, cm (in.)	17.0 (6.7)	16.8 (6.6)
Length/Dome Height - Pilot	2.8	2.2
Length/Dome Height - Main	3.4	2.2
Number of Fuel Injectors - Pilot	30	30
Number of Fuel Injectors - Main	30	30
Space Rate, kW/m ³ , Pa (Btu/hr, ft ³ , atm)	0.72 (7.0 x 10 ⁶)	1.06 (10.3 x 10 ⁶)
Pilot Dome Velocity (Cold), m/sec (ft/sec)	7.6 (25)	9.8 (32.2)
Main Dome Velocity (Cold), m/sec (ft/sec)	19.1 (63)	9.8 (32.2)

The airflow distribution selected for the E³ single-annular design was simulated by modifying the airflow areas in an existing, similar-size combustor. The initial portion of the test program was carried out in a sector-combustor test rig capable of operating at the E³ combustor-inlet conditions at ground idle. A photograph of this five-swirl-cup (90°) test rig is shown in Figure 83. Nine different sector-combustor configurations were evaluated, and the most promising of these designs was selected for evaluation in a full-annular-combustor, high-pressure test.

Based on the available test results, estimates were made of the CO, HC, and NO_x emissions levels expected in the E³ single-annular combustor. As expected, the CO emissions are very high compared to the required levels at the prescribed ground idle conditions corresponding to 4% of the sea level takeoff thrust (Figure 84). At a ground idle thrust of 6%, however, the CO emissions very closely approach the required levels even when the margin for variability effects is included. The NO_x emission levels at both idle settings exceed the E³ project goals. At the conclusion of this testing, it was determined that the double-annular-dome approach exhibited the greatest potential for meeting all of the program emission goals. Therefore, the double-annular-dome concept was retained as the prime approach for the E³ combustor application.

4.3.6 Weight Estimate

As part of the mechanical-design analysis, detailed calculations of the double-annular-combustor system weight have been completed. An estimated weight of 122.6 kg (270 lbm) has been calculated for the complete system in

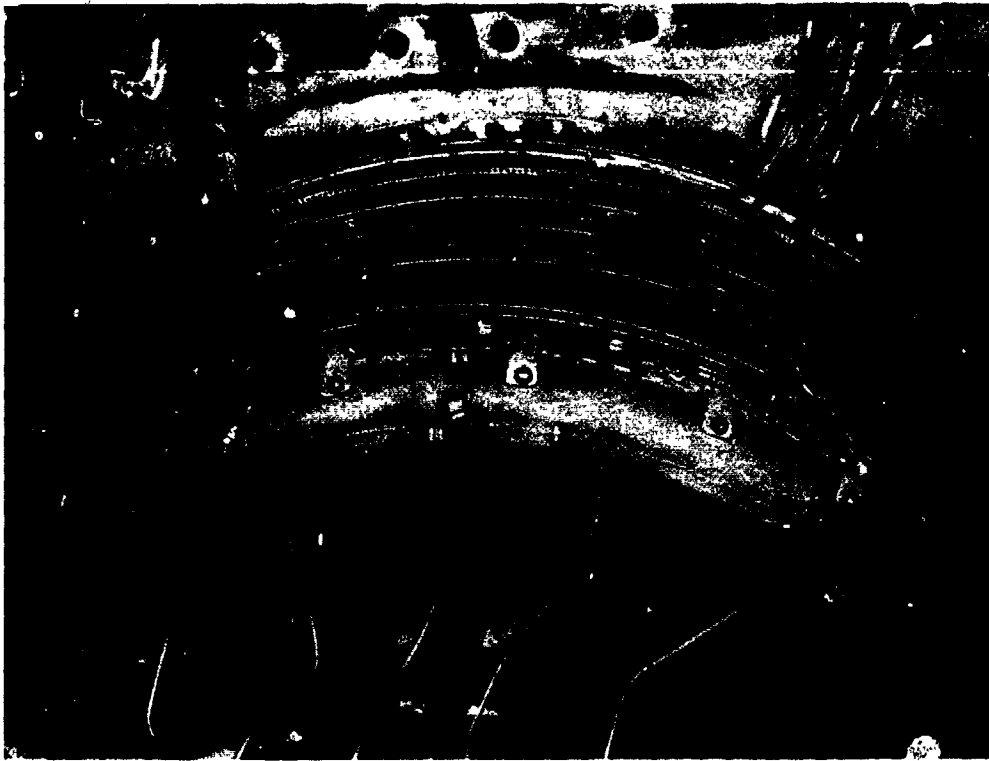


Figure 83. E³ Combustor - Alternate Design Test Configuration.

ORIGINAL PAGE IS
OF POOR QUALITY

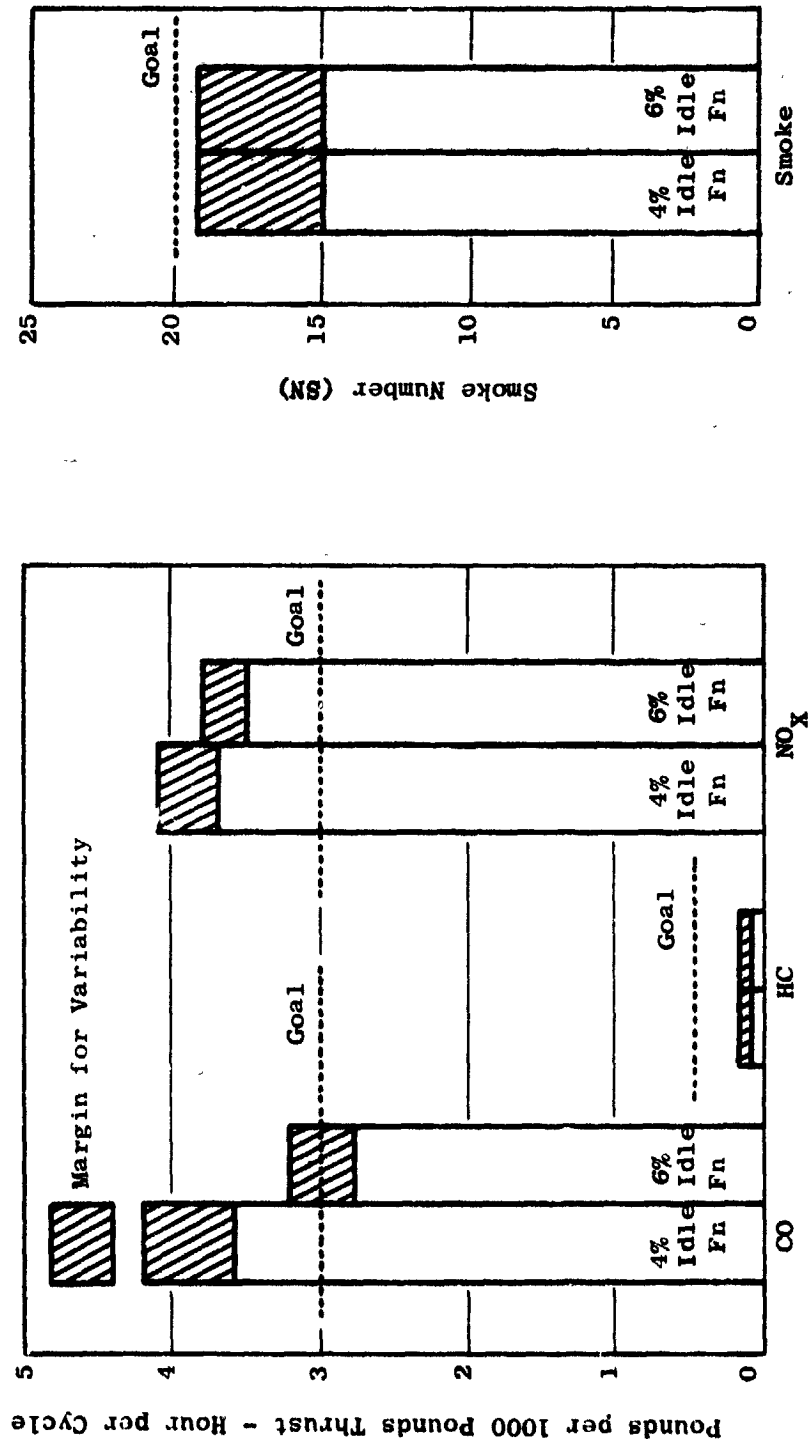


Figure 84. E³ Single-Annular-Combustor Emission Characteristics.

the baseline engine. A breakdown of this weight estimate by major component is provided in Table 48. An increase in combustion-system weight of approximately 4.5 kg (10 lbm) is anticipated for the growth engine due primarily to a required increase in combustor-casing thickness.

Table 48. E³ Double-Annular Combustion System Weight Estimate (Baseline Engine).

Component	Weight kg (lbm)
Outer Combustor Case	31.3 (69)
Fuel Delivery System	44.0 (97)
Combustor and Screens	47.2 (104)
Total	122.6 (270)

4.4 HIGH PRESSURE TURBINE

4.4.1 General Description

The two-stage HPT is an air-cooled design using compressor-discharge and interstage air as coolant for the vanes and blades. Figure 85 shows the general turbine configuration and air passages used for cooling and purging. The components are designed for commercial applications and long service lives. The turbine configuration incorporates advanced design concepts and advanced material applications. Table 49 describes the major technology features of the turbine components.

The major component goals in the FPS engine, shown in Table 50, define the component life goals at a turbine efficiency of 92.4%. The use of two stages, optimized reinjection of cooling air into the flowpath, low windage losses, active clearance control, and advanced aerodynamic design contribute to the high estimated turbine efficiency. An assessment of HPT potential efficiency was made based on CF6-50C testing. Corrections were applied to account for reduced load and for geometry differences, and the resulting efficiency was 91.5% (Table 51). Additional effects of cooling air, reduced tip clearance, and improved aerodynamics resulted in an installed efficiency of 92.4%.

Trade studies showed specific fuel consumption improved as work was shifted from Stage 1 to Stage 2 up to the point where a higher pressure cooling-air source would have been required for the Stage 2 vanes. A power split of 55% on Stage 1 and 45% on Stage 2 was selected, as shown in Table 52, and is near optimum for the Stage 7 vane-cooling system. Stage 8 cooling air resulted in a net system sfc loss. A summary of internal aerodynamic parameters is shown in Table 53.

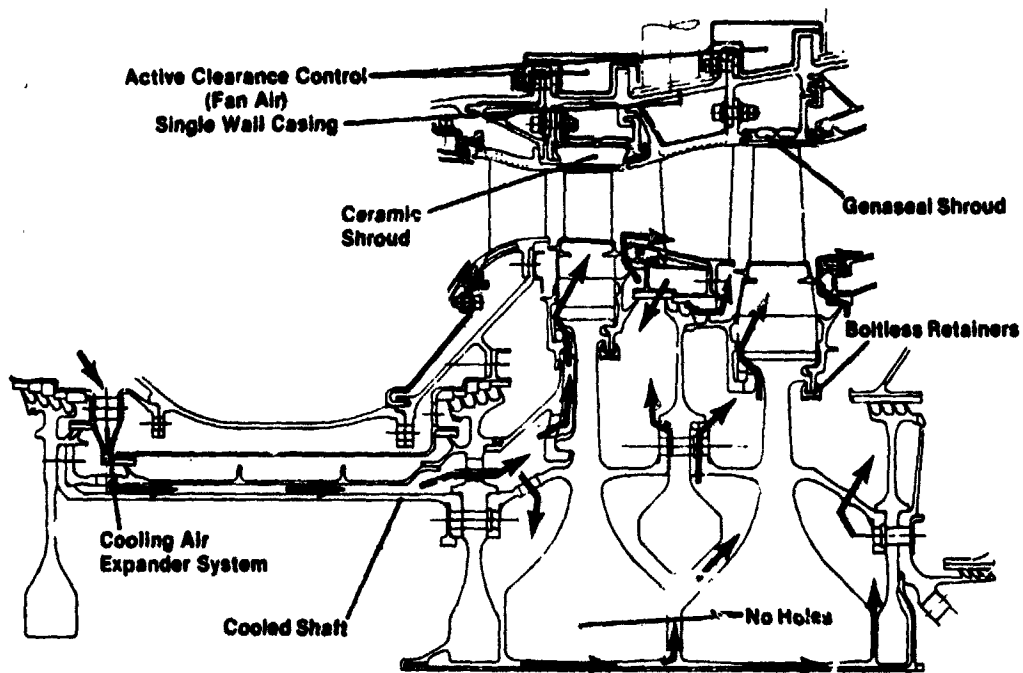


Figure 85. E³ High Pressure Turbine.

Table 49. High Pressure Turbine Major Technology Features.

- Two Stages, 92.4% Efficiency Goal
- Low Windage Loss, Flowpath Seals
- Active Clearance Control
- Blade-Cooling Expander System
- No Holes in Major Disks
- Advanced Materials
- Modular Assembly and Maintainability Features
- Ceramic Shrouds
- Thermal Barrier Coating (TBC) - Incorporation Based on Test Results

Table 50. High Pressure Turbine FPS Goals.

- Rotor Inlet Temperature - Hot Day Takeoff, Sea Level at M = 0.3
 Cycle 1343° C (2450° F)
 Design Red Line 1421° C (2590° F)
- High Pressure Turbine Efficiency - 92.4% (Maximum Cruise, Altitude)

Component	Service Life Installed		Total Life With Repair*	
	Hours	Flight Cycles	Hours	Flight Cycles
Flowpath Components Blade Retainers, Interstage Seals	9000	9000	18000	18000
Disks/Shaft	18000	18000	36000	36000

*Typical Repairs as follows:

- Stripping and recoating blades/vanes
- Crack repairs, seal-tooth build up
- Removing fatigued metal from disk bolt holes

Table 51. Estimated HPT Efficiency.

Item	Turbine Efficiency, %
Aerodynamic Efficiency*	90.4
Net Cooling Effects	+ 0.1
Active Clearance Control	+ 1.6
Improved Aerodynamics	+ 0.3
Installed Efficiency	92.4

*CF6-50C technology level at altitude cruise clearance.

Table 52. HPT Energy Distribution.

- Work Split - Maximum work on Stage 2 up to limit set by Vane 2 cooling air back-flow with Stage 8 cooling air showed a net system degradation.
 - $\Delta h \text{ Stg } 1 / (\Delta h \text{ Stg } 1 + \Delta h \text{ Stg } 2) = 56.9\%$
 - Stg 1 Power/HPT Power = 55%
- Reaction - Set by thrust balance requirements (see Table 53).

Table 53. HPT Aerodynamic Description.

Stage	1	2
Pressure Ratio	2.25	2.11
Loading, $\Delta h/2U^2$	0.74	0.56
Blade Turn	105.5	90.0
Reaction	0.35	0.38
No. of Vanes	46	48
No. of Blades	76	80

Root reaction is moderately high at values of 35% for Stage 1 and 38% for Stage 2 at the aerodynamic design point. These reactions were selected to improve rotor thrust balance by increasing aft pressure load on the bearing system.

Aerodynamic loading is moderately low. Table 54 represents the aerodynamic design requirements for the HPT. The turbine flowpath and the aerodynamic airfoil contours were designed using these parameters.

The present turbine configuration summary for the combined stator and rotor weight is 510 kg (890 lbm). Table 55 illustrates a breakdown of turbine parts by weight. Further refinement of the weight estimates will continue as the detail design of the turbine proceeds.

4.4.2 Cooling

In order to utilize the cooler compressor-discharge air at the pitch-line location for blade cooling, a unique design feature was configured as shown in Figure 86. This system takes advantage of the cooler air at the pitch line relative to the typical hub-extraction system. The extracted air passes through passages within the OGV structure. This air is then brought to a cavity where it passes through the expander system.

The cooling-flow distribution and cooling supply system are shown in Figure 87. The compressor discharge air, after passing through the expander system, is channeled within the torque shaft and outer liner. The air is then pumped to a higher pressure by the impeller located on the front face of the Stage 1 disk. Next, the air enters the disk at the bottom of the disk dovetail post and finally enters the blade through holes located at the bottom of the blade dovetail. The Stage 2 blade cooling air is from the same source; however, air passes through holes located in the forward arm of the Stage 1 disk shaft and then passes below the Stage 1 bore. Disk-bore cooling achieved by this air provides the improved disk thermal-growth response used as part of the active clearance-control system. Air passages are designed into the Stage 2 disk forward arm flange such that the air can pass into the cavity and continue out of the disk dovetail posts. The air then enters the blade through cooling holes at the bottom (base) of the blade dovetail.

A purging system between the Stage 1 disk and the interstage seal disk is used by combining seventh-stage air (used for Stage 2 vane cooling) and the compressor-discharge air.

The Stage 1 nozzle is cooled by compressor-discharge air. The inner coolant source feeds the air in the forward cavity of the vane; the outer coolant air feeds the forward and aft cavity of the vane. Band cooling follows a similar pattern.

Table 54. HPT Aerodynamic Design Requirements.

Cycle Parameter	Aerodynamic Requirement at Max. Climb Standard Day +10° C (+18° F)
$\Delta h/T$, J/kg(K) Btu/lbm (° R)	353.61 0.0844
N/\sqrt{T} , rpm/K rpm/° R	316 236
$W/\bar{T}/P$, kg(K)/sec(Pa) lbm(° R)in. ² /sec(lbf)	0.000867 1766
Ψ (GE) = $g j \Delta h/2 \Sigma U_p^2$	0.649
Ψ (NASA) = $g j \Delta h/\Sigma U_p^2$	1.298

Where:

h is enthalpy

T is temperature

N is rotational speed

W is weight flow

P is pressure

Ψ is loading

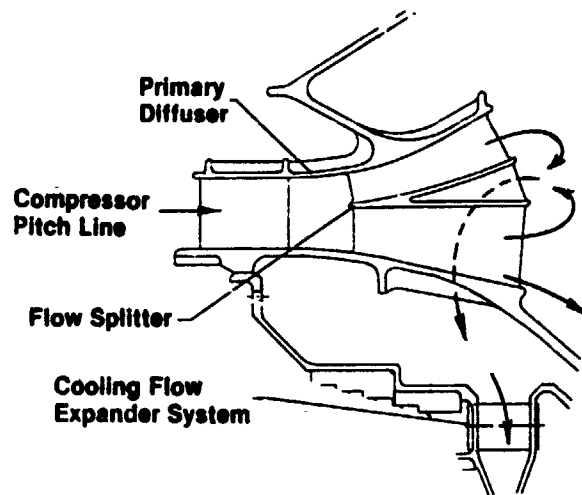
g is acceleration of gravity

j is 778 ft-lb/Btu

U_p is pitch-line velocity

Table 55. HPT Weight Summary.

Item	Weight, kg (lbm)	
Rotor	Stage 1 Blade	12.2 (27)
	Stage 2 Blade	20.4 (45)
	Stage 1 Disk	74.1 (163)
	Stage 2 Disk	78.6 (173)
	Disk Seals, Retainers, Shafts, Paddle Wheel, and Fasteners	110.0 (242)
	Subtotal	295.3 (650)
	Stator	Stage 1 Nozzle
Stage 2 Nozzle		14.1 (31)
Inner Nozzle Support		6.8 (15)
Outer Casing, Seals, Seal Supports, and Fasteners		70.5 (155)
Shrouds		7.7 (17)
Subtotal		109.1 (240)
Total	404.4 (890)	



- Pitch Cooling Source Reduced 21° C (38° F)
- Pitch Line Temperature Constant/Less Deterioration
- No Heat Pick-up From Combustor

Figure 86. E³ Turbine Rotor Cooling Source.

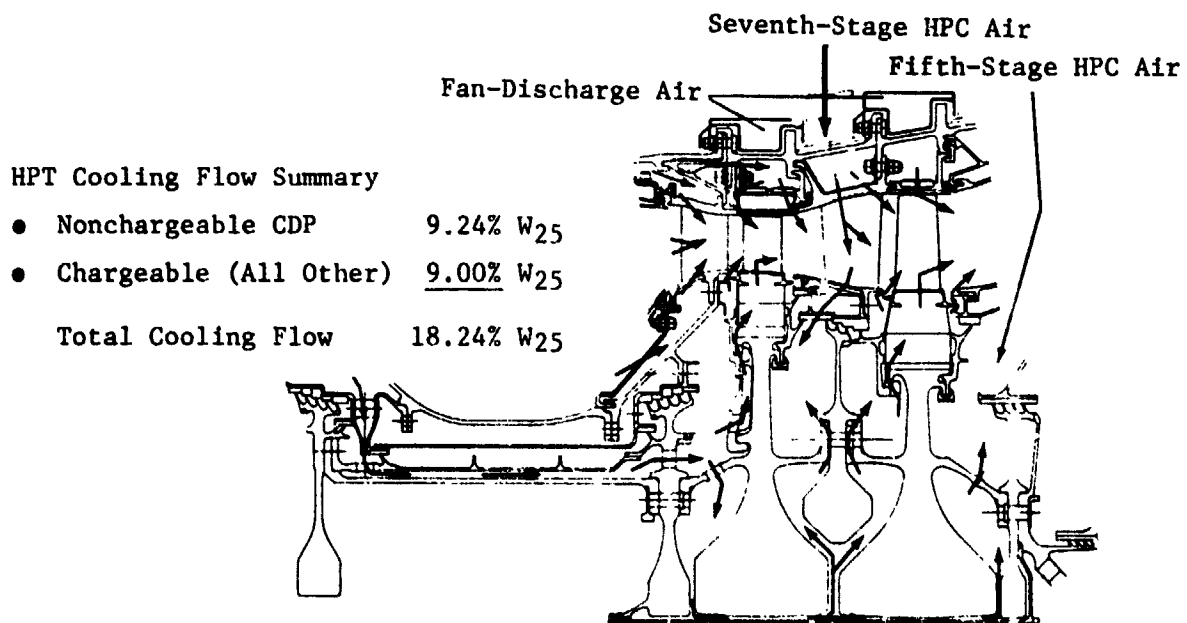


Figure 87. E³ High Pressure Turbine Cooling-Flow Distribution.

4.4.3 Stage 1 Design Features

The Stage 1 nozzle consists of a fabricated assembly. The airfoils are manufactured from an Oxide Dispersion Strengthened (ODS) material (Inconel MA754) and brazed to MAR-M509 bands. Figure 88 defines some of the mechanical features in the nozzle design. The airfoil contains two unconnected cavities. The forward cavity employs two inserts with a slip joint within the cavity. The purpose of the two inserts is to increase the backflow margin of the spent impingement air by allowing air to enter from the inner and outer edges of the vane. This has the effect of doubling the coolant-feed area for the two-insert design.

The two-cavity vane airfoil, as shown in Figure 89, is formed by the use of the rib located within the airfoil and extending along the spanwise direction. Air entering the forward cavity through the inserts impinges on the inner airfoil walls and exits through an array of film holes for further cooling. The leading edge uses a "shower head" film-cooling design to maintain uniform surface cooling.

The inner and outer bands are cooled by a combination of impingement and film cooling. Band compartmentized cooling, as shown in Figure 90, is used to increase the effectiveness. After the air impinges on the band wall, it enters the gas stream through an array of film holes. As the hot gas traverses axially, the outside gas pressure diminishes. This allows a higher impingement pressure ratio for the aft compartments, improving cooling effectiveness.

The Stage 1 blade design incorporates mechanical and heat-transfer features that permit long-life operation in the E^3 environment. There are two basic air-entry circuits within the airfoil, as shown in Figure 91. The forward circuit enters the airfoil in the proximity of the airfoil centerline and radially traverses a three-pass, serpentine flowpath. Within the last cavity, an array of impingement holes allows the air to impinge on the blade leading edge. The spent impingement air exits into the gas path through holes in the leading edge, pressure and suction sides. The suction-side film holes allow improved air ejection and film cooling along the suction side of the airfoil.

Aft-cavity-circuit air enters the airfoil in the vicinity of the trailing edge. An array of metering holes allows this air to enter the trailing-edge slots for cooling. This air then enters the gas field on the pressure side. Incorporating pressure-side bleed permits the use of thinner trailing edges, thereby improving turbine efficiency.

4.4.4 Stage 2 Design Features

The Stage 2 nozzle vane shown in Figure 92 is a fabricated assembly consisting of René 150 airfoils brazed to René 80 inner and outer bands. The airfoil is cooled by using seventh-stage compressor air that enters an impingement insert at the outer band location. After the air impinges on the airfoil,

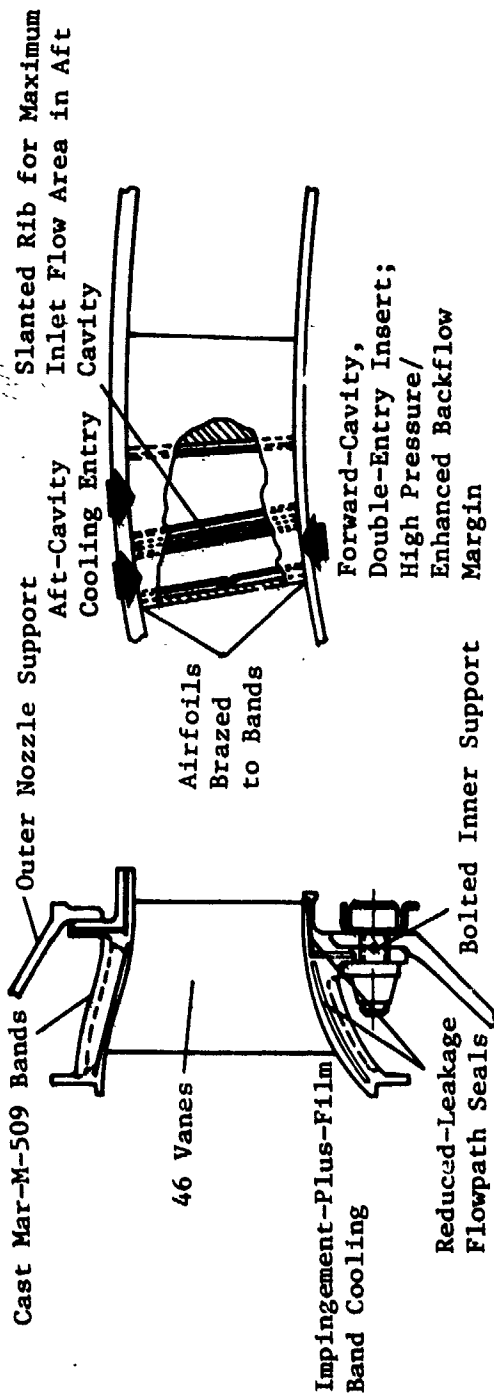


Figure 88. High Pressure Turbine Stage 1 Nozzle Diaphragm Design Features.

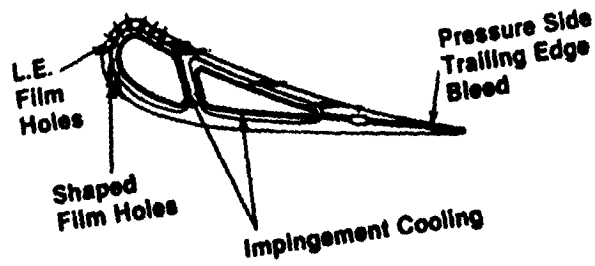


Figure 89. E³ High Pressure Turbine Stage 1 Vane Airfoil Cooling

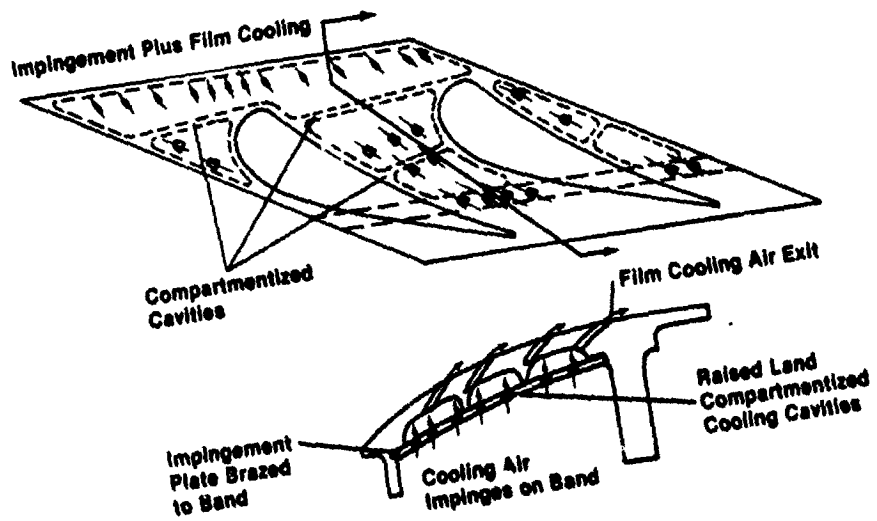


Figure 90. E³ High Pressure Turbine Stage 1 Vane Band Cooling.

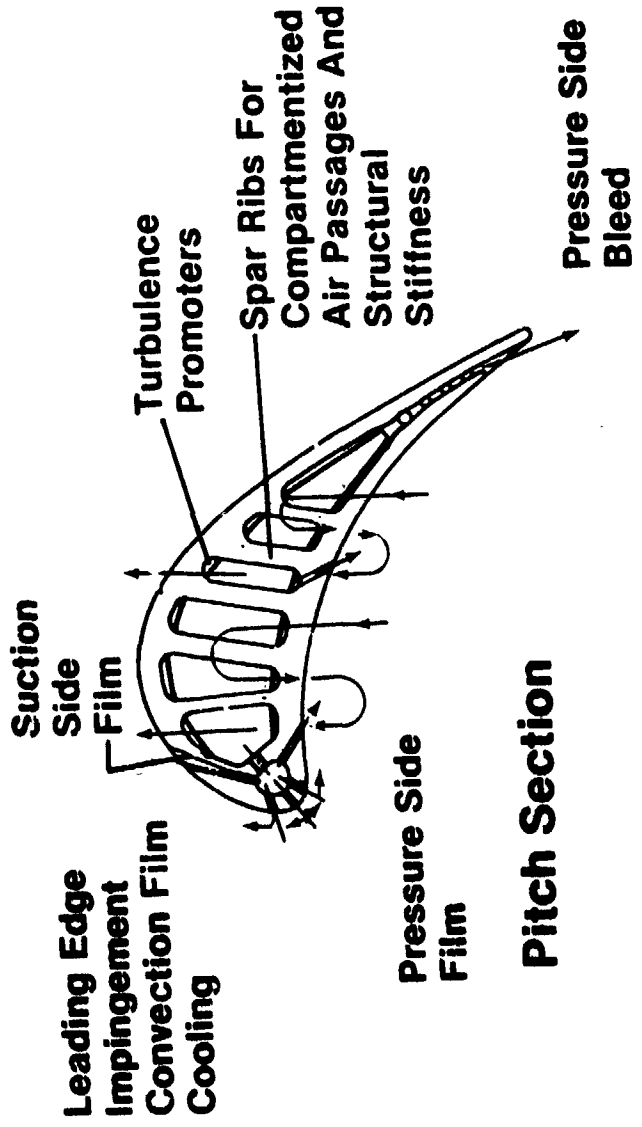
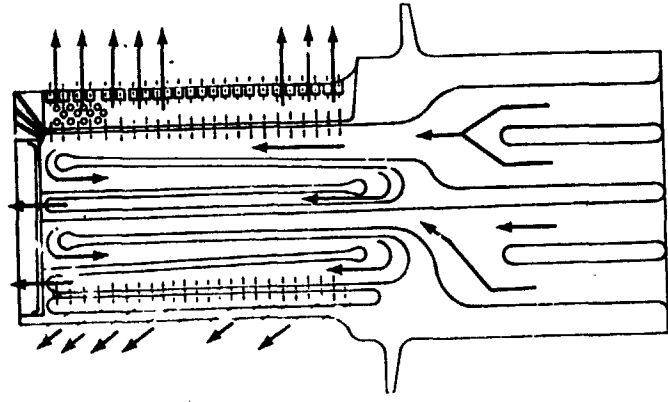


Figure 91. E³ High Pressure Turbine Stage 1 Blade.

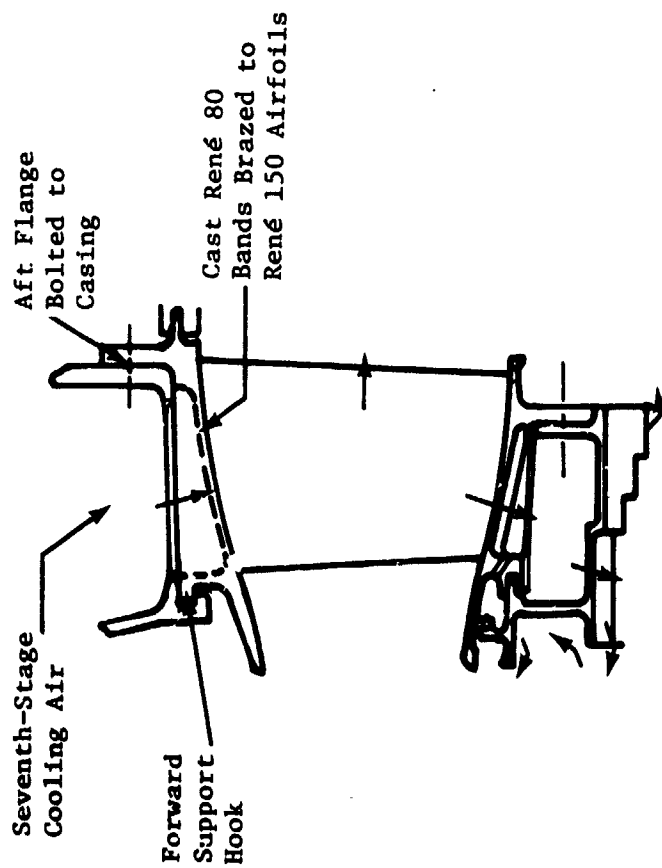
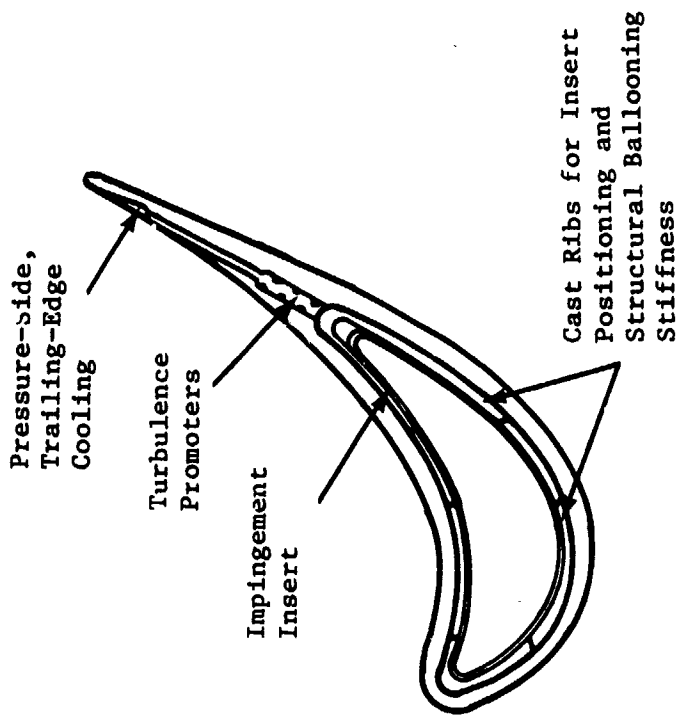


Figure 92. E³ High Pressure Turbine Stage 2 Nozzle Vane.

a portion is fed to the inner cavity for further band cooling and purging the interstage cavity. The remainder of the impingement air is fed through slots to cool the trailing edge of the airfoil. Cast ribs are located along the airfoil chord to locate the insert (control impingement distance) and increase the structural wall stiffness (in order to minimize local airfoil bulging, or ballooning, of the suction-side wall).

The Stage 2 blade design shown in Figure 93 is based on mechanical and heat-transfer technology features that allow it to operate for long life in the high-temperature, FPS environment. The blade is cooled by compressor-discharge air. There are two main cooling circuits. The first circuit enters the airfoil leading-edge cavity and convectively cools the airfoil surface through a three-pass, serpentine flowpath. Turbulence promoters are located along the blade wall to increase the cooling effectiveness. At the end of the serpentine circuit, the air is injected into the gas stream through holes located close to the blade tip at the pressure side. This air ejection at the blade tip contributes to increased turbine work extraction, thereby increasing turbine efficiency. The second main cooling circuit enters the airfoil in the vicinity of the blade center and convectively cools the airfoil in a three-pass circuit. The air exits into the main gas stream through trailing-edge slots that break out in the pressure side. This method of cooling the trailing edge allows the use of thin trailing edges for improved turbine efficiency.

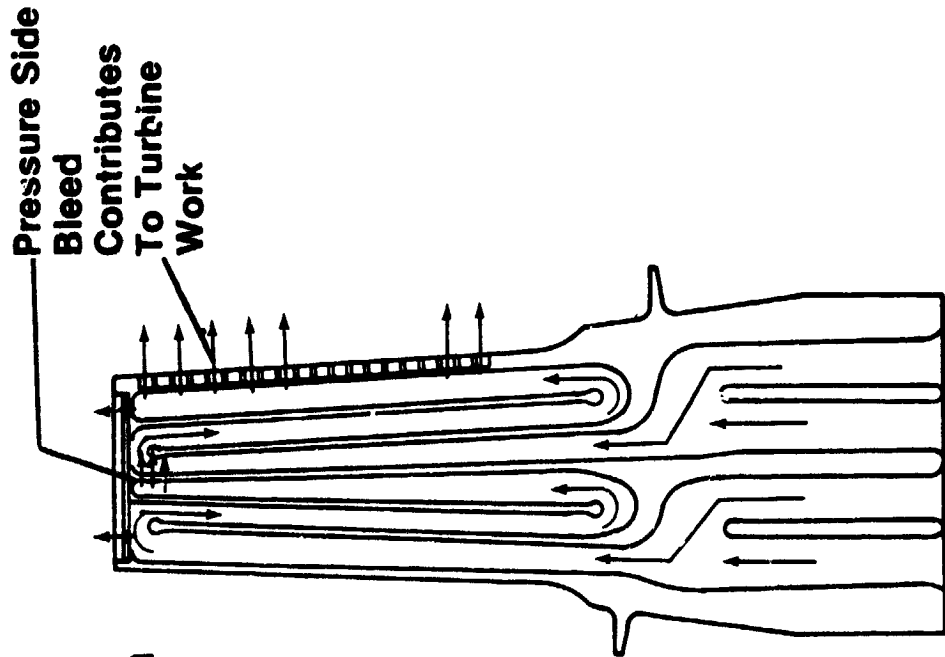
The Stages 1 and 2 blades and vanes are designed for a mission mix of 18,000 hours. Table 56 represents the basic design data for the Stages 1 and 2 blades.

4.4.5 Material

Engine-demonstrated and advanced materials and alloys under present development are used throughout the high pressure turbine, as defined in Figures 94 and 95. René 95, with high strength at elevated temperature, is used to achieve the long-life objectives for the disks. The advanced technique of forming near-net-shape sections of as-HIP René 95 is being utilized for the FPS design. This method allows minimum machining of the final disk form, thereby reducing machining costs and improving the utilization of raw stock material.

AF115, an advanced development alloy, will be used in the turbine. This alloy has the strength capability of René 95 and can operate at even higher temperatures. AF115 was specifically chosen for temperatures in excess of 704° C (1300° F).

Directionally solidified (DS) René 150 blade alloy is currently being used in an advanced development engine and will undergo testing in a CF6-50C Stage 1 HPT blade under the NASA-sponsored Materials for Advanced Turbine Engines (MATE) Project II, Contract NAS3-20074. Designing the Stages 1 and 2 blades with René 150 results in a long-life blade at higher stress and temperature than possible with current alloys.



- Non-Film Hole Design
- Convective Cooling

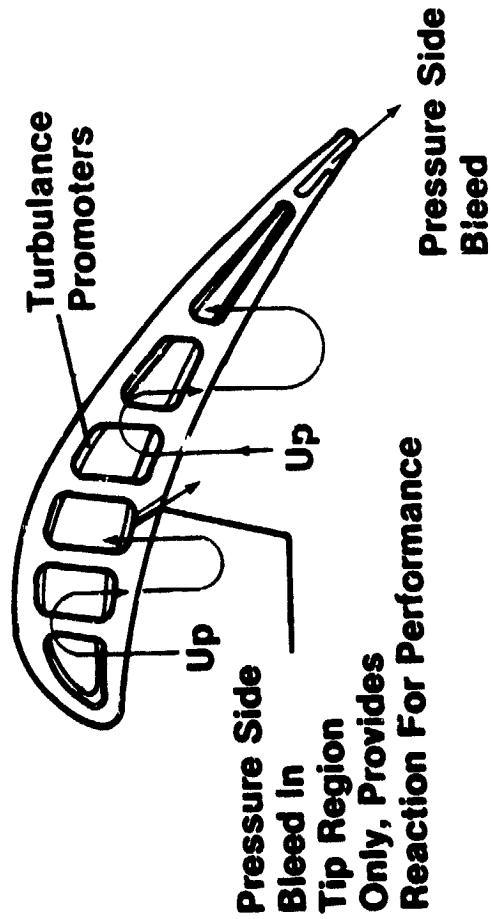


Figure 93. High Pressure Turbine Stage 2 Blade.

Table 56. HPT Stages 1 and 2 Blades and Vanes.

Parameter	Stage 1		Stage 2	
	Blades	Vanes	Blades	Vanes
Quantity	76	46	70	48
Material				
Airfoil	René 150	MA754	René 150	René 150
Bands	---	MAR-M509	---	René 80
Coolant Temperature, ° C (° F)	596 (1105)	610 (1130)	591 (1096)	488 (910)
Pitch Centrifugal Stress, MPa (ksi)	122.0 (17.7)	--- ---	186.2 (27.0)	--- ---
Root Centrifugal Stress, MPa (ksi)	208.2 (30.2)	--- ---	317.2 (46.0)	--- ---
Coolant Source	CDP*	CDP	CDP	Stage 7 Compressor Air
Area Ratio	1.6	---	1.9	---
Life Mission Mix, hours	18,000	18,000	18,000	18,000

*With expander system.

● Engine Demonstrated Advanced Materials

- René 95 PM - HIP
- René 150 DS - Blade Airfoil

● Engine Development Alloys

- AF 115 PM - HIP

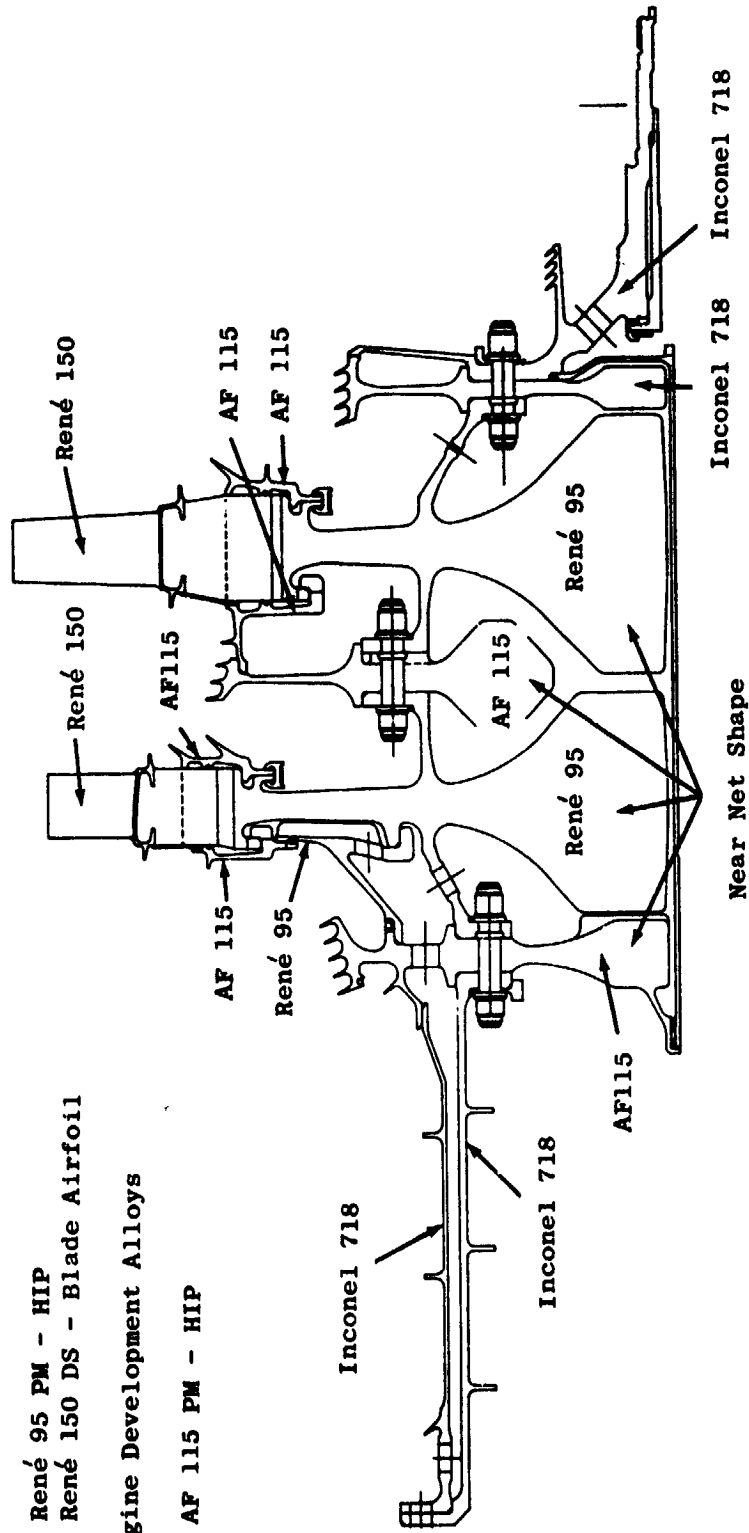


Figure 94. E³ HP Turbine Materials Rotor Components.

- Engine Demonstrator Advanced Materials
 - MA754 ODS Vane 1 Airfoil
 - René 150 DS Vane 2 Airfoil
 - Genaseal (Backup to Stage 1 Ceramic Shrouds)
- Engine Development Materials
 - Ceramic Shrouds
 - CTX-2 Low Thermal Expansion Alloy

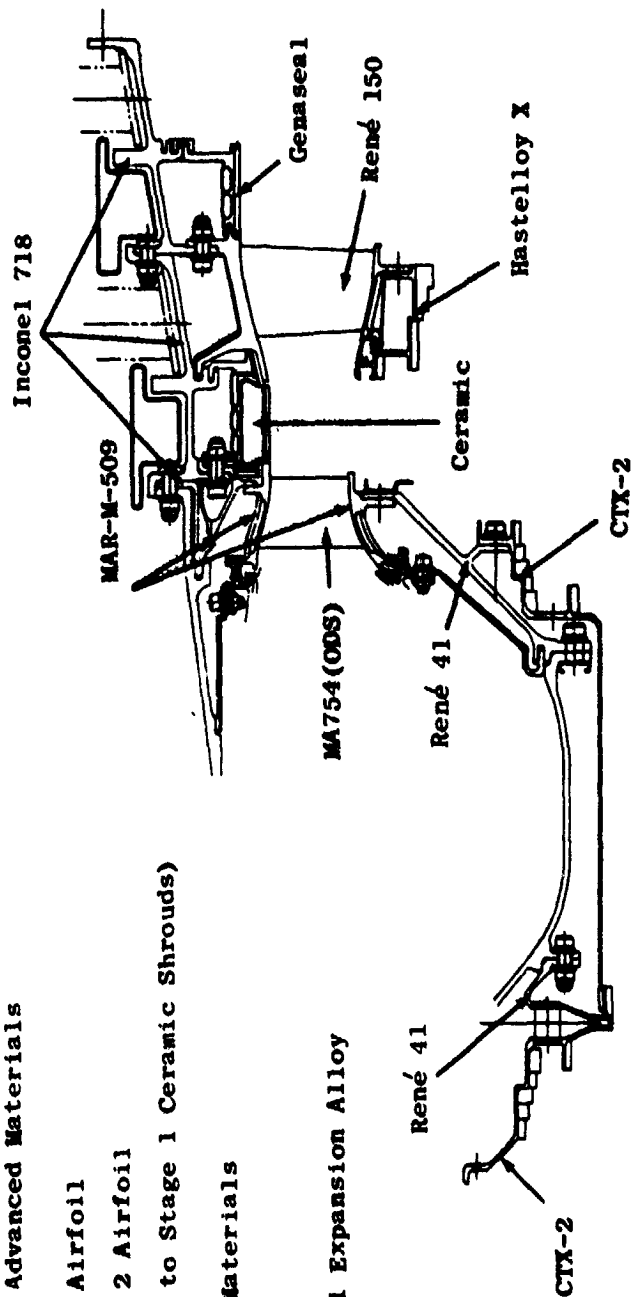


Figure 95. E³ HPT Materials - Static Components.

Design of the static parts also makes use of advanced and demonstrated alloys. The Stage 1 ceramic shroud material is undergoing lab process development as part of this program. CTX-2, a low coefficient of expansion alloy, will allow an improved radial-growth match with the seal disk, thereby allowing closer radial running clearances for reduced leakages and seal deterioration. Use of a thermal-barrier coating is being considered on HPT blades and vanes, and a program is underway to develop such a system and demonstrate adequacy for the E³. The coating will be applied to CF6-50C HPT blades and vanes and run in a factory-engine endurance test.

4.4.6 Active Clearance Control

The active clearance-control system is shown in Figure 96 and Table 57. Operating clearances are maintained by controlling the temperature of the turbine stator; this is accomplished by cooling the stator with fan-discharge air. Cooling flow is modulated by the engine control to produce and maintain proper clearances throughout the engine operating envelope. This in turn improves efficiencies and reduces premature engine deterioration.

4.4.7 Disk Life

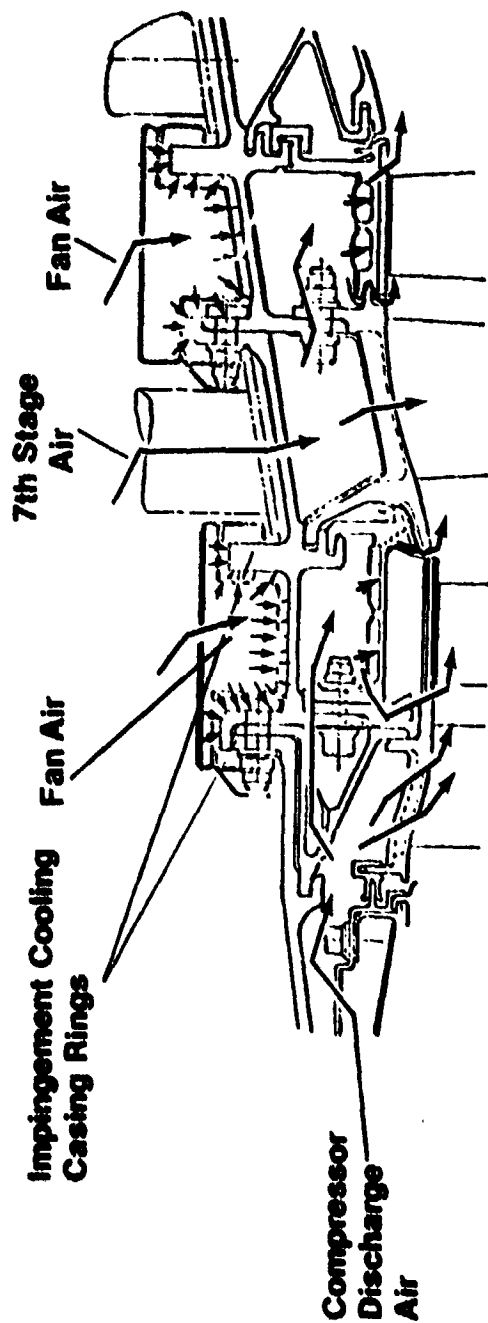
A flight mission profile was used to establish the Low Cycle Fatigue (LCF) endurance for the calculated 36,000-mission-cycle design life. In addition, variations in ambient temperature result in disks being subjected to varying speed and compressor-discharge-temperature conditions. The combination of all the varying operating parameters was used to define a mission-mix life profile for the disk bore as presented in Table 58. The table represents the four ambient temperatures at sea level static conditions used for the disk stress analysis. The stress and life summary, as shown, is the result of combining temperature and stress effects.

Figure 97 represents Stage 1 disk stresses 860 seconds into a typical flight profile. Generation of this type of analysis for various times in the mission was necessary to determine the worst disk-bore-stress condition in order to establish the LCF life capability.

4.5 LOW PRESSURE TURBINE

4.5.1 Component Description

The low pressure turbine (LPT) is a five-stage component designed for high performance with a goal of 91.7% overall efficiency. This goal was established by the current GE LPT technology base with appropriate corrections for Reynolds number and geometry. Additional corrections were made to account for tip clearance, cooling-air effects, and other aerodynamic improvements (Table 59). To achieve this goal, the aerodynamic design incorporates features (Figure 98) such as inner stage blade-to-vane overlaps and attention to rotor/stator cavity design in order to achieve low windage losses. Internal



Design Requirements:

- Close Clearance Over Operating Range
- Accommodate Transients Without Rubs
- Roundness Control/Uniform Casing Temperatures
- Minimal Deterioration

Figure 96. High Pressure Turbine Active Clearance Control.

Table 57. HPT Active Clearance Control.

Stator to Rotor Signature Characteristics:

- Stator Outer Flange Ring Provides
 - Stiffness/Roundness Control
 - Slower Response Constant
- Rotor Blades Response = 5 Seconds
- The Stator-to-Rotor Clearance Setting Point 15 Seconds into Takeoff
- Active Clearance-Control System After 15 Seconds
 - Turbine Inlet Temperature Overshoot Control
 - Performance Improvement in Max. Climb and Cruise

Table 58. HPT Stage 1 Disk - LCF Life with Mission Mix.

- FPS Engine
- As-HIP René 95
- LCF Life Base: 100% Life Used Up 36,000 Flight Cycles.

Case/Cycles In Mission Mix	σ_{eff} At Bore MPa (ksi)	% of Flights in Mission	Bore Temperature ° C (° F)
50° C (122° F) Day/7200	924 (134)	20	486 (907)
30° C (86° F) Day/10800	924 (134)	30	478 (893)
23° C (73° F) Day/7200	910 (132)	20	472 (882)
21° C (69° F) Day/1080	902 (131)	30	467 (872)

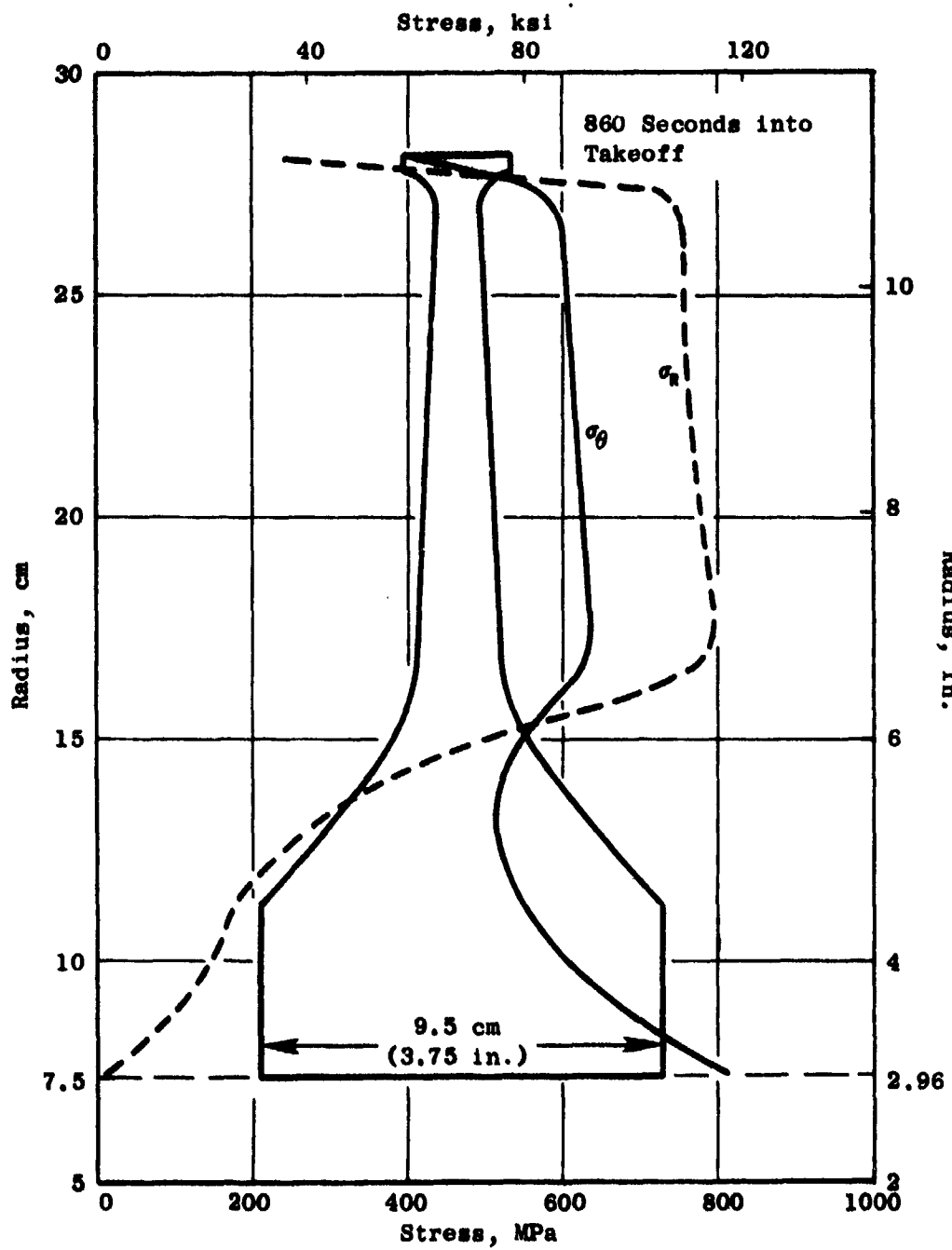


Figure 97. E³ High Pressure Turbine Stage 1 Disk Stresses.

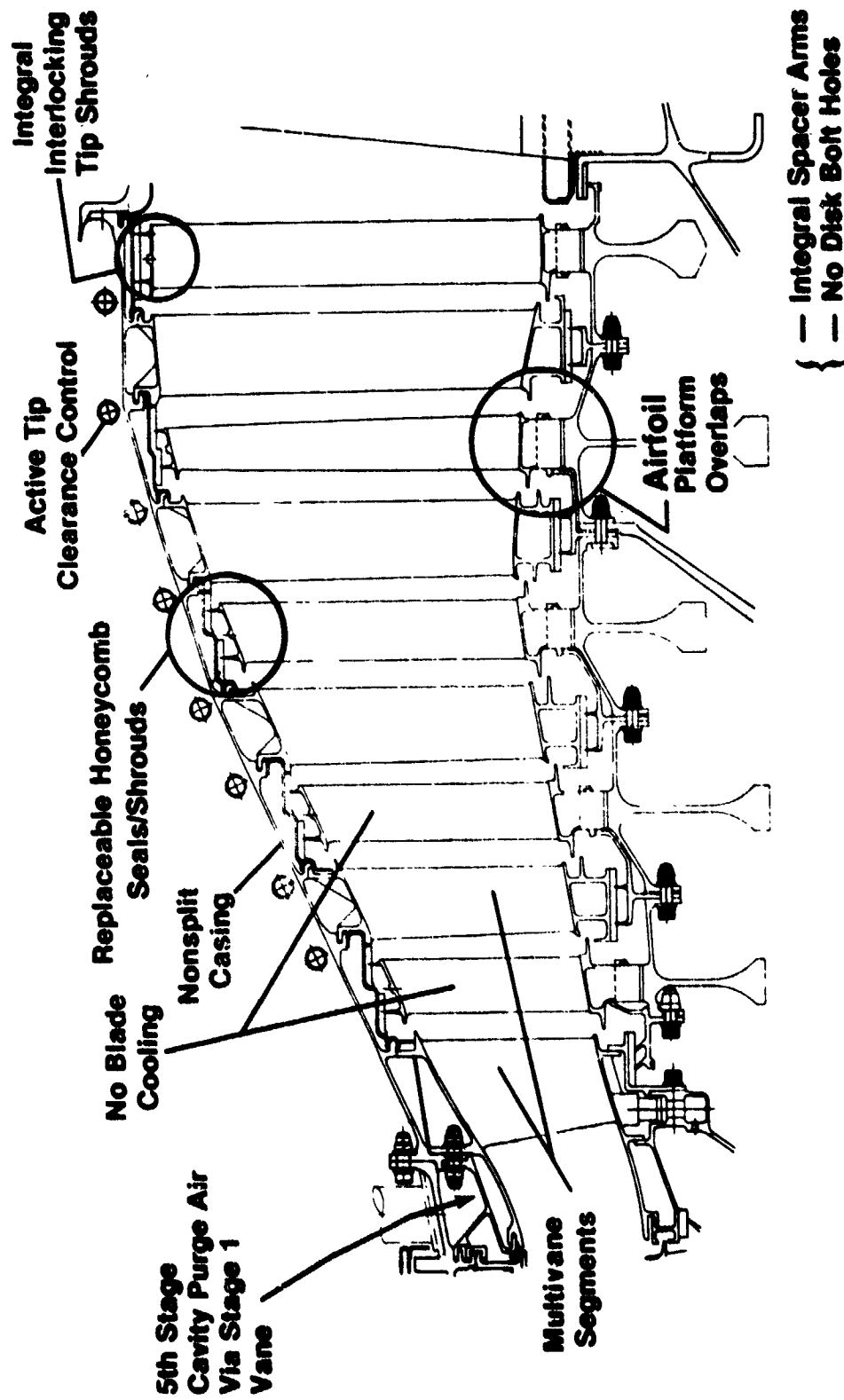


Figure 98. E³ Low Pressure Turbine - Five Stages.

aerodynamic parameters are summarized in Table 60. Blade cooling is not required for any stages, and only the Stage 1 vane is cooled by internal purge air. Honeycomb seals are provided over the tip of each blade and at the inner radius of each nozzle to reduce leakage and flow recirculation. Blade tip shrouds are integral with each blade and interlock with adjacent blades to provide both a smooth outer flowpath and a vibration restraint. Close blade-to-honeycomb clearances will be held by incorporating an unsplit casing that allows uniform circumferential temperatures and through the use of an active clearance-control system to provide rub avoidance during transient engine operation and close clearances during steady-state operation.

Ease of manufacture and assembly is enhanced by the design of nozzles in multivane segments. Long life is aided in the major rotating components by design of the disks with attachment at the ends of integral spacer arms, thus avoiding low cycle fatigue limits that would occur if bolt holes were placed through main disk webs.

Low-noise features have also been incorporated through the selection of blade numbers and vane-to-blade spacings that avoid undesirable passing frequencies and high wake-noise sources.

4.5.2 Design Objectives

Engine operation goals for the FPS LPT, as listed in Table 61, have been set for temperatures, efficiency, and life. Temperature at the LPT rotor inlet is 862° C (1583° F) for the basic engine cycle. The turbine efficiency goal for the fully developed FPS LPT is 91.7%. Component life requirements for commercial engine service are 36,000 hours and flight cycles total life for nonflowpath components, such as the casing and rotor disk, and 18,000 hours and flight cycles for flowpath components. Service life has been established for when these items need to be removed for repairs to enable them to meet the total life. These life values are 18,000 hours and cycles for nonflowpath components and 9,000 hours and cycles for flowpath components.

Materials are indicated in Figure 99. Inconel 718 is used extensively in moderate-temperature regions for the casing, disks, rotating seals, the Stage 1 vane inner seal, and all bolts. Seals are Hastelloy X honeycomb, and nuts are Waspaloy. René 125 was used for the Stage 1 vane, directionally solidified René 80 + hafnium for the Stage 1 blade, and René 80 for the Stage 2 vane. All remaining blades and vanes are made of René 77.

4.5.3 Cooling System

The LPT uses two separate cooling systems: (1) an active clearance control design for exterior cooling of the LPT casing and (2) an interior purge-air system to control interstage-rim hot gas recirculation. The ACC will be described later, but the purge-air design will be outlined here.

Table 59. Estimated LPT Efficiency.

Item	Turbine Efficiency, %
Aerodynamic Efficiency (Base)	90.6
Reduced Tip Clearance	+ 0.4
Cooling-air Effects	+ 0.3
Improved Aerodynamics	+ 0.4
Installed Efficiency Goal	91.7

Table 60. LPT Aerodynamic Descriptions.

Stage	1	2	3	4	5
Pressure Ratio	1.31	1.36	1.41	1.39	1.25
Loading, $\Delta h/2U^2$	1.70	1.62	1.46	1.15	0.77
Blade Turn	101.0	102.5	102.5	101.0	88.0
Reaction	0.27	0.32	0.33	0.27	0.24
No. of Vanes	56	96	96	108	108
No. of Blades	110	112	110	156	102
Tip Clearance, mm (mils)	0.381(15)	0.381(15)	0.381(15)	0.381(15)	0.381(15)

Table 61. Low Pressure Turbine FPS Goals.

- Motor Inlet Temperature - Hot Day Takeoff: 862° C (1583° F)
- 91.7% LP Turbine Efficiency; Fully Developed FPS
- Life Requirements/Commercial Service

Component	Service Life Installed		Total Life With Repairs*	
	Hours	Flight Cycles	Hours	Flight Cycles
Flowpath Components Blades, Vanes	9,000	9,000	18,000	18,000
Rotor Disk, Shaft, Casing	18,000	18,000	36,000	36,000

- *Typical Repairs:
- Removal of Worn Material from Vane Structural Hooks
 - Buildup of Blade Shroud Seal Teeth
 - Blending of Vane/Blade Leading- and Trailing-Edge Dents
 - Reaming Fatigued Metal Out of Bolt Holes

Hastelloy X Honeycomb Stationary Seals, Typical

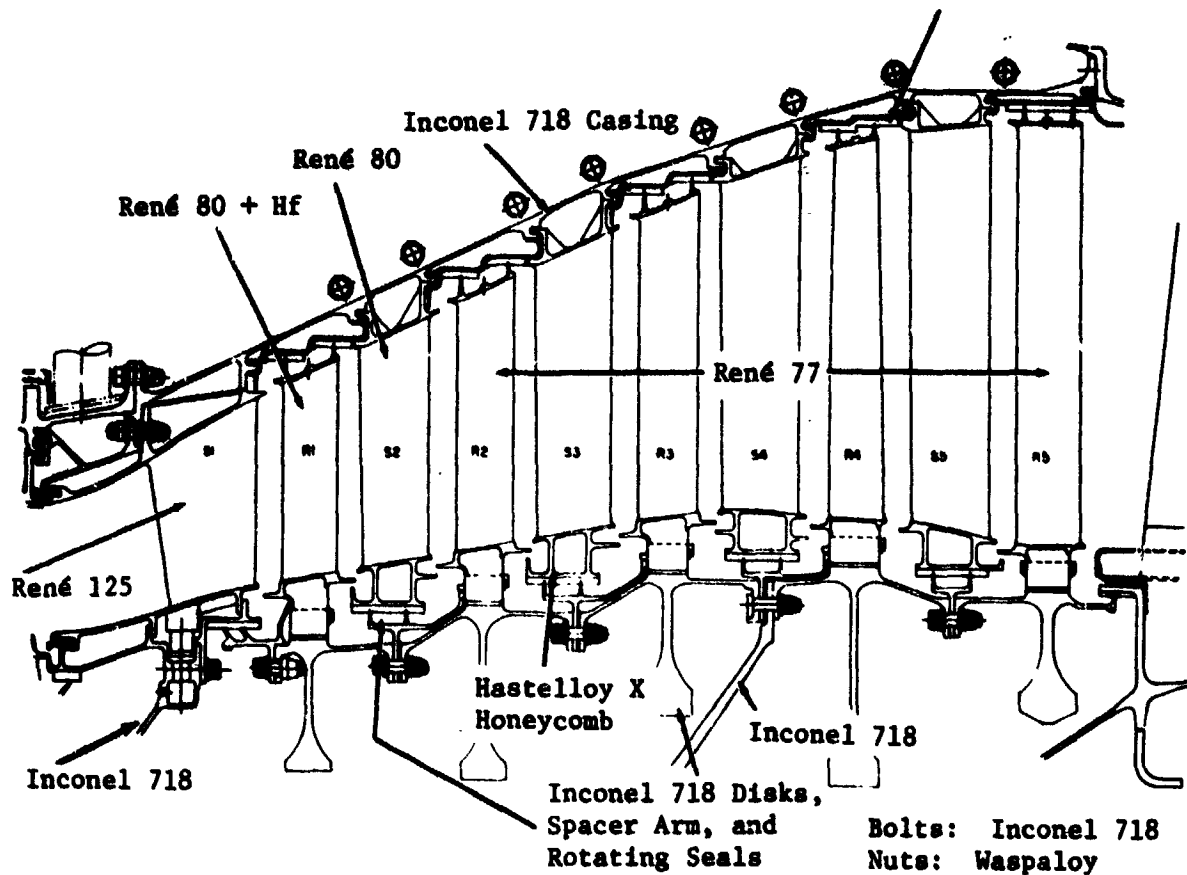


Figure 99. Low Pressure Turbine Materials.

As shown in Figure 100, fifth-stage compressor bleed air is routed back to the LPT casing just forward of the Stage 1 vane attachment. The purge air is isolated from the flowpath by a baffle to prevent leakage and is routed through the hollow Stage 1 vanes and dumped into the HPT-to-LPT inner cavity. As the flow-distribution drawing (Figure 100) shows, this purge air is routed to three main regions: (1) the HPT, where hot gas inflow at the aft-side of the HPT rotor is presented, (2) the sump, for pressurization to prevent sump leakage, and (3) the LPT rotor, where purge is provided through the bolt attachments and up to the disk rims for rim-temperature control.

4.5.4 Active Clearance Control

The LPT active clearance control (ACC) system is designed to achieve a minimum average gap at the engine operating point and to avoid seal damage, during transient conditions, with minimal deterioration. To achieve these requirements, an ACC system has been designed that cools the LPT casing with modulated, external air. The source of this air is the fan stream; the ACC supply is scooped off, routed to the LPT casing, and then discharged back into the fan stream. The distribution of fan air to the LPT casing is through a manifolded system of tubes positioned over the shroud hanger rings as seen in Figure 101. Thus, upon demand from the control system, valving allows fan air to cool the shroud rings; this shrinks them inward and closes down the LPT seal and tip clearances.

4.5.5 Aerodynamic Design

The selection of a five-stage LPT was made to achieve the highest efficiency consistent with weight, cost, and mechanical configuration limits. A selection study considered various numbers of stages (4, 4-1/2, 5, 5-1/2) with various transition-duct lengths [zero, 7.1 cm (2.8 in.), 10.2 cm (4.0 in.)]. Table 62 shows the results of this study. The overall turbine loading was lower for the five-stage, 7.1-cm (2.8-in.) duct design and significantly contributed to the overall greater efficiency of this design. In the five-stage design, several advanced aerodynamic features, noted in Figure 102, are used to achieve high efficiency. Improved velocity distributions and, hence, reduced losses were achieved in the airfoil designs. The radial work gradient has been tailored to match that of advanced General Electric air-turbine designs that have demonstrated significant efficiency gains over previous designs. Improved end-wall gap geometry will be achieved in the form of extended overlaps and lower windage features. The transition duct permits an increase in LPT rotor diameter with a resultant increase in average pitch velocity and decrease in aerodynamic loading. Reduced seal and tip clearances achievable through the use of the active clearance-control system will allow less leakage and higher efficiency.

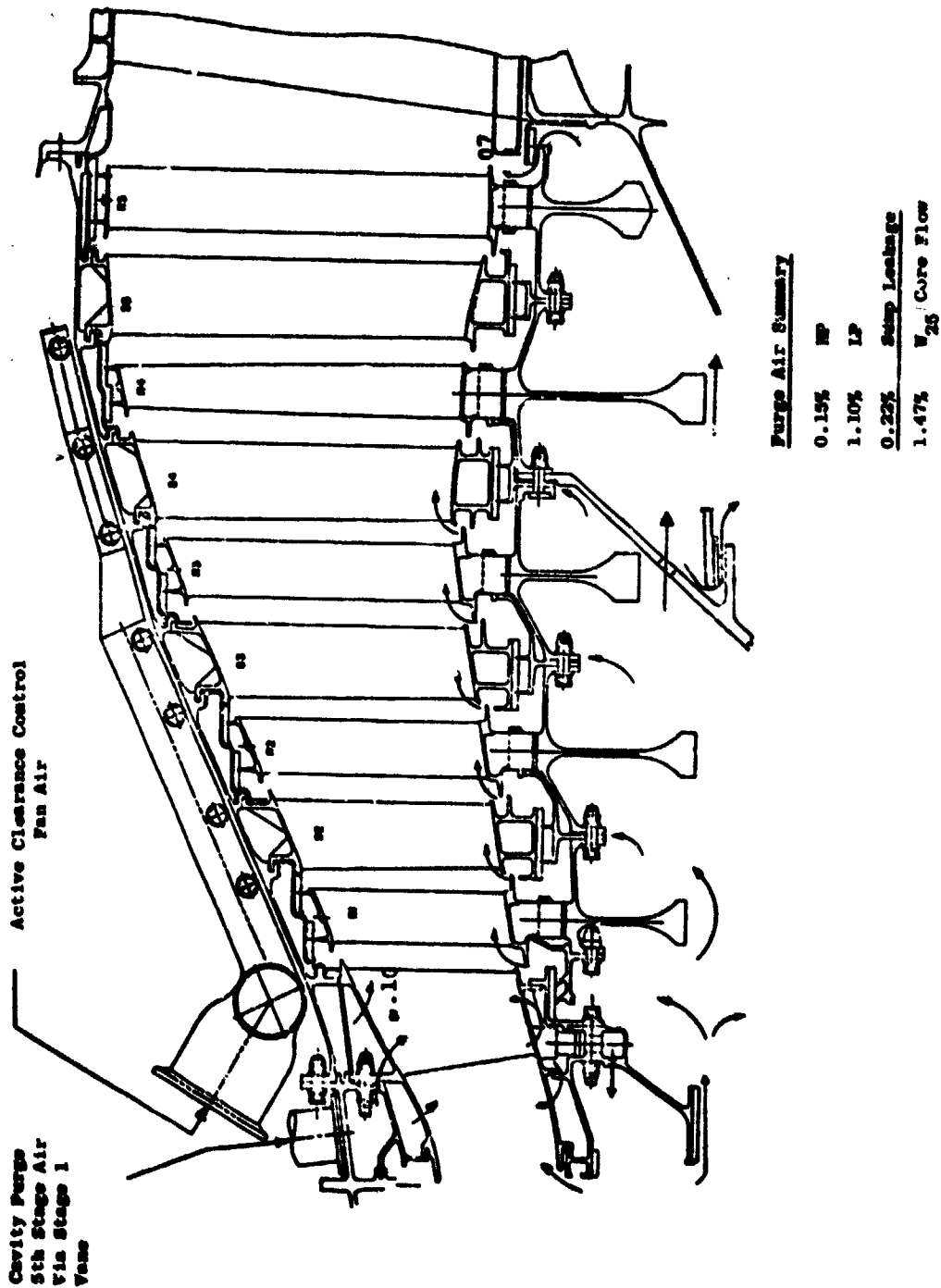


Figure 100. Cooling System - E3 Low Pressure Turbine.

Features:

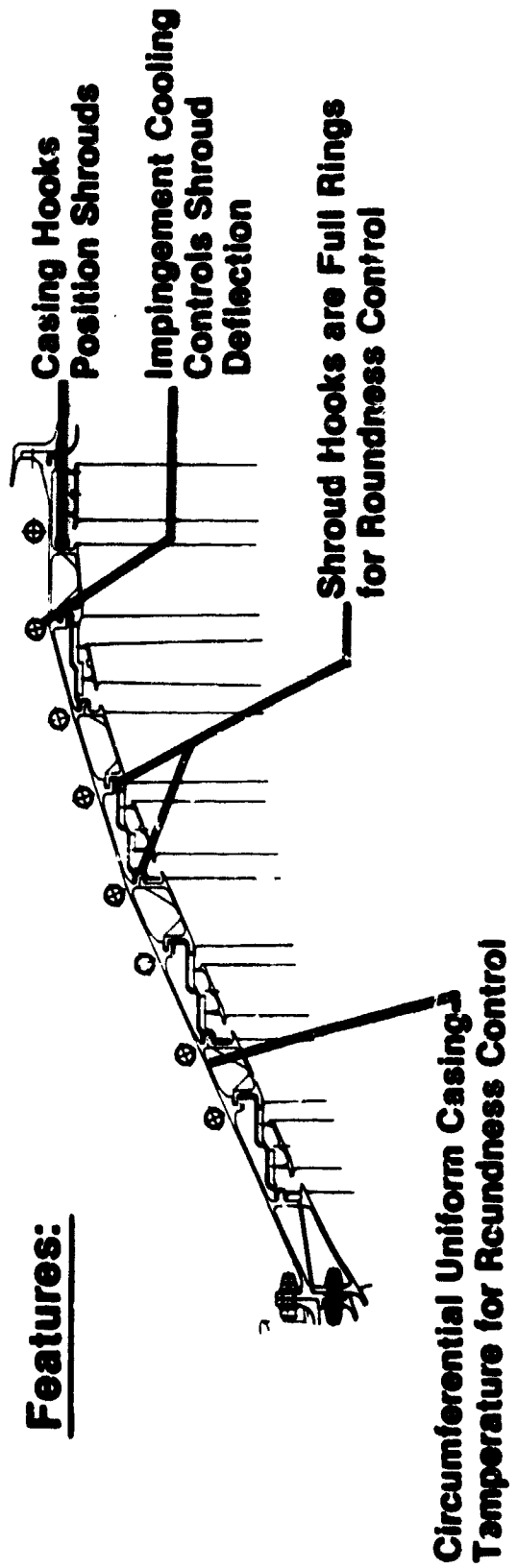


Figure 101. E3 Low Pressure Turbine Active Clearance Control.

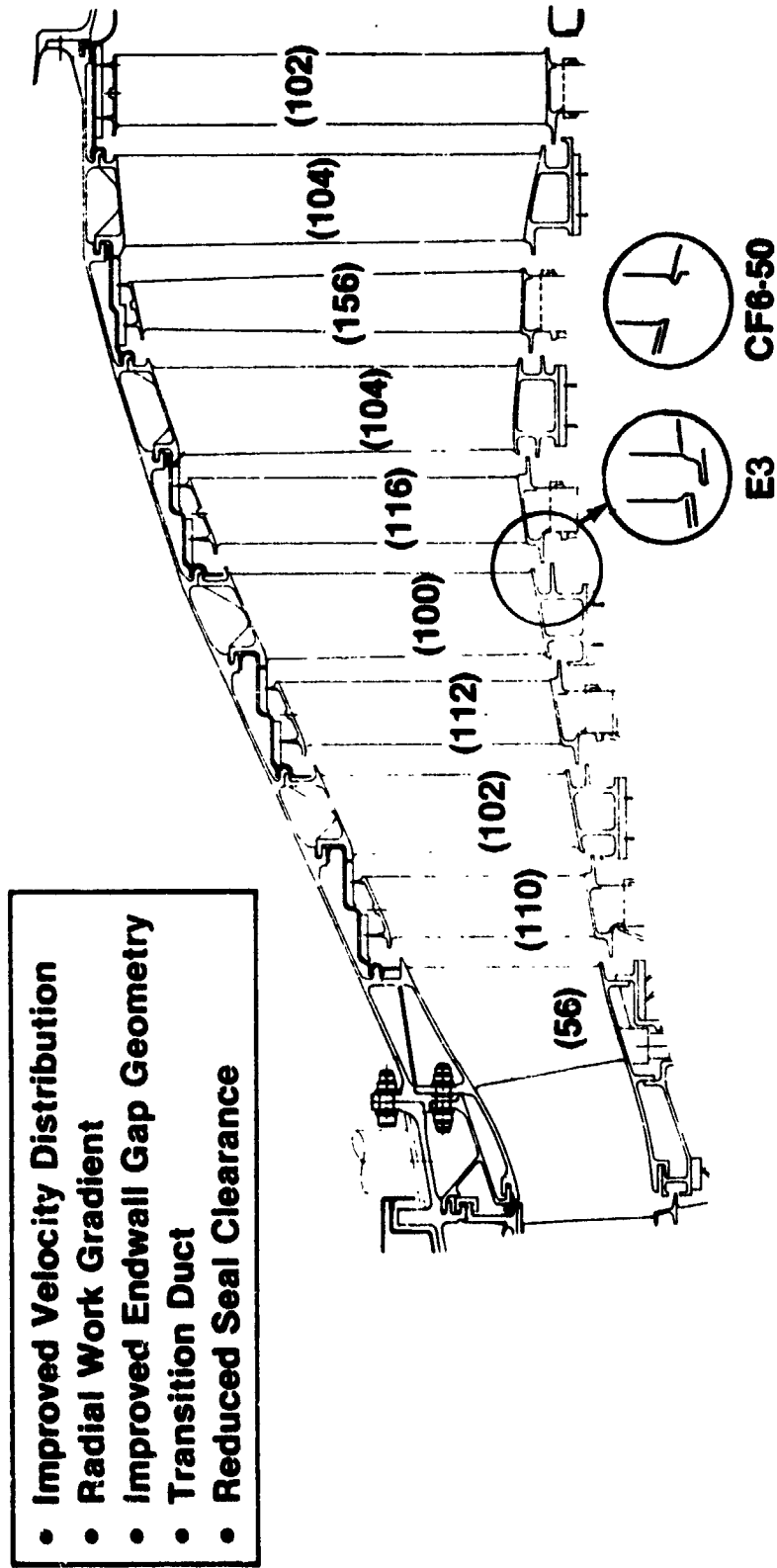


Figure 102. E³ LP Turbine Aerodynamic Design Features.

Table 62. LPT Aerodynamic-Design Selection Study Made for ICLS.

Parameter	4 Stage 7.1 cm (2.8 in.) Transition Duct	4-1/2 Stg 7.1 cm (2.8 in.) Transition Duct	4-1/2 Stg 10.2 cm (4.0 in.) Extended Transition	5 Stage 7.1 cm (2.8 in.) Duct	5-1/2 Stg No Transition Duct
Overall Average Loading	1.70	1.70	1.59	1.30	1.42
Max. Stage Loading	2.46	2.21	1.90	1.69	1.65
Overall Efficiency, %	-2.6	-0.8	-0.5	Base	-0.3
<p>● Efficiency Benefit Favors five-Stage, 7.1-cm (2.8-in.) Duct.</p>					

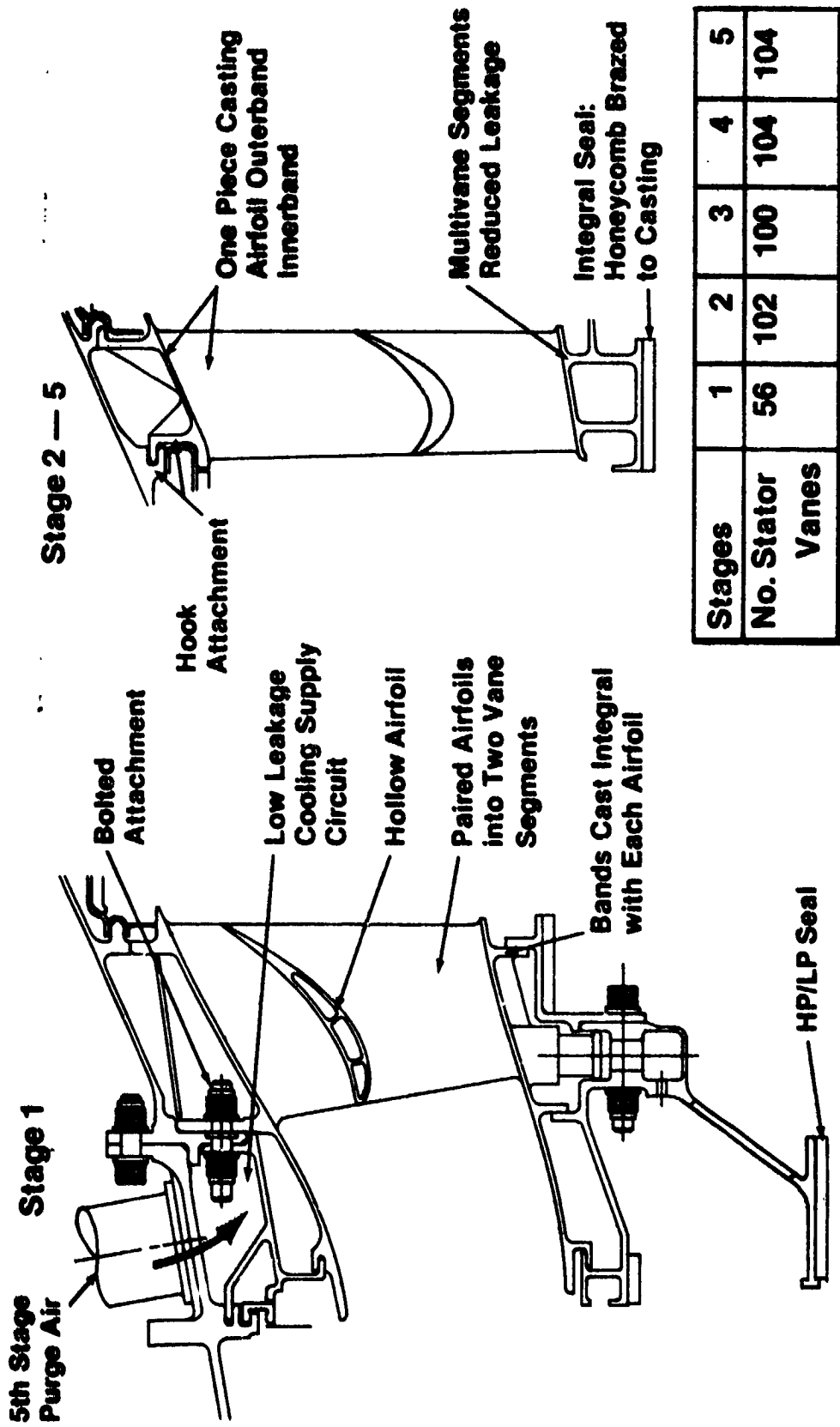
4.5.6 Mechanical Design

The Stage 1 nozzle differs from Stages 2 through 5. As shown in Figure 103, Stage 1 has large, hollow airfoils instead of the smaller type on Stages 2 through 5. This feature allows purge-air passage as discussed in the cooling-system description. Vane attachments vary also; a bolted design is used on Stage 1 (to assure low leakage of the purge air) while all other nozzles use hook attachments. The HP/LP inner seal for Stage 1 must provide three close-clearance rub lands and, therefore, is designed as a ring that is radially and axially positioned by the vane. Stages 2 through 5 nozzles have single rub surfaces that are brazed integral with each nozzle segment.

By comparison, the blades are made as individual pieces rather than multi-airfoil segments like the vanes. All blades are solid, uncooled airfoils with two-tooth seals on integral tip shrouds. In addition Stages 1, 2, and 3 have decambered airfoils for higher efficiency. Figure 104 shows these blade features.

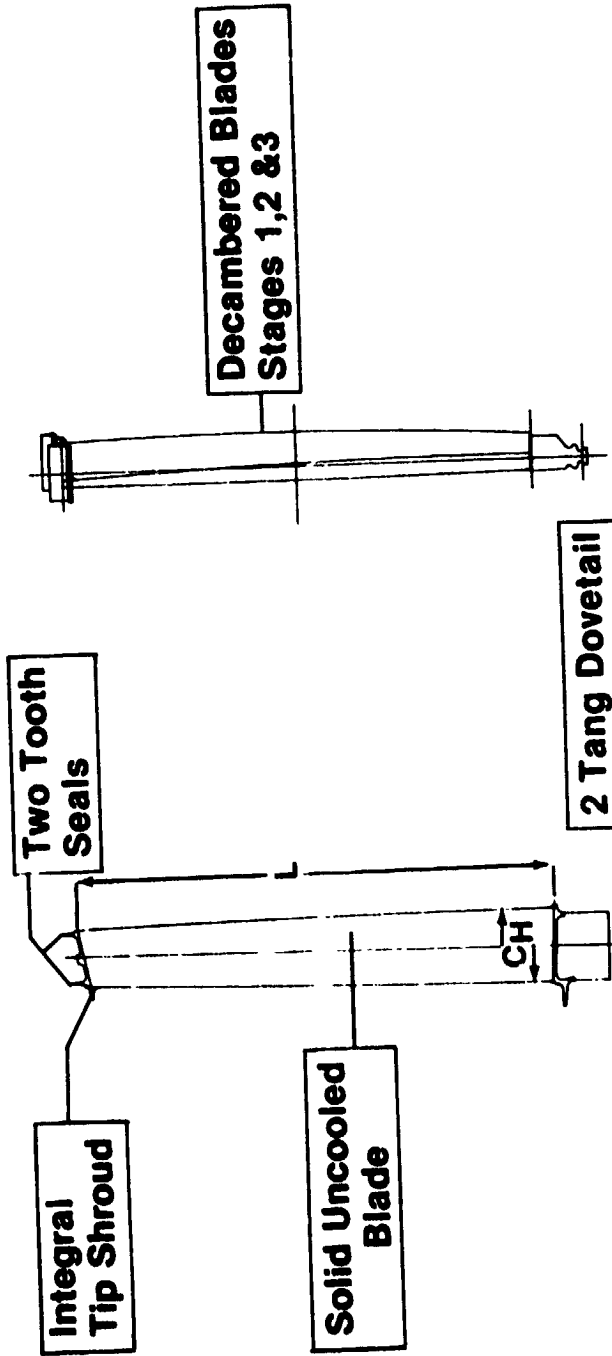
Operating conditions and component lives have been calculated and are shown for the most critical LPT airfoils: the Stage 1 vane and blade. As shown in Table 63, the Stage 1 vane is designed to operate in a 985° C (1805° F) gas stream with internal purge air only. The air loads cause a 109.3 MPa (15,850 psi) bending stress at the most limiting location (the 95% span). Evaluation of vane life at this stress shows an adequate design margin.

Similarly, the Stage 1 blade operates in a 889° C (1650° F) maximum gas stream. The stresses have been analyzed in the major areas and are reported in Table 64.



Stages	1	2	3	4	5
No. Stator Vanes	56	102	100	104	104

Figure 103. LPT Vane Features.



Aspect Ratio L/CH

- 3.53
- 4.35
- 5.00
- 6.50
- 6.27

No. Blades

- 110
- 112
- 116
- 156
- 102

Stage

- 1
- 2
- 3
- 4
- 5

Figure 104. LPT Blades: Stages 1-5.

Table 63. Low Pressure Turbine Stage 1 Vane.

- Material: René 125
 - $T_{g \text{ max}} = 985^\circ \text{ C (1805}^\circ \text{ F)}$
 - $T_{\text{Cooling (Purge)}} = 404^\circ \text{ C (760}^\circ \text{ F)}$
- 1.47% 5th Stage Purge Air
 - Gas Load = 485 N/Blade (109 lbf/Blade)
 - AP Load = 69 kPa (10.3 psi)
 - σ Bending at 95% = 106.5 MPa (15.9 ksi)
- $\frac{\text{Rupture Life}}{\text{Required Life}} > 3$
 $\frac{0.2\% \text{ Creep Life}}{\text{Required Life}} = 1.8$
 $\frac{\text{LCF Life}}{\text{Required Cycles}} > 2.7$

Table 64. Low Pressure Turbine Stage 1 Blade

- Material: René 50 + Hf (DS Alloy)
 - $T_{\text{TB}} = 899^\circ \text{ C (1650}^\circ \text{ F)}$
 - Shroud: $\sigma_b = 103.4 \text{ MPa (15 ksi)}$
- $\frac{\text{Rupture Life}}{\text{Required Life}} > 2$
- Airfoil: $\sigma_c = 61.3 \text{ MPa (8.9 ksi)}$ at Root
- $\frac{\text{Rupture Life}}{\text{Required Life}} = 1.25$
 $\text{LCF: } \frac{\text{Calculated Cycle Life}}{\text{Required Life}} > 2$
- Dovetail: $\sigma_{\text{eff}} = 246 \text{ MPa (35.5 ksi)}$
- $\text{LCF: } \frac{\text{Calculated Cycle Life}}{\text{Required Life}} > 1.4$

A special design study was carried out to investigate the acoustic benefit of a Stage 4 rotor with a high number of blades. As shown in Table 65, the original rotor design had 112 blades. The low-noise, 156-blade design was sized to meet aspect-ratio criteria and, upon analysis, was found to be acceptable in stress. This high-blade-number design produced acoustic benefits in two areas.

The increased number of blades gave: (1) a higher (less objectionable) passing frequency for lower perceived noise and (2) a shorter blade chord that provided a desirable increase in axial vane-to-blade gap. The combined effects gave a 5.0-PNdB reduction in turbine noise and a 1.5-EPNdB benefit in overall engine-system noise.

The FPS configuration weight has been estimated and is broken into a rotor and a stator section. A breakdown of these two sections is given in Table 66.

4.6 TURBINE FRAME AND MIXER

4.6.1 Turbine Frame

Figure 105 shows the turbine frame, mixer, mount structure, and center-body. Engine dynamic considerations require that the rear bearing be located well forward of the turbine frame strut plane. To accommodate this requirement with a rigid, weight-effective structure, a long-hub frame design is used. Preliminary analysis shows that this frame will meet the 87.6 N/m (500,000 lbf/in.) spring rate required for engine-vibration criteria. For additional stiffness, 12 struts are used. These are oriented semitangentially for rigidity while accommodating relative thermal expansion of the struts by allowing for a slight rotation of the hub accompanied by lateral flexing of the struts. The construction is basically formed sheet material with cast fittings at the strut ends and chem-milling with local reinforcement for low weight.

Figure 106 illustrates the location of the rear-sump lube lines with respect to the turbine frame struts. The position of these struts is important because the supply line must gravity-drain into the sump, and the drain and scavenge lines must gravity-drain out of the map, on engine shutdown. These requirements prevent oil from being trapped and coking in the lines on shutdown. The lube lines are double walled through the struts in order to keep the tube-wall temperature below the design limit of 177° C (350° F). This also prevents oil-coking in the service lines. A small bump in the fairing over the turbine casing is required at each lube-line location in order to provide sufficient envelope to get the lube lines into the frame struts. The aft mount for vertical load reaction is also shown on the frame end view.

The major goals of the turbine frame system include a design service life of 36,000 flight cycles and a combined mixer/turbine-frame weight goal of 163 kg (360 lbm). A stiffness requirement of 87.6 MN/m (500,000 lbf/in.) for the turbine frame has been set by overall engine dynamic analysis.

Table 65. Low Pressure Turbine Acoustic Study: 156 Fourth-Stage Blades.

Characteristic	Original Design	Low-Noise Design
Number of Blades	112	156
Mechanical Criteria		
Aspect Ratio	5.9	6.5
Stress Margin (Limit/Actual)	1.7	1.4
Acoustic Payoff, PNdB		Component PNdB
Increased No. Blades	-	3.5
Increased Axial Gap (Reduced Blade Chord)	-	<u>1.5</u>
		5.0
Engine System = <u>1.5ΔEPNdB</u>		
Conclusion: The 156-blade design provides required LPT noise reduction.		

Table 66. Low Pressure Turbine Weight Summary.

Component	Weight, kg (lbm)	
Rotor		
Blade	124	(274)
Disks	109	(239)
Hardware and Seals	39	(87)
Subtotal	272	(600)
Stator		
Casing	52	(114)
Vanes	142	(310)
Manifold	7	(15)
Hardware and Seals	17	(37)
Subtotal	218	(480)
Total	490	(1080)

- Twelve Semitangential Struts
- Stiffness Objective: 87.6 MN/m (5×10^5 lbf/in.)

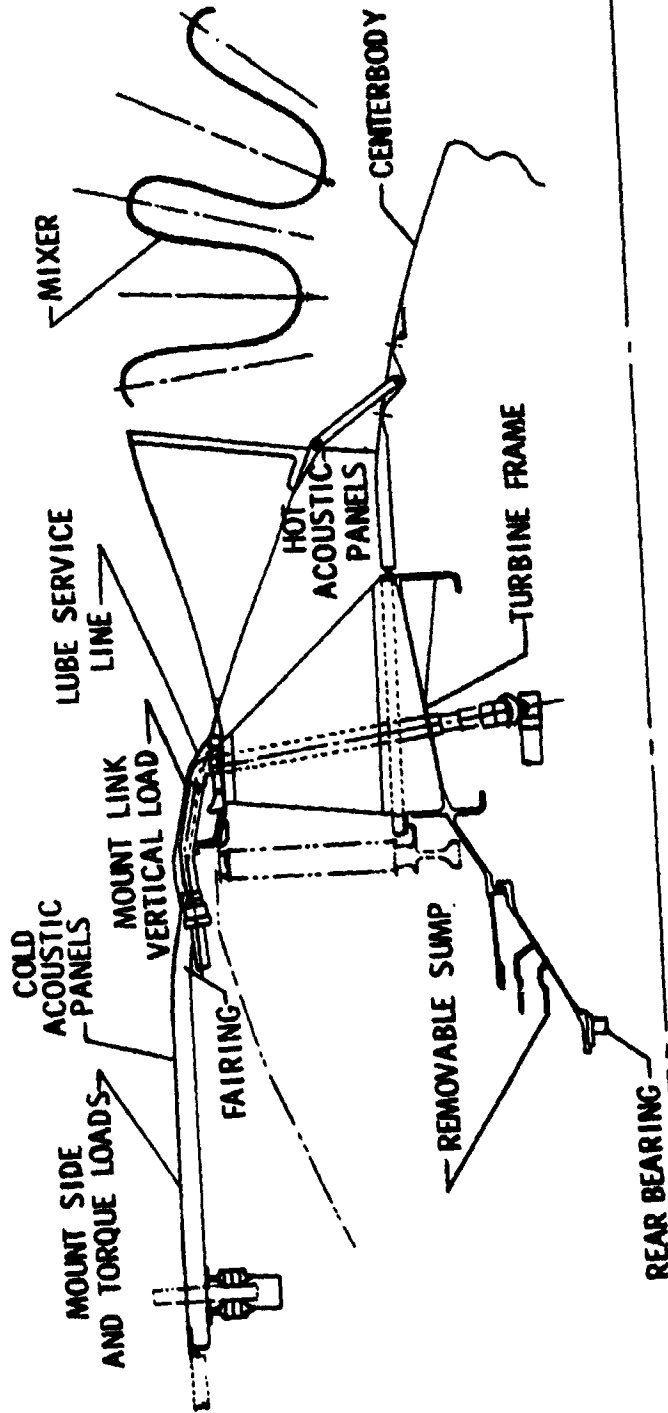


Figure 105. FPS Turbine Frame and Mixer.

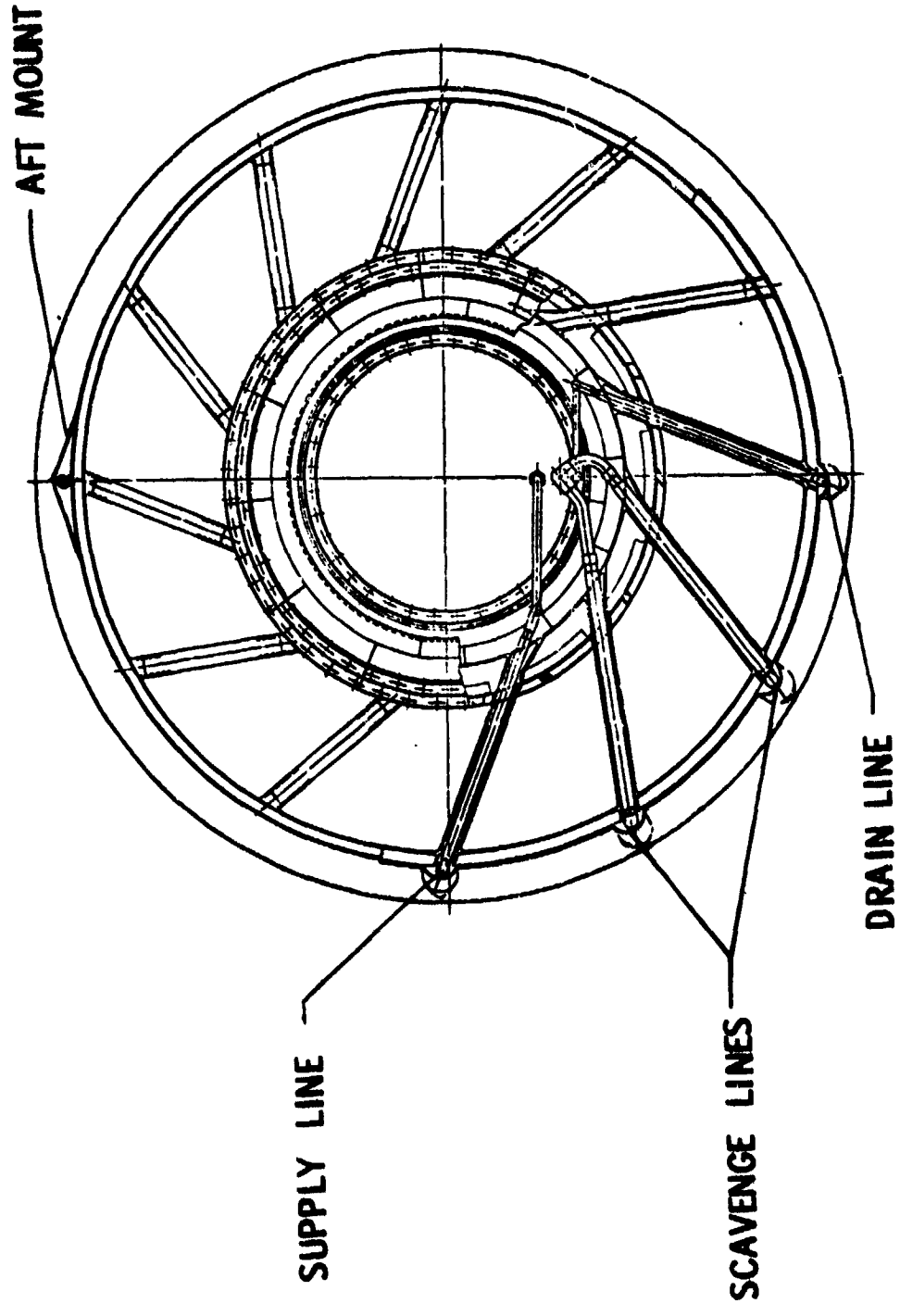


Figure 106. Turbine Frame End View.

Along with fuel efficiency and advanced acoustic characteristics, the Energy Efficient Engine has challenging goals for direct operating cost and maintainability. These objectives are being considered in the design of the turbine frame, mixer mount structure, and centerbody system. As shown in Table 67, some maintainability features include:

- Easy Access to the Aft Bearing Sump for Maintenance Without Engine Disassembly - The centerbody is easily removed for access to the sump area, and the sump flange connection to the turbine frame is designed to allow removal of the sump assembly through the turbine frame hub.
- Acoustic Treatment Panels Independent of the Structure for Easy Removal and Repair - In addition to maintainability, this allows lightweight, nonload-carrying construction of the panels and avoids distortion or fatigue cracking due to cyclic temperature differences between the inner and outer treatment-packaging walls.

In the selection of materials, weight and cost effectiveness were carefully considered for all parts. Listed in the right column of Table 68 are the additional selection considerations applicable to the individual parts. The materials selected for the cold acoustic panels and the outer fairings are limited to an operating temperature of 148° C to 177° C (300° F to 350° F).

4.6.2 Mixer

The prime function of the mixer is to efficiently mix the hot turbine-discharge flow with the relatively cool fan-bypass flow to provide a thermodynamic performance gain in the overall engine cycle. For high bypass ratio engines, this gain can range from 2.5 to 3.5% in sfc. In addition to improving performance, the mixer lowers the overall engine jet noise by providing a more uniform nozzle-exit velocity compared to an unmixed, separate-flow exhaust system.

The preliminary mixer design is convoluted with 24 lobes contoured for effective mixing. The end view shown in Figure 105 points out the convoluted shape which incorporates continuous-curvature walls throughout the mixer. Since the mixer is not a highly loaded part, the mechanical design primarily requires rigidity and stiffness to maintain shape. The continuous-curvature walls will provide a stiff, rigid mixer that can be made with thin walls and, thus, low weight with no adverse effect on performance. The mixer is fabricated from 2.29 mm (0.090 in.) Inconel 718 formed sheet chem-milled to 0.56 mm (0.022 in.) wall thickness over most of the surface area. Added thickness at the trailing edge provides needed stiffness.

The mixer is bolted to the turbine frame and linked to the centerbody, providing easy access to the engine aft-bearing and sump area. Convoluted mixers are inherently flexible, and the links to the centerbody provide the required structural support at the mixer exit. The links are aerodynamically shaped to minimize pressure loss.

Table 67. Direct Operating Cost and Maintainability Features.

- **Design Emphasis On**
 - Life
 - Repairability
 - Assembly and Service Access

- **Turbine Frame and Mixer Features**
 - Centerbody and Mixer Designed for Access to Rear Bearing Sump
 - Materials and Manufacturing Processes Selected for Low Manufacturing and Maintenance Cost
 - Acoustic Treatment Panels Independent of Structure

Table 68. Turbine Frame Assembly Material Summary.

Part	Material	Basis for Selection
Turbine Frame	Inconel 718	High Modulus - Heat Resistance High Strength
Rear Mount Structure	6-4 Titanium	Low Density - High Strength
Centerbody	Inconel 625	Heat Resistance - Fatigue Resistance
Hot Acoustic Panels	Inconel 625 Astroquartz Absorber	Heat Resistance - Fatigue Resistance
Cold Acoustic Panels	Glass-Reinforced Epoxy Kevlar Absorber	Low Density
Outer Fairing	Aluminum 2618	Low Density

The mixer aerodynamic design is based on a combination of General Electric engine and model-test experience and analytical studies. Previous tests of mixer configurations, both on subscale-model and full-scale engine test vehicles, provided the data base for the selection of the mixer overall cross section including the penetration (size) and the number of lobes. The FPS combination of mixer size and number of mixer lobes should provide high mixing effectiveness with only a small pressure drop. The detailed flowpath coordinates were defined with the aid of a stream tube curvature (STC) computer program in combination with a boundary-layer program. These programs were used to ensure that favorable area and Mach number distributions were achieved through the mixer and that no boundary-layer separation will occur in the mixer.

The mixer and turbine frame strut are relatively close coupled, as shown by the cross section in Figure 105. The STC program was also used to analyze the core flow field to determine if an interaction between the strut and mixer would occur which might degrade performance. The STC flow-field solution was obtained in a circumferential plane, as shown in Figure 107, with and without the strut. Results indicate the flow streamlines and Mach number distributions going into the mixer were unaffected by the presence of the strut. Likewise, comparison of the flow field around the strut with previous STC runs of the isolated strut indicated that the mixer did not affect the strut aerodynamics.

The mixer design goals are summarized in Table 69. The performance goals (Figure 108) include a mixing effectiveness of at least 75% and a mixer pressure loss of 0.2%. The chart puts the performance goals in perspective and points out the significance of the goals in terms of payoff to engine performance. A performance gain of slightly over 3% sfc will be achieved due to 75% mixing at the Mach 0.8/10.7 km (35,000 ft) max cruise design point. The mixer will also provide a jet-noise reduction, relative to an unmixed system, compatible with the overall FPS noise goals. A status weight summary for the turbine frame, rear mount structure, and centerbody is shown in Table 70. A major activity during the remaining design process will be weight improvement of the overall turbine-frame/mixer-system design. This will be accomplished by closer consideration of the stress distributions and the reduction of material thicknesses in the low-stress areas. Finally, the mixer mechanical design will allow a service life of 36,000 flight cycles. This will require adequate acoustic-fatigue margin during normal, forward-thrust operation and creep resistance during high-temperature, reverse-thrust operation.

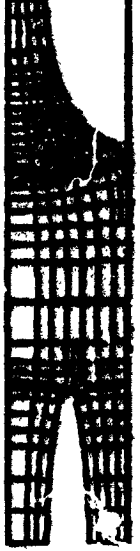
The mixer material selection, Inconel 718, was based on four main requirements: (1) fatigue resistance for normal, forward-thrust operation, (2) heat resistance (creep) for reverse-thrust operation, (3) low weight, and (4) low cost. Two materials were analyzed for the mixer: titanium 6-2-4-2 and Inconel 718. The titanium mixer was creep-distortion limited with a maximum allowable sidewall deflection of 0.5 cm (0.2 in.). This deflection is the maximum allowable which will not result in significant mixer performance degradation. In order not to exceed the 0.5 cm criteria, a chute-wall thickness of 0.89 mm (0.035 in.) was required. This resulted in a mixer weight of 21 kg (46 lbm). The Inconel 718 mixer was fatigue limited. The resulting chute sidewall thickness was 0.56 mm (0.022 in.) in order to

STC FLOWFIELD SOLUTION

Without Strut



With Strut



**STC ANALYSIS
ALONG STREAMLINE**

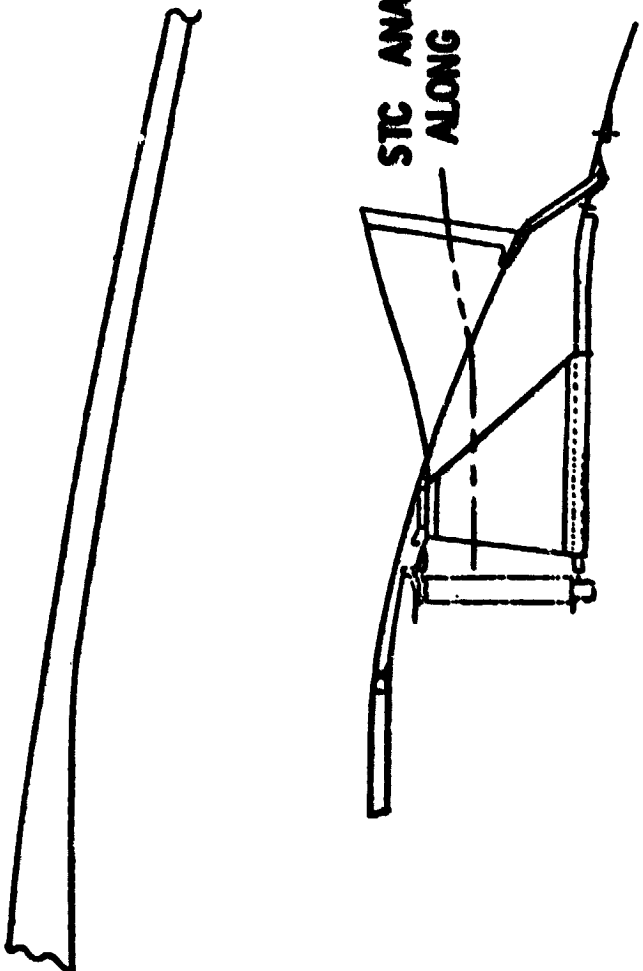


Figure 107. Turbine Frame - Mixer Flow Field STC Analysis.

Table 69. Mixer Design Goals.

- Mixing Effectiveness $>75\%$
- Mixer Pressure Loss 0.2%
- Flight Jet Noise Compatible With System Goals
- Meet Flight Design Weight
- 36,000 Flight Cycles
 - Adequate Acoustic Fatigue Margin
 - Adequate Reverse Thrust Temperature Margin

Table 70. Turbine Frame/Mixer Status Weight Summary.

Part	Material	Calculated Weight, kg (lbm)
Turbine Frame	Inconel 718	95 (210)
Rear Mount Structure	6-4 Titanium	39 (85)
Mixer	Inconel 718	24 (52)
Centerbody	Inconel 625	22 (48)
Hot Acoustic Panels	Inconel 625	11 (24)
Cold Acoustic Panels	Polyimide - Glass	9 (20)
Outer Fairing	2618 Aluminum	4 (8)
Status Weight Total		204 (447)
Design Goal Weight		163 (360)

● Mach 0.8/10,700 m (35,000 ft) Mx Cr

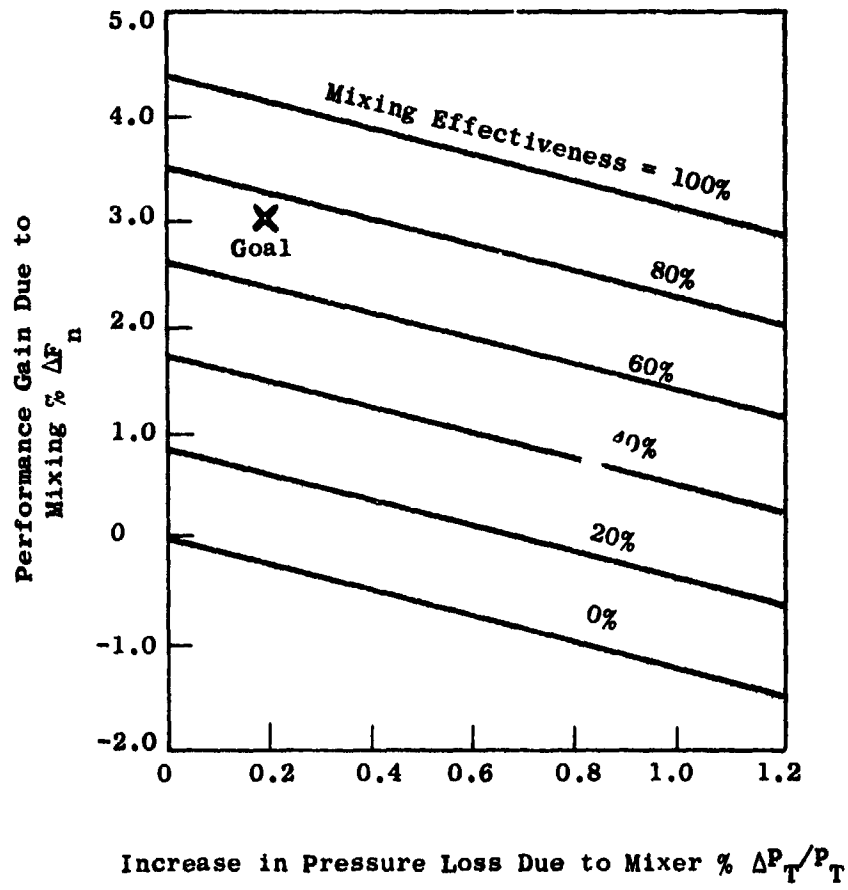


Figure 108. ³E Mixed-Flow Thrust Gains.

maintain the acoustic stress level below the endurance limit of 317 MPa (46 ksi). This results in a mixer weight of 24 kg (53 lbm). In terms of fatigue and creep strength, Inconel 718 is high in both categories whereas titanium, on a relative basis, is moderate in fatigue strength and lower yet in creep strength. Based on these analyses, it was concluded that Inconel 718 provides high fatigue and creep strength margin with a small weight penalty.

4.7 BEARING SYSTEMS, DRIVES, and CONFIGURATION

The FPS bearings, lube system, and configuration components have been designed to meet the major design goals shown in Table 71. Besides meeting requirements for engine life and producing a viable design as far as cost and weight are concerned, attention is also given to maintainability and fire safety. Modular concepts are being applied to the sump designs; in particular, the forward sump is designed such that the core and fan modules can be separated at the core thrust bearing.

Fire safety is enhanced in the aft sump by surrounding the sump with cool fan-discharge air and providing oil-seal drains to carry away oil leakage. It is anticipated that a single seal failure in the aft sump will not produce a fire hazard in any way.

The FPS mechanical arrangement for locating major components of the sump and drive system is shown in Figure 109. A comparison of various FPS features to the CF6-50C baseline engine is shown in Table 72. The short rotor system and the elimination of a high pressure turbine frame have reduced the number of sumps from four to two. Only five bearings are required to support the rotor system as compared to seven for the CF6-50C. The FPS presently incorporates a gearbox mounted in the lower quadrant of the core compartment. Studies comparing various locations of the accessory gearbox (see Section 4.9) showed slightly higher sfc and DOC for a fan-case- or pylon-mounted accessory gearbox (AGB) as compared to a core-compartment gearbox. However, it is anticipated that future users of the FPS might prefer a fan-case-mounted AGB, so provisions have been made to permit this type of installation as well. To reduce the main-shaft bearing loads due to rotor critical speed, the core thrust bearing and the intershaft bearing are spring mounted with provision for fluid dampers. Currently, it is planned to incorporate a damper on the No. 3 thrust bearing but not on the No. 4 differential bearing. It will use labyrinth seals based on the excellent experience of the General Electric family of high bypass commercial engines.

Table 73 shows the major areas of study during the preliminary design of the FPS engine. As originally configured, the sumps were to be pressurized with internal compressor interstage bleed. A study was made in conjunction with the compressor rotor drum-cooling study. The results of this study indicated fan-booster air (core-inlet air) is the best choice for both compressor rotor drum cooling and sump-seal pressurization.

Table 71. FPS Major Design Goals.

- 36,000 Flight Cycles
- Life of All Bearings >35,000 hr
 - Less Than Two Events/Million Flight Hours
- Employs Modular Design Concepts
 - Can Separate Fan/Core Modules
- Fire Safety
 - Sumps Surrounded by Cool Air
 - Seal Drains Provided
- Meet Specified Weight and Cost Goals

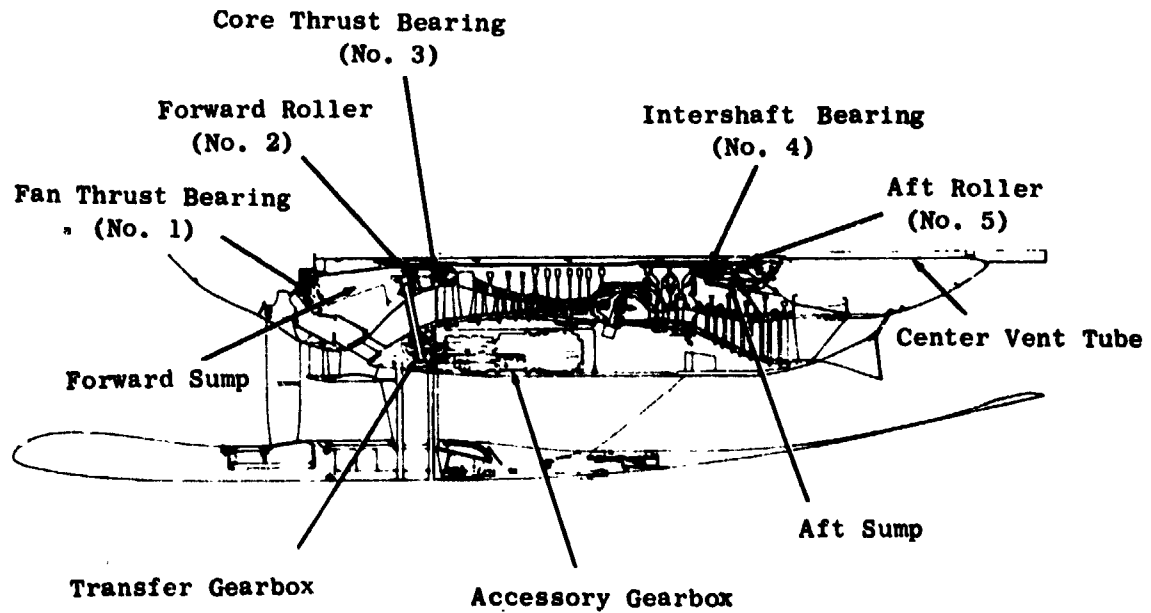


Figure 109. FPS Engine.

Table 72. FPS Comparison to Baseline (CF6-50).

Comparison	E ³ (FPS)	Baseline (CF6-50C)
Number of Sumps	2	4
Number of Bearing Positions	5	7
Accessories Location	Core	Fan Case
Spring Mounted Bearings	2	0
Fluid Damped Bearings	1	1
Seals	Labyrinth	Labyrinth

Table 73. Major Areas of Study.

- Determine Source of Sump Seal Pressurization
 - Completed in Conjunction with Compressor Rotor Drum Cooling Study
- Rotor Thrust
 - Determined Balance Piston Diameters
- Design Support of Rotor Dynamics Studies
 - Fan Shaft Sized for Maximum Stiffness
 - Bearing DN* is Maintained Below 2.20×10^6
 - Capability of Spring/Damper for No. 3 and No. 4 Bearings is Provided
- Drive System
 - Determined Feasibility for Core-Mounted Gearbox
 - Configuration

* DN = Bearing bore diameter (mm) × rpm

Calculations were made to determine the effects of balance-piston diameters on the core and fan thrust-bearing loads. The various engine seal diameters have been chosen to limit the thrust-bearing loads to values that will meet bearing life requirements.

During the rotor dynamics studies, a fan shaft system of maximum stiffness within the confines of the engine design was determined. A bearing DN of 2.5×10^6 (see Table 73) was used as a limit, and the maximum allowable diameter through the HPT rotor system was also a restriction. Going to 2.5×10^6 DN for the bearing would require a spline joint in the aft sump because of the diameter restriction through the HPT rotor system. When considering a fan shaft that would go with a 2.5×10^6 DN core thrust bearing, it was found that the rotor critical speed did not change significantly compared to a shaft sized to be compatible with a bearing DN of 2.2×10^6 . This also allows for a stiff, bolted joint in the aft sump rather than a spline joint. The rotor dynamics studies also showed the advantages of incorporating spring mounting to the core support bearings. Fluid dampers at these bearings have been provided for although it has not been determined that a fluid damper is necessary at the intershaft bearing location.

The drive system has been configured to incorporate a core-mounted gearbox. This study included packaging the accessory gearbox and the major piping adjacent to it. It was concluded that a gearbox could be mounted in the available space in the core compartment without any core cowl distortion.

Figure 110 shows the major components of the sumps and drive system for the FPS engine. The forward sump, also shown in Figure 111, contains the No. 1 thrust bearing, the No. 2 roller bearing, and the No. 3 core thrust bearing. From the forward end of the compressor stub shaft, the power takeoff (PTO) gearing is driven; this, in turn, drives the transfer gearbox (TGB). The accessory gearbox (AGB) is driven from the TGB. All driven engine accessories are mounted on the AGB. The TGB is mounted in a cavity provided in the front fan frame.

The sump seals are pressurized with fan booster air directed from the leading edge of the core struts to the cavity shown in Figures 110 and 111. This air pressurizes the seal just forward of the No. 1 bearing and is allowed to flow rearward to the aft sump through the annulus formed by the inside diameter of the fan shaft and the outside diameter of the center vent tube. An air/oil separator is provided in the forward sump and prevents oil from entering the sump vent.

Referring to Figure 112, the No. 3 bearing is mounted in a squirrel-cage spring housing secured to the No. 2 bearing housing. The fluid damper is a multisleeve design mounted in the fan-frame housing. The labyrinth seal shown aft of the No. 3 bearing is pressurized with the same air source that cools the compressor drum rotor.

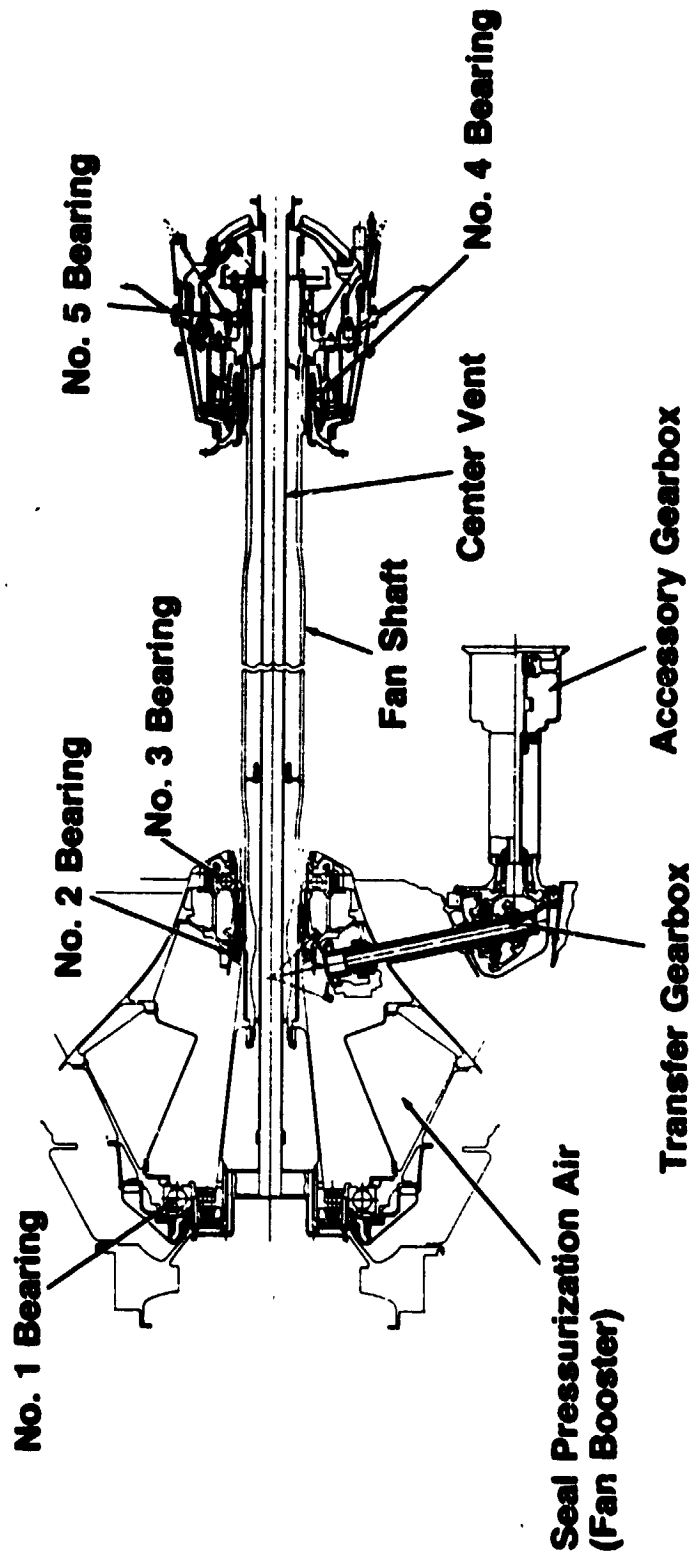


Figure 110. FPS Sumps and Drive System.

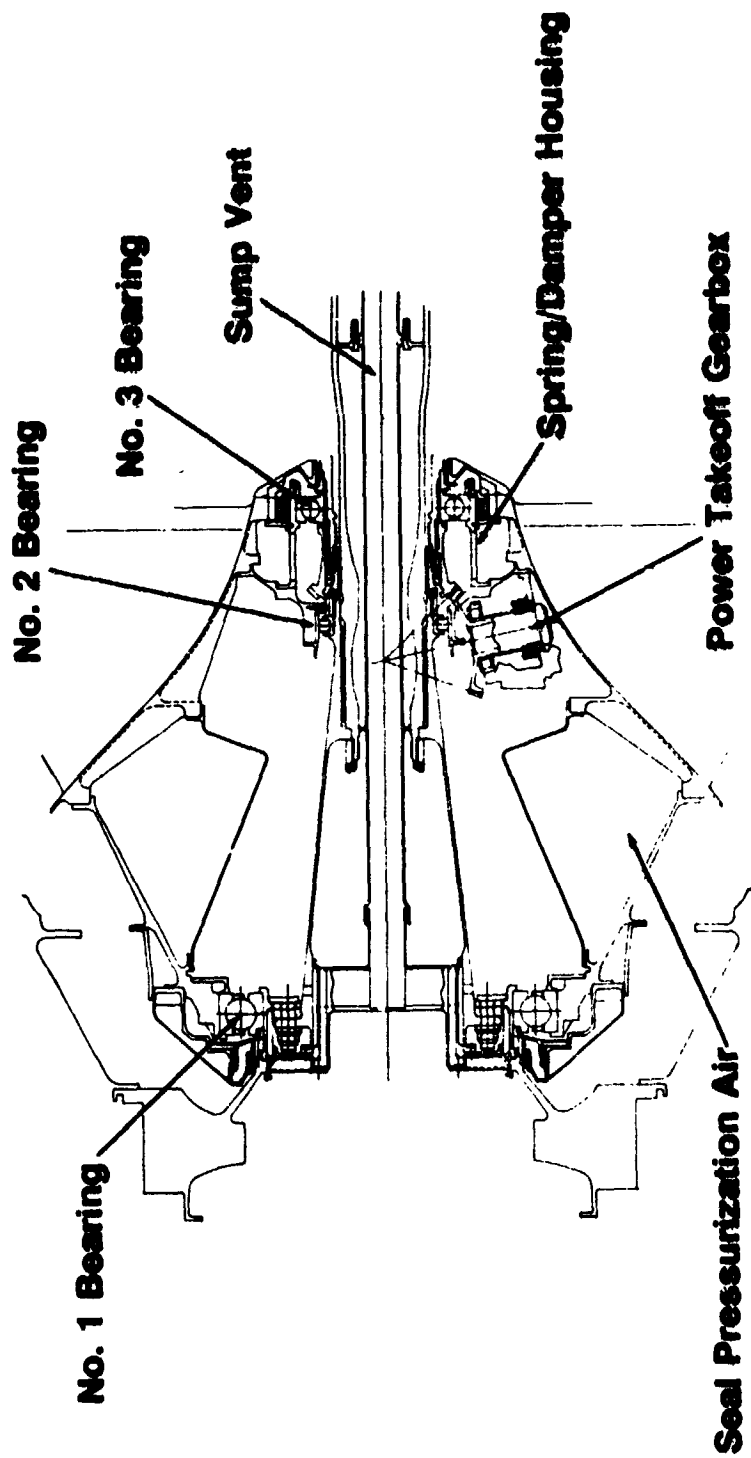


Figure 111. FPS Forward Sump.

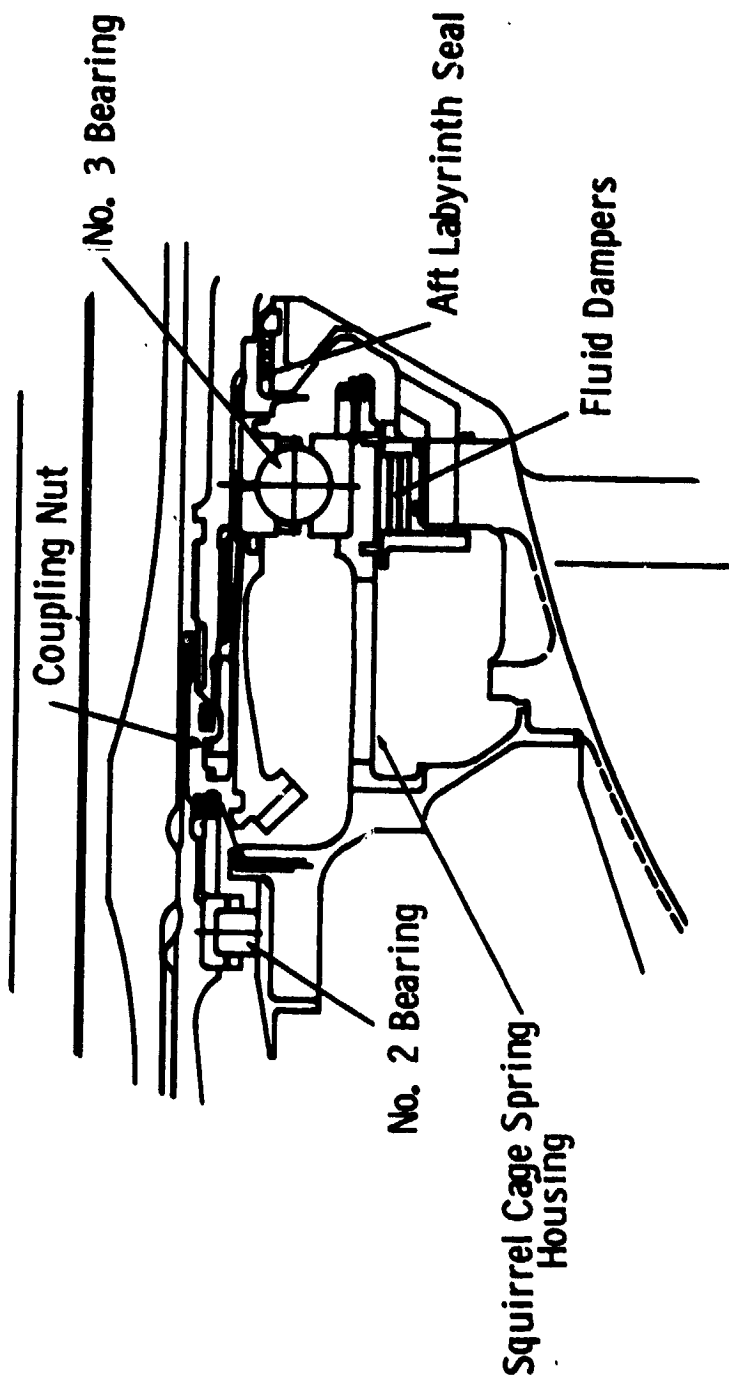


Figure 112. FPS No. 3 Bearing Spring/Damper Housing.

The No. 3 bearing is cooled and lubricated by applying oil under the race. This is accomplished by introducing oil over a lip provided in the horizontal PTO gear shaft. This method of lubrication is especially important with bearing DN's greater than 2.0×10^6 .

Separation of the core from the fan module requires access to the coupling nut which clamps the horizontal PTO gear and the No. 3 bearing to the compressor stub shaft. Access is obtained by arranging the fan forward stub shaft so it can be removed without removing the fan assembly.

The aft sump configuration is shown in Figure 113. The aft sump contains the No. 4 intershaft bearing and the No. 5 low pressure system aft support bearing. Since the aft sump contains only roller bearings, it must also allow for relative thermal axial growth of the high pressure and low pressure systems. The No. 4 bearing is spring mounted, and provisions are made to incorporate fluid damping if required. Lubrication oil is centrifuged into the No. 4 bearing, and the No. 5 bearing is under-race cooled.

The aft sump is surrounded by cool fan-discharge air (478 K/400° F) which is used to pressurize the sump seals. Outside of that is another cavity containing compressor rotor cooling air at 663 K (734° F). These two cavities protect the sump from the hotter turbine-cavity air. An oil-seal drain is provided in the 478 K (400° F) cavity to prevent oil from getting into the hotter outside cavities. All the rotating walls of the sump are designed to "pump" the leakage to drain. An air/oil separator is provided which discharges into the center vent tube common with the forward sump vent. The total vent flow directed overboard is 0.24% of the core flow.

Detailed information on the engine main-shaft bearing is shown in Figure 114 and Tables 74 and 75. All bearings used in the FPS design are VIM-VAR M50 with drain-flow control. The ball or roller bearing separators are premium grade AMS 6414, silver plated. The No. 1 bearing (350.5-mm bore) is the largest. The size and number of balls and rollers are defined to obtain maximum capacity in the bearing to withstand "blade out" conditions. Table 74 is a tabulation of the rotor thrust on the low and high pressure systems. Rotor thrust varies at each flight condition, and these loads are combined to obtain a cubic-mean load of 24,096 N (5417 lbf) and 9724 N (2186 lbf) for the low pressure and high pressure rotors, respectively. These loads, along with the radial load shown in Table 75, are used to determine the calculated bearing life in hours. For the thrust bearing, the lives of the No. 1 and No. 3 bearings are 133,000 and 35,000 hours, respectively. Also shown in Table 75 are the calculated lives of the No. 2, No. 4, and No. 5 bearings.

Labyrinth oil seals based on General Electric commercial-engine experience will be used in the sumps. Table 76 presents the design philosophy for the sump-sealing system. Figure 115 shows the labyrinth seal used just aft of the No. 3 bearing. Epoxy composite housings and rub material will be utilized in the forward sump, based on experience gained from application in the CF6 engine.

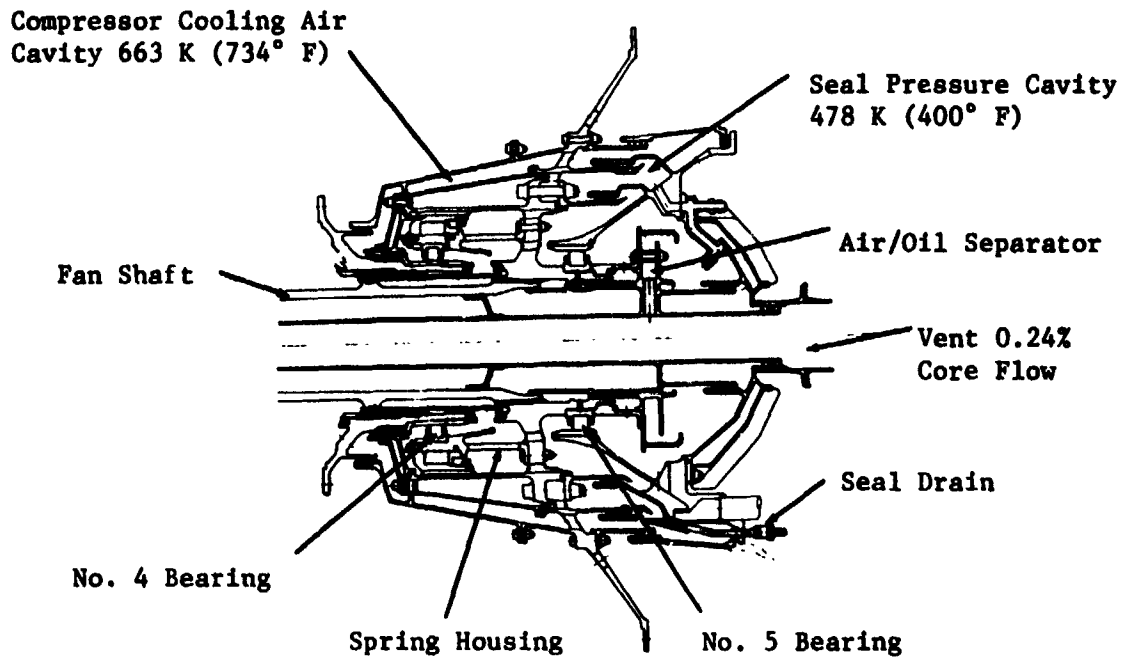


Figure 113. FPS Aft Sump.

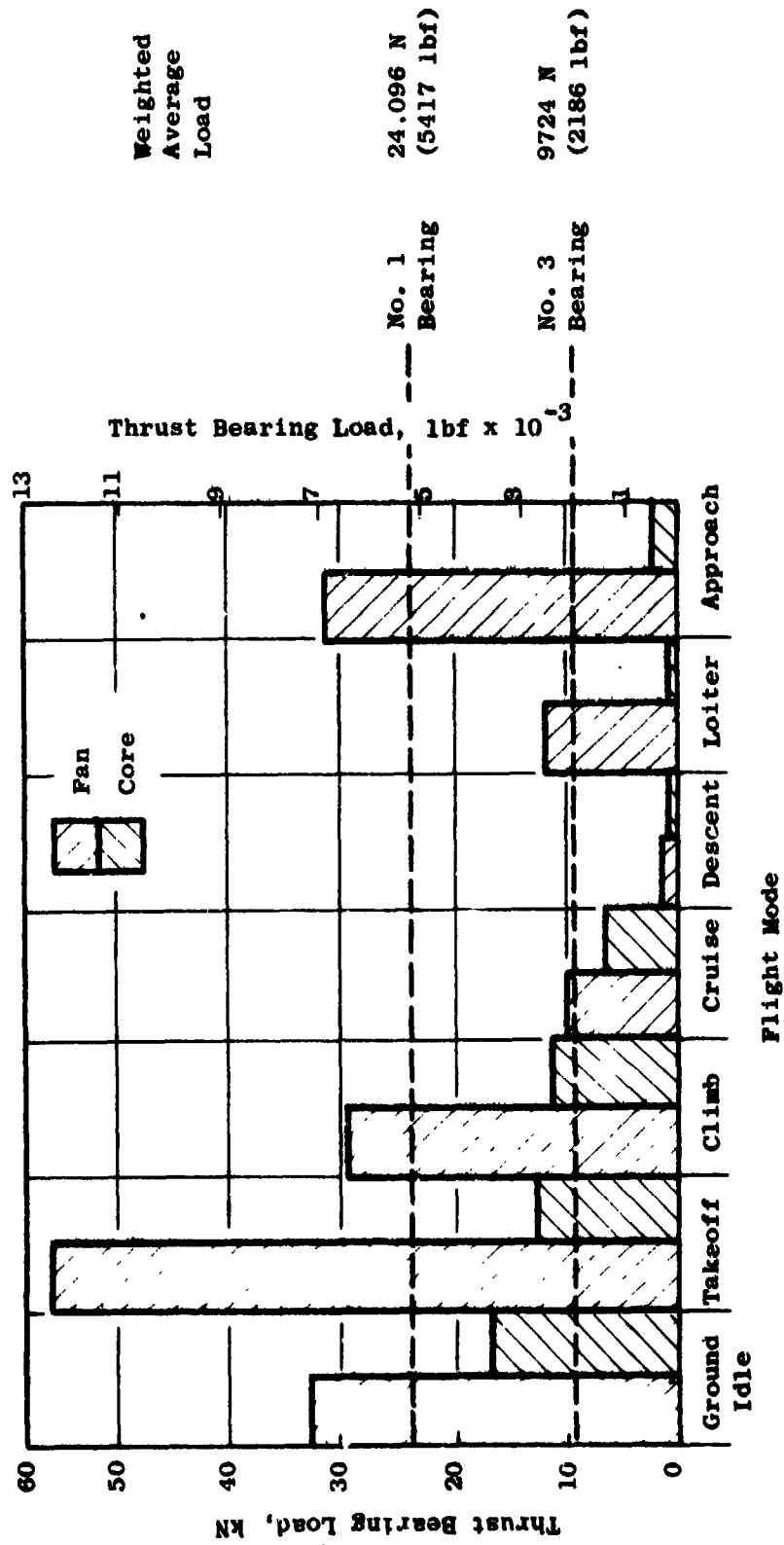


Figure 114. FPS Rotor Thrust Summary.

Table 74. FPS Main-Shaft Bearing Description.

Bearing No.	1	2	3	4	5
Bearing Bore, mm	350.5	139.7	162.6	170.7	150.4
Ball Diameter, mm	41.27	-	27	-	-
Roller Diameter/Length, mm	-	15/15	-	14/14	17/17
No. of Rollers or Balls	28	26	20	28	24
Materials					
Rings, Balls, and Rollers	VIM-VAR M50				
Cages	Premium 4340, Silver Plated				

Table 75. FPS Bearing Loads and Life.

Bearing No.	1	2	3	4	5
DN Max $\times 10^6$	1.28	0.51	2.18	1.67*	0.55
Radial Load, N	15,591	2,447	5707	4,439	8,861
(lbf)	(3,505)	(550)	(1,283)	(998)	(1,992)
Thrust Load, N	24,096	-	9,724	-	-
(lbf)	(5,417)	-	(2,186)	-	-
Calculated Life, hr	133,000	$>27 \times 10^6$	35,000	38,900	4×10^6
* DN = Bearing Bore Diameter (mm) \times (Fan Speed - Core Speed) (rpm)					

Table 76. FPS Sump Labyrinth Seals.

- Labyrinth Seal Philosophy
 - a. Reliability
 - b. Repairability
 - c. Low Heat Generation
 - d. Allows Use of Lightweight Material in Forward Sump
 - e. Long Life
- Total Sump Airflow (Vented) = 0.24% Core Flow

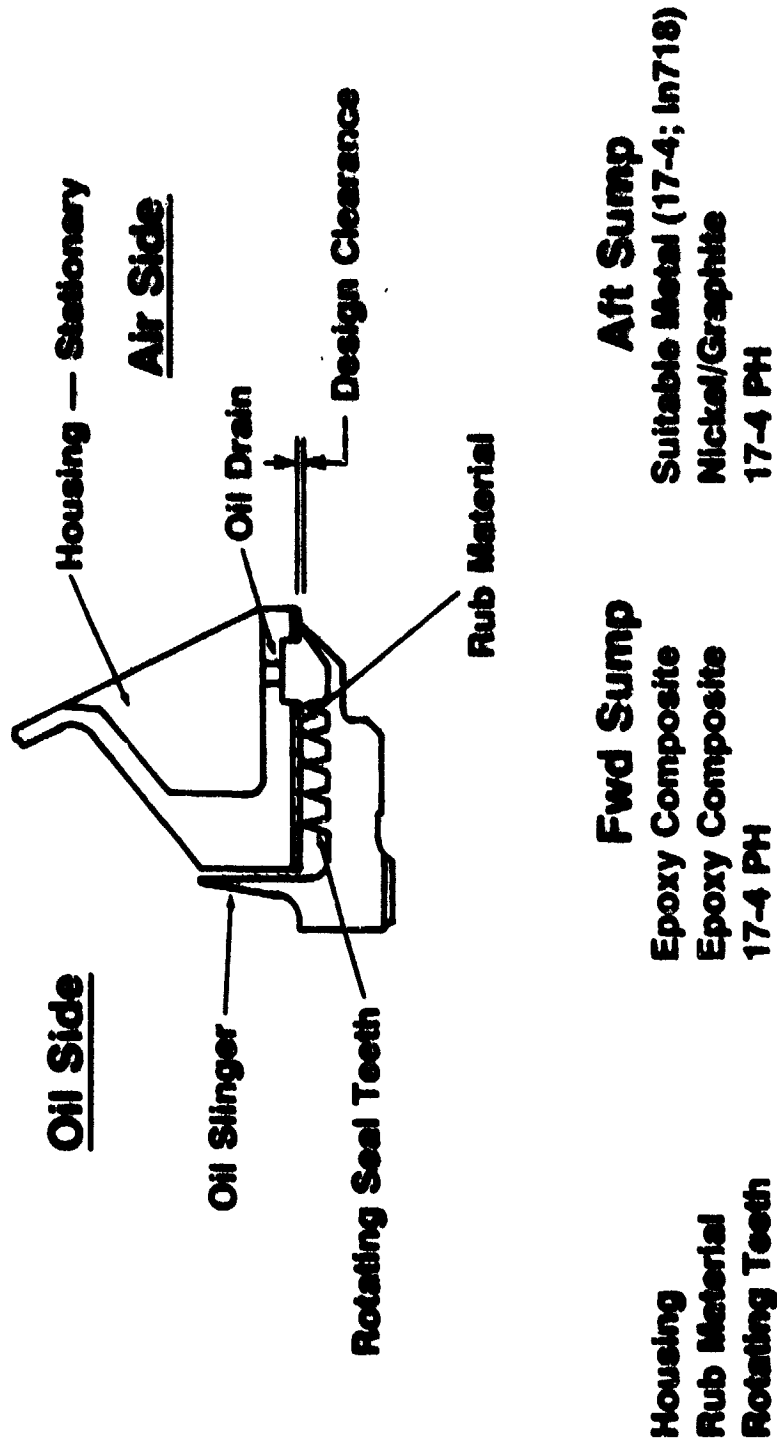


Figure 115. FPS Sump Labyrinth Seals - Typical.

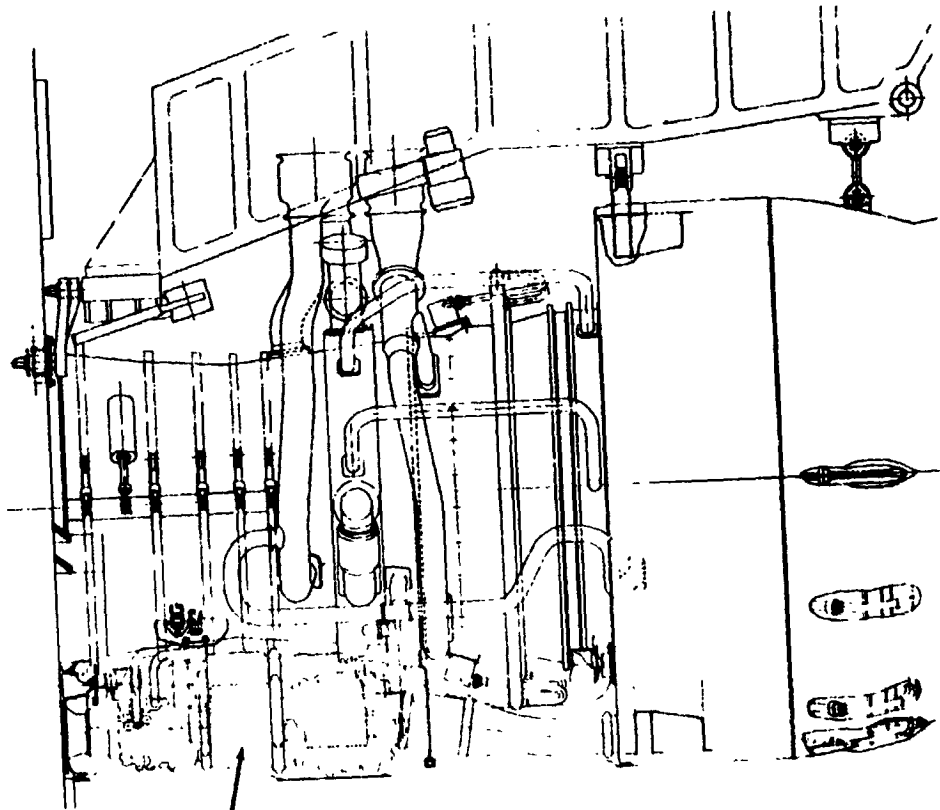
The sump seal teeth will not be hard-coated. This will prevent the possibility of hard-coating flakes entering the sump and damaging the bearings. In the aft sump, where higher temperatures exist, the seal rub material will be nickel graphite.

Figures 116 through 119 show the accessory drive system for the E³. This system transmits mechanical power from the engine high pressure system to the engine- and airframe-required accessories. The drive system consists of a PTO located in the forward sump as shown in Figure 111. The PTO horizontal bevel gear is mounted to the forward end of the compressor stub shaft and meshes with a bevel gear to give a slanted shaft angle of 78.05°. A slanted shaft is used to allow the TGB to be mounted in a cavity in the fan frame as shown in Figure 109. From the TGB, horizontal shafting drives aft to the AGB located in the lower core cowl area as shown in Figure 116. (It should be noted, however, that accessories could just as readily be located on the fan case if this location were preferred by the aircraft company.) Figures 117 and 118 show the forward-looking-aft view and the bottom view of the AGB. Mounted and driven from the AGB are:

- Engine Starter
- Lube and Scavenge Pump
- Control Alternator
- Fuel Pump
- Two Hydraulic Pumps
- Variable-Speed, Constant-Frequency (VSCF) Generator

The AGB is mounted in a separate enclosure ventilated with fan-discharge air to create a cool environment for the accessories. The mounting system for the accessory gearbox and the enclosure is designed so that the AGB/enclosure assembly can be swung down to provide access to the compressor casing. Figure 119 illustrates the gearing schematic for the E³ FPS system.

The lube system schematic for the E³ FPS engine is shown in Figure 120. The engine lube and scavenge pump is driven from the accessory gearbox. The pump contains four scavenge elements to return oil from the two sumps and the TGB and AGB gearboxes. The supply element, also contained in the pump, supplies oil under pressure to bearing and gearing systems requiring cooling and lubrication. The system features a filter both in the supply and in the scavenge circuits. The oil tank and fuel/oil heat exchangers are also part of the lube system.



**Accessory
Gear Box**

Figure 116. FPS Engine Side View.

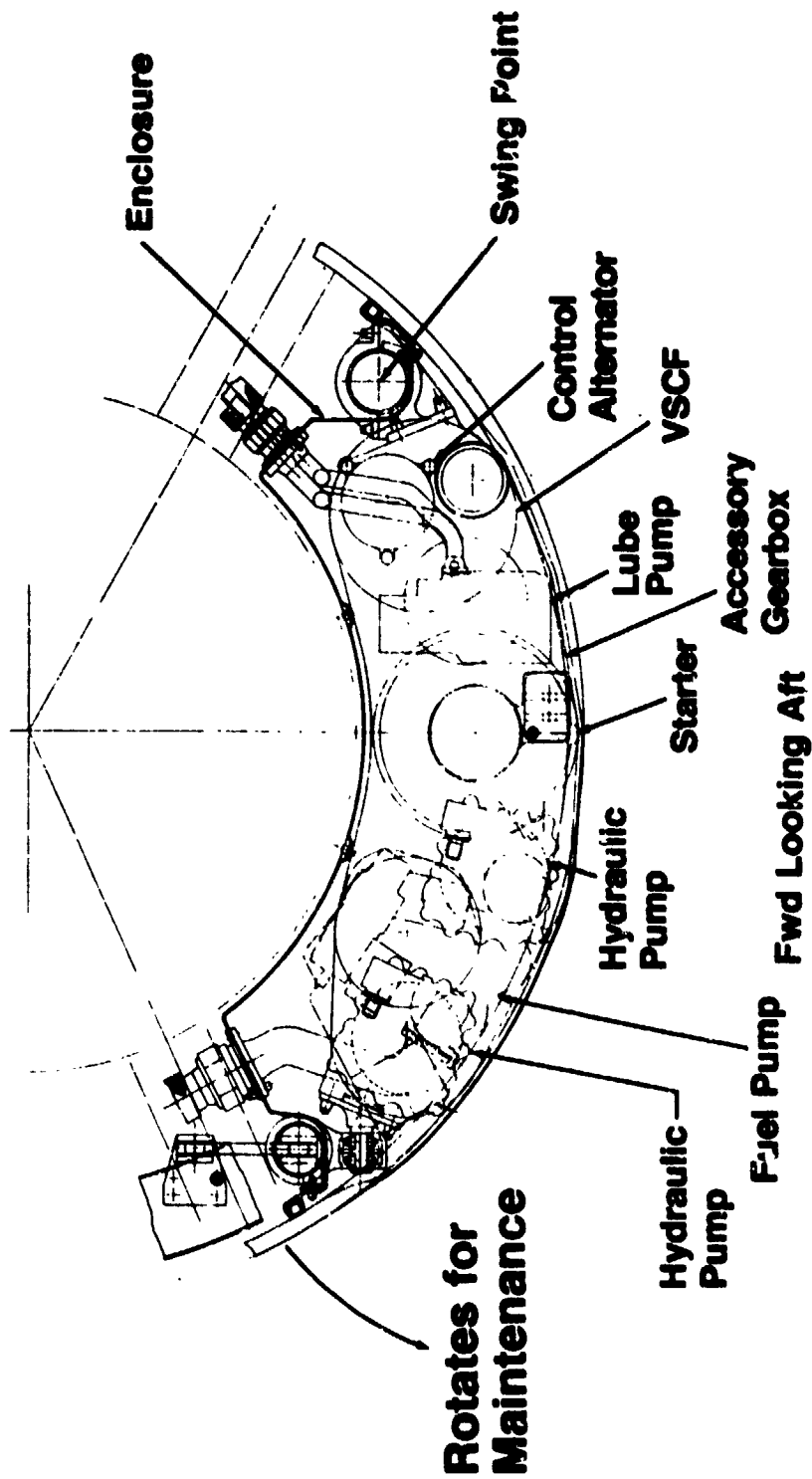


Figure 117. FPS Accessory Gearbox.

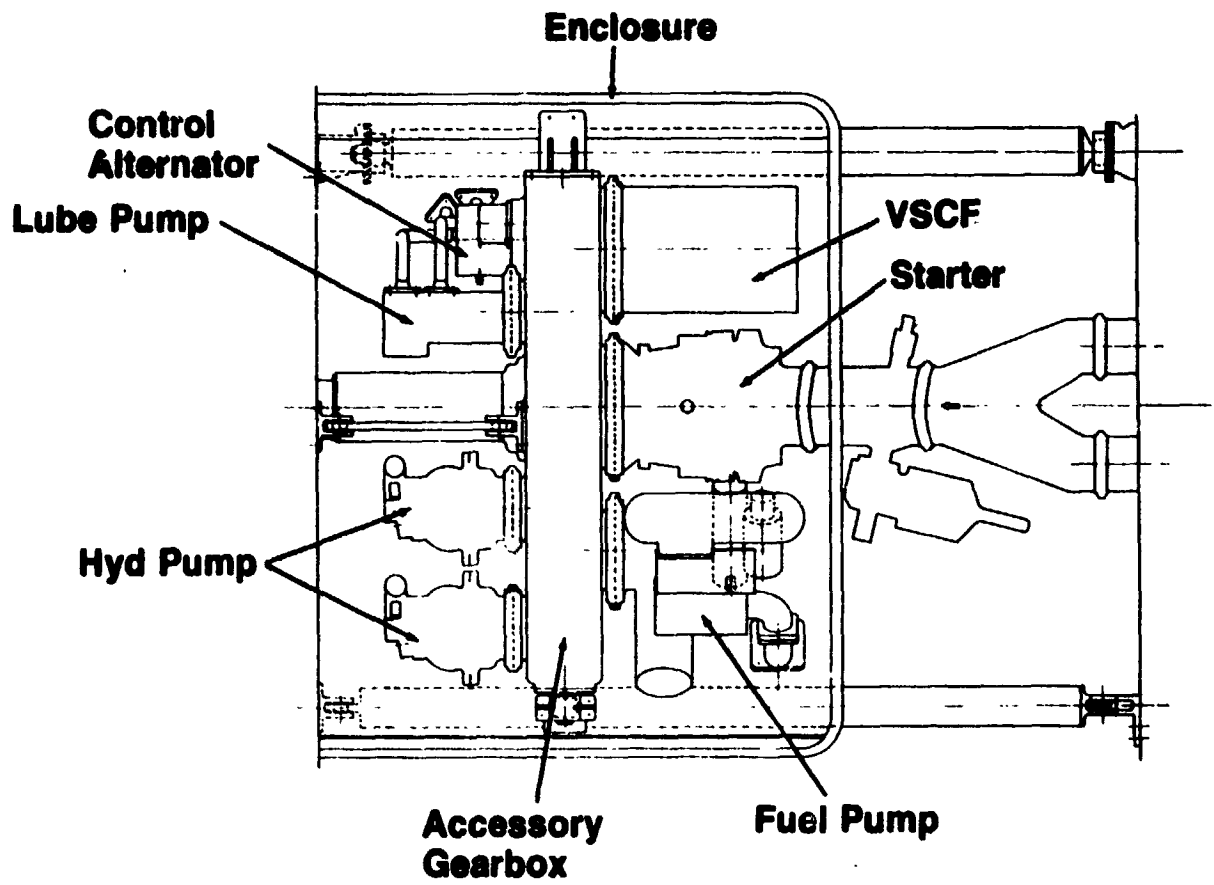


Figure 118. FPS Accessory Drive System.

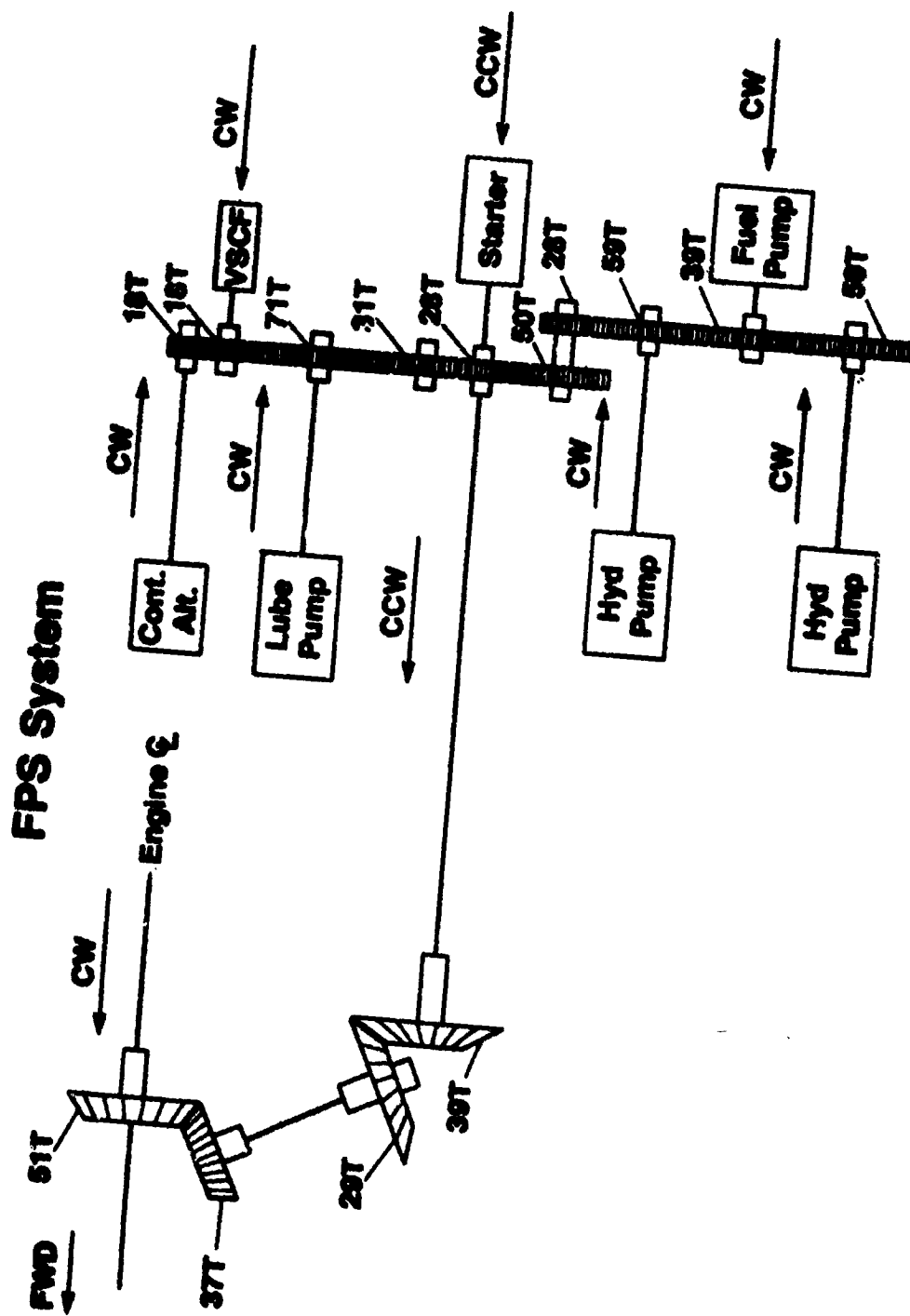


Figure 119. E³ Accessory Drive Gear Schematic.

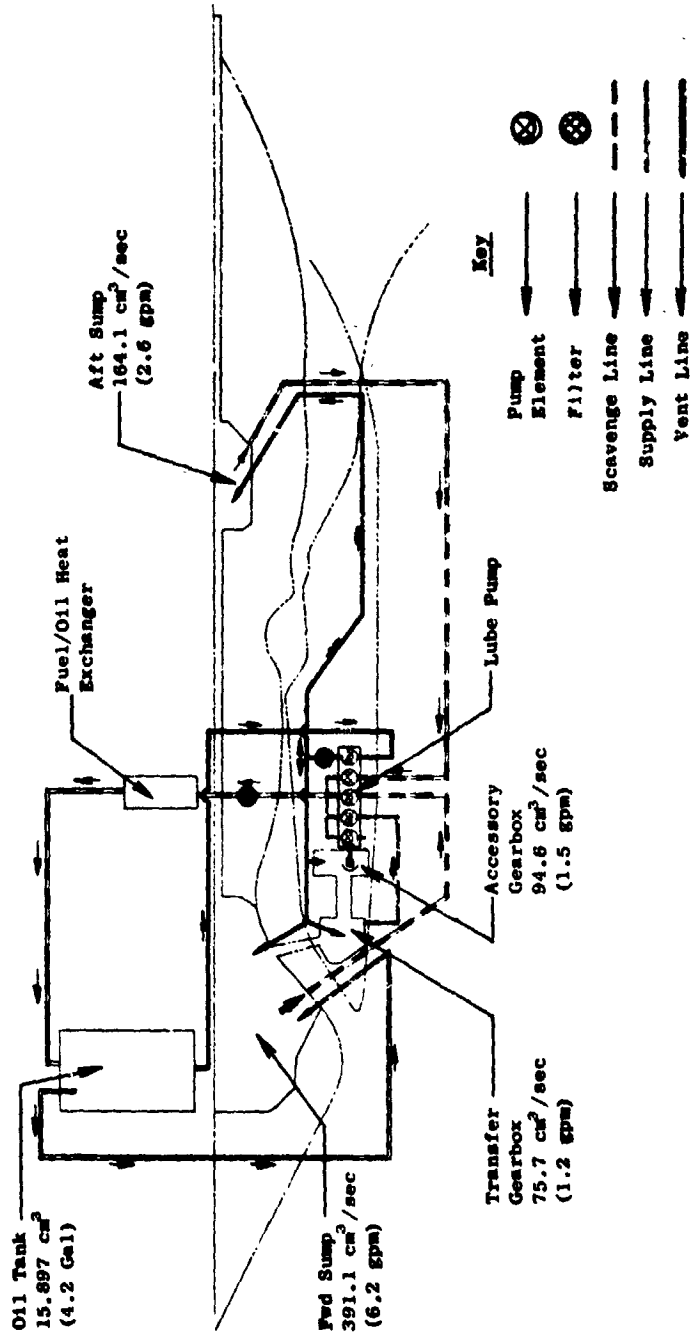


Figure 120. FPS Lube System.

4.8 CONTROL SYSTEM

The E³ incorporates a control system that utilizes digital electronic computation and associated control and accessory elements to control fuel flow, fuel distribution, compressor variable stators, starting bleed air, active clearance control air, and the thrust reverser. Requirements for the control system are outlined below and are followed by a description of the system and its elements.

4.8.1 Design Requirements

Most of the basic control system functional requirements evolve from the engine design definition; this establishes the variables to be controlled and the fundamental control characteristics required. The major control system functional requirements thus established are to:

1. Modulate fuel flow to control thrust.
2. Divide the fuel flow into the two zones of the double-annular combustor as required to meet exhaust emission goals.
3. Position the compressor variable stators for best compressor performance.
4. Position the air valves in the three separate active-clearance-control systems (compressor, high pressure turbine, and low pressure turbine) to achieve the minimum rotor clearances possible at important operating conditions and to prevent rubbing at any condition.
5. Position compressor bleed valves to unload the compressor in the starting region.
6. Control thrust-reverser actuation and integrate it with other controlled variables on the engine.
7. Sense, process, and transmit engine and control-system data for engine-condition monitoring.

In addition to these functional requirements, some general design requirements were established for the control system. One such requirement, established early in the engine preliminary design phase, was that the control system would employ digital electronic computation rather than the hydro-mechanical computation used in most current commercial-engine controls. There are a number of reasons for this, one being that this engine has more functions to be controlled than current engines. In addition, because of higher engine pressure ratio and higher efficiency in some engine components, more accurate and more flexible control of existing functions is required. This can be achieved with digital computation.

Another factor favoring a digital control is that, in the late 1980's when this engine is to go into service, it is anticipated that aircraft control systems will be predominately digital and that digital aircraft/engine-control interfaces will be required.

Cost is another factor favoring digital electronic control. The time-sharing capabilities of a digital computer make possible the control of a number of separate functions with a single computer processor; a hydromechanical computer or a hybrid hydromechanical/electronic analog computer generally requires separate computing elements for separate functions. Also, good progress is being made in developing automated manufacturing techniques for digital electronics, and this will tend to reduce costs.

Another general requirement imposed on the control system for this engine is in the area of reliability. Even though this system will perform more functions and will have considerably more capability than current commercial-transport engine controls, it is considered necessary that reliability be equal to or better than that of current controls.

4.8.2 Control System Design

A simplified schematic of the control system is shown in Figure 121. The main element in the system is the digital control. The control is being designed basically for single-channel operation with the intent that in-service development will eventually result in a digital control equal in reliability to current hydromechanical controls which have had extensive military and commercial operational development. However, for initial service, redundant controls are considered necessary to achieve the desired operational reliability. The two units will be functionally identical; software logic will cause one to serve as the primary control and the other as an active standby, brought on line automatically if a primary-unit malfunction is detected by self-test within that unit. When satisfactory in-service digital control reliability has been demonstrated, the standby unit will be eliminated from the system.

The system will be designed to operate with input commands and data from the aircraft in the form of multiplexed, digital, electronic signals. Because of the critical nature of the input commands, it is anticipated that these signals will be generated using power from the top-priority aircraft electrical bus, that dual (redundant) signals will be supplied, that the signals will be transmitted over separate lines, and that the signals will include a periodic test word to identify signal malfunctions. It is further anticipated that these signals will be in the form dictated by the applicable specification for aircraft avionics digital-data transfer.

The controls also receive a number of inputs from electrical sensors on the engine. Most of these will be dual-element devices with separate elements supplying each control. The digital control program includes a sensor-failure-accommodation feature in which a simplified model of the engine and an

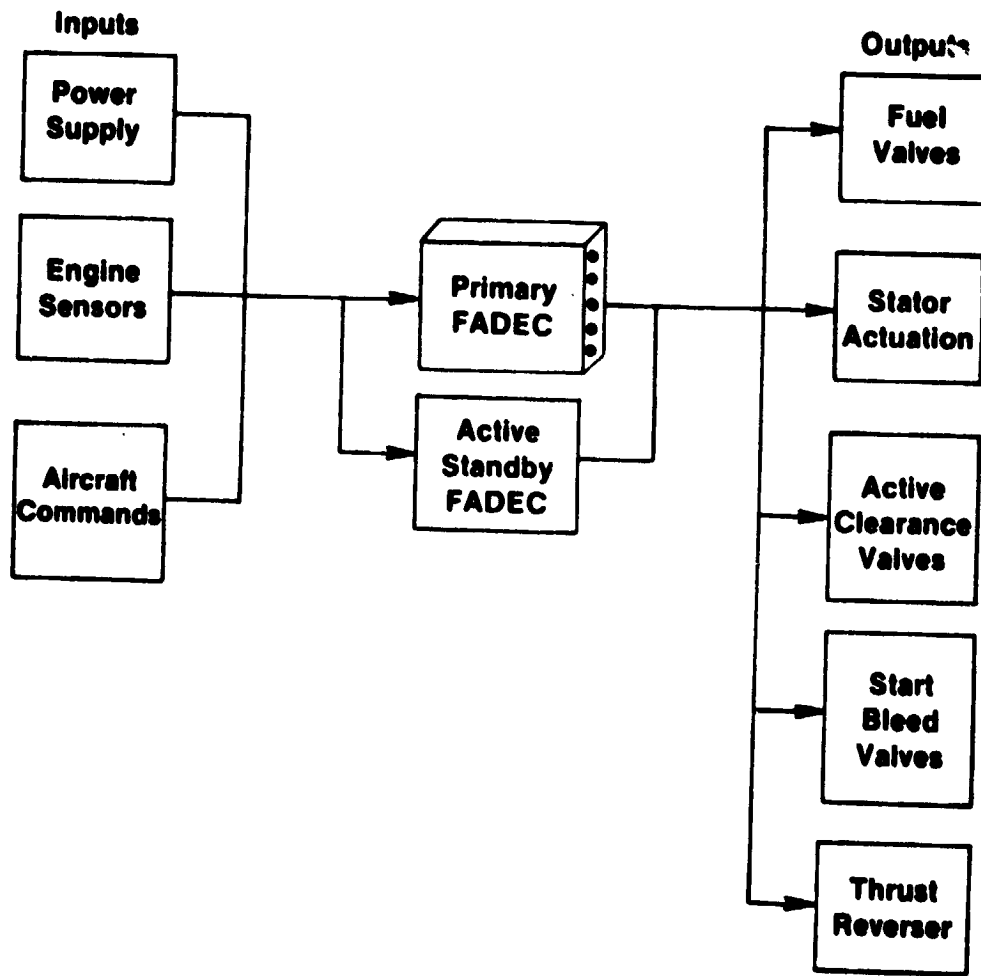


Figure 121. Full Authority Digital Control (FADEC).

extended Kalman filter combine to detect faulty sensor input and replace it with computed input to allow continued operation with a failed sensor.

An engine-driven control alternator, with separate coils for each, will be the primary source of electrical power for the digital controls. Aircraft power from the 28-volt d.c. system will serve as a backup and will provide power for static control checkout and for engine starts. Use of aircraft power for starts reduces the design speed range of the control alternator and results in a smaller, more efficient design.

Outputs from the digital control operate servovalves which, in turn, control the actuation of the various controlled elements in the system. The servovalves will be multiple-coil electrohydraulic or electropneumatic devices incorporating a fail-safe design feature which causes the element being controlled to remain fixed, or to drift slowly in a safe direction, if the signal from the digital control fails to zero or to maximum current.

The basic engine cycle inputs to the control system are shown pictorially on Figure 122. T_{12} , P_{T0} , and T_{25} serve primarily as control-scheduling parameters, but N_1 , N_2 , and T_{49} serve primarily as feedback in the fuel-control loop. T_3 and P_{S3} are involved in a turbine inlet temperature calculation, and P_{S3} is also used in transient fuel scheduling. The inputs will also be used for condition monitoring and for the sensor-failure-accommodation feature noted in Figure 122.

Two types of temperature sensors are used: resistance temperature detectors for the fan and core inlets, and thermocouples for the compressor discharge and LPT inlet. Pressures are sensed by probes or static taps at appropriate locations and are converted to variable-frequency electrical signals by transducers in the digital control. Fan rpm is sensed by a magnetic pickup in conjunction with a multitoothed disk on the fan shaft to provide a pulsing signal, with a frequency proportional to fan speed, to the digital control. Core rpm is sensed by measuring the frequency of the digital control power supply from the control alternator.

The outputs controlled by the system are shown pictorially on Figure 123. The controlled outputs include three air valves (compressor, HPT, and LPT clearance control), two fuel valves (main fuel and fuel-flow split), and two actuation systems (core stator and reverser). The boxes on Figure 123 indicate additional controlled outputs beyond those incorporated on a typical, current, transport engine: the CF6.

4.8.3 Digital Control Design

The digital control for this engine is a solid-state electronic device designed specifically as an aircraft engine control. The design has evolved over a period of years at General Electric, beginning with off-engine units

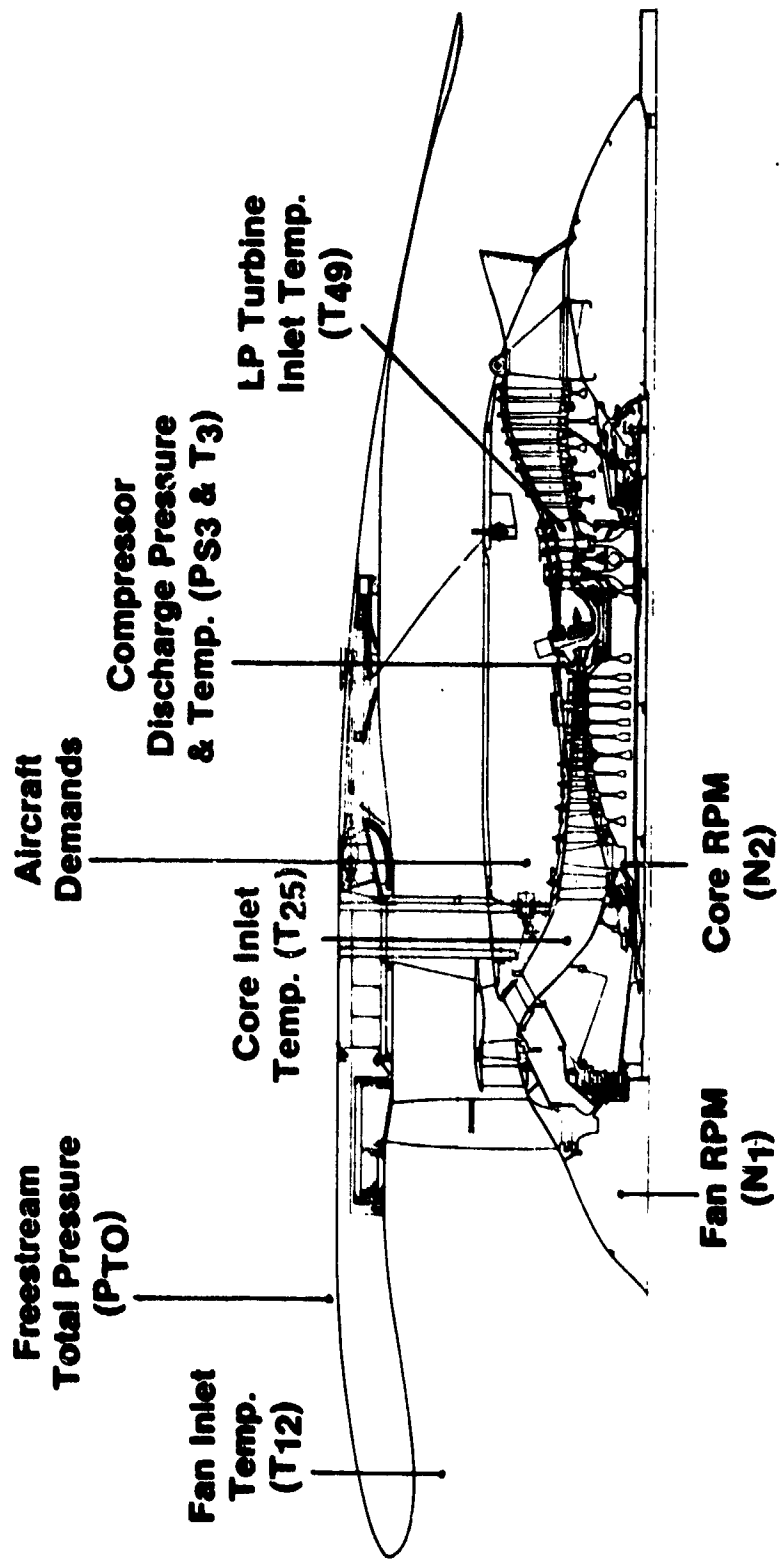


Figure 122. Control System Inputs.

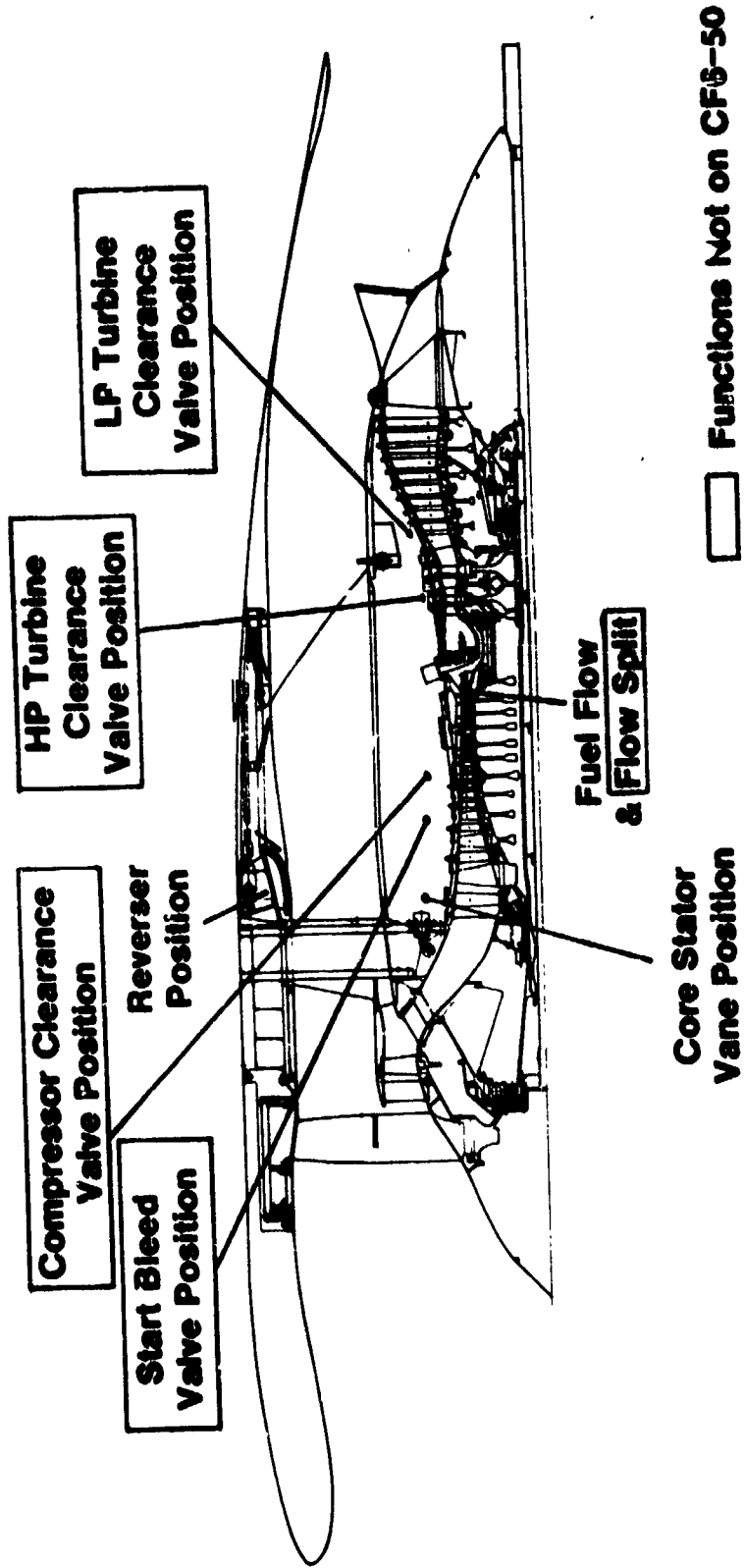


Figure 123. Control System Outputs.

in the early 1970's and proceeding to refined, on-engine designs for the NASA/GE QCSEE program (References 13 and 14) and the U.S. Navy/General Electric Full Authority Digital Electronic Control (FADEC) program, Contract N00019-76-C-0423 (Reference 15). The design incorporates a single, time-shared, digital microprocessor operating in conjunction with solid-state memory elements to perform essentially all of the computation and logic required for the various control functions of the engine. Also included are timing and control elements which control processor/memory operation and circuit elements which handle input/output-signal functions. The basic clock rate of the computer is 3.5 megahertz, and program running time will be in the 0.010 to 0.015-second range.

The digital control design is tailored for operation in an aircraft engine environment and incorporates features aimed at reducing the effects of factors which are known to be major sources of problems. Extensive experience on General Electric military engines with limited-authority electrical controls has shown that most problems are associated with mechanical-interconnection failures between electrical elements, caused by thermal and vibratory stresses, or with electrical-element degradation caused by high temperature. In the digital control, extensive use is made of integrated circuit chips to reduce the number of elements requiring interconnection. In addition, most circuit elements are mounted on ceramic, multilayer circuit boards; this further reduces the number of interconnections exposed to vibration and atmospheric effects. Figure 124 is a schematic of this circuit board design. The materials utilized (i.e., Kovar leads, tungsten circuit runs, and alumina boards) all have low and well-matched thermal-expansion coefficients to reduce thermal stresses. The circuit boards are mounted to a fuel-cooled aluminum plate to reduce the effects of environmental and internally generated heat.

4.8.4 Fuel Control System

A schematic of the fuel system is shown in Figure 125. The system uses a positive-displacement fuel pump with integral centrifugal boost. Ports on the pump are provided so that fuel from the boost element can be passed through the fuel heater (shown in Figure 126 and discussed in Section 4.8.7).

Fuel from the positive-displacement pump element enters the fuel valves where a metering-valve/bypass-valve combination meters fuel to the engine and bypasses surplus fuel back to the pump. Metering-valve position and (thus) fuel flow are controlled by the digital control by means of an electrohydraulic metering servovalve and an electrical metering-valve-position feedback transducer. The fuel valve includes a mechanical core-overspeed governor that operates on the bypass valve, a fuel shutoff valve, and a pressurizing valve to maintain sufficient fuel pressure to operate servos at low flow conditions.

From the fuel valve, metered engine fuel passes through an engine-oil cooler and into the flow divider where a metering-valve/throttling-valve combination splits the flow as required for the double-annular combustor. The flow-divider metering valve is controlled by the digital control through a position-control loop similar to that used for the main-fuel metering valve.

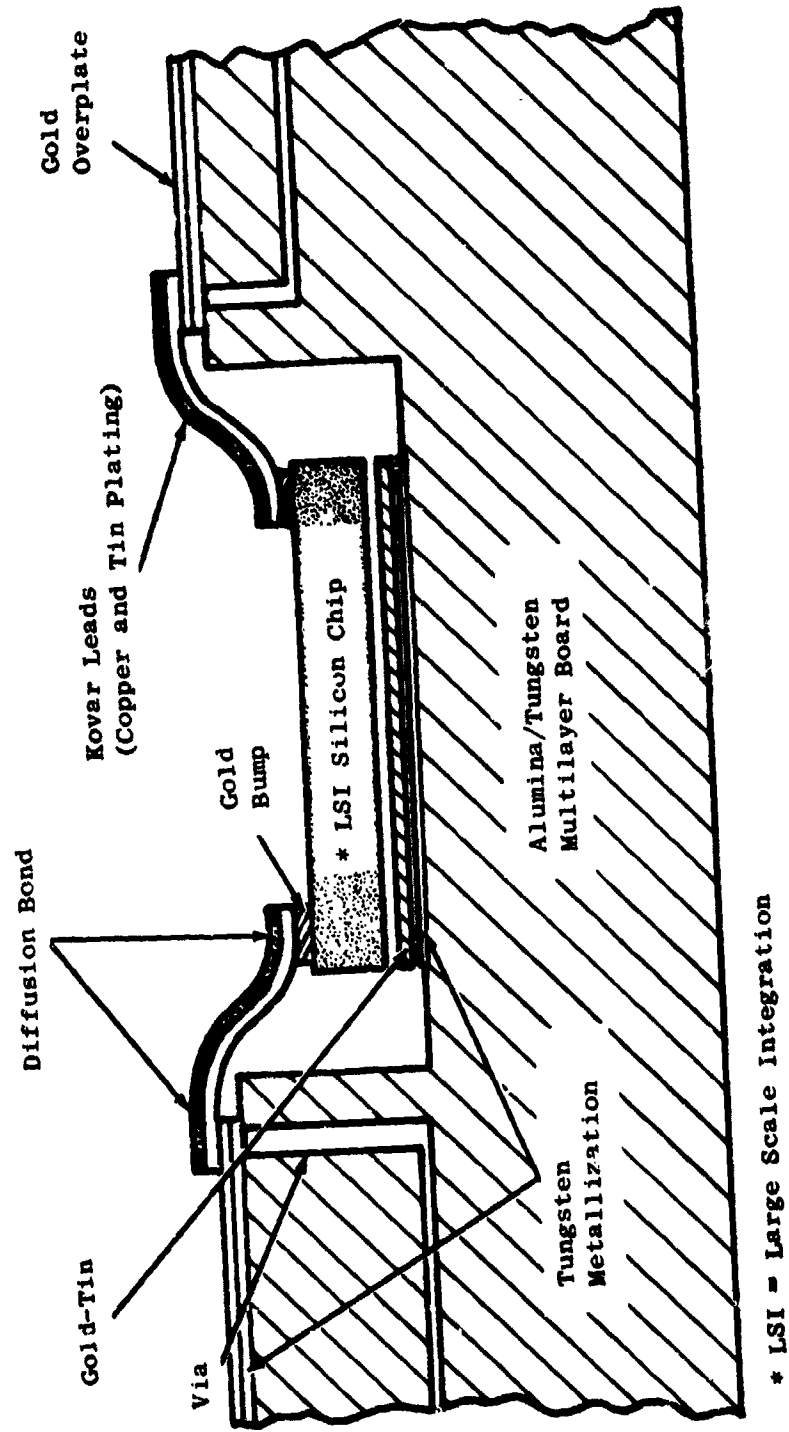


Figure 124. Hybrid Electronics.

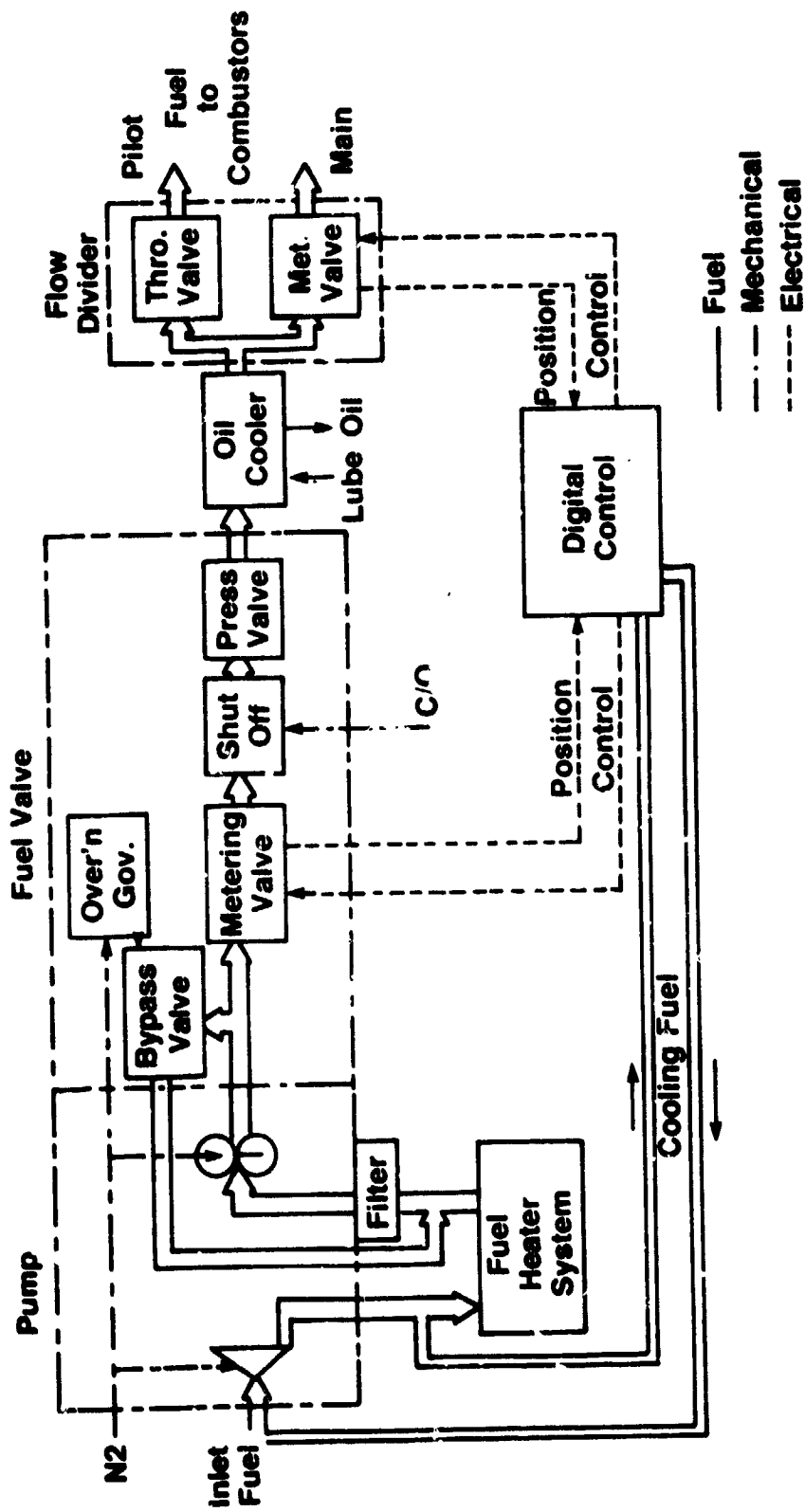


Figure 125. Fuel System.

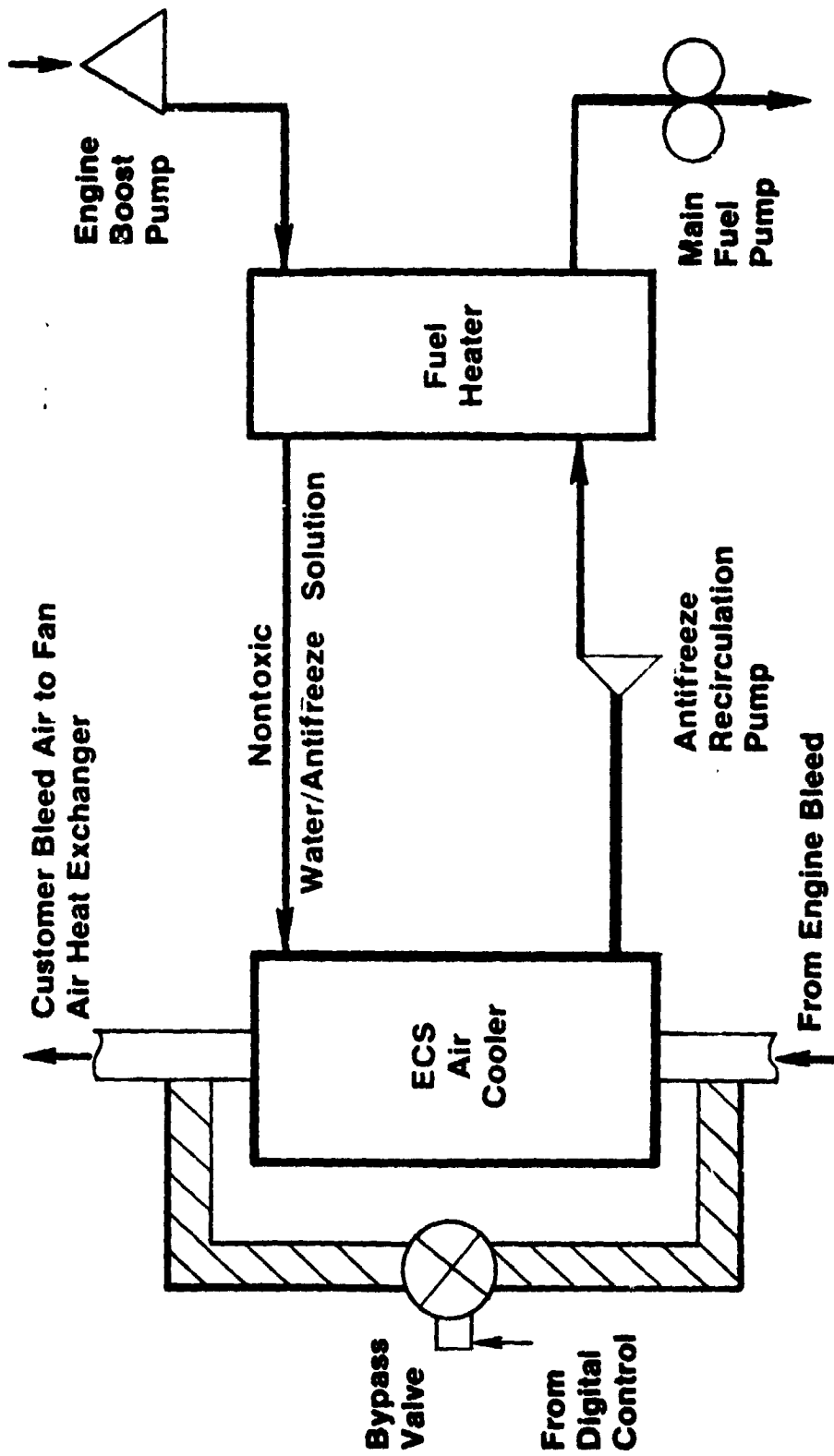


Figure 126. Fuel Heater/Regenerator Schematic.

Control of fuel flow is basically achieved by modulating flow to set thrust in response to the thrust-command input from the aircraft. Because no practical method is available to sense thrust directly, a study was performed comparing 14 engine variables which can be sensed or computed by the control system and used as a measure of thrust. Included among the candidate parameters were fan rpm, core rpm, a fuel-flow-related parameter, and various parameters computed from pressure and/or temperature at various points in the engine flowpath. The potential thrust parameters were compared by using a special computer model that operated the engine with each parameter (taken one at a time) in control and applied typical engine and control-component tolerances at key operating conditions to define thrust-setting accuracy.

Of the 14 thrust parameters compared, corrected fan rpm provided the best thrust-setting accuracy, and it was selected as the primary fuel-controlling parameter. Thus, during normal steady-state operation, fuel flow is modulated to control corrected fan rpm. Fuel-flow limits are applied by the digital control to prevent overspeed, overtemperature, compressor stall, or combustor blowout. The flow is then split for the two zones of the combustor, with pilot-zone flow only at low power settings and flow in both zones at high power.

4.8.5 Stator Control System

The core compressor stator control system is shown schematically on Figure 127. A pair of fuel-driven ram actuators operates the stator-actuation system of levers and annular rings around the compressor case. Fuel to the actuators is controlled by an electrohydraulic servovalve on one of the actuators. The servovalve control signal is supplied by the digital control. A position transducer in one actuator provides a feedback signal to the digital control. Actuation synchronization is achieved through the rigidity of the actuation linkage.

The digital control schedules Variable Stator Vane (VSV) position in accordance with a basic corrected-core-speed schedule, much the same as is done on the CF6-50C, but it also applies a number of compensating biases to exploit the capabilities of variable compressor stators to accommodate the engine transients and widely varying steady-state operating conditions. The exact nature of these biases will be determined during engine development testing. Some of the potential stator biases are listed below.

Rain Reset - Heavy rain causes a reduction in core inlet temperature (T_{25}), and rapid termination of rain, combined with T_{25} sensing lag, can cause compressor stalls. This bias is applied in the closing direction when sensed T_{25} is less than calculated T_{25} (as it will be in heavy rain), thus increasing stall margin.

Stall Avoidance - CF6 experience has shown that the optimum stator setting in the cruise corrected-speed region is different than the optimum setting in this region on the ground. This schedule modification can be accomplished with a power-demand reset of the stators.

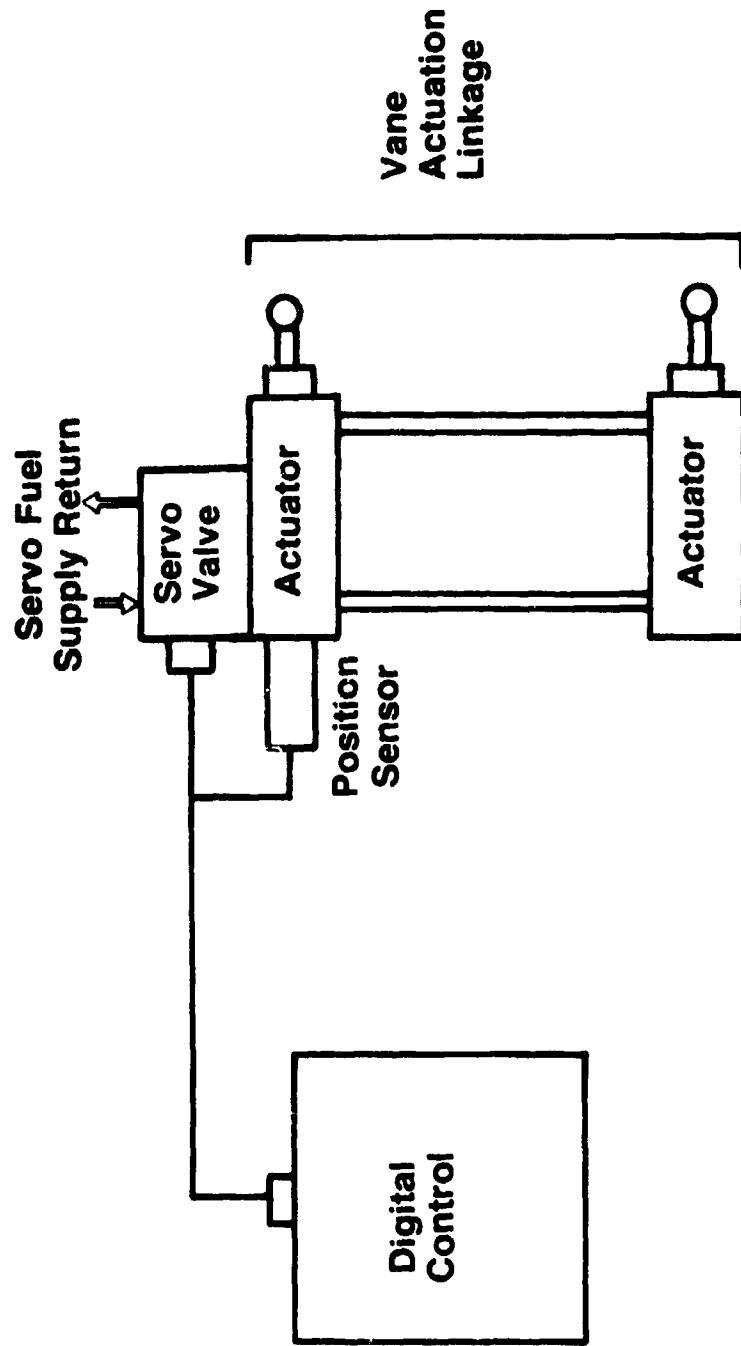


Figure 127. Compressor Stator Vane Control.

Stall Recovery - Experience has shown that recovery from a compressor stall can often be accomplished by temporarily shifting the stators in the closed direction. When a rapid drop in compressor-discharge pressure occurs, as it will during a stall, this function creates a temporary stator closure and, simultaneously, a fuel-flow reduction. If recovery does not occur, shut-down or power reduction by the pilot will be required as on current engines. If recovery does occur and then the engine stalls a second time, the stator-closing bias would be reapplied and left on to provide additional stall margin until the engine is shut down.

Reverse Reset - Experience has shown it is desirable to bias the stators in the closed direction to accommodate the inlet disturbances that can accompany thrust-reverser operation.

Deterioration Compensation - Experience has shown that engine deterioration results in a change in the core-speed/fan-speed relationship. Stator reset can restore the original relationship and regain some lost internal efficiency.

Bleed Compensation - It has been suggested that a stator reset might be used to adjust the compressor operating point and improve efficiency when customer bleed air is being extracted. Such a reset is being shown in the preliminary control system design.

Transient Compensation - It is quite probable that some adjustment to the basic stator schedule would improve transient operation of the compressor and thereby improve transient response. Also, as demonstrated successfully in the NASA/GE QCSEE Program (Reference 16), transient response at approach conditions can be improved by resetting the stator schedule in the closed direction so that core rpm is higher than normal at approach, and maximum thrust can be reestablished with less rpm change than normally required. Development testing would be required to determine if this could be done without causing aeromechanical compressor instability or unsatisfactory engine efficiency changes.

4.8.6 Active Clearance Control

As noted in previous sections, this engine has three separate active-clearance-control systems. Clearance control in compressor Stages 6 through 10 is achieved by modulating the flow of fifth-stage bleed air over the aft compressor casing. Clearance control in the turbines is achieved by modulating the flow of air extracted from the fan duct into separate annular manifolds surrounding the HPT and LPT casings.

The control system elements involved in active clearance control are shown schematically in Figures 128 and 129. In the current design, compressor clearance-control air is regulated by three separate three-way, modulating butterfly valves actuated by fuel and controlled by an electrohydraulic servovalve operated by a signal from the digital control. An electrical position transducer is included in each valve package to supply feedback to the digital control.

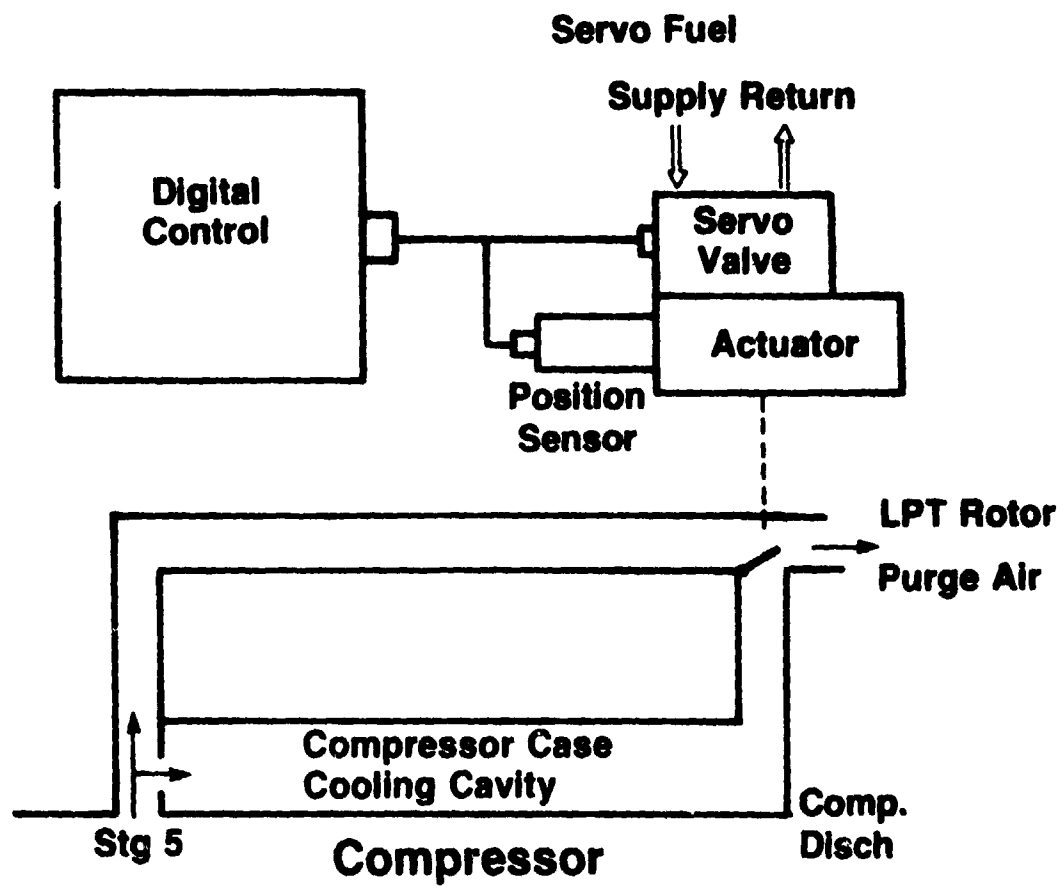


Figure 128. Compressor Clearance Control System.

(2 Separate, Identical Systems — HPT & LPT)

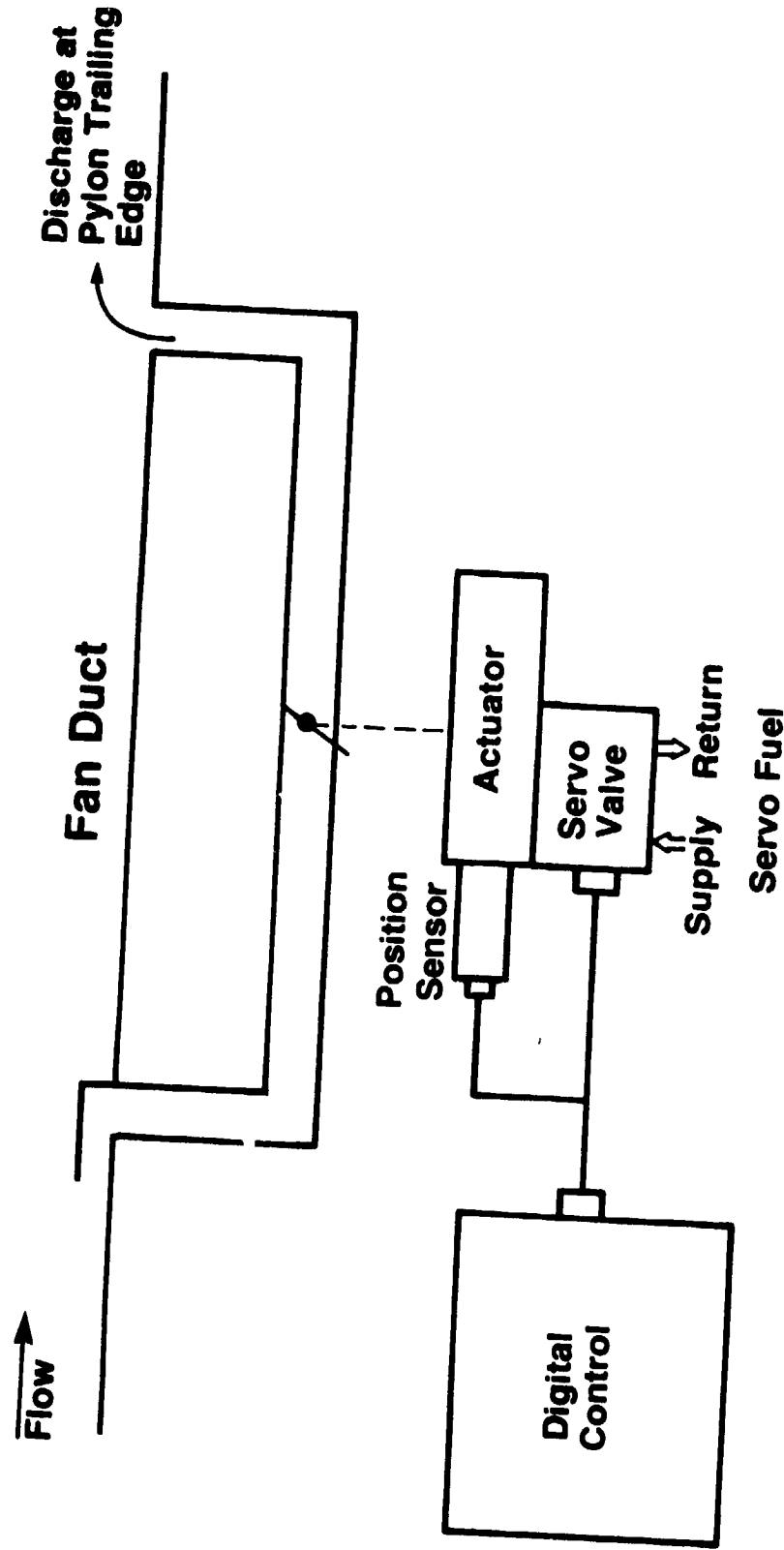


Figure 129. Turbine Clearance Control Systems.

The air to each turbine clearance-control system is regulated by a two-way, fuel-operated, modulating butterfly valve. Separate valves are included for the HPT and LPT. The digital control operates both valves through electrohydraulic servovalves. Position-feedback transducers are included on both valves.

The strategy for active clearance control has not yet been firmly established. One possible approach is to schedule the air-valve positions as functions of rpm and operating condition with compensation applied to accommodate transient thermal lags. Another concept is to include thermal and mechanical equations in the digital control program for computing clearance from sensed input variables. The control would modulate the air valves to maintain the desired clearances, again compensating for transient thermal lags. Use of sensed rather than calculated clearance here has been considered, but it is not likely that a fully developed sensing method will be available when this engine goes into service. However, development programs currently underway (including a NASA-funded program at General Electric, Contracts NAS3-21006 and NAS3-21843) (Reference 17) may produce practical rotor-clearance-sensing techniques that could be introduced at a later date.

4.8.7 Starting Bleed

The engine incorporates provisions for seventh-stage bleed to unload the compressor during starting. As presently configured, this bleed is controlled by three fuel-actuated, two-way air valves modulated in unison by the digital control through servovalves on each valve. Position transducers on each valve provide position-feedback signals to the digital control.

4.8.8 Fuel-Heating System

The engine fuel system incorporates a heat-exchanger network that transfers heat into the engine fuel. The primary purpose of this feature is to recover heat energy otherwise lost to the engine cycle.

It was originally proposed that the heat be extracted from the compressor bleed air used for active clearance control, but this concept proved unattractive because this cooled, clearance-control air returns to the cycle at a relatively high energy point, and the cycle gain from heated fuel is nearly cancelled by the reduced work capability of the reinjected air. Further study identified the following two heat sources with potential for improvement over the original systems.

- Heat could be removed from compressor-bleed air used for the aircraft environmental control system (ECS). ECS air is a heat loss which cannot normally be recovered by the engine. In addition to compressor bleed, fan air is also lost to the cycle as it is used to cool the compressor air below 232° F (450° F) so that it can be safely carried through the wings of the aircraft. The net sfc gain would be the sum of the gain for fuel heating and the gain for elimination of fan bleed.

- The LPT exhaust is another potential heat source if it can be used without a significant pressure loss. The net sfc gain is the gain for fuel heating and the gain for elimination of fan bleed.

Three fuel-heating-system concepts were studied: (1) using ECS air for the heat source, (2) using LPT exhaust air, and (3) using either source. These studies indicated that the concept using ECS air as a heat source offers the most promise; so ensuing design effort was concentrated on that approach.

The fuel-heating feature also provides fuel anti-icing by heating the fuel sufficiently to prevent fuel blockage by ice in the fuel-handling components.

Figure 126 is a schematic of the current fuel-heating system. It includes two separate heat exchangers and uses a pressurized water/antifreeze intermediate fluid to eliminate the possibility of fuel leakage into the ECS air. The intermediate fluid is nontoxic and is circulated by an engine-driven pump picking up heat from the ECS system in one heat exchanger and transferring the heat into the fuel in the other heat exchanger.

An air bypass valve around the air-to-water heat exchanger controls fuel-heating-system temperatures and prevents excessive ECS air pressure loss at high bleed-flow conditions. This valve will be operated by the digital control.

Based on current ECS bleed flow and temperature estimates from E³ air-frame subcontractors for a late 1980's transport aircraft employing cabin air recirculation, the fuel-heating feature offers an sfc reduction of 0.8%, at the cruise design point, made up of 0.35% due to the fuel energy recovery and 0.45% due to the elimination of fan-air cooling of the ECS. It is estimated that the fuel-heater weight effect will be +20 kg (44 lb), and the cost effect will be +\$14,500. Combining the sfc, weight, and cost effect yields a reduction in DOC of 0.37% for the aircraft system.

4.8.9 Aircraft Generator Cooling

Certain characteristics of this engine and fuel system make it possible to provide cooling for the aircraft electrical-generation system using engine fuel rather than using fan air like current CF6 installations. This provides an sfc benefit at the cruise design point of 0.33%. This, in combination with weight and cost reductions of 3.6 kg (8 lb) and \$1500 which result from elimination of the air/oil cooler, reduces net DOC 0.19%.

The key factors which make possible the fuel-cooling of aircraft generator oil are as follows:

1. This engine has a lower heat load on the lube-oil system because it has fewer bearings and sumps than current engines.

2. Higher fuel temperature can be tolerated because the fuel/oil cooler is downstream of the fuel pump. On the CF6, the cooler is upstream of the main pump element, and fuel temperature is limited by pump-cavitation considerations.
3. The aircraft generator is anticipated to be a high speed VSCF (variable speed, constant frequency) design producing less heat than current generator/constant-speed-drive combinations.
4. A more efficient fuel pump will be available when this engine enters service in the late 1980's.

4.8.10 Control System Configuration

The major fuel and control-system components will be located in the space between the core compressor casing and the inner wall of the fan flowpath, as discussed in Section 4.7. The digital controls are mounted on the wall at the forward end of this space; the fuel pump, fuel valve, starter, and control alternator are mounted on the accessory gearbox. The remaining components are mounted to the core engine casing in various locations.

Estimated total weight for fuel and control system components is 136 kg (299 lbm).

4.9 NACELLE DESIGN

The E³ Flight Propulsion System was designed with an integrated nacelle to permit a significant weight reduction for the total installed system. Major elements of the nacelle design include:

- Integral, composite construction of the fan frame, the outer portion of which forms the outer surface of the nacelle.
- Substantial use of composite materials in the inlet and aft cowling and in acoustic treatment of the exhaust flowpath.
- Lightweight fan containment based on the use of Kevlar fibers to trap and hold engine-generated debris in the event of fan damage.
- A long-duct, mixed-flow exhaust system to enhance propulsive efficiency, achieving a higher level of engine performance with a smaller fan and low pressure turbine than would be required for a comparable separate-flow system.
- A reverser contained entirely in the outer wall of the nacelle, without need for bifurcation and cross-duct linkage, and extensive application of composite materials in the reverser to reduce the weight of the design.

- An engine mount system chosen with particular attention to minimization of engine deflections due to mount loads in order to promote close control of turbomachinery clearances.
- Nacelle aerodynamic lines chosen for slimness and low cruise drag. To achieve as small an external-nacelle profile as possible, the accessory package is located in the core component.
- A reverser hinged at the pylon attachment and latched at the bottom for ease of maintenance access to the core engine and accessories. The core cowl panels are hinged to the pylon to form a separate inner-door system.

The aggressive use of advanced structural design and low-drag aerodynamics was estimated to contribute a 0.6% cruise drag reduction and a 15 to 20% installation weight saving relative to the current technology of the CF6-50C nacelle that was the E³ program baseline.

The general arrangement of the E³ nacelle is shown in Figure 130.

4.9.1 Fan Reverser

The preliminary fan thrust-reverser design is a fixed-cascade, translating-sleeve/blocker-door configuration. The reverser is made in symmetrical circumferential halves, each half hinged to the aircraft pylon and latched to the other half along the bottom centerline, allowing ready access to the engine (Figure 131). The reverser consists of the fixed support structure including the cascade section, the outer translating sleeve, the blocker doors and linkage mechanism, and the actuation system. Since the actuation system is located outboard of the cascades, the cascade section is made in circular-arc sectors with passageways (slots) between them for the blocker door links to pass through. The blocker door is a floating design with the forward section supported by rollers located at the corners. The aft portion of the blockers is supported by a slider-link mechanism consisting of a drive link connected to a unison ring and a drag link with a fixed pivot on the aft support structure. Drive links connect each blocker door to the translating sleeve.

The unison ring is located outboard of the cascades and is supported by "T" shaped ends riding in a slot in the fixed-structure main axial beams. A forward-acting load is imparted to the unison ring by a series of compression springs mounted between it and the translating sleeve. This load is sufficient to hold the blocker doors in the stowed position during forward-thrust operation. The floating feature of the unison ring also serves to eliminate the effect of manufacturing and assembly tolerance accumulation in the system. The translating sleeve is driven by the actuation system and serves as the blocker door and unison ring driver as well as the outer nacelle flow-surface fairing. Figure 132 shows the translating sleeve, unison ring, and compression springs.

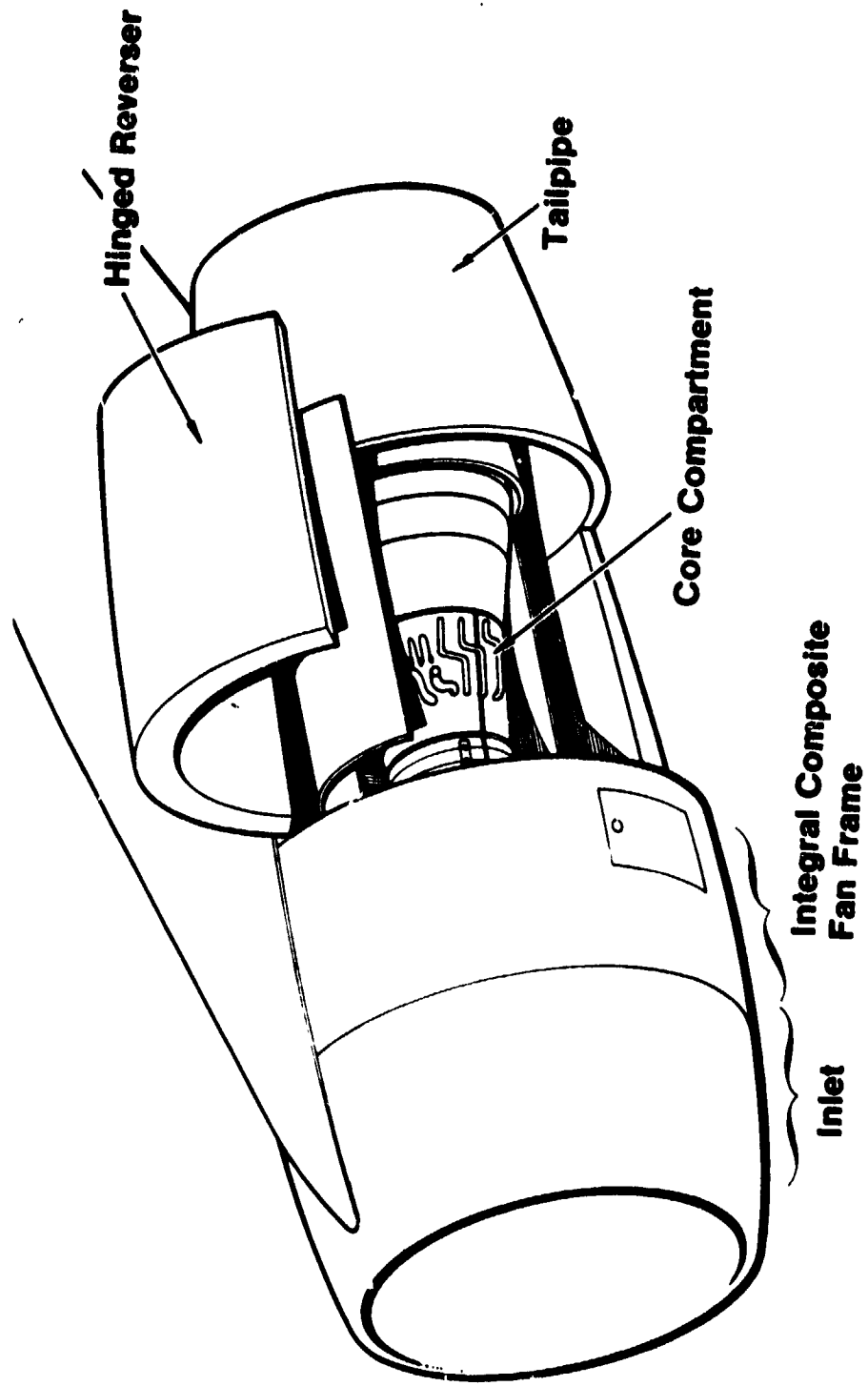


Figure 130. Nacelle General Arrangement.

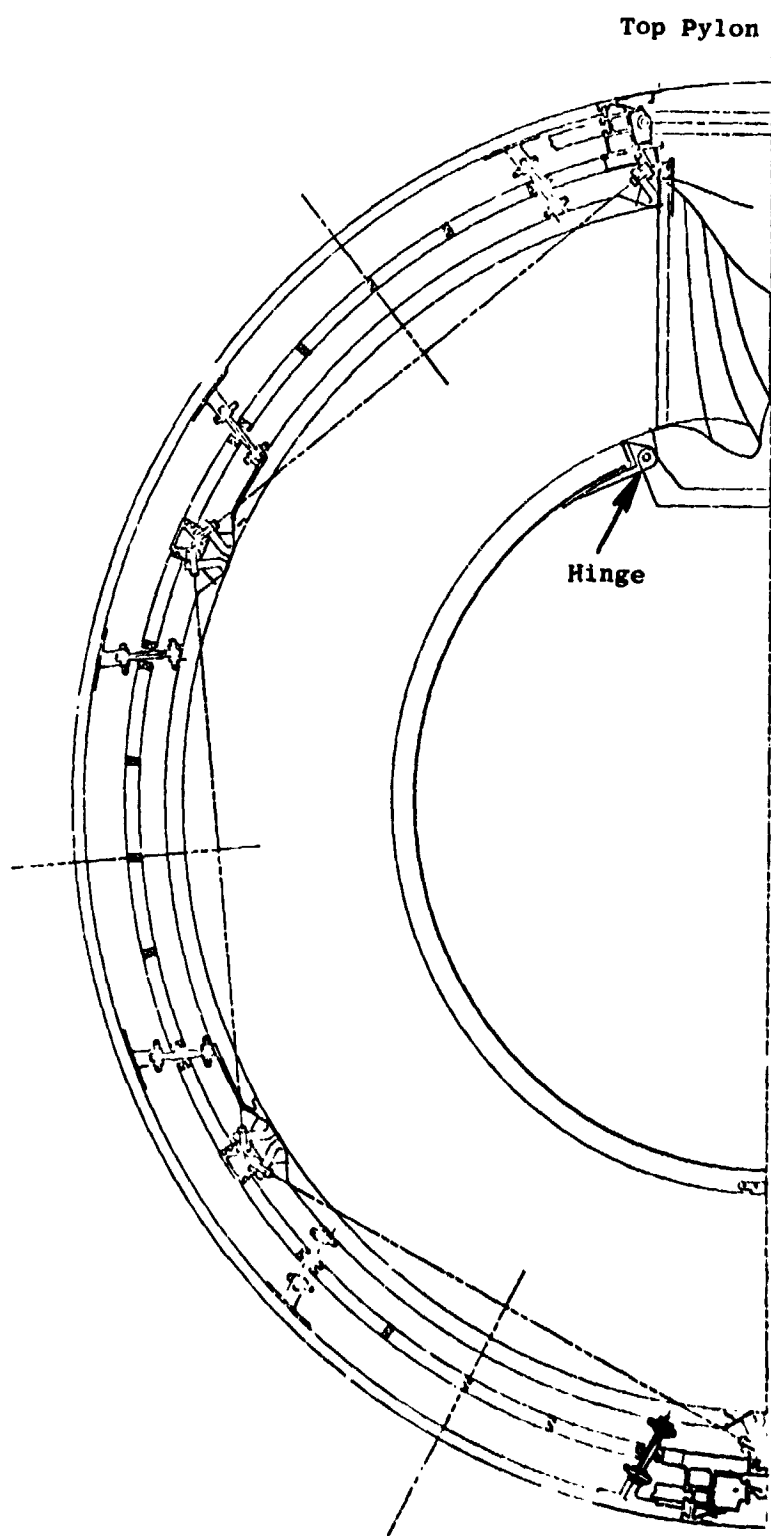


Figure 131. Front View, Reverser Cross Section.

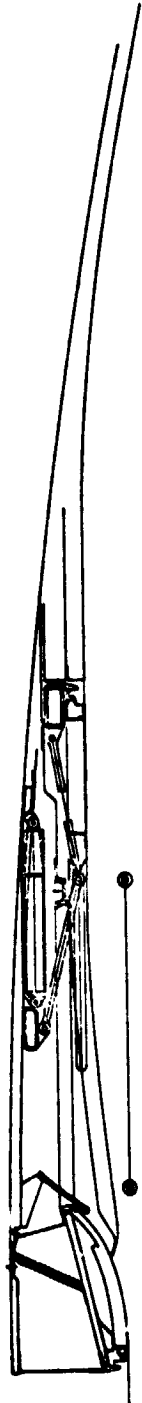
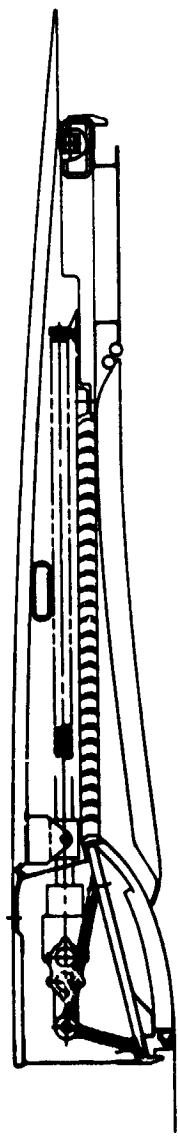
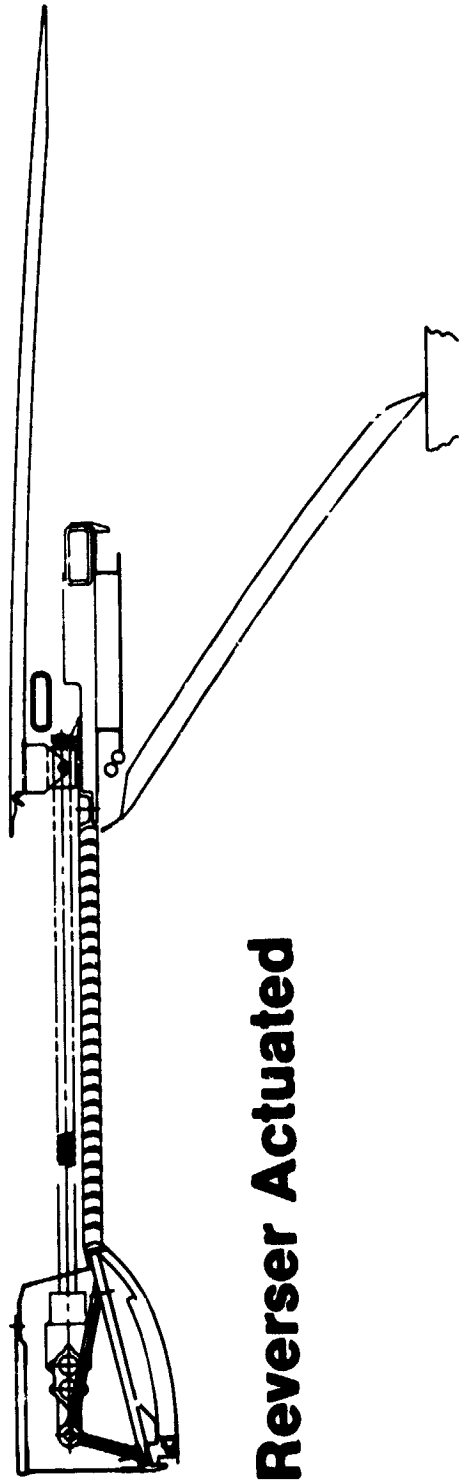


Figure 132. Side View of Reverser Translating Sleeve and Blocker Door.



Reverser Stowed



Reverser Actuated

Figure 133. Thrust Reverser Actuation.

As the translating sleeve is moved aft by the actuators to uncover the cascades, the blocker doors are moved aft along with it. Because the unison ring is not being driven at this time, the unison ring spring load tends to cause the aft end of the blocker doors to stay in the stowed position. To prevent interference of the blockers with fixed structure aft of the doors as the blockers move aft, a set of rollers at the edge of the structure at the blocker door cavity ride along a ramp surface on the back side of the blocker, forcing the door into the fan stream sufficiently to clear the fixed structure but not enough to cause a large decrease in fan-duct flow area. At a predetermined point in the sleeve translation, a bumper on the sleeve contacts the forward face of the unison ring, causing it to move aft with the sleeve and blockers for the remainder of the actuator stroke. The aftward movement of the unison ring forces the slider-link mechanism to rotate towards the engine centerline, causing the blocker doors to rotate about the forward support rollers, blocking the fan stream and diverting it through the cascades.

Figure 133 illustrates the reverser in stowed and deployed positions. The aerodynamics of the reverser are based on previous General Electric experience with large-turbofan reverser designs. Cascade area was sized to provide an adequate effective-area margin, fully deployed, relative to the discharge-flow requirements of the fan bypass. The desired fan operating line for reverse thrust is lower in pressure ratio at corrected airflow than the normal forward-thrust-mode fan operating line at static conditions. This was done in order to provide additional stall margin if required and to provide a reduction in core engine speed and turbine temperature at fan speed relative to forward-mode operation.

Overall thrust effectiveness of the fan reverser is improved by the core-thrust spoiling of the mixed-exhaust system. In the reverse mode, the absence of bypass flow in the tailpipe causes a reduction in low pressure turbine back pressure and allows the core speed to be reduced relative to forward-mode operation. This "rotor matching" effect causes a significant reduction in core-stream thrust potential which is reduced still further by the aerodynamic-spoiling effect of dump-diffusion out of the mixer core chutes into the tailpipe. These effects, evaluated in a cycle computer model, are based on previous, scale-model, exhaust-mixer tests.

The overall system reverse-thrust effectiveness is shown in Figure 134 compared to a CF6-50C with and without the turbine reverser. The E³ effectiveness compares closely to the effectiveness achieved with the CF6-50C with turbine reverser and exceeds the -50C level without turbine reverser.

4.9.2 Engine Mount System

The mount system design was selected to achieve the following important objectives:

- c Compatibility with aircraft pylon structural design requirements.

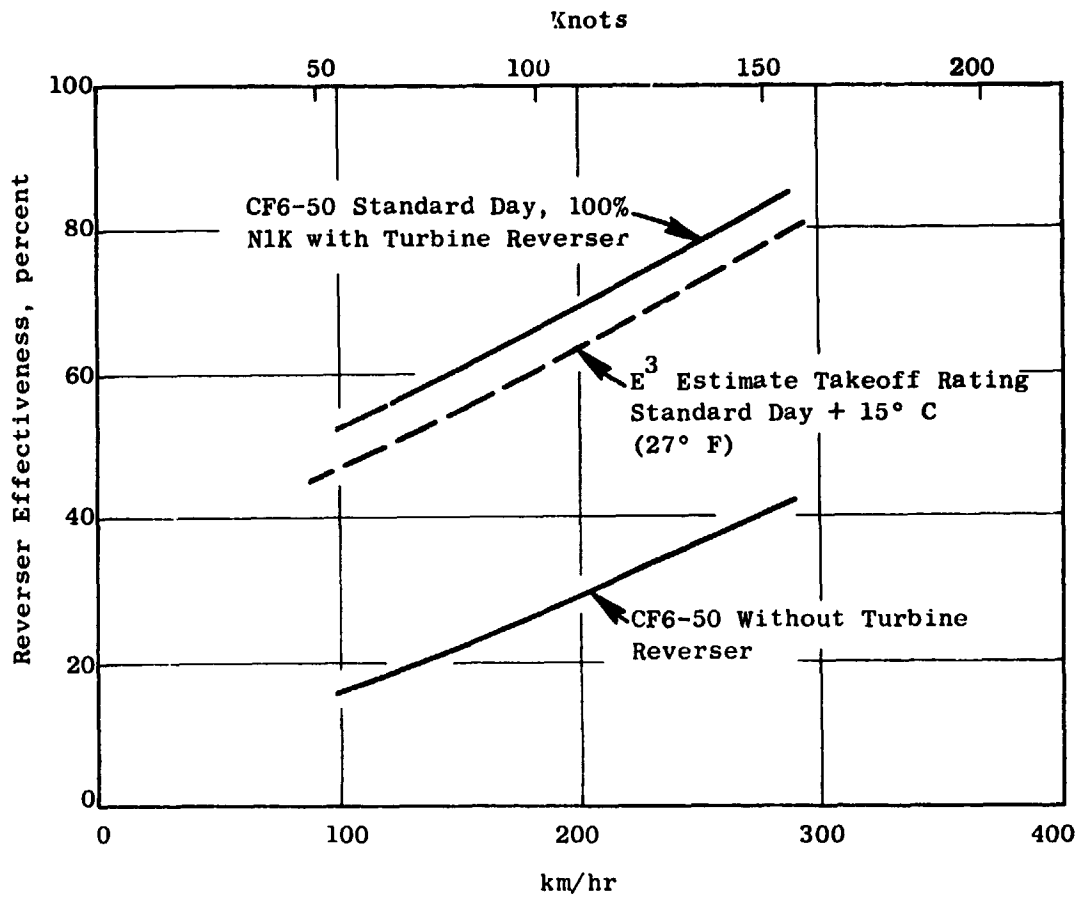


Figure 131. Overall Engine Reverse Thrust Comparison.

- Reduction or elimination of concentrated "punch" loads into the engine structure.
- Reduction of engine ovalization and bending loads due to mount reactions.

The mount system chosen for the E³ is shown in Figure 135. It consists of a front mount with twin thrust links and a uniball to take vertical and side loads, a midmount to take roll and side loads, and an aft mount to take only vertical loads. The mount reactions are shown schematically in Figure 136.

The front mount was derived from the improved CF6-50C mount with additional emphasis on lowering the thrust-reaction line closer to the engine centerline to reduce the thrust-induced moment. The two links were made self-adjusting by means of a whiffletree arrangement; this also helped to reduce load concentrations at the fan-frame attachment points.

The midmount was evolved to provide sufficient wheelbase to take out rolling moment without making the pylon too wide in the bypass flowpath. More conventionally, or in a separated-flow installation, the rolling moments would be taken out on the low pressure turbine rear frame, along with vertical and side loads. But the pylon width required for this, about 41 cm (16 inches), would be excessive at a location just upstream of the mixer in a mixed-flow installation. Movement of the side-and-roll mount to the midengine location was accomplished by use of a mount-extension ring attached to the low pressure turbine rear frame. This ring appeared to perform another useful function in the distribution of mount reactions over the periphery of the rear frame, thereby, avoiding punch-load deflections.

The aft vertical mount was originally incorporated in the midmount, but it was found that a longer wheelbase between the fore and aft vertical mounts was beneficial in reducing engine bending. Therefore, it was decided to move the vertical load member aft to the turbine rear frame, as shown in Figure 135.

Structural analyses of the FPS engine in response to typical thrust, aerodynamic, and maneuver loads have indicated encouragingly low engine deflections. Figure 137 shows maximum local deflections versus engine axial length for a takeoff rotation condition where the nacelle (air) load moment is near maximum (370K in.² lbs). The maximum deflection (approximately 0.02 mm or 9 mils) was found to occur over the turbine area. These deflections would be in addition to clearance changes resulting from thermal and elastic behavior of the engine.

4.9.3 Accessory Package

The accessory package location for the FPS was selected to help reduce fuel consumption and DOC.

The principal choices for accessory arrangement were as follows:

- Fan-case-bottom-mounted aircraft and engine accessories.

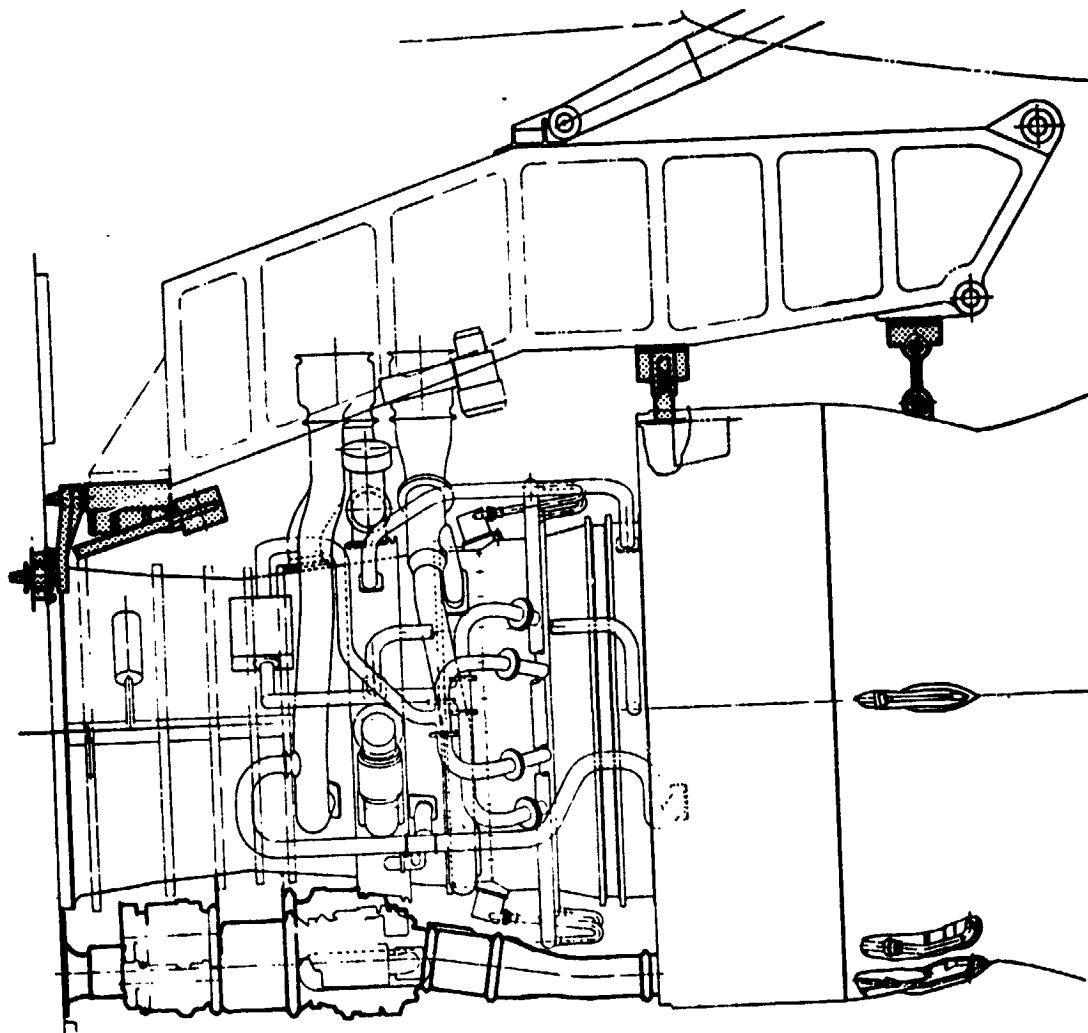


Figure 135. Engine Mount System.

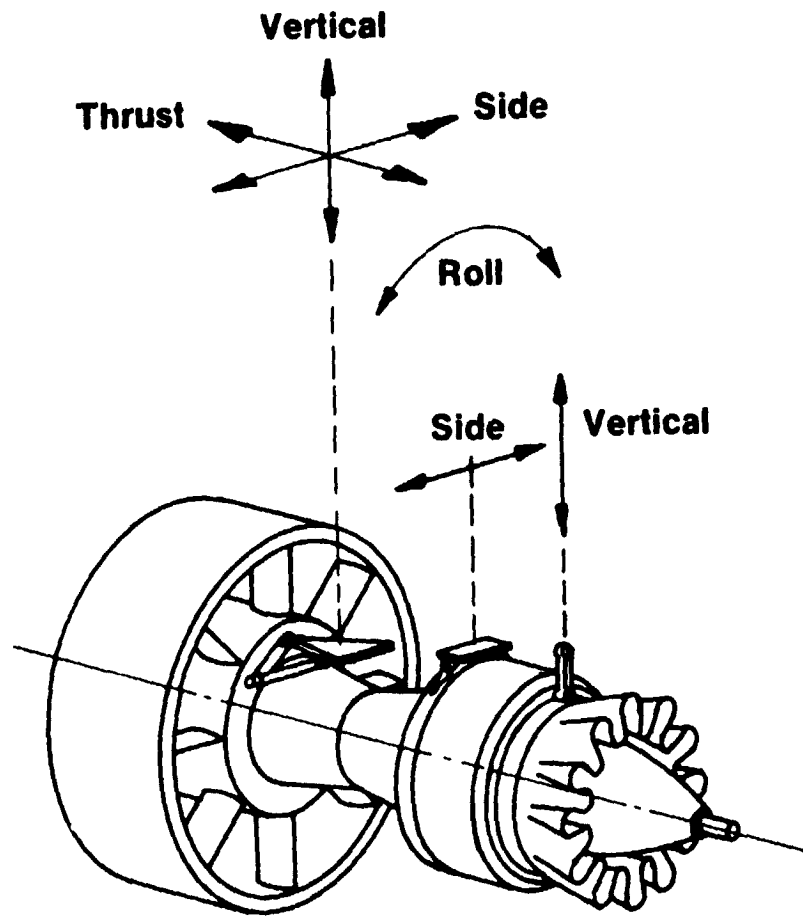


Figure 136. Mount Reactions Schematic.

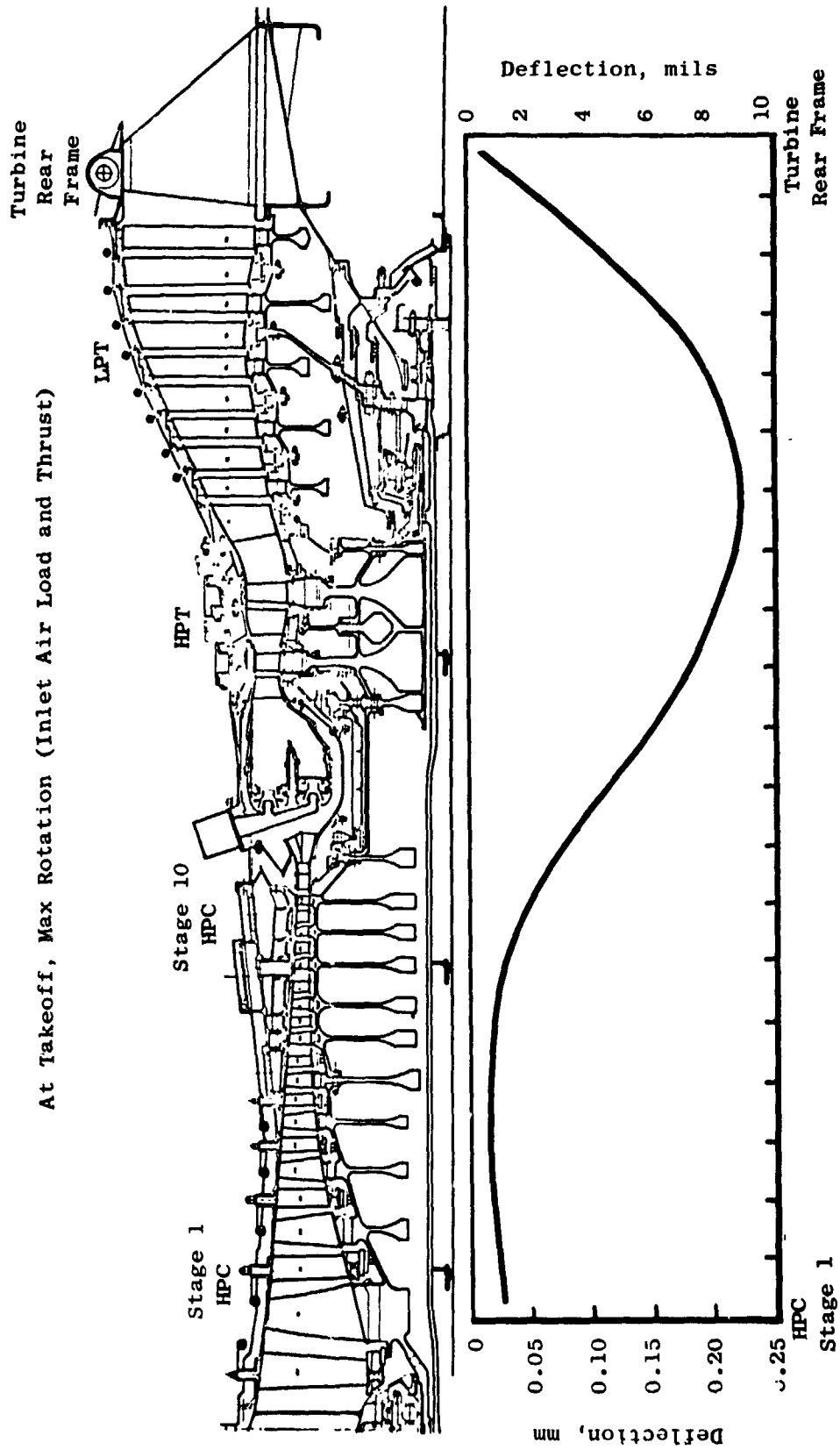


Figure 137. Preliminary E^3 Ovalization.

- Core-component-mounted aircraft and engine accessories, thermally isolated in a shielded and vented compartment.
- Pylon-mounted aircraft accessories with engine accessories in the core compartment.

Evaluation of these systems included consideration of differences in installation drag and pressure losses, weight, maintenance cost, and the impact of these on mission fuel and DOC. Summaries of the results are shown in Tables 77 and 78. Because these results tended to favor the core-compartment arrangement, this was chosen as the baseline configuration for the E³. However, the engine design retains the ability to be modified to other arrangements if desired by users.

Figures 138 and 139 show front and bottom views of the core-mounted accessory package chosen for the E³ FPS. A side view is shown on Figure 135.

4.9.4 Aircraft Company Subcontracts

In order to ensure that the E³ FPS design is consistent with the installation requirements of advanced commercial transports, the aircraft subcontracts with Boeing, McDonnell-Douglas, and Lockheed included reviews and critiques of the nacelle design. As a result, the major elements of the nacelle design (including choice of external aerodynamic lines, mount system, accessory arrangement, thrust reverser, and maintenance access provisions) were reviewed with the aircraft companies, and many of their recommendations were incorporated in the design. An Aircraft Integration Report, now in preparation, will document the details of these reviews with the aircraft companies.

Table 77. Accessory Gearbox Location Trade Study Results.

Location	Pylon (Aircraft Accessories) Core (Engine Accessories)	Fan Case (All)	Core Mount (All)
Δ Weight, kg (lbm)	+22.7 (+50)	34.0 (-75)	0
Δ Maintenance Estimated \$/EFH	+1.84 + +2.69	-0.42 + -1.27	0
Δ SFC (Drag, ΔP), %	-0.1	+0.65	0
Δ DOC, %	+0.26	+0.13	0
ΔW_F , %	0	+0.72	0

Table 78. Nonquantitative Factors in Accessory Package Selection.

Fan Case Mount

- Must be Designed to Comply with FAA wheels-Up Landing Regulation
- Accessory Fairing Tends to Block Reverser if Side-Mounted
- Aircraft Asymmetry or Left-Hand/Right-Hand Engines if Side-Mounted
- Best Accessibility of Candidate Configurations

Core Compartment Mount

- Some Airline Disfavor from Maintenance, Accessibility Aspect

Pylon Mount

- Airline Disfavor from Accessibility Aspect
- May have Significant Drag Penalty in Close Nacelle/Wing Placement
- Access and Mounting Problem with DACO-Type Tail Engine Installation

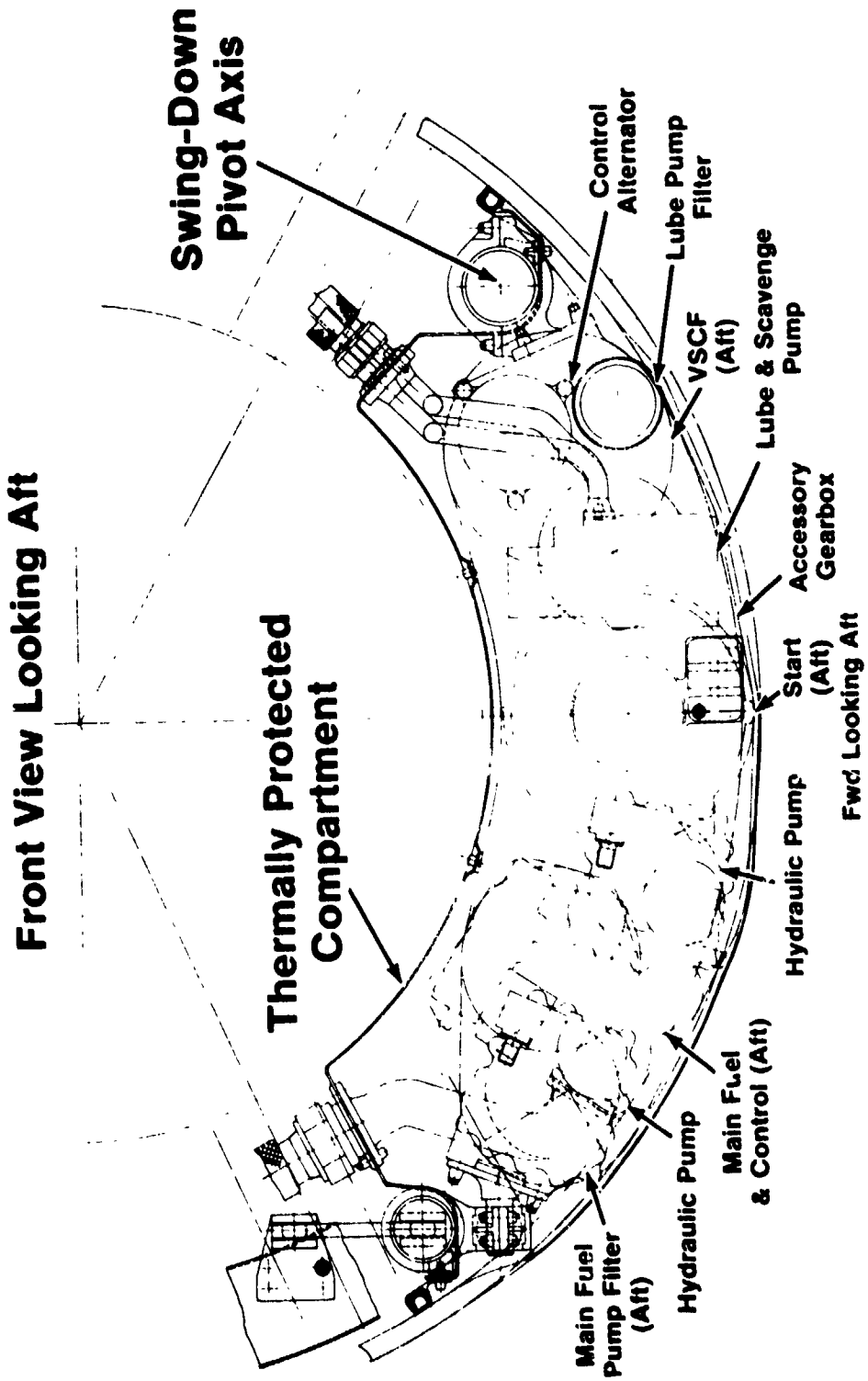


Figure 138. Accessory Package.

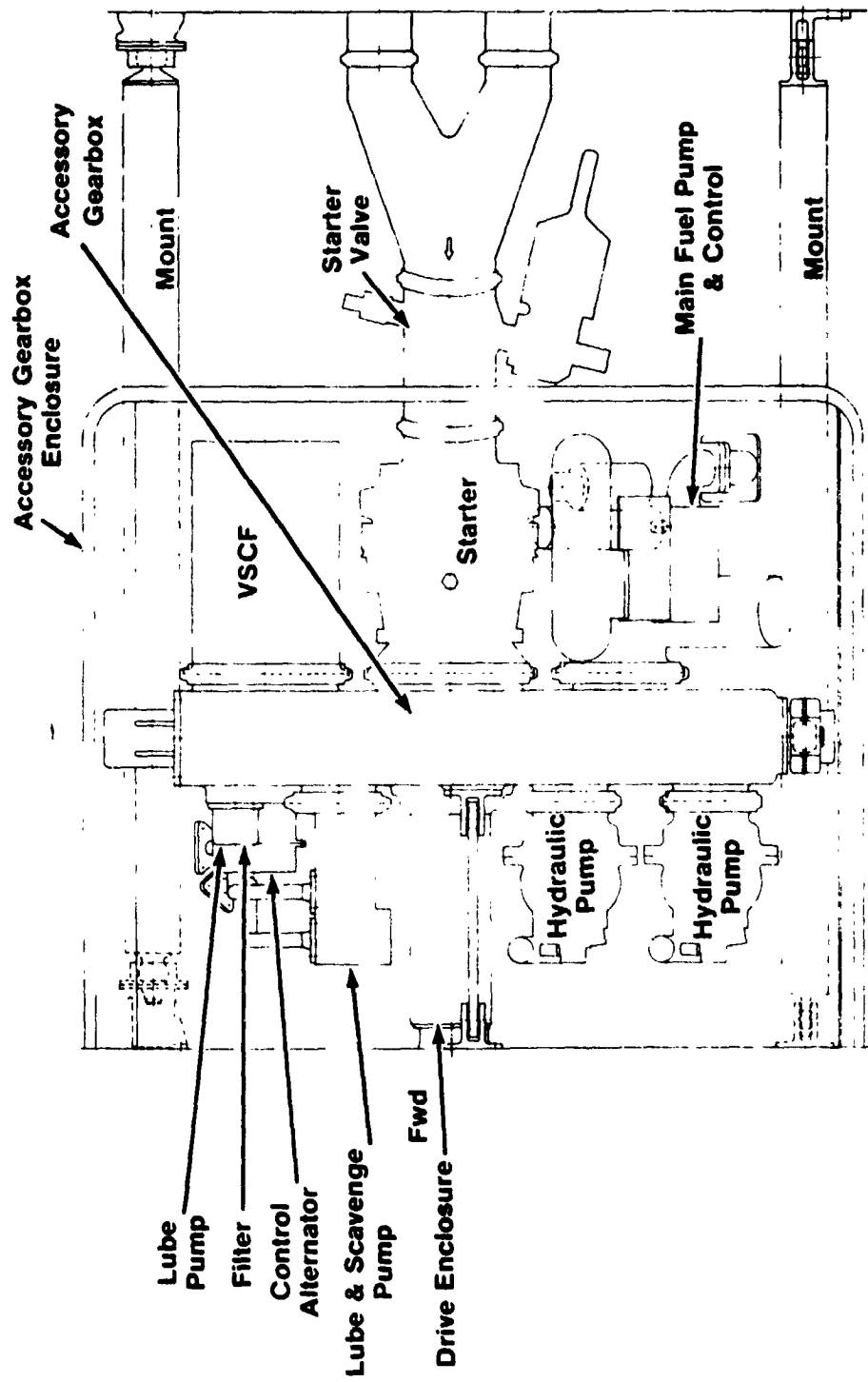


Figure 139. Accessory Package.

5.0 CONCLUSIONS

The preliminary design of the Flight Propulsion System (FPS) has indicated that all NASA goals for the General Electric Energy Efficient Engine (E³) Project can be met. The current status of the FPS design, as compared to the NASA program goals, is as follows:

<u>NASA Goal</u>	<u>FPS Status</u>
● 12% Reduction in sfc (Installed, Altitude Max. Cruise)	14.2% Reduction Projected
● 5% Reduction in DOC	5 to 11.6% Reduction depending on mission/aircraft
● Meet FAR 36 (March 1978) noise requirements for new engines	Meets with a minimum 3 EPNdB margin at all points
● Meet Proposed EPA (1981) Emissions Standards for new engines	CO/HC with margin, no margin on NO _x
● Half of the in-service performance deterioration of current engines	Projected to meet

The installed FPS sfc reduction of 14.2% at maximum cruise compared to the CF6-50C has been estimated based on performance goals for the components and anticipated reductions in isolated-nacelle drag. If a fully installed engine is considered (one with customer bleed and power extraction), the relative sfc reduction increases to 14.6%. Aircraft integration studies indicate that with the FPS projection of installed engine weight and performance achieved, reductions in block fuel consumption ranging from 14.5 to 21.7%, depending on the aircraft/mission, can be attained.

The studies have estimated that a 5 to 11.6% reduction in DOC is achievable with the above FPS characteristics and the projected, initial engine cost, and maintenance costs.

Achievement of the performance-retention goal would increase the projected fuel and DOC savings. The fuel savings would then become 15.4 to 22.9%, and DOC savings would range from 5.3 to 12.3%. Since many of the advanced design features of the engine such as mounting, active clearance control, improved shroud materials, and the quarter-stage debris separation (for example) enhance performance retention, General Electric is projecting that the retention goal will be met.

Evaluation of the acoustic performance of the FPS when integrated with advanced aircraft indicates that the FAR 36 (March 1978) acoustic requirements for newly certified engines will be satisfied. Calculation of noise levels for various study aircraft showed that a 3 EPNdB margin could be maintained for the most critical aircraft condition (approach) on the aircraft that required the highest approach power setting. Calculation of the noise levels that could be expected with the growth version of the FPS (+20% thrust) indicated that this engine could also be certified under FAR 36 (March 1978) rules but without a 3 EPNdB margin at all points.

Meeting the emissions goals under the proposed EPA (1981) standards for nitrous oxide (NO_x) will be very difficult. Projected NO_x levels meet the goal, but do not permit any margin for engine-to-engine variation. The hydrocarbon (HC), smoke, and carbon monoxide (CO) goals should be met with adequate margin to ensure that all production engines meet the standard. The double-annular combustor, although potentially controlling emissions better than any other General Electric configuration, does add a weight and cost penalty to the overall FPS system. Future emission requirements will determine if it is retained or replaced by a simpler combustor.

6.0 REFERENCES

1. Johnston, R.P., et al., "Energy Efficient Engine - Preliminary Design and Integration Study," NASA Lewis Research Center, CR-135444, September 1978.
2. Neitzel, R.E., Hirschkron, R., and Johnston, R.P., "Study of Turbofan Engines Designed for Low Energy Consumption," NASA Lewis Research Center, CR-135053, August 1976.
3. Neitzel, R.E., Hirschkron, R., and Johnston, R.P., "Study of Unconventional Engines Designed for Low Energy Consumption," NASA Lewis Research Center, CR-135136, December 1976.
4. Ross, E.W., Johnston, R.P., and Neitzel, R.E., "Cost Benefit Study of Advanced Materials Technology for Aircraft Turbine Engines," NASA Lewis Research Center, CR-134702, November 1974.
5. Hillery, R.V., and Johnston, R.P., "Cost Benefit Study of Advanced Materials Technology for Aircraft Turbine Engines," NASA Lewis Research Center, CR-135235, September 1977.
6. Wisler, D.C., Koch, C.C., and Smith, L.H., Jr., "Preliminary Design Study of Advanced Multistage Axial Flow Core Compressors," NASA Lewis Research Center, CR-135133, February 1977.
7. Tyler, J.M., and Sofrin, T.G., "Axial Flow Compressor Noise Studies," SAE Aeronautic Meeting, Paper No. 345D, 1961.
8. Patt, R.F., et al., "Flight Propulsion System Aircraft Integration Evaluation," NASA Lewis Research Center, CR-159584, publication pending.
9. Koch, C.C., and Smith, L.H., Jr., "Loss Sources and Magnitudes in Axial-Flow Compressors," Transaction of ASME, Journal of Engineering for Power, Vol. 98, Series A, No. 3, July 1976, p. 411.
10. Gleason, C.C., and Niedzwiecki, R.W., "Results of the NASA/General Electric Experimental Clean Combustor Program," AIAA 76-763, July 1976.
11. Burrus, D.L., Sabla, P.E., and Bahr, D.W., "Quiet Clean Short-Haul Experimental Engine, Double-Annular Combustor Technology Development Final Report," NASA Lewis Research Center, CR-159483, July 1978.
12. Niedzwiecki, R.W., and Jones, R.E., "The Experimental Clean Combustor Program - Description and Status," NASA Lewis Research Center, TNX-715471, May 1974.
13. "Quiet Clean Short-Haul Experimental Engine (QCSEE) Over-the-Wing Engine Digital Control System Design Report," NASA Lewis Research Center, CR-135337, December 1977.

14. "Quiet Clean Short-Haul Experimental Engine (QCSEE) Under-the-Wing Engine Digital Control System Design Report," NASA Lewis Research Center, CR-134920, January 1978.
15. "Full Authority Digital Electronic Control, Phase I Final Report, Revision A," General Electric Aircraft Engine Group, Advanced Engineering and Technology Programs Department, R79AEG411, 1979.
16. "Quiet Clean Short-Haul Experimental Engine (QCSEE) OTW Propulsion System Test Report, Volume III - Mechanical Performance," NASA Lewis Research Center, CR-135325, February 1978.
17. Poppel, G.L., "Analysis and Preliminary Design of an Optical Digital Tip Clearance Sensor for Propulsion Control," NASA Lewis Research Center, CR-159434, September 1978.